Investigation into the potential of bilosomes (bile salt-containing liposomes) to increase the bioavailability of phenolic compounds

Aygul Can

Submitted in accordance with the requirements for the degree of

Doctor of Philosophy

The University of Leeds

School of Food Science and Nutrition

August, 2023

This thesis is dedicated to my parents, my sister and my brother-in-law for their love, support, and encouragement.

The candidate confirms that the work submitted is his/her own, except where work which has formed part of jointly-authored publications has been included. The contribution of the candidate and the other authors to this work has been explicitly indicated below. The candidate confirms that appropriate credit has been given within the thesis where reference has been made to the work of others.

Details of the contribution of each member are outlined below.

Aygul Can: Conceptualization, Methodology, Data Curation, Formal Analysis, Writing-Original Draft Preparation.

Alan R. Mackie: Project Administration, Supervision, Conceptualization, Validation, Writing-Review and Editing.

Arwen I. Tyler: Project Administration, Supervision, Conceptualization, Validation, Writing-Review and Editing.

James Doutch: Data Collection and Formal Analysis for SANS experiment

Taskeen Niaz: Data Collection and Formal Analysis for absorption through murine intestinal tissue.

List of Publications

Chapter 1. Can, A., Tyler, A.I. and Mackie, A.R., 2021. Potential use of bile salts in lipid self-assembled systems for the delivery of phytochemicals. Current Opinion in Colloid & Interface Science, 56, p.101502.

List of Accepted Conference Abstracts

Oral and Poster Presentations

- 7th School of Food Science & Nutrition Annual PhD Conference (26-27 November 2020), University of Leeds, UK - Investigation into the potential of bile salt-containing liposomes to increase the bioavailability of phenolic compounds. (Online-Oral Presentation)

- The 35th ECIS 2021 Conference of the European Colloid & Interface Society (5-10 September 2021), Athens, Greece - Potential of Bile Salt-Containing Liposomes as Carriers of Health-Promoting Resveratrol. (Oral Presentation)

- Food Physics 2022 Conference, (1-2 February 2022)- Potential of Bile Salt Containing Liposomes as Carriers of Health Promoting Resveratrol (Online-Oral and Poster Presentation)

- 8th School of Food Science & Nutrition Annual PhD Conference (6 December 2022), University of Leeds, UK - Investigation into the potential of bile salt-containing liposomes to increase the bioavailability of phenolic compounds. (Oral Presentation)

- 12th International Colloids Conference (11-14 June 2023 | Palma, Mallorca, Spain) - Design and characterisation of bilosome-based oral delivery system for trans-resveratrol. (Poster Presentation)

Acknowledgements

Foremost, I would like to express my sincere appreciation to my supervisors, Prof. Alan R. Mackie, Dr. Arwen I.I. Tyler, and Dr. Christine Bösch, for their guidance, assistance, patience, and invaluable support. Their expertise and insights have been instrumental, significantly enhancing the quality of my work. I am genuinely grateful for the opportunity to collaborate with them.

I extend sincere appreciation to Dr. Taskeen Niaz for her vital contributions to the absorption experiment, to Dr. James Doutch for his role in the SANS experiment, to Prof. Michael Rappolt for his invaluable assistance in SAXS data analysis, and to Mohammed Asaf for his technical guidance with FT-IR.

Furthermore, my gratitude goes out to the entire team at the School of Food Science and Nutrition, including Miles Ratcliff, Gita Winder, Dr. Nataricha Phisarnchananan, Dr. Joanna Sier-Fuller, and Neil Rigby. Your unwavering support and assistance throughout my Ph.D. journey have been deeply valued.

In addition, I wish to express my deep appreciation to the ISIS Neutron and Muon Source for providing me with beam time (proposal STJA01606) and for their financial support. A special acknowledgement also goes to Diamond Light Source (Beamline I22), Prof. Nick Terrill, and Dr. Tim Snow for their invaluable guidance and support.

I reserve a special note of thanks to Dr. Sam Stubley and Dr. Frances Brown for their support during my Ph.D. journey.

Finally, I would like to acknowledge the Republic of Turkey - The Ministry of National Education for providing me with the opportunity to conduct this research and for their financial support.

Abstract

Phenolic compounds offer health-promoting functions, but they suffer from low bioavailability. Bilosomes (bile salt-containing liposomes) have the potential to improve the bioavailability of encapsulated phenolic compounds for oral administration. The hypothesis of this thesis is that incorporating bile salts into self-assembled vesicles can enhance the bioavailability of phenolic compounds. This thesis focuses on investigating the effects of bilayer modification with sodium cholate (NaC) and surface modifications using chitosan (CH) and polygalacturonic acid (PGA), on the physicochemical properties and stability of the lipid bilayer under various conditions. Additionally, it examines behaviours of the modified bilayers during simulated digestion, the bioaccessibility, and absorption of encapsulated *trans*-resveratrol *(t*-res), a model phenolic compound, with/without a food matrix.

The incorporation of NaC into the lipid bilayers and the biopolymer coating strongly affected the physical properties of the bilayers. Liposomes and bilosomes showed high stability at different pH, during thermal treatment and during storage. Despite some challenges (pKa and swelling properties of biopolymers), biopolymer-coated bilosomes exhibited good stability and protected the encapsulated t-res. While the incorporation of NaC increased the bioaccessibility of t-res from 40% to 83-90%, it was ~20% and ~40% for CH-coated and PGA/CH-coated bilosomes, respectively. The bioaccessibility increased significantly when t-res, liposomes, and bilosomes were digested with oat milk. For the absorption of samples, t-res concentration in the basolateral chamber at 2 hours for free t-res, liposomes, and bilosomes ranged from 0.379 µM to 0.487 µM. Accumulated t-res in tissue, ready for absorption, reached remarkably 3.345 µM and 16.801 µM with the incorporation of 10 mM and 7.5 mM NaC into the bilayers, respectively.

In conclusion, bilosomes provided stability and enhanced bioaccessibility and absorption of t-res, consequently enhancing bioavailability, compared to the liposomes. For food applications, while bilosomes are promising for intestine-targeted oral delivery of phenolic compounds, biopolymer-coated bilosomes have the potential for colon-targeted oral delivery.

Table of Contents

List of Tables

List of Figures

Chapter 1: General introduction

1.1 Research objectives

Phenolic compounds have received considerable attention and extensive research due to their health-promoting functions, such as antimicrobial, antioxidant, anti-carcinogenic, anti-aging, etc. (Mouhid et al., 2017; Shishir et al., 2018). To demonstrate these biological activities, phenolic compounds should reach sufficient plasma concentration. However, many phenolic compounds face challenges like solubility and poor absorption. Ellagic acid, for instance, exhibits low intestinal permeability and thus cannot be completely absorbed. Similarly, resveratrol and curcumin suffer from low solubility in aqueous media and, consequently, in biological fluids, making it challenging to incorporate them into many food products (Tønnesen et al., 2002). In addition to solubility and permeability issues, environmental stress factors (food matrix, storage conditions, food processing steps, or gastrointestinal tract (GIT)) can cause the degradation of phenolic compounds. As a result, their bioavailability may not be high enough, and they may not reach a sufficient concentration to exhibit their biological activity at the site of action (Arzani et al., 2015; Bonechi et al., 2012; Wenzel & Somoza, 2005).

Thus, when oral administration is the goal, bilosomes (bile salt-containing liposomes) can be beneficial for encapsulating phenolic compounds to enhance their bioavailability. This can be achieved by improving their solubility and intestinal permeability, protecting them from chemical and enzymatic degradation, and controlling their release rate and location. Bilosomes have been shown to enhance the solubility of poorly aqueous soluble phenolic compounds (Abbas et al., 2022). The incorporation of bile salts induces membrane curvature of phospholipid bilayers in a concentration-dependent manner and results in a range of lipid structures, including ellipsoid shapes, rod-like formations, smaller vesicles, and micelles. Due to differences in the physicochemical properties, the loading capacities (LC) of these structures may differ, resulting in different bioaccessible concentrations (Lichtenberg et al., 2013; McClements, 2013). Moreover, bile salts can increase the elasticity of the bilayer and show a penetration-enhancing effect that facilitates the absorption and bioavailability of bilosomes (Aburahma, 2016; Hu et al., 2013; Tang et al., 2021).

Previous studies have demonstrated that bilosomes can effectively enhance the bioavailability of phenolic compounds. However, there exists a knowledge gap in the literature concerning the comprehensive structural analysis of the impact of bile salts and biopolymers on lipid bilayers, the food application of phenolic compound-loaded

bilosomes, as well as their behaviours in the food matrix, during GIT, and their absorption.

Data from the literature search (in Chapter 1) outlined below led to the hypothesis of the current research: Incorporation of bile salts into the self-assembled vesicles can enhance the bioavailability of phenolic compounds.

The overall objective of the project: To explore the use of bilosomes as carriers for the delivery of trans-resveratrol (*t*-res) as a model phenolic compound.

More specifically, the objectives of this research were:

- to optimize the bilayer properties of both empty and *t*-res loaded bilosomes and investigate their characteristics.
- to modify the surface properties of empty and *t*-res loaded bilosomes using chitosan (CH) and polygalacturonic acid (PGA) and characterise the effects on the bilayer properties.
- to examine the stability of *t*-res loaded liposomes, bilosomes, CH-coated bilosomes, and PGA/CH-coated bilosomes under various stability conditions.
- to investigate the behaviour of *t*-res loaded liposomes, bilosomes, CH-coated bilosomes, and PGA/CH-coated bilosomes during simulated gastrointestinal conditions and assess the bioaccessibility of *t*-res.
- to study the impact of oat milk (OM) as a food matrix on the behaviour of *t*-res-loaded liposomes, bilosomes, CH-coated bilosomes, and PGA/CH-coated bilosomes during simulated GIT conditions and assess the bioaccessibility of *t*-res.
- to assess the absorption mechanisms of free *t*-res, *t*-res-loaded liposomes, and bilosomes, as well as the absorption of *t*-res loaded samples digested with OM.

1.2 Thesis outline

The thesis is divided into the following sections;

Chapter 1, General Introduction: The main purpose of the first chapter is to present essential subjects necessary for comprehending and valuing the content of the subsequent chapters. The following topics were discussed in this chapter: (i) the advantages and disadvantages of liposomes as a lipid self-assembled system. (ii) the investigation of the effect of bilayer modification and surface modification on the physicochemical properties and behaviours of lipid self-assembled systems (LSAS) in different environments based on the literature. (iii) the exploration of bioaccessibility, absorption, and bioavailability of LSAS. (iv) general information about resveratrol and the bioavailability of resveratrol as a model bioactive compound.

Chapter 2, Design, and characterisation of empty and t-res loaded liposomes, bilosomes, and CH-coated bilosomes and PGA/CH-coated bilosomes: This chapter describes the preparation, optimization, and characterization of empty and *t*-res-loaded liposomes, bilosomes, CH-coated bilosomes, and PGA/CH-coated bilosomes as carriers for oral delivery. The physical properties of the prepared systems were determined through a combination of dynamic light scattering (DLS), small-angle X-ray scattering (SAXS), and small-angle neutron scattering (SANS). Additionally, cryo-transmission electron microscopy (cryo-TEM) was employed to observe and analyse the morphology and lamellarity of the systems. Fourier transform infrared spectroscopy (FT-IR) was utilized to examine the effect of CH coating and PGA coating on the systems and to investigate the interactions between the compounds present in the formulations. Finally, the encapsulation efficiency (EE) (%) and LC (%) of the prepared systems were determined.

Chapter 3, The stability of t-res loaded liposomes, bilosomes, CH-coated bilosomes and PGA/CH-coated bilosomes: This chapter comprises the stability experiments (pH stability, thermal stability, and storage stability) of *t*-res-loaded liposomes, bilosomes, CH-coated bilosomes, and PGA/CH-coated bilosomes. The aim is to investigate the effect of lipid bilayer modification using bile salt (sodium cholate (NaC)) and bilayer surface modification using biopolymers (CH and PGA) on the stability of *t*-res loaded liposomes, bilosomes, CH-coated, and PGA/CH-coated bilosomes. During the stability conditions, the physicochemical properties of the systems, including hydrodynamic diameter (D_H), polydispersity index (PDI), zeta (ζ) potential, and drug retention (DR %), were determined.

Chapter 4, In vitro gastrointestinal digestion and absorption of t-res loaded liposomes, bilosomes, CH-coated bilosomes, and PGA/CH-coated bilosomes: In this chapter, static *in vitro* simulated digestion experiment was conducted to investigate the effect of bilayer modification using bile salt (NaC) and surface modification using biopolymers (CH and PGA) on the behaviour of *t*-res loaded liposomes, bilosomes, CH-coated, and PGA/CH-coated bilosomes during GIT. Additionally, these systems were digested with OM to observe the effect of the food matrix on their behaviours during GIT. The physical properties of the systems were determined during static *in vitro* simulated digestion in terms of D_H, PDI, and ζ potential. The bioaccessible *t*-res, which was in a form available for absorption at the end of digestion, was measured. Finally, the absorption of t-res from free *t*-res, *t*-res loaded liposomes, and bilosomes as well as the absorption of *t*-res from samples digested with OM were determined using the Ussing chamber system for intestinal permeability of the *t*-res.

Chapter 5, General discussion: The section includes a comprehensive discussion that integrates the findings from the previous chapters and concludes with final remarks on potential modifications of the prepared systems for utilization in food applications. Additionally, suggestions for future studies are provided.

Appendix: The Appendix contains detailed information about the various experimental methods employed and results from the preliminary study for the development and optimization. In Appendix A, the theoretical information about the methods (DLS, ζ potential, and small-angle scattering) used during the characterization of prepared samples was given. The data analysis of SAXS and SANS, models used for SANS data, and electron density profile calculation were also given in this section. In Appendix B1, the procedures for preparing 1-palmitoyl-2-oleoyl-sn-glycero-3-phosphocholine (POPC)-bilosomes, assessing their storage stability, and applying CH and PGA coatings were explained. Appendix B2 covers the optimization of CH and PGA coatings for POPC/1,2-dioleoyl-sn-glycero-3-phospho-(1'-rac-glycerol)(sodium salt) (DOPG)-bilosomes.

1.3 Systematic literature search

Research Question: Could the usage of bile salts in self-assembly systems enhance the bioavailability of plant-based active compounds?

Study objectives: The main objective of this systematic review is to investigate the potential roles of bile salts in self-assembly systems and to examine the effect of their presence on the bioavailability of plant-based active compounds.

Search strategy: Keywords were composed of self-assembly systems, bile salts, and plant-based bioactive compounds. In order to increase searching efficiency, terms related to different self-assembly systems that may contain bile salt, the specific name of bile salts, and some terms related to plant-based bioactive have been added to the keywords. Keywords were combined with Boolean operators (“AND” and “OR”) and searching was performed using databases (Web of Science, PubMed, Medline, Embase, and Scopus). Searching keywords were limited between 2000 and 2021. The last update search was conducted on 08 January 2021.

The keywords were composed following: (nanodelivery OR delivery OR self-assembl* OR self assembl* OR vesic* OR micell* OR carrier* OR particle* OR nanoparticle* OR phospholipid* OR liposome* OR nanoliposome* OR proliposome* OR bilosome* OR probilosome* OR niosome* OR proniosome* OR transfersome* OR phytosome* OR polymersome* OR ethosome* OR chitosome*) AND (bile salt* OR bile acid* OR cholate OR cholic OR chenodeoxychol* OR deoxychol* OR

glycochol* OR glycochenodeoxychol* OR glycodeoxychol* OR glycolithochol* OR glycoursodeoxychol* OR hyodeoxychol* OR lithochol* OR murichol* OR taurochol* OR taurochenodeoxychol* OR taurodeoxychol* OR taurolithochol* OR tauromurichol* OR tauroursodeoxychol* OR ursodeoxychol* OR biosurfactant* OR surfactant* OR detergent* OR edge activator*) AND (pharmaceutical* OR biopharmaceutical* OR bioactive* OR nutraceutical* OR phyto* OR polyphenol* OR phenol* OR caroten*).

Study selection and inclusion/exclusion criteria: After searching the keywords in the databases, full-text research articles published in English were selected. Reviews, book and book sections, conference papers, letters, and dissertations were excluded. The titles of the research articles have been screened in line with the objectives of the systematic review. Research articles that not addressing lipid-based self-assembly systems, compositions including phospholipid, bile salts, and plant-based active compounds, and bioavailability of plant-based active compounds were excluded. An abstract screening of the included articles was conducted with a focus on "bile salts in self-assembly systems and the effect of their presence on the bioavailability of plant-based active compounds" and articles with insufficient data were excluded. Full text of included articles was assessed for eligibility and additional records identified from the references of full-text articles were screened by hand searching. Some of full- text articles were excluded because of insufficient data and not addressing the topic. The articles were determined according to selection criteria defined by the first author and included articles were checked and evaluated by co-authors. The results of the study selection criteria/process for systematic review are shown in the PRISMA diagram **(Fig 1.1).**

Data extraction and tabulation: Data were extracted from relevant articles using PICO (P: sources, I: interventions, C: control study, O: outcomes) standards. The data collected include the properties of the safe (non-toxic biodegradable and biocompatible) and stable (particle size, PDI, ζ potential, encapsulation, and loading efficiency) self-assembly system and *in vivo* and *in vitro* interactions (release profile, cytotoxicity, and pharmacokinetic parameters). Data including the route of administration, self-assembly system and active material, composition and optimum formulation, and key findings were exported to Microsoft Excel.

Data analysis: In this systematic review, the potential roles of bile salts in self-assembly systems and the effect of their presence on the bioavailability of plant-based active compounds were investigated. The composition of the self-assembly systems and their effect on morphology were evaluated. Key findings including morphological properties, EE of the system, release profile, and *in vivo* and *in vitro* interactions of the self-assembly system according to the delivery route were summarized.

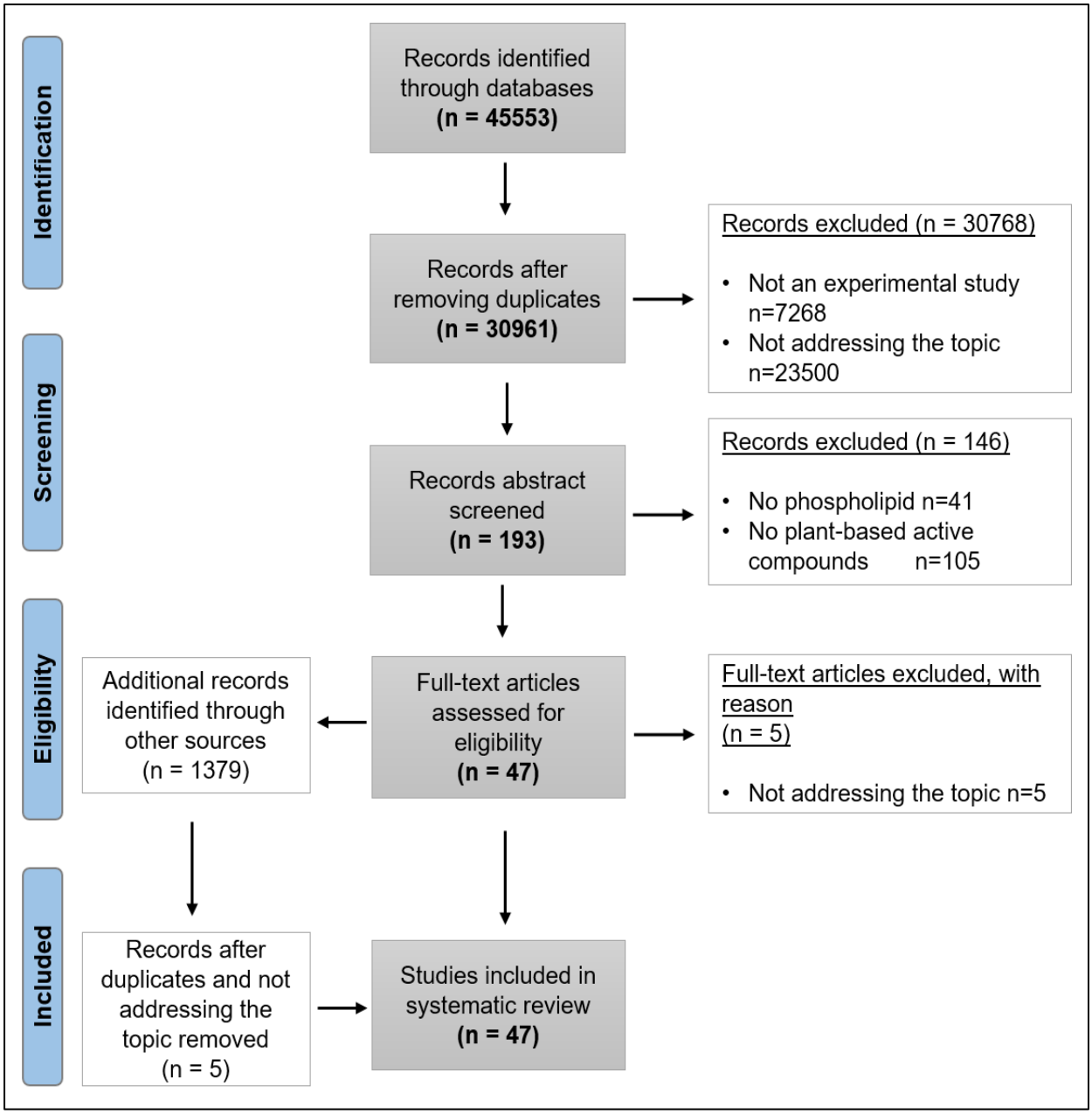

Figure 1.1 Flowchart of selection criteria/process and included studies.

Study description: After searching the keywords in the databases, a total of 45533 studies were found. Duplicates were removed and studies that were not experimental (7268) and not addressing the topic (23500) were excluded during title screening. After the title screening, an abstract screening was performed for the remaining research articles (193). Research articles that reported compositions did not contain phospholipids and plant-based active materials were excluded. 5 out of the 47 articles were excluded from the full-text assessment. 1379 additional records were identified from the references of full-text assessed research articles. The 5 relevant research articles were also determined from additional records and were included in the synthesis of the systematic review.

A total of 47 articles were found after the systematic search. The results of the study selection process are given in the PRISMA diagram **(Fig 1.1).** Due to the heterogeneity of the studies, a meta-analysis could not be carried out.

1.4 Key topics

1.4.1 Encapsulation technology

In recent years, consumers have shown increased interest in including functional foods in their diet. Of particular interest are functional products containing health-promoting phytochemicals, such as phenolic compounds, terpenes, phytosterols, and others (Mouhid et al., 2017; Shishir et al., 2018). There is a growing body of literature that highlights the potential of phytochemicals in the food, beverage, and pharmaceutical industries, due to their desirable biological functions, including antioxidant, anti-microbial, anti-inflammatory, and anti-carcinogenic activities. However, these biological functions are highly dependent on the bioavailability of these compounds.

The bioavailability of phytochemicals can be low due to limited bioaccessibility or absorption, as well as rapid metabolism in the body. Low bioaccessibility can be attributed to factors such as limited liberation, poor solubility in the GIT, and interactions with components in the GIT. On the other hand, absorption can be limited by the intestinal mucus layer, as well as the compound's innate properties, such as surface charge, ζ potential, polarity, size, and hydrophobicity. Once absorbed, phytochemicals pass into the systemic circulation through the liver or lymphatic system (McClements et al., 2015). However, their bioavailability may still be hindered by factors like bioaccessibility, absorption, transformation, and rapid clearance from the circulation, resulting in low plasma concentration, which is insufficient to exert significant pharmacological effects at target sites (Walle et al., 2004).

To overcome these limitations and enhance the bioavailability of phytochemicals, encapsulation technology, and delivery systems offer a promising solution (Amri et al., 2012). Phytochemicals can be loaded into carriers that release them under controlled conditions at the target site. Encapsulation techniques are widely used to enhance the stability of active compounds during processing and storage, mask undesirable taste, reduce toxicity, protect them from the harsh GIT environment, control their release, and improve cellular uptake and biological activities (Esfanjani et al., 2018; Jafari & McClements, 2017; Shishir et al., 2018).

Different encapsulation technologies and materials can be used depending on the desired properties and function of active compounds such as increased surface area,

solubility, homogeneity, stability, intracellular uptake, and bioavailability. The choice of bioactive compounds, wall materials, and encapsulation techniques plays a crucial role in achieving successful encapsulation. Encapsulation materials must be "generally recognized as safe" (GRAS) and approved for use in food products by authorized organizations (Shishir et al., 2018). Physicochemical properties of active and wall materials, such as molecular weight, polarity, solubility, size distribution, structural morphology, rheological behaviours, and processing cost, are essential considerations for developing carrier systems for food applications from an industrial perspective (Dias et al., 2017; Souza et al., 2015). Different encapsulation technologies, such as spray or freeze-drying, fluid bed coating, extrusion, coacervation, emulsification, and liposome entrapment, can be employed depending on the desired properties and functions.

Additionally, encapsulation can produce different particle sizes, including macrocapsules (>5000 µm), microcapsules (0.2-5000 µm), and nanocapsules (<0.2 µm) (Jafari, 2017). Among these, nanocapsules are particularly advantageous for providing desired properties to active compounds, such as increased surface area, solubility, homogeneity, stability, intracellular uptake, and bioavailability (Shishir et al., 2018). Nanostructures are generally considered to be below 1 µm, according to the European Food Safety Authority, and are described as "for 50% or more of the particles in the number size distribution, one or more external dimensions are in the size range 1 nm - 100 nm" (EC, 2011).

1.4.2 Lipid self-assembled systems

Among encapsulation techniques, there has been a growing interest in encapsulating bioactive compounds into novel and promising LSAS, such as (phospho)lipid-based carriers (liposomes, bilosomes, transfersomes, cubosomes, hexosomes), surfactant-based carriers (niosomes), emulsions (single, double, microemulsions) and solid lipid nanocarriers (solid lipid nanoparticles, nanostructured lipid carriers (NLCs), nano-oleogels) (Assadpour & Jafari, 2019).

1.4.2.1 Liposomes

Liposomes are the most widely used carriers among LSAS and play a key role in addressing the limitations of phenolic compounds. Composed of phospholipids with polar head groups and apolar acyl chains, liposomes form self-closed structures when placed in water (Reza Mozafari et al., 2008). The inner aqueous phase of the liposome is separated from the external water phase by a phospholipid bilayer, whose shape is determined by hydrogen bonding between head groups/phosphates/carbonyl and water, hydrophilic interactions between head groups and water, and van der Waals interactions between hydrocarbon chains (Pattni et al., 2015; Shishir et al., 2018). Due

to this unique structure, liposomes can encapsulate both hydrophilic and hydrophobic compounds, making them versatile carriers (Maurer et al., 2001; Rezaei et al., 2019).

Liposomes can be produced using various methods such as thin-film hydration, reverse phase evaporation, ethanol injection, and microfluidic-based methods, which can be combined with size reduction techniques like sonication and extrusion (Sarabandi et al., 2019; Van Tran et al., 2019). Depending on the production methods, liposomes can come in different shapes and sizes, including small unilamellar vesicles (SUV) (>20-100 nm), large unilamellar vesicles (LUV) (>100 nm), giant unilamellar vesicle (GUV) (>1000 nm), and multilamellar vesicle (MLV) (>500 nm) (Borel & Sabliov, 2014).

Liposomes have numerous advantages as carriers. They can reduce the required drug dosage frequency, especially for drugs with short half-lives that require multiple dosages to show a therapeutic effect. Liposomes provide a more uniform drug distribution in circulation due to the controlled release of encapsulated compounds. They are biocompatible and biodegradable, reducing the systemic toxicity of drugs and allowing delivery to specific organs, minimizing cytotoxicity in drug-sensitive tissues (Çağdaş et al., 2014). Furthermore, liposomes can be easily modified by altering their size, charge, and bilayer structure. Liposomes have been shown to enhance the solubility of flavonoids (Goniotaki et al., 2004) stability and solubility of tea polyphenol (Zou, Liu, et al., 2014), stability, and bioavailability of epigallocatechin gallate (EGCG) (Zou, Peng, et al., 2014), the antioxidant activity of resveratrol (Kristl et al., 2009), permeation of catechin (Fang et al., 2006), and bioavailability of quercetin (Priprem et al., 2008).

Although liposomes have considerable potential for encapsulation of bioactive compounds, they may suffer from instability during storage and digestion. The physical stability of grape seed extract (0.1% w/w) loaded in liposomes for 98 days was investigated by Gibis et al. According to the results, the D_H and PDI of liposomes did not change for 58 days ($p > 0.05$). After 58 days, a broad particle size distribution was seen because of the oxidation of the unsaturated fatty acids in soy lecithin (Gibis et al., 2013). Astaxanthin-loaded liposomes showed 82.29% of retention during storage (15 days at 4°C). The retention rate decreased to 61.32% at 25°C due to the increased storage temperature which accelerates the hydrolysis rate of phospholipids and adversely affects the structure of liposomes (Pan et al., 2018).

The chemical instability of liposomes is generally related to lipids which are used in formulations. Unsaturated fatty acids of phospholipids are prone to oxidation and the ester moieties can undergo hydrolysis, both of which can lead to structural disruption of liposomes and drug leakage (Rideau et al., 2018). During digestion, the properties

and composition of liposomes, as well as digestion conditions (pH, enzymes, bile salts, etc.), have a considerable effect on the biological fate of liposomes. The composition of liposomes depends on the structure of phospholipids, including polar head groups, length, and degree of saturation of the acyl chain (Liu et al., 2019). The average pore size of human mucus is 100 nm, allowing particles smaller than 100 nm to diffuse through mucus easily. While particles of 200 nm have also been reported as absorbable, particles bigger than 200 nm suffer from a short circulation time in the blood, leading to decreased bioavailability (Borel & Sabliov, 2014). Although liposomes can generally remain stable in gastric conditions, they cannot maintain their integrity in the presence of intestinal enzymes and bile salts, especially in the small intestine, particularly the duodenum. Phospholipases (A_1, A_2, B, C, and D) hydrolyse phospholipids, producing lysophospholipids and free fatty acids. Phospholipase B shows the combined effect of phospholipase A_1 and A_2, capable of cleaving acyl chains of phospholipids from both the sn-1 and the sn-2 positions. Phospholipase C cleaves the glycerophosphate bond to produce diacylglycerol and a phosphate-containing head group, while phospholipase D cleaves the terminal phosphate ester bond of phospholipids to produce phosphatidic acid and an alcohol. Other major intestinal enzymes include pancreatic lipase (which hydrolyses dietary fat molecules) and cholesterol esterase (which hydrolyses tri-, di-, and monoglycerides, cholesterol esters, and phospholipids) (Liu et al., 2019). Interaction with intestinal bile salts leads to the destruction of vesicle integrity. When intestinal bile salts reach the critical micelle concentration, they use phospholipids from liposomes to form mixed micelles. Even if not completely disintegrated, liposomes may rapidly release active materials from enlarged pores (Hu et al., 2013).

The stability of bovine serum albumin-loaded liposomes was investigated and results show that while liposomes can protect their membrane from the simulated gastric fluid (SGF) and pepsin hydrolysis, most of the liposomal membrane was damaged in simulated intestinal fluid (SIF) (2015). After incubation of liposomes composed of lipids with low transition temperatures (T_m) (<37°C) in 10 mM bile salts at pH 7.4, all encapsulated active material was released because of disruption of the lipid bilayer (Richards & Gardner, 1978). These instability problems limit the usage of liposomes in the food and pharmaceutical industries. However, these difficulties can be overcome through several approaches. The properties of conventional liposomes can be enhanced by using different lipids and lipid combinations, incorporating materials such as cholesterol (Chol), non-ionic surfactants, and bile salts in the bilayer structure, and modifying the surface with coating techniques (Kotla et al., 2017).

1.4.3 The bilayer modification of lipid self-assembled systems

1.4.3.1 Phospholipids

The properties of LSAS can be enhanced with the use of different lipids, surfactants, or their combinations or by incorporation of several compounds such as Chol or bile salts in the bilayer structure **(Fig 1.2).** Phospholipids are classified into natural and synthetic depending on their sources. Natural phospholipids are produced from soybeans, egg yolk, etc. by purification. Synthetic phospholipids are manufactured using a synthetic way and they have a specific polar head group and fatty acid composition (Van Hoogevest & Wendel, 2014). Phospholipids such as phosphatidylcholine (PC), phosphatidylethanolamine (PE), phosphatidylglycerol (PG), and phosphatidylserine (PS), are the main materials of liposomes (Pattni et al., 2015).

Phospholipids have different T_m, causing them to transition from a solid gel state ($<T_m$) to a liquid crystalline state ($>T_m$). The T_m of phospholipids changes depending on their hydrophilic phosphatidyl head group and hydrophobic fatty acid tails. Different head groups, lengths, and degrees of saturation of the fatty acid chains affect the T_m of phospholipids. The T_m of POPC (16:0–18:1) is -2°C, whereas that of 1-palmitoyl-2-oleoyl-sn-glycero-3-phosphoethanolamine (POPE, 16:0-18:1) is 25°C. Phospholipids with longer fatty acid chains have higher T_m. The T_m of 1,2-dimyristoyl-sn-glycero-3-phosphocholine (DMPC, 14:0), 1,2-dipalmitoyl-sn-glycero-3-phosphocholine (DPPC, 16:0), and 1,2-distearoyl-sn-glycero-3-phosphocholine (DSPC, 18:0) are 24°C, 41°C, and 55°C, respectively. With the same head group and fatty acid chain length, higher saturation causes a higher T_m. The T_m of DSPC (18:0), 1,2-dioleoyl-sn-glycero-3-phosphocholine (DOPC, 18:1), 1,2-dilinoleoyl-sn-glycero-3-phosphocholine (DLPC, 18:2), and 1,2-dilinolenoyl-sn-glycero-3-phosphocholine (18:3) are 55°C, -17°C, -57°C, and -60°C, respectively (Liu et al., 2019). Selecting the appropriate phospholipids for liposome formulations is important for achieving the desired stability and release profile. Using phospholipids with higher T_m during liposome preparation provides a more stable structure compared to using phospholipids with low T_m. Phospholipids with low T_m may not protect their structure and can lead to active material leakage, but when combined with Chol, the stability of the structure can be enhanced (Lee, 2020).

The effect of phospholipid composition (docosahexaenoic acid, salmon, and soybean phosphatidylcholine (SPC)) on the properties of liposome membrane showed that lipid type significantly affects the T_m, elasticity, and fluidity of the membrane and consequently membrane stability and rigidity (Bouarab et al., 2014).

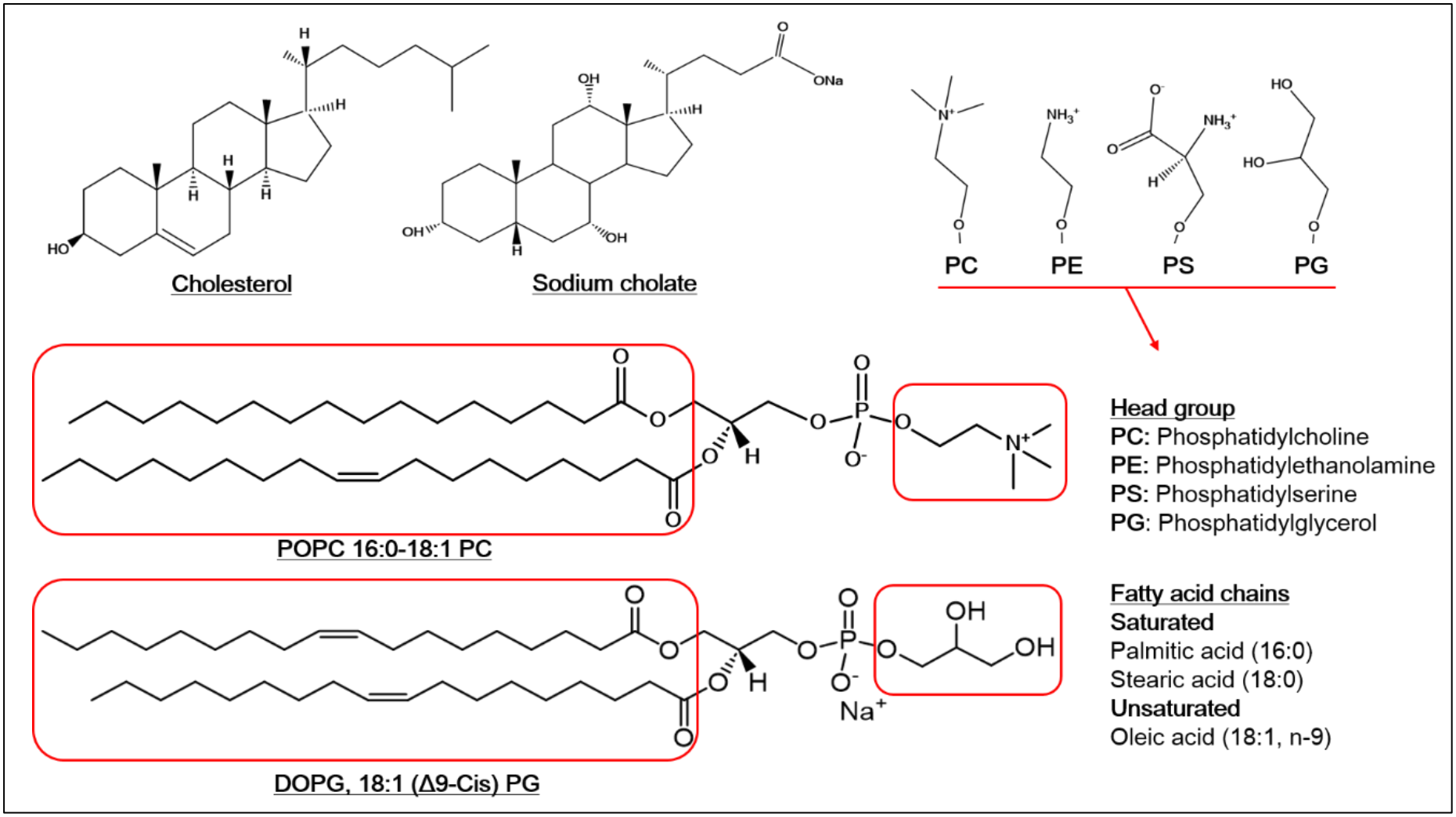

Figure 1.2 Structure of, cholesterol (Chol), sodium cholate (NaC), 1-palmitoyl-2-oleoyl-sn-glycero-3-phosphocholine (POPC, 16:0–18:1), and 1,2-dioleoyl-sn-glycero-3-phospho-(1'-rac-glycerol)(sodium salt) (DOPG, 18:1(Δ9-cis)).

The effect of NaC and sodium taurocholate (NaTC) on the membrane integrity of liposomes which were produced using lipids with a low T_m (PC and DMPC) and lipids with a high T_m (DPPC), DSPC, and sphingomyelin) was studied. Bile salts were shown to be less destructive to liposomes consisting of lipids with high T_m (Kokkona et al., 2000).

Chol **(Fig 1.2)** is the most known sterol and has a significant effect on the membrane properties of liposomes by enhancing the rigidity and hydrophobicity of vesicles. The effect of types of phospholipid (POPC, DPPC, and Lipoid H100) and sterol (Chol and β-sitosterol) on liposome structure was reported by Jovanović et al. Results showed that when each sterol was added into the bilayer of DPPC below T_m, 1,6 diphenyl-1,3,5-hexatriene (DPH) polarization decreased compared to the DPPC bilayer without sterol. Above T_m, DPH polarization values were higher than DPPC bilayer without sterol. Hence bilayer of DPPC was more ordered above T_m (Jovanović et al., 2018). When sterols are added to the liquid phase of the bilayer, they further order the bilayer, while their incorporation into the gel phase results in a disordered bilayer (Silva et al., 2011).

1.4.3.2 Bile salts

Recently there has been an interest in the incorporation of exogenous bile salts into the liposome bilayer to reach desired properties of lipid bilayers. Bile salts **(Fig 1.2)** are potential bio-surfactants formed from conjugated bile acids that form complexes with sodium. Primary bile acids (cholic acid (CA) and chenodeoxycholic acid (CDCA) are synthesized from Chol in the liver. These primary bile acids are conjugated to either taurine or glycine at the C-24 carboxyl group to increase their hydrophilicity.

Intestinal bacteria convert primary bile acids to a secondary form ((deoxycholic acid (DCA) and lithocholic acid (LCA)) (Ridlon et al., 2016). Bile salts such as NaC, NaTC, and sodium deoxycholate (NaDC) are characteristic amphipathic molecules that contain a steroid nucleus **(Fig 1.3).** The presence of hydroxyl groups provides hydrophilic properties to the concave side of the molecule, whereas the convex side is hydrophobic due to methyl groups. Because of their steroid skeleton, bile salts have a rigid structure that is very different compared to head-tail surfactants (Pabois et al., 2019). Due to their amphiphilic nature, bile salts form primary (aggregation number 2-10) or secondary (aggregation number 10-100) micelles in aqueous solutions above the critical micelle concentration (CMC) (Moghimipour et al., 2015). Their CMC value is also not well defined, so it is given as a range. They have smaller aggregation numbers which are 4-6 molecules for NaC and 7-12 molecules for NaDC (Garidel et al., 2007).

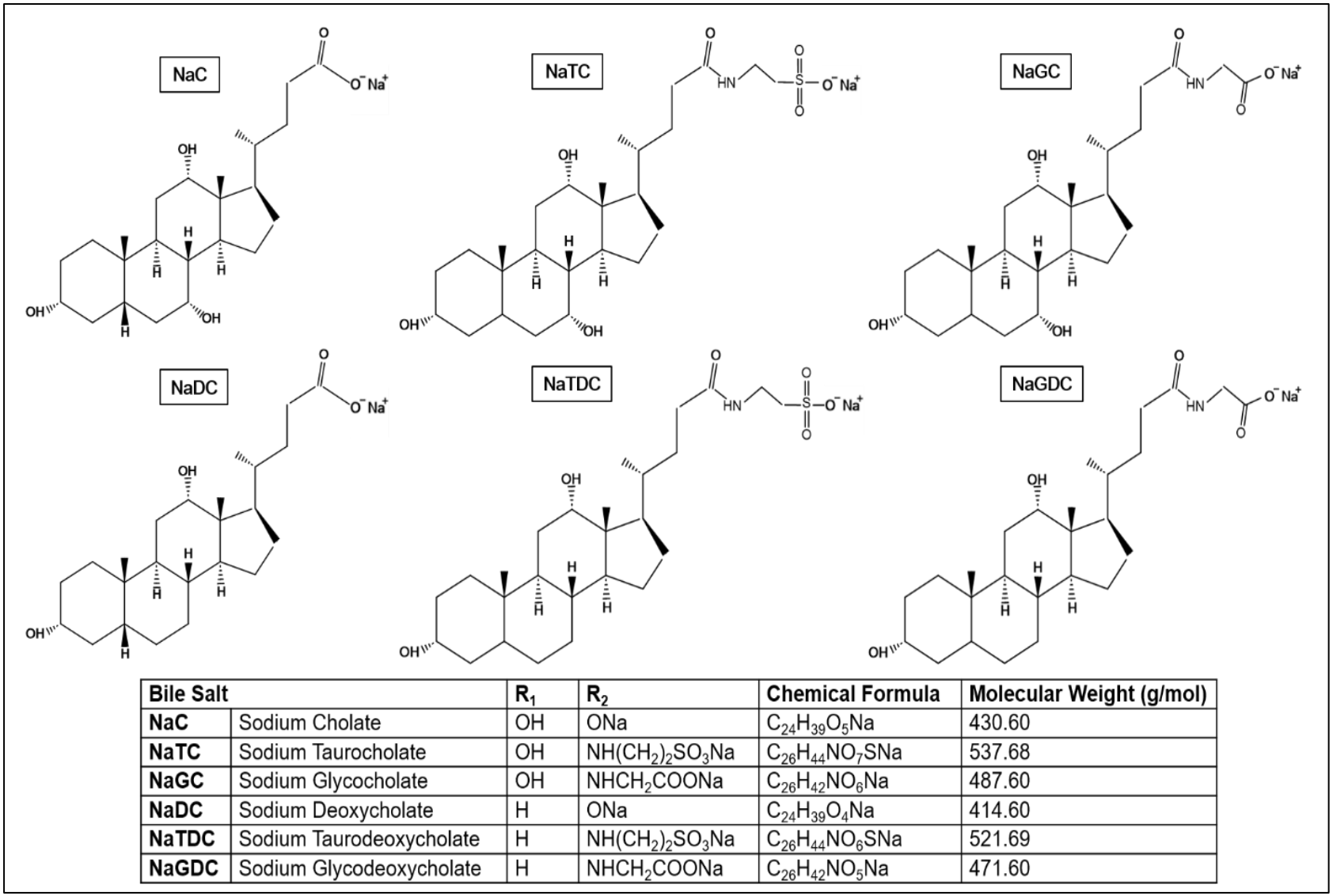

Bile Salt		R_1	R_2	Chemical Formula	Molecular Weight (g/mol)
NaC	Sodium Cholate	OH	ONa	$C_{24}H_{39}O_5Na$	430.60
NaTC	Sodium Taurocholate	OH	$NH(CH_2)_2SO_3Na$	$C_{26}H_{44}NO_7SNa$	537.68
NaGC	Sodium Glycocholate	OH	$NHCH_2COONa$	$C_{26}H_{42}NO_6Na$	487.60
NaDC	Sodium Deoxycholate	H	ONa	$C_{24}H_{39}O_4Na$	414.60
NaTDC	Sodium Taurodeoxycholate	H	$NH(CH_2)_2SO_3Na$	$C_{26}H_{44}NO_6SNa$	521.69
NaGDC	Sodium Glycodeoxycholate	H	$NHCH_2COONa$	$C_{26}H_{42}NO_5Na$	471.60

Figure 1.3 Chemical structure of bile salts. Adapted from (Aburahma, 2016).

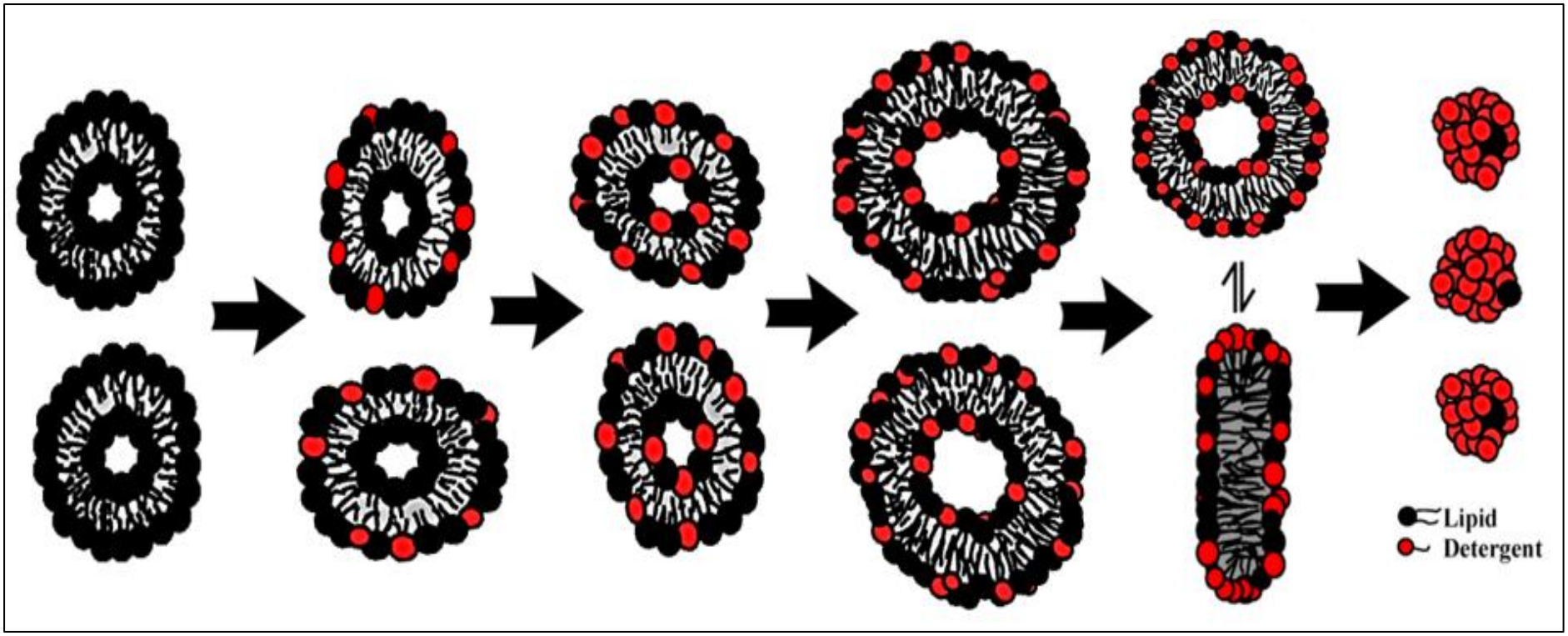

Figure 1.4 A schematic representation of the transition from phospholipid vesicles to mixed micelles caused by the membranolytic effect of bile salts on phospholipid bilayers. Below CMC, bile salts first locate the outer layer of the phospholipid bilayer, and then bile salts transport to the inner layer of the bilayer. When the bile salt concentration reaches the saturation phase boundary, the phospholipid bilayer cannot incorporate more bile salt molecules. Therefore, bilayer transforms into coexisting mixed vesicles and mixed micelles. Further increased bile salts concentration, the solubilisation phase boundary is reached, and bile salts-rich mixed micelles are formed. Adapted from (Garidel et al., 2007).

Bile salts solubilize the vesicles into mixed micelles due to its powerful solubilisation potential against phospholipid bilayers. show powerful solubilisation potential against phospholipid bilayers (Wüstner et al., 2000). The solubilisation effect of bile salts on the phospholipid bilayer is represented in **Fig 1.4**. Bile salts are incorporated into the outer layer of the phospholipid bilayer below their CMC and upon further increase of bile salts concentration, bile salts transport to the inner leaflet of the bilayer. When the total bile salts concentration reaches the saturation phase boundary, the system transforms into coexisting micelles and vesicles. Upon further increase of bile salts concentration, the solubilisation phase boundary is reached, and bile salts-rich mixed micelles are formed. During solubilisation, all steps have aggregates with bile salts monomers (Garidel et al., 2007). The incorporation of bile salts leads to the curvature of phospholipid bilayers, creating various lipid structures such as ellipsoid shapes, rod-like formations, smaller vesicles, and micelles, depending on the concentration of bile salts. These structures may exhibit different LCs due to their physicochemical properties, resulting in varying bioaccessible concentrations (Lichtenberg et al., 2013; McClements, 2013). Furthermore, bile salts can enhance the elasticity of the bilayer and promote penetration, thereby facilitating the absorption and availability of bilosomes(Aburahma, 2016; Hu et al., 2013; Tang et al., 2021).

Bile salts-containing lipid bilayers was generally reported as bilosomes (Waglewska et al., 2020; H. Yang et al., 2019), transfersomes (Arora et al., 2020; Hosny et al., 2020), and ultra-deformable or elastic liposomes (Barone et al., 2020; Z. Wu et al., 2019). Bilosomes **(Fig 1.5)** are designed based on the structure of liposomes which can encapsulate both hydrophilic and hydrophobic bioactive compounds (Van Tran et al., 2019). They have a promising potential to enhance the bioavailability of poorly soluble drugs like hydrophobic phenolic compounds. Bile salts interact with phospholipid membranes differently. A considerable amount of literature has been published on bile salts-containing LSAS **(Table 1.1).**

Table 1.1 Bile salts containing self-assembled system for delivery of phytochemicals.

Self-assembled System	Application	Active Compound	Biological Activity	Bile Salts	Composition	Reference
Liposomes	Topical application	Ammonium glycyrrhizinate	Anti-inflammatory Activity	NaC	SPC: 88mg, NaC:12 mg in 6 mL water/EtOH, Ammonium glycyrrhizate: 0.3% mass concentration (w/v) of the drug in the lipid	(Barone et al., 2020)
Liposomes	Oral application	Doxorubicin and Silybin	Cardio protective activity	CA	PC: 40 mg/mL, DSPE-poly (ethylene glycol) (PEG)- Cholic acid: 3 mg/mL, Chol: 8 mg/mL, Silybin:5 mg/mL, Doxorubicin: 1 mg/mL	(Li et al., 2019)
Liposomes	Oral application	Biflavonoids extract from *Selaginella doederleinii*	Anti-tumour Activity	NaDC	Optimum: SPC: 30 mg/mL, Chol: 3 mg/mL, NaDC: 3 mg/mL, Extract: 3 mg/mL, Isomaltooligosaccharide/ lipid, 2:1, w/w)	(Chen et al., 2019)
Liposomes	Oral application	[6]-gingerol	Anti-tumour Activity	NaC	Optimum: PC: 75 mg, Isopropyl myristate: 0.08 mg, NaC: 0.04 mg, [6]-gingerol: 5 mg	(Wang et al., 2018)
Liposomes	Oral application	Notoginsenoside R1	-	sodium glycocholate (NaGC)	Optimum: SPC: 50 mg, Chol: 10 mg, DSPE-PEG2000: 10 mg, NaGC: 6 mg, Notoginsenoside R1: 8 mg	(Fan et al., 2018)

Liposomes	Topical application	Pogostone	-	NaC	SPC, NaC, Chol, Vitamin E, Pogostone: 0.07%	(Z. Wu et al., 2019)
Transfersomes	Oral application	Genistein	Antioxidant and Neuroprotective Activity	NaDC	PC: 693 mg, NaDC: 297 mg, Genistein: 10 mg in 50 mL water	(Langasco et al., 2019)
Transfersomes	-	Resveratrol	Antioxidant activity	NaC	Optimum: SPC: 90.7 mg, NaC: 12.5 mg, Resveratrol: 100 mg in 5 mL phosphate-buffered saline (PBS) buffer (pH 7.4)	(Arora et al., 2020)
Transfersomes	Topical application	Phenylethyl resorcinol	Anti-tyrosinase activity	NaDC	SPC: 3% (w/v), Chol: 0.5% (w/v), phenylethyl resorcinol: 0.5% (w/v), NaDC: 15% (w/w) in water: up to 100% volume concentration (v/v)	(Amnuaikit et al., 2018)
Transfersomes	Oral application	Sodium pravastatin and Naringenin	Anti-hyperlipidemic and Antioxidant Activity	NaDC	Desirability values of the numerical optimization: Omega-3 PC: 0.7908 NaDC: 1, Naringenin: 1	(Hosny et al., 2020)
Bilosomes	-	Tripterine	Anti-arthritic Activity	NaDC	SPC: 80 mg, DOTAP: 20 mg, NaDC: 2 mg/mL, Tripterine: 10 mg, Hyaluronic acid: 10 mg in water: 10 mL	(H. Yang et al., 2019)

Bilosomes	Oral application	Sulphated polysaccharide-protein complexes of *Enteromorpha intestinalis*	Anti-cancer activity	NaC, NaDC and sodium taurodeoxycholate (NaTDC)	Chol/ Span 65: 1:5 molar ratio, Active compounds: 10 mg, NaC: 0.5 M in 10 mL saline solution (0.9% w/v sodium chloride (NaCl))	(Matloub et al., 2018)
Surface-modified bilosomes	Intravenous and topical Application	Methylene blue and Curcumin	Anticancer Activity	NaC	Optimum: L-α-PC: 1.00 mass fraction (wt) %, Chol: 0.30 wt%, Pluronic P123: 0.60 wt%, NaC: 0.50 wt% in water: 97.60 wt%	(Waglewska et al., 2020)
Hexosomes	Topical application	Catechin	Antioxidant activity	NaC, NaGC and NaTC	Optimum: GMO: 3.0 wt%, Oleic acid: 0.5 wt%, NaTC: 0.3 wt%, Pluronic F108: 0.3 wt% in water: 5.9 wt%	(Fornasier et al., 2021)
Ethosomes	Transdermal application	Doxorubicin and Curcumin	Cytotoxic and Chemo sensitizing Activity	NaC	Lecithin: 100 mg, Chol: 10 mg, polyethylenimine (PEI) or SC: 5 mg in 10 ml of water/ethanol	(Ma et al., 2019)
NLCs	Oral application	Gypenosides	-	NaGC	Oleoyl macrogolglycerides, glyceryl monolinoleate, glycerol monostearate, SPC, Gypenosides, NaGC, Polysorbate 80	(G. Yang et al., 2019)

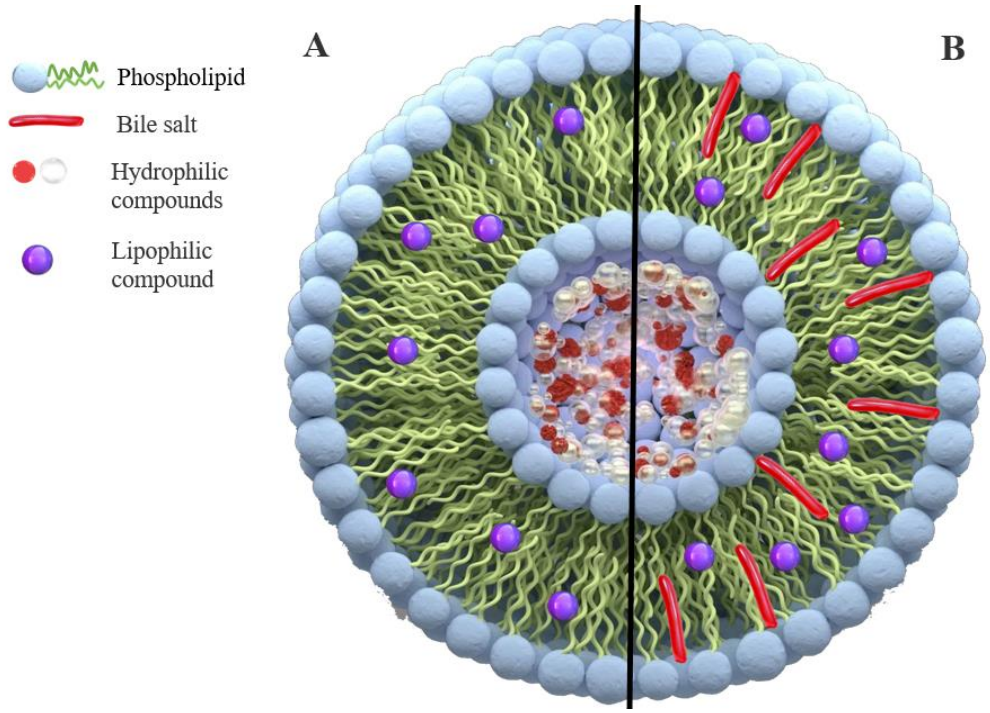

Figure 1.5 Schematic representation of hydrophilic and lipophilic compounds loaded (A) liposome and (B) bilosomes (Can et al., 2021).

1.4.4 The effect of bile salts on lipid self-assembled systems

1.4.4.1 The effect of bile salts on the morphology of lipid self-assembled systems

NaDC-transfersomes were designed and optimized using response surface methodology to encapsulate sodium pravastatin and naringenin (Hosny et al., 2020). The independent variables chosen were the concentration of omega-3 phospholipid, NaDC, and naringenin. The dependent variables assessed included D_H, EE, cumulative percentage of drug permeated, levels of alanine aminotransferase (AAT) (IU/L), and levels of malondialdehyde (MDA) (mmol/mg protein). The reported influence of the independent variables was as follows: omega-3-phospholipid>NaDC>naringenin. Optimization results showed that increasing NaDC concentration significantly reduced the D_H of transfersomes (D_H: 86-249 nm) ($p<0.0001$).

76% of sodium pravastatin and naringenin were loaded in NaDC-transfersomes (D_H: 191 nm) for the optimum composition (desirability values: omega-3 PC (0.7908), NaDC (1), naringenin (1)). In the same way, the concentration of bile salts and D_H showed a contrary trend for resveratrol-loaded NaC-transfersomes (Arora et al., 2020) and notoginsenoside R_1-loaded NaGC-liposomes (Fan et al., 2018).

Resveratrol loaded-NaC-transfersomes were optimized using a face-centred central composite design. The amount of SPC and NaC were chosen as independent variables and their effect on D_H and EE (%) were chosen to optimise NaC-transfersomes. The D_H and PDI of the optimized formulation were 178.9±12.87 nm and 0.132, respectively. Their shape was found to be nearly spherical and uniform by transmission electron microscopy (TEM). According to the results, once NaC concentration was increased, the D_H of transfersomes decreased (Arora et al., 2020).

Notoginsenoside R_1-loaded NaGC-liposomes were prepared, and the D_H of NaGC-liposomes (200 nm) was smaller than conventional liposomes and when the concentration of NaGC increased, D_H and EE (%) decreased (Fan et al., 2018). These findings indicate that the concentration of bile salts in the formulations plays a significant role in the D_H of lipid bilayers(Aburahma, 2016; Arora et al., 2020).

Biflavonoid extract from *Selaginella doederleinii* was encapsulated using liposomes and bilosomes (Chen et al., 2019). The SPC/biflavonoid extract ratios (15:1, 10:1 and, 5:1 w/w) and SPC/NaDC ratios (15:1, 10:1, and 5:1 w/w) were chosen for optimization to see the effect on EE (%). The SPC/biflavonoid extract ratios showed the lowest effect among the four variables and a 10:1 w/w ratio was chosen for optimum formulation. The SPC/NaDC ratio had the second-highest effect among the four variables. Optimized bilosomes (SPC/NaDC, 10:1 w/w) had a D_H of 249.77±15.68 nm, ζ potential of −21.89±1.51 mV, and a PDI of 0.184±0.002. 91.39±0.88% of the extract was encapsulated in the optimized liposomes.

Comparable results were also reported by Yang et al. who studied tripterine-loaded hyaluronic acid-coated NaDC-bilosomes. Effects of concentration of NaDC (1, 2, and 3 mg/mL), on the D_H and EE (%) of bilosomes, were evaluated. With increased NaDC concentration from 1 mg/mL to 2 mg/mL, D_H decreased from ~140 nm to ~90 nm. However, when NaDC concentration was increased to 3 mg/mL, the D_H of bilosomes increased to ~110 nm (H. Yang et al., 2019). A possible explanation for these results is up to a specific concentration of bile salts reduces the surface tension that induces membrane curvature and stabilizes the system and leads to decreased D_H. Further increase in BS concentration and an increase in the D_H may be related to aggregation in the system and increased medium viscosity (Madsen & Herlo, 2017; Waglewska et al., 2020; H. Yang et al., 2019). The 2 mg/mL NaDC in the bilosome formulation had the lowest D_H (~90 nm) and the highest EE (%). For the hyaluronic acid coating particles, 2 mg/mL of NaDC was chosen and the D_H was 95.3 nm and 118.4 nm for the bilosomes and hyaluronic acid-coated bilosomes, respectively.

Ammonium glycyrrhizate-loaded liposomes composed of SPC and NaC prepared by Barone et al. Loading of ammonium glycyrrhizate did not affect the D_H, PDI, ζ potential,

and deformability index (DI) of vesicles significantly. D_H increased from 109±3.8 to 128±4.6 nm and the ζ potential decreased from -17±0.5 to −22±0.6 mV. The decrease in the ζ potential mainly results from the presence of NaC in the formulation. The self-assembled system with ζ potential values more than ±30 mV shows moderate stability. As the ζ potential comes close to zero, the system loses its stability, and agglomeration and precipitation are seen (Riddick, 1968).

Surface-modified bilosomes were prepared and triblock copolymer Pluronic P123 was used to stabilise the surface (Waglewska et al., 2020). Three different concentrations of NaC were added into formulations (0.25, 0.50, and 1.00 wt %). The effect of the presence of NaC in the bilosome formulation was similar to those shown by (Barone et al., 2020). The negative ζ potential of the formulation results from the negative charge of NaC (Holm et al., 2014).

Sulphated polysaccharide-protein complexes of *Enteromorpha intestinalis*-loaded bilosomes were prepared using three different bile salts (NaC, NaDC, NaTDC) and two different surfactants including Span 40 (hydrophilic-lipophilic balance (HLB): 6.7 (Foo et al., 2020) and Span 65 (HLB: 2.1) (Thakare et al., 2017). Span 40-bilosomes had more than double the D_H compared to span 65-bilosomes for all bile salt formulations. The lower D_H of Span 60-bilosomes resulted from the lower HLB value of span 65. Low HLB results in a decrease in the surface free energy and shows increased lipophilic affinity that leads to smaller vesicles (Yoshioka et al., 1994). Higher HLB values lead to water uptake into the vesicles and cause increased vesicle size due to hydrophilicity (Al-Mahallawi et al., 2015).

Bile salts had a significant effect on the D_H of bilosomes. The D_H of bilosomes were reported as NaTDC-bilosomes (Span 40: 1982±24.74 nm, Span 65: 740.56±5.52 nm)>NaDC-bilosomes (Span 40: 870.65±2.33 nm, Span 65: 305±0.14 nm)>NaC-bilosomes (Span 40: 350.1±19.73 nm, Span 65: 181.1±16.80 nm). The ζ potential of all bilosomes was around -1 mV and EE (%) ranged from 69.66% to 71.60% ($p>0.05$). Span 65/NaC-bilosomes had the highest EE (%) (71.60±0.25%) with D_H: 181±16.80 nm (Matloub et al., 2018). In phenylethyl resorcinol-loaded transfersomes, NaDC (HLB: 16), Tween 80 (HLB: 15), Tween 20 (HLB: 16.7), Span 80 (HLB: 4.3), Span 20 (HLB: 8.6) were used as skin enhancers in the formulation (Amnuaikit et al., 2018). In contrast to previous work (Matloub et al., 2018), the D_H of NaDC-transfersomes was 353.70±10.90 nm, and the PDI, ζ potential, and EE (%) of NaDC-transfersomes were 0.111±0.038, −41.86±0.73, and 92.49±0.01, respectively. TEM and scanning electron microscopy (SEM) analysis also revealed that NaDC-transfersomes had a unilamellar to multilamellar structure with a smooth surface (Amnuaikit et al., 2018).

Catechin-loaded hexosomes for topical application have been prepared using NaC, NaDC, and NaTC in the formulations and the D_H of hexosomes was 148 nm without bile salts but the D_H decreased to 107–110 nm after 0.6 wt% BS addition (Fornasier et al., 2021). SAXS measurements showed that after the addition of 0.02 wt% of bile salts in the formulation an inverse bicontinuous cubic phase completely transitioned to unilamellar vesicles (ULVs). The phase transition could have been caused by the amphiphilic structure of bile salts that are in contact with the bulk water thus decreasing the negative interfacial curvature of the system (Fornasier et al., 2021).

Surfactant concentration (NaGC and polysorbate 80) was chosen as one of the independent variables for the optimization of gypenosides loaded-NLCs (G. Yang et al., 2019). While the surfactant concentration did not show a significant effect on D_H and LC (%), it had a significant effect on EE (%). The EE (%) increased with increased surfactant concentration and the D_H, PDI, and ζ potential of the optimized NLCs formulation were reported as 146.7±6.8 nm, 0.137±0.011, and −56.0±3.4 mV respectively with 74.22% in EE (%) and 4.89% in LC (%).

D_H of self-assembled systems is a considerable parameter in the delivery of active compounds and, consequently, their passage through a biological membrane. According to the results, a decrease in D_H is correlated to an increase in bile salts up to a specific concentration. Bile salts stabilize the vesicles by reducing the interfacial tension of the vesicles. Further increased bile salts concentration, bile salts begin to show a disruption effect on the self-assembled system.

1.4.4.2 The effect of bile salts on encapsulation efficiency, release, and stability of lipid self-assembled systems

The EE of LSAS varies depending on the stability of the dispersion and the methods and parameters chosen for vesicle loading. The general stability of LSAS comprises the stability of active material and the retention capacity of the membranes. Membrane stability that provides integrity to the system has a direct effect on EE (Uchegbu & Florence, 1995).

NaDC-liposomes and hyaluronic acid-coated NaDC-bilosomes were prepared to encapsulate tripterine (H. Yang et al., 2019). Both formulations showed a narrow PDI and the ζ potential decreased from 4.8 mV to -34.2 mV due to the use of the negatively charged polysaccharide coating. EE (%) and LC (%) were 99.56% and 8.15% respectively. Doxorubicin-silybin-loaded liposomes prepared using CA to improve the oral treatment of actives (Li et al., 2019). The D_H of CA-liposomes was 97.03±2.17 nm with a narrow PDI and both active compounds had an EE (%) of approximately 95%. *In vitro* release of doxorubicin-silybin-loaded CA-liposomes was investigated in PBS buffers (pH 2 and 7.4) to mimic the SGF and SIF conditions. While ~25% of silybin

was released from liposomes at pH 2, ~50% of silybin was released at pH 7.4 in 12 hours (h). In addition, the stability was determined in rat gastric fluid, rat intestinal fluid, and serum. After 12 h incubation, the EE (%) of all liposomes in different steps was still more than 80%. It shows that CA-liposomes protect their integrity during different steps of digestion. However, some active material leakage problems were also reported because of the presence of a high concentration of bile salts. When the effect of NaC concentration on EE (%) of resveratrol-loaded transfersomes was studied, high (EE (%) was seen at intermediate NaC levels and a decrease in EE (%) was seen as NaC was increased. Higher NaC amounts also can cause leakage of active material because of the formation of lipid pores in the membrane. The ζ potential of the optimized formulation was reported as -23.2±1.4 mV (Arora et al., 2020).

EE (%) of the self-assembled system mainly depends on lipid concentration in the formulation. EE (%) increases with increased lipid concentration which enhances lipophilicity and increases the D_H of particles so a higher amount of drug can be loaded (Boseila et al., 2019). Although EE (%) depends on lipid concentration, the addition of bile salts below CMC into the formulation can also enhance EE (%). The flexibility of vesicles increases with the presence of bile salts and the bilayer, and the aqueous core can be flexed to encapsulate the drug more (Ahad et al., 2018). Bile salts above CMC show the solubilisation effect on vesicles so vesicles transit to micelles and increase the drug solubility consequently decreasing EE (%). In addition, drug leakage can be seen because of opened lipid membrane pores (Mahmood et al., 2014).

In vitro release studies are important to give a prediction about the *in vivo* release profile (Nkanga et al., 2019). *In vitro* dissolution profiles of NLCs and NaGC-NLCs were compared with gypenosides powders. The cumulative dissolution of gypenosides powders (29.4%) was slightly higher than both NLCs in 6 h. Although NaGC-NLCs showed slightly higher release, the release of NLCs and NaGC-NLCs was not significantly different after 48 h. While ~55% of gypenosides was released from both NLCs at 48 h, the cumulative dissolution of gypenosides powders did not change significantly after 6 h. The most probable cause of slow release from NLCs is due to lipid layers slowing the diffusion of the active compounds (G. Yang et al., 2019). Sulphated polysaccharide-protein complexes of *Enteromorpha intestinalis*-loaded bilosomes were prepared using three different bile salts (NaC, NaDC, NaTDC) and two different surfactants (Span 40 (HLB: 6.7) and Span 65 (HLB: 2.1)). Span 65-NaC-bilosomes and Span 40-NaC-bilosomes released ~70% and ~40% of active compounds respectively, while other formulations prepared with NaDC or NaTDC released less than ~20% in PBS (pH 6.8) at 37°C in 24 h (Matloub et al., 2018). It was reported that while ~50% of [6]-gingerol was released, using NaC-liposomes significantly increase the cumulative release of [6]-gingerol (~90% in 24 h) ($p<0.01$)

(Wang et al., 2018). *In vitro* release from bilosomes and hyaluronic acid-coated bilosomes were investigated (H. Yang et al., 2019). Bilosomes released only 40.51% of tripterine in PBS (pH 7.4) in 24 h, which may be due to the hydrophobic nature of tripterine. The hyaluronic acid coating also slowed the release of actives from bilosomes; 11.35% and 23.24% of tripterine were released at 8 h and 24 h, respectively. The release of active compounds can be controlled by loading the active into the system that acts as a barrier. Also, these barriers can be modified using coatings which provide additional layers to slow down the release. The presence of bile salts in the self-assembled formulation enhances the physical stability of the system and thus can slow the release (Zhang et al., 2016).

The physical and chemical stability is important to protect the structure of LSAS from the harsh conditions of the GIT, to keep the structure in circulation longer, and to provide long-term shelf-life (Hashemzadeh et al., 2020). Several factors such as lipid type, PDI, and ζ potential of the system, etc. are known to affect the stability of LSAS. Bile salts are only one of many factors that can affect and enhance stability. Phenylethyl resorcinol-loaded NaDC-transfersomes were stored at different temperatures for 4 months (Relative humidity (RH): 75%). At 4±1°C and 30±1°C, NaDC-transfersomes were stable for 4 months. While the D_H (~400 nm) and EE (%) (~90%) were quite stable, an increase in ζ potential was seen from ~-70 mV to ~-40 mV. At 45±1°C, NaDC-transfersomes could retain their stability for 2 months. As it was at 4±1°C and 30±1°C, ζ potential increased, and D_H (~400 nm) did not change significantly. ~10% decline was seen in EE (%) (Amnuaikit et al., 2018). The presence of NaGC in NLCs was evaluated in terms of the D_H and EE (%) (G. Yang et al., 2019). The accelerated stability of NLCs and NaGC-NLCs was monitored and both NLCs showed stable structures. The D_H and EE (%) of NLCs did not change significantly during storage at 40±2°C, RH: 75±5% for 6 months. Likewise, methylene blue and curcumin-loaded NaC-bilosomes showed minimum changes during storage at 4ºC for 28 days. The D_H and PDI of the formulations were reported as ~100 nm and < 0.25.EE ((%) were 85% and 70% for methylene blue and curcumin, respectively (Waglewska et al., 2020). The physical stability of ammonium glycyrrhizate-loaded NaC-liposomes (EE: 57.3±3.7%) was determined at 25°C and 37°C for 4 weeks. According to delta backscattering and delta transmittance profiles, variations were measured below ±5% showing a long-term stable structure. During 4 weeks of storage, while the D_H of vesicles did not change significantly at 25°C, a significant increase was observed at 37°C after 2 weeks. An increase in the D_H can be related to the gel-to-fluid lamellar phase transition at 37°C (Barone et al., 2020). However, stability problems during storage were also reported. The effect of different bile salts on the stability of hexosomes was evaluated. NaC and NaDC-hexosomes (0.2-0.5 wt %) were

destabilised after ~2 weeks. While NaTC-hexosomes remained stable for 2 months for NaTC concentrations of 0.2-0.5 wt%, hexosomes outside this range lost their stability after a few weeks (Fornasier et al., 2021).

PDI and ζ potential of the self-assembled system are important parameters that reflect the homogeneity (PDI<0.3) of population and stability (more than ±30 mV) of particles, respectively. Aggregation, flocculation, or precipitation problems can be seen during storage with the decrease of ζ potential below ±30 mV (Danaei et al., 2018). The net surface charge of particles comes from the combination of lipids, active compounds, and other compounds that are used to modify the structure. The addition of bile salts into the self-assembled system decreases ζ potential which results in increased repulsion between particles. A decrease in ζ potential of the system is correlated to an increased bile salts concentration due to the negative charge of bile salts.

1.4.4.3 The effect of bile salts on the bioavailability of lipid self-assembled systems

The biological fate of the self-assembled system that aims to enhance the bioavailability of active compounds differs depending on their administration. While digestion is one of the main steps for the oral delivery of active materials, skin penetration is taken into consideration for the topical application of active materials. zeta Much research is already being undertaken about LSAS for further exploiting the biological activities of phytochemicals.

Gypenosides are triterpenoid saponins from *Gynostemma pentaphyllum*. Gypenosides have been used for medical purposes for many years however they are sensitive to the environment and suffer low solubility both in lipid and water (G. Yang et al., 2019). In a study designed to assess the delivery of gypenosides for oral application. The time to peak plasma concentration (T_{max}), maximum plasma concentration (C_{max}), the area under the plasma concentration ($AUC_{0-\infty}$), and mean retention time ($MRT_{0-\infty}$) were investigated in rats after oral administration of gypenosides powders, NLCs, and NaGC-NLCs. Loading of gypenosides into NLCs prolonged the absorption time from 0.79±0.10 h to 1.42±0.28 h and retention time from 6.22±0.34 h to 11.83±1.41 h ($p<0.05$). The C_{max} of NLCs (0.671±0.073 mg/mL.h) also increased ~1.5-fold compared to the powder, so it shows that NLCs remained longer in circulation. The addition of NaGC in the NLCs formulation increases the T_{max} and $MRT_{0-\infty}$ significantly ($p<0.05$). The plasma concentration of gypenosides increased compared to gypenosides powders and NLCs ~1.9-fold and 1.3-fold, respectively. Intestinal absorption of NLCs and NaGC-NLCs was also compared with the gypenosides powder. The apparent absorption coefficient (P_{app}) of NLCs showed increased permeability and bioavailability compared to gypenosides powder ($p<0.05$)

in all sections of the intestine. The presence of NaGC in NLCs increased the P_{app} 5.11-fold compared to gypenosides powder and ~2-fold compared to NLCs in the jejunum ($p<0.05$). In addition, Caco-2 cell viability was increased from ~70% to ~90% at 100 µg/mL gypenosides due to loading the gypenosides into NaGC-NLCs that reduced the cytotoxicity of gypenosides (G. Yang et al., 2019).

The delivery of tripterin isolated from *Tripterygium wilfordii* was investigated (H. Yang et al., 2019). Tripterin also known as celastrol shows antioxidant, anti-angiogenic, and anti-rheumatic effects. However, it is poorly soluble in water and consequently shows low solubility in biological fluids (Ng et al., 2019). Cellular uptake of free tripterine, bilosomes, and hyaluronic acid-coated bilosomes in RAW264.7 cells was compared. Loading tripterine into bilosomes doubled its cellular uptake from ~75 ng/mg protein to ~150 ng/mg protein ($p<0.01$). Compared to uncoated bilosomes, hyaluronic acid enhanced the internalization of bilosomes and provided higher cellular uptake (~275 ng/mg protein) ($p<0.01$). This enhanced internalization ability was further confirmed by confocal laser scanning microscopy. Bioavailability and biodistribution results of free tripterine, bilosomes, and hyaluronic acid-coated bilosomes showed that C_{max} and $AUC_{0-\infty}$ of hyaluronic acid-coated bilosomes significantly different from free tripterine and bilosomes. The C_{max} and $AUC_{0-\infty}$ of bilosomes (23.57±0.49 µg/mL and 76.19±1.13 µg/mL.h) and coated bilosomes (25.24±0.57 µg/mL and 112.19±0.85 µg/mL.h) were higher than the C_{max} of free tripterine (22.62±0.71 µg/mL and 35.86±0.53 µg/mL.h). In addition, the elimination time of the drug decreased from 0.279±0.086 L/h to 0.131±0.054 L/h (bilosomes) and 0.089±0.063 L/h (coated bilosomes). Encapsulation improved the resistance of tripterinein in circulation. The relative bioavailability of tripterine in bilosomes and coated bilosomes were 480.3% and 799.9% respectively, compared to free tripterine (H. Yang et al., 2019).

Notoginsenoside R_1 derived from *Panax notoginseng* poorly dissolves in water and cannot exhibit its biological functions sufficiently (Liang & Hua, 2005). For the oral application of notoginsenoside R_1, *in vitro* cellular uptake in Caco-2 cells and intestinal absorption of notoginsenoside R_1-loaded NaGC-liposomes and liposomes were compared. NaGC-liposomes showed 1.5-fold higher cellular uptake compared to liposomes ($p<0.01$) so the presence of NaGC enhanced the cellular uptake of notoginsenoside R1. Intestine absorption of notoginsenoside R_1 was reported as duodenum>jejunum>ileum>colon. Notoginsenoside R_1 accumulated more in the duodenum compared to other regions of the intestine. The P_{app} of notoginsenoside R_1 was NaGC-Liposomes> liposomes> notoginsenoside R_1 solution for the same drug concentration (20 µg/mL and 100 µg/mL) and in the same section of the intestine ($p<0.05$). The addition of NaGC increased P_{app} 1.85-fold (20 µg/mL notoginsenoside R_1) and 3.19-fold (100 µg/mL notoginsenoside R_1) compared to notoginsenoside R_1.

NaGC-liposomes enhanced the C_{max} (210.95±43.58 µg/L) and elimination half-time ($T_{1/2}$) (4.69±1.20 h) of notoginsenoside R_1 compared to liposomes (C_{max}: 113.97±35.84 µg/L and $T_{1/2}$:1.86±0.80 h). The presence of NaGC also improved AUC0-t 1.32-fold and 2.68-fold compared to liposomes and notoginsenoside R_1 solution (Fan et al., 2018). Loading into NaC-liposomes increased the relative bioavailability (16.4-fold) and $T_{1/2}$ of [6]-gingerol (~2.5-fold) which shows that [6]-gingerol can stay longer in circulation (Wang et al., 2018). Similarly, an *in vivo* pharmacokinetic study showed that while C_{max}, $AUC_{0-\infty}$ and $MRT_{0-\infty}$ of all biflavonoids were increased when biflavonoids loaded into NaDC-liposomes. Encapsulation did not show a significant difference in the $T_{1/2}$ of biflavonoids. A pharmacokinetic study showed that the relative bioavailability of biflavonoids in the extract was enhanced between 191%-995% due to loading into NaDC-liposomes. Moreover, the cytotoxicity of the biflavonoids extract-loaded liposomes was evaluated on HT-29 cells. Encapsulation into NaDC-liposomes reduced the half-maximal inhibitory concentration (IC_{50}) of the extract by 37% (Chen et al., 2019).

Ammonium glycyrrhizinate is isolated from *Glycirrhiza glabra* and is used for supplements and medical purposes. Ammonium glycyrrhizinate shows an anti-inflammatory effect against inflammation of the skin (Kubo et al., 2016). The applicability of the ammonium glycyrrhizate-loaded NaC-liposomes for topical application was investigated and at 24 h, only 40% of ammonium glycyrrhizate was released from vesicles and showed pseudo-first-order kinetics (Barone et al., 2020). Permeation and skin tolerability studies were done with the topical application of vesicles on humans. 134.9 µg/cm^2 ammonium glycyrrhizate penetrated through the stratum corneum and epidermis and permeation through the skin layers showed zero-order kinetics. For topical application, drugs need to pass through the stratum corneum and epidermis as well as protect their structure (Barone et al., 2020). Erythema index values were measured below 4.5 that shows ammonium glycyrrhizate-loaded NaC-liposomes can be tolerated by human skin without any toxicity. In order to determine the effect of NaC on the deformability of liposomes composed of DPPC, the deformability of liposomes and NaC-liposomes (DPPC/NaC 4:1) were compared using the vesicle-pore model where both liposomes are pushed to pass through narrow pores and deformability parameters are measured (Z. Wu et al., 2019). According to the results, NaC improves the flexibility of liposomes and decreases the deformability through pores.

Resveratrol is a well-known natural antioxidant (Huang et al., 2017). Spreadability, skin permeation, and deposition of resveratrol-loaded NaC-transfersomes cream were compared with a conventional resveratrol cream (Arora et al., 2020). The spreadability of the vesicular cream was 47.90±3.65% spread by weight (conventional resveratrol

cream: 39.14±1.59%). The permeation flux of the resveratrol-loaded NaC-transfersomes cream and conventional cream was determined as 4.95±0.69 and 2.70±0.73 μg/cm^2 respectively (at 24 h). When deposition in the skin layer was evaluated, drug deposition of NaC-transfersomes cream (335.2±4.12 μg/cm^2 with skin retention: 70.16±0.87%) was reported to be significantly higher than conventional cream (67.12±19.63 μg/cm^2 with skin retention: 14.05±4.11%). *In vitro* skin permeation and deposition of phenylethyl resorcinol-loaded NaDC-transfersomes were investigated. Compared to liposomes (skin permeation: 20.65 μg/cm^2, accumulation: 28.18 μg/cm^2), transfersomes (skin permeation: 72.66 μg/cm^2, accumulation: 71.21 μg/cm^2) provided higher permeation and accumulation of phenylethyl resorcinol in new-born pig skin ($p<0.05$) (Amnuaikit et al., 2018). According to the results, the enhanced permeation ability of the resveratrol-loaded NaC-transfersomes cream (Arora et al., 2020) and phenylethyl resorcinol-loaded NaDC-transfersomes (Amnuaikit et al., 2018) is possibly due to the presence of bile salts that can enhance the penetration (Moghimipour et al., 2015). Sodium pravastatin and naringenin-loaded NaDC-transfersomes were optimized and NaDC showed a significant impact on the cumulative % permeated (<0.0001). When NaDC concentration (20-60 mg) increased, cumulative (%) permeated increased from 37% to 59%. Results also showed that NaDC did not show a considerable effect on ALT level (p: 0.8767) and MDA (p: 0.4490) levels (Hosny et al., 2020). The deformability of phenylethyl resorcinol-loaded NaDC-transfersomes and liposomes were compared before and after filtering through a 200 nm polycarbonate filter (Amnuaikit et al., 2018). While transfersomes (D_H: 398.37±9.82 nm, PDI: 0.06±0.08) passed through the filter, liposomes (D_H: 600.23±11.92 nm, PDI: 0.21±0.07) could not pass because of their rigid structure. After filtration, the D_H, PDI, and DI of NaDC-transfersomes were 371.97±8.72 nm, 0.13±0.09, and 6.63% respectively. These results confirm that incorporating NaDC into the lipid bilayers enhances the flexibility of vesicles.

Catechin is a widely studied phenolic compound that shows mainly antioxidant activity. *In vitro* skin permeation performance of catechin-loaded NaTC-hexosomes was tested on the skin of new-born pigs and compared with catechin-loaded hexosomes and vesicles. Due to the presence of NaTC, NaTC-hexosomes showed better permeation through skin layers and higher drug accumulation in the skin layers including stratum corneum: ~14%, epidermis: ~7%, dermis: ~8%, and receptor compartment: ~9%. While liposomes showed max accumulation (~9%) in the dermis, no drug accumulation was detected in and receptor compartment. Hexosomes showed a max ~5% drug accumulation both in the stratum corneum and receptor compartment (Fornasier et al., 2021).

Loading of active compounds into the self-assembled system prolonged the absorption time and retention time compared to free active compounds. The addition of bile salts to the LSAS further increases the absorption time and retention time of the active compounds compared to the LSAS. Due to the presence of bile salts, the C_{max} and $AUC_{0-\infty}$ of circulating active compounds are increased, therefore improved relative bioavailability has been reported. In addition, bile salts increase the elasticity of particles and enhance the penetration and accumulation of active compounds (Ahad et al., 2018).

1.4.4.4 The effect of bile salts on the biological activity of lipid self-assembled systems

Phytochemicals show numerous biological activities such as antioxidant, anti-inflammatory, anti-tumour, anti-arthritic, anti-tyrosinase activity, etc. LSAS can provide increased solubility, enhanced diffusion properties, and stability to phytochemicals and promote these biological functions (Can et al., 2019). *In vivo* anti-tumour activity of biflavonoids extract-loaded liposomes was determined on HT-29 colon cancer cells. NaDC-liposomes almost doubled the antitumor activity of biflavonoid extracts ($p<0.001$) without systemic toxicity (Chen et al., 2019). In the same way, the anti-tumour activity of [6]-gingerol (100 µg/mL, 15% inhibition) on HepG2 cells was improved significantly due to loading into NaC-liposomes (inhibition rate: ~100%) ($p<0.01$) (Wang et al., 2018). In addition, *in vitro* anti-tumour effect of curcumin-loaded PEI-ethosomes and doxorubicin-loaded NaC-ethosomes (7:3 v/v) on B16 cells were determined. PEI-loaded NaC-ethosomes) and doxorubicin-loaded NaC-ethosomes showed similar inhibition (~55%) against B16 cells, PEI-ethosomes, and doxorubicin-loaded NaC-ethosomes (7:3 v/v) exerted stronger inhibition against B16 cells and cell survival was decreased to ~30% ($p<0.01$). Comparable results were also seen for *in vivo* antitumor effects. Melanoma tumour inhibition rates were 21.9%, 35.5%, and 46.38% for curcumin-loaded PEI, doxorubicin-loaded NaC-ethosomes and curcumin-loaded PEI, doxorubicin-loaded NaC-ethosomes (7:3 v/v) respectively ($p<0.01$) (Ma et al., 2019). Loading the phytochemicals in the bile salts system enhanced their anti-tumour activity significantly.

The anti-inflammatory activity of ammonium glycyrrhizate-loaded NaC-liposomes was investigated in human volunteers (Barone et al., 2020). Free compound and liposomes were applied topically on chemically (0.2% w/v) methyl nicotinate) stimulate erythema and NaC-liposomes showed ~10-30-fold increase in anti-inflammatory activity compared to an equivalent of ammonium glycyrrhizate solution.

Anti-arthritic activity of tripterine-loaded hyaluronic acid-coated NaDC-bilosomes on arthritic mice was studied (H. Yang et al., 2019). Mediators that show the inflammation

level was measured and coated and uncoated bilosomes were compared with the model control. While bilosomes reduced the concentration of mediators in serum approximately double times compared to model control, hyaluronic acid-coated bilosomes reduced mediators approximately fourfold compared to model control ($p<0.01$).

The anti-tyrosinase activity of phenylethyl resorcinol-loaded NaDC-transfersomes and liposomes was evaluated after topical application on pigskin. Kojic acid was chosen as a positive control. Liposomes (95.54 ±0.13%) and NaDC-transfersomes (91.09 ±1.23%) showed better anti-tyrosinase activity than kojic acid (87.35±0.76%). Accumulation of phenylethyl resorcinol from NaDC-transfersomes (80.47±0.22%) was nearly the same as liposomes (79.53±0.45%). Tyrosinase activity and melanin content in B16 melanoma cells were also measured after NaDC-transfersomes and liposome application. Compared to liposomes (tyrosinase activity: 71.27% and melanin content: 82.11%), NaDC-transfersomes decreased tyrosinase activity to 64.36% and melanin content to 64.85%. NaDC-transfersomes showed effective skin-lightening properties (Amnuaikit et al., 2018).

In vitro antioxidant activity of catechin-loaded NaTC-hexosomes was measured. Using the 1,1-diphenyl-2-picrylhydrazyl (DPPH) assay, NaTC-hexosomes, hexosomes, vesicles, and catechin in methanol solution could all inhibit 88% of DPPH radicals (Fornasier et al., 2021). Similarly, the antioxidant activity of a resveratrol solution (95%) and resveratrol-loaded NaC-transfersomes (~92%), were not significantly different ($p>0.05$). In addition, empty transfersomes also showed the ability to inhibit ~21% of 25 µM DPPH radical (Arora et al., 2020). The presence of bile salts in formulations and loading into bile salts systems did not show a significant effect on the antioxidant activity of catechin and resveratrol.

In general, the presence of bile salts in the LSAS increased the biological activity of the phytochemicals. Although increased permeation and accumulation of catechin and increased skin retention of resveratrol were reported due to loading into bile salts-LSAS, no significant changes were observed in the biological activities of resveratrol and catechin.

1.4.5 The surface modification of lipid self-assembled systems

The properties of LSAS also can be enhanced through surface modification using biopolymers such as CH (Bang et al., 2011), PGA (Lopes et al., 2017), alginate (Liu et al., 2013), etc. The surface modification with biopolymers can decrease the leakage of encapsulated compounds, control the circulation time and release properties of the particles (Refai et al., 2017), enhance the stability against environmental stress (Tai et al., 2020), decrease the lipid oxidation (Panya et al., 2010), provides additional

functionality such as mucoadhesion (Tahara et al., 2018), and permeation-enhancing effects (Sebaaly et al., 2021).

1.4.5.1 Chitosan

CH is a biodegradable, biocompatible cationic biopolymer, composed of β-(1,4) linked D-glucosamine (acid dissociation constant (pKa): ~6.5) and N-acetyl-D-glucosamine (uncharged) units **(Fig 1.6)** (Espinal-Ruiz et al., 2014; Tahara et al., 2018). It is widely used for coating liposomes due to the electrostatic interaction between the negatively charged phosphate group ($-PO_4^{3-}$) of phospholipids and the positively charged amine group ($-NH_3^+$) of CH (Henriksen et al., 1994).

The positively charged CH-coated liposomes can interact with negatively charged mucosa and due to the mucoadhesive properties of CH lipid bilayers can stay adherent to the intestinal epithelia. Since nanocarriers stay longer in the GIT, the elimination half-life is prolonged, consequently, intestinal absorption of encapsulated compounds can be enhanced (Hejazi & Amiji, 2003). CH coating can also open tight junctions of epithelial cells thus enhancing the bioavailability of the phenolic compounds (Chen et al., 2016). After CH coating, CH acts like a protective layer that reduces the chance of contact between the bilayer and pancreatic lipase, thereby effectively reducing damage to the liposome (Hui & Huang, 2021).

CH is also resistant to hydrolysis by the digestive enzymes secreted by the upper GIT (the oral, stomach, and intestine). The digestion of CH was reported in the colon by lysozymes, nonspecific cellulases, and enzymes secreted by colonic microflora (Kim et al., 2016). CH-coated lipid bilayers show potential as carriers for colonic drug delivery (Yu et al., 2009). The stability of vitamin E-loaded liposomes and CH-coated liposomes at 4℃ for 12 weeks was investigated. The stability of liposomes increased from 60.76% to 97.02% due to the CH coating (Liu & Park, 2009). CH-coated liposomes were less thixotropic compared to uncoated liposomes and the stability of curcumin-loaded liposomes was enhanced due to the CH coating (Hasan et al., 2016). Coating resveratrol-loaded liposomes using low molecular weight (LMW) CH (0.1%) prevented liposome aggregation and increased the stability of the liposomes (Park et al., 2014). The effect of succinyl CH coating on quercetin and resveratrol-loaded liposomes was investigated and results show that physical stability and the release profile (pH 7.0) of liposomes were increased due to the succinyl CH coating (Caddeo et al., 2017). (Y. Liu et al., 2015) studied the effect of CH coating on the stability of curcumin-loaded liposomes. After 40 days, the stability of curcumin was reported 90.68% for coated liposomes and 60.13% for liposomes at 4°C and 75.77% for coated liposomes, and 26.03% for liposomes at 23°C (Y. Liu et al., 2015). Compared to the effect of LMW-CH and high molecular weight (HMW) CH with different concentrations

(low; medium and high) on curcumin-loaded liposomes, results showed that all CH coatings affected positively the stability properties of liposomes against salt, light, heat, accelerated centrifugation, and long-term storage at 4°C. High concentration-HMW CH coating provided better stability (Tai et al., 2020).

Cuomo et al. investigated the effect of LMW-CH coating on the bioavailability of curcumin-loaded liposomes. According to *in vitro* digestion results, after the oral and gastric phases, a slightly higher curcumin concentration was detected compared to uncoated liposomes. A higher concentration of curcumin was determined for CH-coated liposomes after the intestinal phase. CH coating provided better absorption of curcumin in the intestinal phase (Cuomo et al., 2018). Mucoadhesive properties of C-phycocyanin-loaded liposomes were improved (Manconi et al., 2010), and mucoadhesive properties of liposomes were increased 2-fold due to the thiolated CH coating (Gradauer et al., 2012).

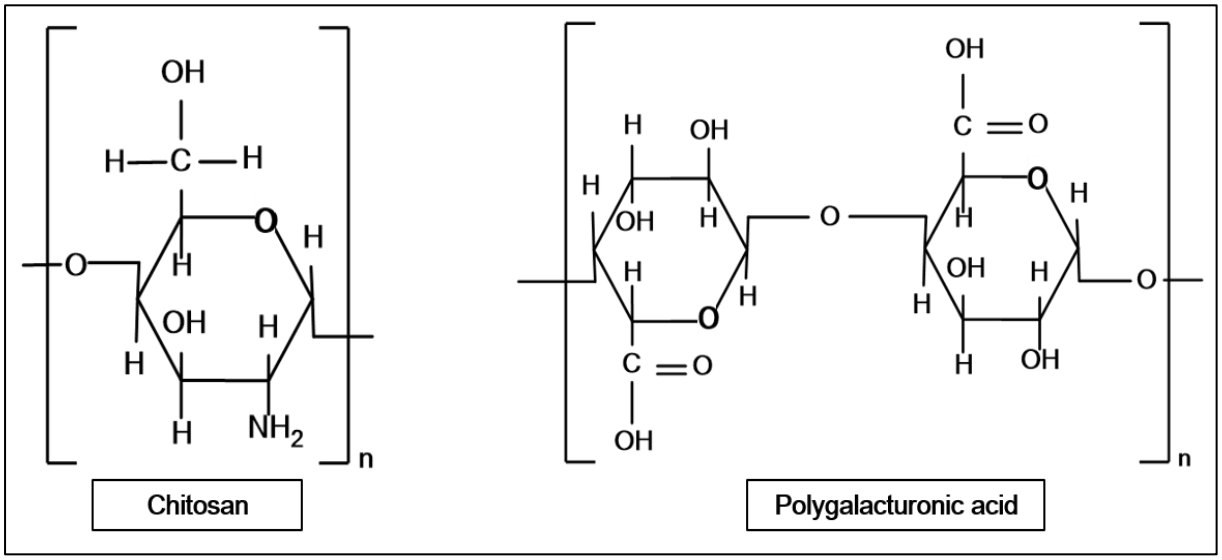

Figure 1.6 Chemical structure of chitosan (CH) and polygalacturonic acid (PGA).

1.4.5.2 Pectin and Polygalacturonic acid

Pectin, a type of plant-derived polysaccharide, is a negatively charged biopolymer composed of linear chains of galacturonic acid units linked through α (1–4) bonds with varying degrees of methyl-esterified carboxyl groups (Cheewatanakornkool & Sriamornsak, 2015; Espinal-Ruiz et al., 2014). The degree of esterification (DE) or amidation of the galacturonic acid units is a common method to characterize pectin and provides insight into the properties of pectin. Two main categories are high methoxy pectin (HM-pectin), which has a DE exceeding 50%, and low methoxy pectin (LM-pectin), characterized by a DE below 50% (Sriamornsak, 2011). Pectin is a well-known polysaccharide for its low toxicity and cost-effectiveness. It finds application in the food industry as a gelling and thickening agent, as well as a stabilizer. Its gelling

properties, along with other properties such as bioadhesive and biocompatibility, make it valuable for food application (Nguyen et al., 2011). PGA is a biocompatible and biodegradable anionic biopolymer, and derived from the demethylation of plant pectin **(Fig 1.6)** (Zhang et al., 2020). This linear homopolymer is linked by α-(1,4) glycosidic bonds (pK_a ~2.9-3.5) (Lopes et al., 2017; Müller et al., 2018). Pectin and PGA are also resistant to enzymes secreted by upper GIT whereas can be digested by pectate lyase and pectate hydrolase secreted by colonic microflora (Matsuura, 1991).

The release profiles of nisin-loaded liposomes, PGA-coated liposomes, and pectin-coated liposomes were examined. When compared to the uncoated liposomes, which exhibited a release of approximately 80% within 30 h, the coated liposomes demonstrated a slower release of the encapsulated nisin, reaching only around 50% release within 30 h (Lopes et al., 2017). Beta-carotene-loaded liposomes, CH-coated liposomes, and pectin/CH-coated liposomes were prepared. The EE for all samples exceeded ~82%. Double-coated liposomes offer effective protection for the encapsulated beta-carotene, leading to the prolonged-release duration compared to both uncoated liposomes and CH-coated liposomes (Wang et al., 2023).

1.4.6 Bioaccessibility, absorption and bioavailability of lipid self-assembled systems

The biological fate of LSAS (liposomes, emulsions, etc.) aiming to enhance the bioavailability of drugs differs depending on their digestibility. Digestible LSAS contains dietary fats and surfactants, while indigestible LSAS contains a mineral oil core or an indigestible shell (CH, pectin, etc.). Optimizing and designing LSAS can be achieved by modifying the properties of the nanocarriers, such as surface charge, size, and polarity, as these properties directly affect the digestion and absorption of LSAS (Roger et al., 2010).

Digestion is a crucial step to consider for the oral delivery of drugs. After oral administration, LSAS passes through the oral cavity and esophagus, followed by the stomach. In the gastric cavity, LSAS interacts with gastric fluids (pH 1-3) and a high concentration of calcium and sodium salts. During this interaction, physical properties begin to change, and some lipophilic compounds in the structure start to get digested by gastric lipases in the stomach (10–30%). After the gastric phase, LSAS that can survive the acidic environment of the stomach enters the small intestine (pH 6-7.5). In the small intestine, when digested food compounds mix with bile salts from the gall bladder and pancreatic secretions, lipophilic compounds are broken down to free fatty acids and monoglycerides by pancreatic lipases (70–90%). Bile salts, free fatty acids, monoglycerides, and phospholipids then form mixed micelles, which can be absorbed through the intestinal enterocytes. LSAS may lose their integrity after the gastric and

intestinal phases, but the structure can be protected from harsh conditions due to the indigestible coatings of LSAS (Elnaggar, 2015; Wang & Luo, 2019).

Absorption is one of the main mechanisms for oral delivery, and determining the absorption site is crucial for the design of controlled delivery vehicles. Enterocytes, covered with microvilli and two mucus layers, facilitate the absorption of bioactive compounds and lipids. Electrical charges and polarity of molecules are key factors for their diffusion across the mucus layers (Roger et al., 2010).

Digestible LSAS are digested like dietary lipids. Encapsulated compounds that pass-through enterocytes carried by mixed micelles are transported to the portal vein or lymphatic system. Short-chain triglycerides pass directly to the portal vein. Highly hydrophobic drugs (partition coefficient (LogP) > 5 and solubility > 50mg/g) are attached to chylomicrons, which enter the lymphatic system and carry these hydrophobic drugs to the tissues. Hydrophobic drugs are released from chylomicrons by hydrolysis of lipoprotein by lipases for the absorption of drugs in the tissue. Later, chylomicrons are taken by liver cells. Amphiphilic drugs follow the portal vein and systemic circulation (Roger et al., 2010; Wang & Luo, 2019).

The absorption, distribution, metabolism, and excretion of bioactive compound-loaded carriers are affected by the physicochemical properties of the vesicular carriers, such as size, hydrophilicity/hydrophobicity, charge, and the target site.

Size is one of the crucial factors in the absorption and uptake of LSAS. Large particles (>500 nm) cannot be absorbed in the intestine because the absorption of large particles across the mucous layer and transport of large vesicles through Enterocytes/M cells are very low, leading to their excretion in the faeces. Hydrophilic LSAS smaller than 10 nm are excreted in the urine (Borel & Sabliov, 2014; Roger et al., 2010). Cellular uptake of intact LSAS is provided by several mechanisms, including transcellular transport, paracellular transport, or persorption, to pass the intestinal barrier (Roger et al., 2010). For cellular uptake, intact LSAS needs to penetrate through the mucus layer that acts like a filter (~200 nm). The surface charge of LSAS affects interactions and penetration through the mucus layer. Cellular uptake of cationic LSAS is higher than anionic LSAS because of the high electrostatic interactions with the negatively charged mucus layer (Borel & Sabliov, 2014; Wang & Luo, 2019). Jubeh et al. investigated the adherence of neutral, anionic, and cationic liposomes to the healthy epithelium of the rat colon. Liposomes were prepared in L-histidine buffer (5 mM in normal saline) at pH 6.5. The adherence of cationic liposomes (64 mV) to mucus was ~50% and about three times higher than anionic liposomes (-66 mV) and neutral liposomes (-12 mV) (Jubeh et al., 2004).

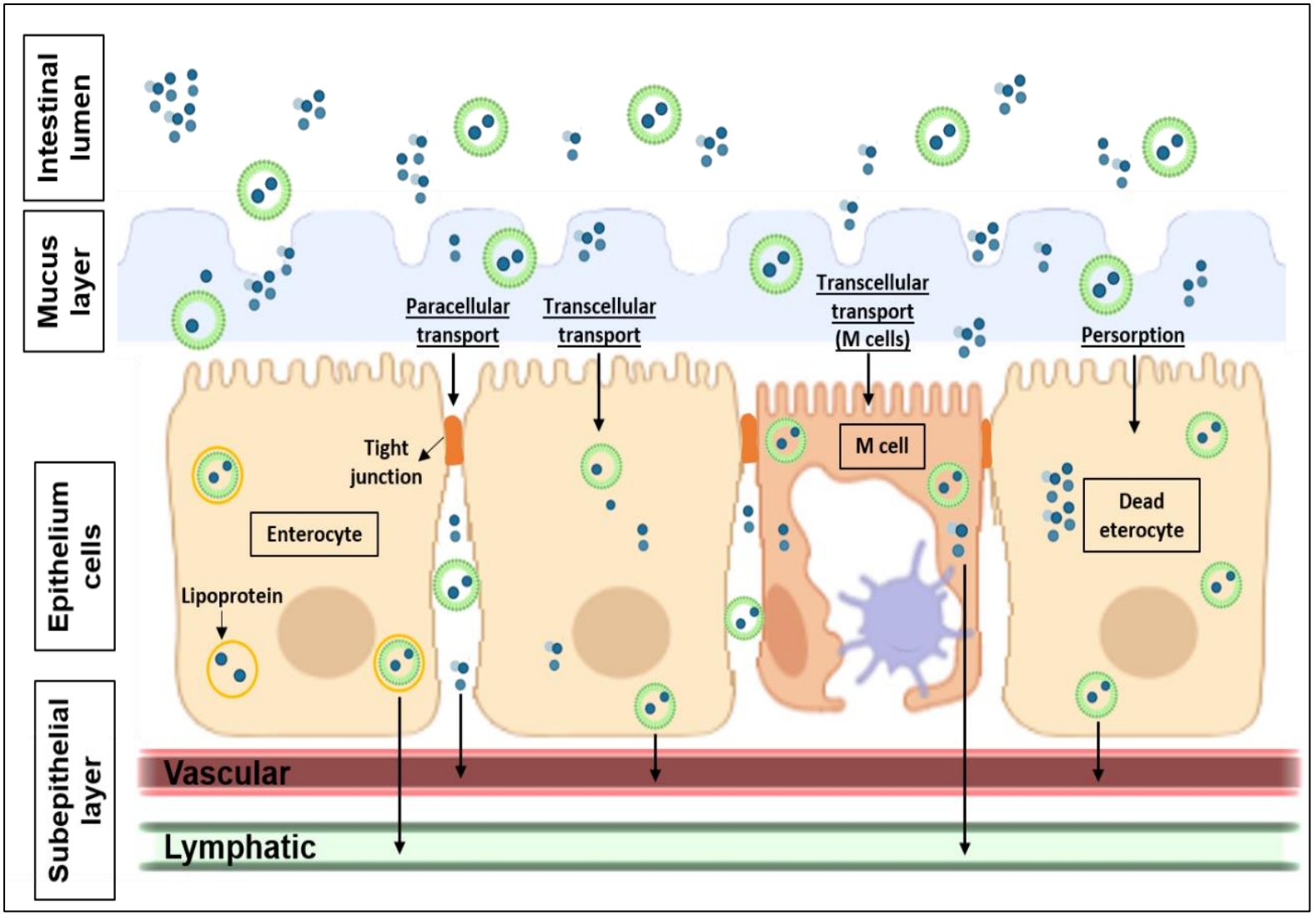

Figure 1.7 Schematic representation of uptake of LSAS across the intestinal epithelium. Adapted from (Mouhid et al., 2017; Wang & Luo, 2019).

Transcellular transport, which occurs through enterocytes and M cells, is facilitated by transcytosis **(Fig 1.7)**. Transcytosis involves the transportation of extracellular materials into the cell through endocytosis, which is the first step. Various mechanisms are responsible for transcellular transport across enterocytes, including clathrin-mediated endocytosis (for particles < ~200 nm), caveolae-mediated endocytosis (for particles ~60-100 nm), micropinocytosis (for particles > ~200 nm), and phagocytosis (for particles up to several µm). M cells are situated in gut-associated and mucosa-associated lymphoid tissues. In comparison to enterocytes, M cells, which are responsible for the transportation of viruses, bacteria, and antigens to immune cells, exist in fewer numbers in the GIT. M cells possess a unique structure, such as a thin mucus layer and undeveloped microvilli, which facilitates endocytosis and transcytosis as compared to enterocytes (Roger et al., 2010; Wang & Luo, 2019).

Paracellular transport, on the other hand, occurs between epithelial cells and involves the uptake of LSAS through tight junctions **(Fig 1.7)**. However, tight junctions have a small area of only approximately 3-4 nm, accounting for just 0.1% of the total absorption area of the intestine. Consequently, this uptake process is inefficient. The efficiency of uptake through tight junctions may be increased by using penetration enhancers, such as CH, bile salts, etc. (Wang & Luo, 2019). Persorption is another mechanism for the uptake of intact particles and involves the uptake of particles through dead or dying enterocytes (Wang & Luo, 2019).

1.4.7 Recent advances in resveratrol

1.4.7.1 General aspects of resveratrol

In recent years, consumers have shown increased interest in functional foods to regulate their diet. Functional foods can contain some health-promoting compounds such as phenolic compounds, terpenes, and phytosterols (Mouhid et al., 2017; Shishir et al., 2018). Phenolic compounds are one of the most widely studied groups among these health-promoting compounds, and there is a growing body of literature that shows their potential in the food and pharmaceutical industries. Phenolic compounds are found in fruits, vegetables, and other plant sources and range from simple phenolic molecules to polymerized forms. They can be categorized into phenolic acids, flavonoids, stilbenes, and curcuminoids based on their chemical structures (number of rings with one or more hydroxyl groups), physical properties (hydrophobicity or hydrophilicity), distribution and concentrations in plants, and their biological actions (Craft et al., 2012; Porrini & Riso, 2008).

Resveratrol (3,5,4′-trihydroxytrans-stilbene) is a well-known natural phenolic compound, produced by several plants in response to stress caused by pathogens. The molecular weight of resveratrol is 228.25 g/mol and the molecular formula is

$C_{14}H_{12}O_3$ (P. Devi et al., 2019; P. S. Wu et al., 2019). Resveratrol consists of two benzene rings linked by a heterologous bridge (Kasiotis et al., 2013). Resveratrol exists in isomeric *cis*- and *trans*- forms **(Fig 1.8)** but only *t*-res shows health benefits and is more bioactive and common in nature compared to *cis*-resveratrol (*c*-res). When *t*-res in solution is exposed to light for 1 h, 80-90% of *t*-res was converted to *c*-res (Vian et al., 2005). While *t*-res can remain stable in buffers (pH 1-7), *c*-res is only stable in neutral pH without light exposure (Peng et al., 2018). Resveratrol may undergo auto-oxidation. According to Yang yet al., 96% of resveratrol was degraded due to oxidation at 37℃ for 24 h and produced hydrogen peroxide (Yang et al., 2010).

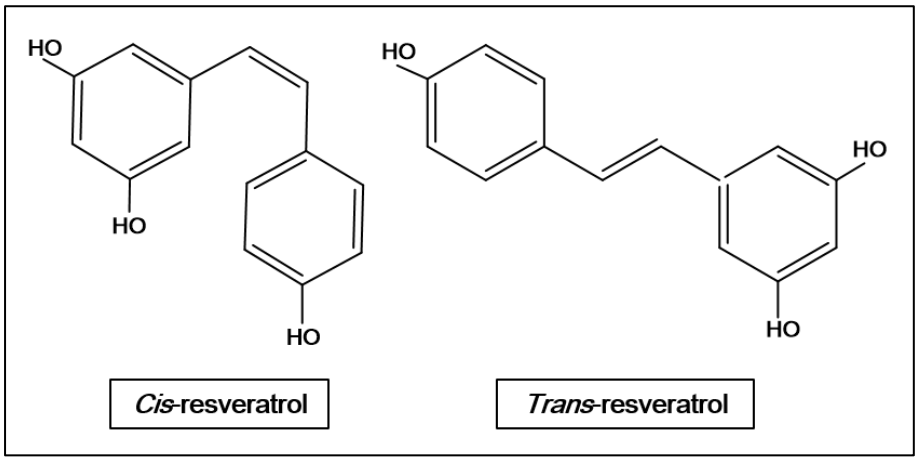

Figure 1.8 Chemical structure of *cis*-resveratrol (*c*-res) and *trans*-resveratrol (*t*-res).

Daily intake of resveratrol may be up to 4 mg/person/day with the consumption of foods (Vang et al., 2011). Daily intake of different doses (0.5, 1.0, 2.5, and 5.0 g) of resveratrol for a short-term human study (29 days) was studied, and up to 5 g/day, resveratrol intake is reported as safe according to toxicology studies. However, some gastrointestinal symptoms occurred in the volunteers who intake 2.5 and 5 g of resveratrol in a day (Brown et al., 2010). Resveratrol exists in many plants, majorly grapes, berries, and peanuts, and their products wine and peanut butter, and shows many desirable biological activities including antioxidant (Huang et al., 2017), anti-microbial (Ferreira & Domingues, 2016), anti-inflammation (Svajger & Jeras, 2012), anti-carcinogenic (Guo et al., 2015), anti-ageing (Li et al., 2018) properties. These functions depend on the bioavailability of resveratrol. The oral absorption of resveratrol reaches 75% in humans. However, the bioavailability of resveratrol is lower than 1% due to its rapid first-pass metabolism and rapid clearance from the circulation. This low bioavailability leads to low plasma concentration, which is not enough to exhibit significant pharmacological effects at target sites (Vaz-da-Silva et al., 2008; Walle, 2011).

1.4.7.2 Bioavailability of resveratrol

Bioavailability is defined as the fraction of a compound that is absorbed and reaches the systemic circulation, providing nutritional benefits (Carbonell-Capella et al., 2014; Rein et al., 2013). The bioavailability of phenolic compounds can be affected because of their bioaccessibility, absorption, and transformation during digestion (McClements et al., 2015). The first step in assessing the bioavailability of phenolic compounds is to determine bioaccessibility, which is the fraction of phenolic compounds released from the food matrix in the GIT and available for absorption (Saura-Calixto et al., 2007). The bioaccessibility of phenolic compounds can be influenced by their liberation, solubility, and interaction with components in the GIT (McClements et al., 2015).

Solubility and release from the food matrix play a significant role in the bioaccessibility of resveratrol. Resveratrol's incorporation in foods and pharmaceuticals is limited due to its instability and poor solubility in aqueous media (<0.001 mol/L) and consequently, in gastrointestinal fluids (Bonechi et al., 2012). The release of resveratrol from the plant matrix can be affected depending on the production methods. Resveratrol is a reference stilbene in grapes, and during winemaking, the concentration of *c*-res and *t*-res increases depending on the hydrolysis of *cis*- and *trans*-species in the products. Resveratrol can be extracted more from grape tissues with an increasing concentration of ethanol produced during fermentation (King et al., 2006). Compared to the aqueous solubility of resveratrol, solubility in ethanol (~50 mg/mL) is quite high (Gambini et al., 2015) so alcoholic beverages may be utilized to increase the peak plasma concentrations and bioavailability of resveratrol (Weiskirchen & Weiskirchen, 2016).

Absorption and transformation are other important steps for the bioavailability of phenolic compounds, and absorption can broadly be defined as the fraction of phenolic compounds that can pass through the mucosa and reach systemic circulation. The absorption of phenolic compounds can be limited by mucus layers of the epithelium, depending on electrical charges, polarity, and size of phenolic compounds. Following the mucus layer, absorption through the epithelial cell also depends on the permeability of phenolic compounds. For the characterization of permeability, oil/water LogP of phenolic compounds can be used. When the hydrophobicity of phenolic compounds increases, membrane permeability also increases because highly hydrophobic compounds can directly pass through the hydrophobic phospholipid membranes (McClements et al., 2015). According to the Biopharmaceutical Classification System which classifies compounds based on their solubility in aqueous media and intestinal membrane permeability, resveratrol is classified in Class II (low solubility and high permeability). Despite its low solubility in gastrointestinal fluids, it

has high intestinal membrane permeability due to its hydrophobic nature (LogP 3.1) (McClements et al., 2015). The absorption of resveratrol is reported to be around 70% in humans (Walle, 2011).

Absorption of resveratrol is by rapid passive diffusion or carrier-mediated transport and transformation occurs by the first-pass metabolism in the intestine (Lancon et al., 2004). During absorption, free and conjugated forms of resveratrol can be transported through the apical membrane and basolateral membrane. Resveratrol and its metabolites interact with multidrug resistance-associated proteins (MRP)-2 and MRP-3. MRP-2, which is in the apical membrane, is being responsible for the efflux transport of resveratrol and its metabolites back to the epithelial cell. In the basolateral membrane, MRP-3 transports them to the circulation (Planas et al., 2012). When resveratrol and its metabolites pass into the systemic circulation, they interact with lipoproteins and serum proteins such as hemoglobin and albumin (only binding occurs when the concentration of resveratrol is high) via hydrophilic and hydrophobic interactions. Thus, resveratrol remains at a high concentration in the serum, consequently improving its functional effect (Delmas et al., 2011).

Further transformation of phenolic compounds occurs through phase I and II metabolism in the liver. Phase I metabolism, which includes hydrolysis, reduction, and oxidation, alters the polarity of phenolic compounds, leading to excretion through urine. Conjugation reactions occur during phase II metabolism between phenolic compounds, phase I metabolites, and other compounds (McClements et al., 2015). Phase I metabolism is not observed for resveratrol. Sulfation and glucuronidation enzyme-catalysed conjugations of resveratrol occur through sulfotransferases and uridine 5'-diphospho-glucuronosyltransferases during phase II metabolism (Springer & Moco, 2019). Phase II metabolism results in conjugated metabolites such as resveratrol monosulfate, resveratrol monoglucuronide, dihydroresveratrol monosulfate, and dihydroresveratrol monoglucuronide. Phase II metabolism is reported to be a major limitation of the bioavailability of resveratrol (Delmas et al., 2011). Resveratrol and its metabolites reach the systemic circulation and are absorbed by specific tissues like adipose. Resveratrol and metabolites are finally excreted into the urine through renal excretion. The excretion of resveratrol and metabolites in humans ranges from 70% to 98% (Walle et al., 2004).

Meng et al. studied the concentration of resveratrol and metabolites in the blood after the consumption of free resveratrol and grape juice. While resveratrol and conjugated metabolites were detected in human plasma after high-dose free resveratrol intake (0.5-1 mg/kg), no related compound was detected after grape juice consumption (containing 0.6-1.8 mg resveratrol) (Meng et al., 2004). The bioavailability of

resveratrol from white wine, grape juice, and vegetable juice was reported by Goldberg et al. After oral consumption (*t*-res, 25 mg/70 kg), only 1.7% to 1.9% of free *t*-res was detected in blood and urine samples (Goldberg et al., 2003).

The concentration of glucuronide and sulphate conjugates is considerably higher than free *t*-res after absorption. Much research is already being undertaken on the bioavailability of resveratrol, which is reported to be quite low after oral administration. In order to overcome the limitation of the bioavailability of resveratrol, some metabolic inhibitors can be administered together with resveratrol to control metabolism, and the functionalities of resveratrol metabolites can be investigated. A more promising method is encapsulation technology and proper carriers that can be used to overcome the limitations of utilizing resveratrol as a bioactive compound (Amri et al., 2012).

Chapter 2: Design and characterisation of empty and *t*-res loaded liposomes, bilosomes, CH-coated and PGA/CH-coated bilosomes

2.1 Abstract

Recently, modifying the lipid membrane with the addition of some surfactants or coating the system using biopolymers to enhance their desired properties have gained increasing attention for their potential applications as delivery systems.

In this study, *t*-res-loaded bilosomes composed of POPC, DOPG, and different concentrations of NaC were prepared and coated with CH and PGA. Samples were characterised by combining DLS, SAXS, SANS, cryo-TEM, and FT-IR. The results showed that liposomes were mostly unilamellar, with a small subpopulation of bi- and tri-lamellar vesicles. The addition of NaC induced a vesicle-to-micelle transition as shown by the presence of different colloidal structures composed of either vesicle, core-shell ellipsoid, micelles, or their mixtures. After CH coating, well-defined Bragg peaks were observed in the SAXS spectra possibly because CH coating pushed the structural order of the bilayer from unilamellar to multilamellar due to the osmotic pressure of CH. SANS data showed that CH-coated and PGA/CH-coated bilosomes were highly swollen, fuzzy, and polydisperse. FT-IR analysis confirmed the conjugation of CH and PGA onto the bilosomes and the successful entrapment of *t*-res. The EE of samples was above 87%.

The present findings demonstrate that the incorporation of bile salts leads to a disruption in the POPC/DOPG lipid bilayer in a concentration-dependent manner, resulting in the formation of different lipid structures. The combined presence of bile salts and biopolymers also caused changes in the structural order of the bilayers due to the increased osmotic pressure.

Keywords: bilosomes, chitosan, polygalacturonic acid, *trans*-resveratrol, small-angle x-ray scattering, small-angle neutron scattering

2.2 Introduction

Resveratrol (3,5,4′-trihydroxytrans-stilbene) is a well-known hydrophobic phenolic compound, produced by several plants in response to stress caused by pathogens. Resveratrol exists in isomeric *cis* (*c*-res) and *trans* forms (*t*-res). Compared to *c*-res, *t*-res is common in nature and displays more health-promoting functions such as anti-microbial, antioxidant, or anti-carcinogenic (Vian et al., 2005). However, its therapeutic efficacy is restricted by its low solubility in aqueous media and consequently in

biological fluids. Its bioavailability has been reported as lower than 1%, which is not enough to show a biological effect at the target site because of first-pass metabolism and rapid clearance from the circulation that causes low plasma concentration (Vaz-da-Silva et al., 2008). Much research has already been undertaken on the bioavailability of resveratrol, which is reported as quite low after oral administration. In order to overcome the limitations of utilizing resveratrol, nanocarriers can be used (Amri et al., 2012).

Liposomes are widely used nanocarriers and have many advantages for the encapsulation of bioactive compounds. They can reduce the required drug dosage frequency to maintain the bioactivity of drugs with short half-lives which require multiple dosages to show a therapeutic effect. Liposomes can provide a more consistent concentration of drugs in circulation due to the controlled release of encapsulated compounds. They are biocompatible and biodegradable and reduce the systemic toxicity of drugs. The cytotoxicity of drugs may be minimized by targeted delivery to specific organs and by decreasing their distribution to drug-sensitive tissues (Çağdaş et al., 2014). Moreover, the properties of liposomes like size, and charge can be easily changed by the incorporation of varied materials into the bilayer (Torchilin, 2005). Although liposomes have considerable potential for encapsulation of bioactive compounds, they suffer from instability during storage. Liposomes may lose their chemical stability because the unsaturated fatty acids of phospholipids are prone to oxidation and the ester moieties can undergo hydrolysis. These chemical changes can cause instabilities of liposomes which may result in drug leakage (Rideau et al., 2018). Moreover, during digestion, the properties and composition of liposomes and digestion conditions (pH variations, enzymes, bile salts, etc.) have a considerable effect on the biological fate of liposomes. While liposomes can generally stay stable in gastric conditions, they cannot maintain their integrity in the presence of intestinal enzymes and bile salts in the small intestine, especially the duodenum (Liu et al., 2019). These instability problems limit their use in the food and pharmaceutical industries. The oxidation of the phospholipid in the food and the release of the encapsulated compound during storage can cause undesirable properties in the product and reduce the shelf life of the product. Since controlled delivery and the release of the encapsulated compound are required in pharmaceutical products, instability during digestion before the target site can affect the bioaccessibility, and consequently bioavailability of the compound.

These difficulties can be overcome by using different lipids and lipid combinations, incorporating several materials such as Chol, non-ionic surfactants, and bile salts in the bilayer structure, and modifying the surface with a coating (Kotla et al., 2017). Recently there has been renewed interest in the incorporation of exogenous bile salts

into the liposome bilayer. Bile salts are physiological bio-surfactants involved in the digestion and absorption of dietary lipids. They take the form of conjugated bile acids that form complexes with sodium (Ridlon et al., 2016; Thomson et al., 1989). Bile salt-containing liposomes have been labelled as bilosomes (Hao et al., 2016) or transfersomes (Guan et al., 2016) in the literature. Bile salts can increase the elasticity of the bilayer which may increase LC of bilosomes and show a penetration-enhancing effect which facilitates the absorption and bioavailability of bilosomes (Aburahma, 2016; Hu et al., 2013; Tang et al., 2021). Another promising technique to improve the stability of liposomes is by modifying the surface using biocompatible and biodegradable biopolymers such as CH and PGA. CH is a cationic biopolymer, composed of β-(1,4) linked D-glucosamine (pKa ~6.5) and N-acetyl-D-glucosamine (uncharged) units (Espinal-Ruiz et al., 2014; Tahara et al., 2018). It is commonly used for coating negatively charged liposomal surfaces because of its positive charge resulting from amino groups (He et al., 2019). Furthermore, PGA, an anionic biopolymer, is a linear homopolymer linked by α-(1,4) glycosidic bonds (Müller et al., 2018). Coating the liposomes not only enhances the stability during storage and protects them from the harsh environment of the GIT, but also provides additional functionality such as mucoadhesion (Tahara et al., 2018), and permeation-enhancing effects (Sebaaly et al., 2021). In this study, the effects of bile salt addition on the structure of lipid bilayers were investigated comprehensively and bilosomes, CH-coated bilosomes, and PGA/CH-coated bilosomes were characterized as carriers for oral delivery for the first time. The *t*-res was used as a model hydrophobic bioactive compound. The physical properties of the bilosomes and coated bilosomes were determined by a combination of DLS, SAXS, and SANS. The lamellarity and shape of samples were also determined using cryo-TEM in support of the scattering techniques. The coating of bilosomes with CH and PGA and the interaction of compounds in the formulations were analysed by FT-IR. Finally, the EE and the LC were measured.

2.3 Materials and methods

2.3.1 Materials

POPC (16:0-18:1 PC), and DOPG (18:1 (Δ9-Cis) PG) were purchased from Avanti Polar Lipids, USA. NaC hydrate (BioXtra, ≥99%), Tris base, 3,4′,5-Trihydroxy-trans-stilbene (*t*-res), LMW-CH with 75-85% deacetylation, PGA with ≥85% (titration) from oranges, sodium tripolyphosphate pentabasic (TPP) and Triton X-100 were purchased from Sigma Aldrich, UK. Chloroform, methanol, NaCl, and ethylenediaminetetraacetic acid (EDTA) were purchased from Merck, UK.

2.3.2 Preparation of empty and *t*-res loaded liposomes and bilosomes

POPC: DOPG (10:3.3 molar ratio) liposomes and bilosomes were prepared using thin-film hydration followed by the extrusion method with minor modifications reported by (Coreta-Gomes et al., 2015). POPC, DOPG, and NaC (only for bilosome formulations) were dissolved in a mixture of chloroform and methanol (80:20, v/v). The organic solvent mixture was evaporated using Genevac (EZ-2 plus) (Fisher Scientific Ltd, Leicestershire, UK) (25℃, Method: Very Low BP Mix) to obtain dried lipid films. The solvent-free lipid film was hydrated with 10 mM Tris buffer (pH 7.4 and containing 150 mM NaCl and 1 mM EDTA) prepared in water and vortexed at room temperature (RT). The hydrated suspension underwent 5 freeze-and-thaw cycles and was vortexed after each cycle. Samples were sonicated using QSonica Sonicator (80% amplitude, 1 second (s) on, 2 s off for 5 minutes (min)) to achieve homogeneous liposomes. An ice-water bath was used to avoid damage due to sample heating during sonication. After sonication, samples were extruded (Avanti Polar Lipids, USA) through a 100 nm polycarbonate membrane (Nuclepore, Whatman Inc., UK) 21 times to obtain ULVs. Finally, the samples were stored in a refrigerator at 4°C in the dark for further analysis. For the preparation of empty **(Table 2.1)** and *t*-res-loaded samples **(Table 2.2)**, *t*-res was dissolved in organic solvent at the same time as POPC, DOPG, and NaC, and the same method was followed. All liposomes and bilosomes were prepared in triplicates.

2.3.3 Preparation of CH-coated and PGA/CH-coated bilosomes

The stock solution of CH (3 mg/mL, protonated in hydrochloric acid (HCl) aqueous solution) and PGA (3 mg/mL) were hydrated overnight under magnetic stirring (500 rpm) at RT and the solution was filtered through a 1.5 µm nylon filter. Stock solutions were stored at 4°C until used.

Bilosomes (pH 5.5) were added dropwise into the CH solution (3 mg/mL, pH 5.5) under magnetic stirring (500 rpm) at RT to form CH-coated bilosomes. A 0.1% TPP (v/v) solution was used as a cross-linker and added to the solution while stirring. Samples were stirred overnight under magnetic stirring (500 rpm) at RT and subsequently, pH was adjusted to 5.5. Samples were sonicated using QSonica Sonicator (35% amplitude, 1 son, 2 s off for 10 min) to achieve homogeneous particles. An ice-water bath was used to avoid damage from sample heating upon sonication. CH-coated bilosomes with different NaC/CH ratios (w/w) from 5.0 to 0.23 (w/w) were prepared. The optimum NaC/CH ratio (w/w) was identified as 0.5 according to their physical properties in terms of D_H, PD, and the ζ potential of samples **(Fig. B.13-15)**.

Table 2.1 Composition of empty liposomes, bilosomes, and CH-coated and PGA/CH-coated bilosomes.

Sample	POPC (mM)	DOPG (mM)	NaC (mM)	*t*-res (mM)	NaC/CH (w/w)	CH/PGA (w/w)
L-0	10	3.3	-	-	-	-
B-5:0	10	3.3	5	-	-	-
B-7.5:0	10	3.3	7.5	-	-	-
B-10:0	10	3.3	10	-	-	-
CH-B-5:0	10	3.3	5	-	0.5	-
CH-B-7.5:0	10	3.3	7.5	-	0.5	-
CH-B-10:0	10	3.3	10	-	0.5	-
PGA/CH-B-5:0	10	3.3	5	-	0.5	0.4
PGA/CH-B-7.5:0	10	3.3	7.5	-	0.5	0.4
PGA/CH-B-10:0	10	3.3	10	-	0.5	0.4
POPC: 2-oleoyl-1-palmitoyl-sn-glycero-3-phosphocholine, DOPG: 1, 2-dioleoyl-sn-glycero-3-phospho-(1'-rac-glycerol) (sodium salt), NaC: Sodium cholate, CH: Chitosan, PGA: Polygalacturonic acid.						

Table 2.2 Composition of *t*-res loaded liposomes, bilosomes, and CH-coated and PGA/CH-coated bilosomes.

Sample	POPC (mM)	DOPG (mM)	NaC (mM)	*t*-res (mM)	NaC/CH (w/w)	CH/PGA (w/w)
L-1	10	3.3	-	1	-	-
B-5:1	10	3.3	5	1	-	-
B-7.5:1	10	3.3	7.5	1	-	-
B-10:1	10	3.3	10	1	-	-
CH-B-5:1	10	3.3	5	1	0.5	-
CH-B-7.5:1	10	3.3	7.5	1	0.5	-
CH-B-10:1	10	3.3	10	1	0.5	-
PGA/CH-B-5:1	10	3.3	5	1	0.5	0.4
PGA/CH-B-7.5:1	10	3.3	7.5	1	0.5	0.4
PGA/CH-B-10:1	10	3.3	10	1	0.5	0.4
POPC: 2-oleoyl-1-palmitoyl-sn-glycero-3-phosphocholine, DOPG: 1, 2-dioleoyl-sn-glycero-3-phospho-(1'-rac-glycerol) (sodium salt), NaC: Sodium cholate, *t*-res: trans-resveratrol, CH: Chitosan, PGA: Polygalacturonic acid						

Different CH/PGA ratios from 2 to 0.2 (w/w) were prepared to optimise PGA coating. CH-coated bilosomes (pH 5.5) were added dropwise into PGA solution (3 mg/mL, pH 5.5) under magnetic stirring (500 rpm) at RT to form PGA/CH-coated bilosomes. Samples were stirred overnight under magnetic stirring (500 rpm) at RT and subsequently, pH was adjusted to 5.5. Samples were sonicated using QSonica Sonicator (35% amplitude, 1s on, 2 s off for 3 min) to achieve homogeneous liposomes. An ice-water bath is used to avoid damage from sample heating upon sonication. The optimum CH/PGA ratio (w/w) was identified as 0.4 according to the D_H, PDI, and ζ potential of the samples **(Fig. B.16)**. CH-coated and PGA/CH-coated bilosomes were filtered through a 1.5 µm nylon filter and finally were stored in a refrigerator at 4°C in the dark for further analysis. All biopolymer-coated bilosomes were prepared in triplicates.

2.3.4 Characterization of liposomes, bilosomes, CH-coated and PGA/CH-coated bilosomes

2.3.4.1 Hydrodynamic diameter, polydispersity, and zeta potential

The D_H and PDI of samples were determined by DLS using a Zetasizer Nano (ZS series, Malvern Instruments, Malvern, UK) at 25 °C. The refractive index (RI) of liposomes used was 1.45, and the absorption coefficient was 0.001. The type of cuvette used was DTS0012. The ζ potential of samples was analysed by the Zetasizer Nano ZS series equipped with a 633 nm helium/neon laser at a detector angle of 90°. The type of cuvette used was DTS1070. Samples were diluted 50-fold using Millipore water to avoid multiple light scattering effects. Measurements were performed on triplicate samples.

2.3.4.2 Cryo-transmission electron microscopy

The cryo-TEM experiments were carried out in the Astbury Biostructure Laboratory at University of Leeds. Briefly, 3 µL of samples were applied to the copper (Cu) grids (Quantifoil R 1.2/1.3 grid: Cu 300), and the grids were blotted for 6 s (blotting force: 1) at RT under 100% RH (Xu et al., 2021). After blotting, grids were plunged into liquid ethane by using a Vitrobot mark IV (Thermo/FEI). Grids were kept under liquid nitrogen before measurement. For liposome and bilosomes samples, grids were glow discharged at 10 mA for 30 s. Data acquisition was performed on a Titan KRIOS microscope (Thermo Fisher Scientific, US) with an accelerating voltage of 300 kV and a defocus value of −2 µm at a nominal magnification of 96k.

2.3.4.3 Small-angle x-ray scattering

Samples were analysed by SAXS. The X-ray experiments were carried out at Diamond Light Source (Didcot, UK) on the beamline I22, using a beam energy of 18 keV

(wavelength (λ)=0.69 Å). The distance between the sample and detector (Pilatus 2M) was set at 6.22 m and Q-range was 3×10^{-3} to 0.40 $Å^{-1}$. Samples were loaded into a glass capillary (1.56x2.00x50 mm) and measured at 25 °C. Silver behenate was used as a calibrant. SAXS data were analysed using DAWN (2.25.0) and OriginPro (2020) software. The details of the data analysis and models are provided in **Appx A3.2** and **Appx A3.3**, respectively.

2.3.4.4 Small-angle neutron scattering

Samples were analysed by SANS. SANS experiments were performed on the SANS2D beamline at ISIS Neutron and Muon Source (Didcot, UK). For SANS experiments, Tris buffer was prepared in heavy water (D_2O), and the same preparation method was followed for liposomes, bilosomes, and CH-coated and PGA/CH-coated bilosomes. 1 mm pathway Hellma macro quartz cells were used during measurements at 25°C. The scattered intensity, I (Q), is measured as a function of the scattering vector, Q, where Q is defined as $Q= (4\pi/\lambda). \sin\theta$, and 2θ is the scattering angle and λ the neutron wavelength. On SANS2D a neutron λ was ranging from 1.75 to 14.4 Å. The distance between the source to sample and sample to the detector was set at 8 m and beam size 8 mm, giving Q-range from 2×10^{-3} to 0.965 $Å^{-1}$. The sample scattering was normalised with respect to incident intensity, transmission, sample thickness, acquisition time, and background. SANS data were analysed using SasView (5.0.6) software. The details of the data analysis and models are provided in **Appx A3**.2 and **Appx A3.3**, respectively.

2.3.4.5 Fourier transform mid-infrared spectroscopy

The FT-IR spectra of samples were measured to investigate the conjugation of CH and PGA onto the bilosomes and the interaction of compounds in the formulations. The FT-IR spectra of *t*-res, POPC, DOPG, NaC, CH, and PGA were measured to detect the main peaks of compounds. A dry or liquid sample was placed on zinc selenide crystal at RT and the FT-IR spectra of samples were recorded in the attenuated total reflectance mode between 4000 cm^{-1} and 550 cm^{-1} with 100 scans using a Spectrum One FT-IR Spectrometer (PerkinElmer Instruments, USA). FT-IR spectrum of samples was analysed using irAnalyze (Version 7.1.0.0, Labcognition GmbH&Co) software.

2.3.4.6 Encapsulation efficiency and loading capacity

Free *t*-res was separated from samples by centrifugation of 0.5 mL liposome and bilosome samples using a high-speed centrifuge (Beckman Coulter, Avanti Centrifuge J-30I) at 108800 x g for 60 min at 4°C and 1.5 mL coated bilosome samples (Thermo Scientific, Fresco 21) at 21000 x g for 60 min at 4°C. The supernatants were collected,

supernatants and pellets were mixed with Triton X-100 to disrupt the lipid bilayer and then were dried using a Genevac (EZ-2 plus) (Fisher Scientific Ltd, Leicestershire, UK) (25℃, Method: Aqueous). The dried samples were dissolved in methanol and were filtered through a 0.20 µm PTFE filter for high-performance liquid chromatography (HPLC). The HPLC method (Ares et al., 2015) described below determined the free *t*-res and the amount of *t*-res loaded in formulations. Measurements were performed on triplicate samples. EE and LC of samples were calculated by using the following equations **(Eq. 2.1** and **2.2)**.

$$EE\ (\%) = \frac{\text{total tres (mg)-free tres (mg)}}{\text{total tres (mg)}} x100 \qquad \textbf{Eq. 2.1}$$

$$LC\ (\%) = \frac{\text{total tres (mg)} - \text{free tres (mg)}}{\text{total tres(mg)+lipids(mg)+NaC(mg)}} x100 \qquad \textbf{Eq. 2.2}$$

2.3.4.7 Quantification of *t*-res using HPLC-DAD

The concentration of *t*-res in the filtrate was determined using a liquid chromatography–mass spectrometry (LC-MS) (Shimadzu, Japan) system controlled by LabSolutions software (version 5.97) (Ares et al., 2015) with a diode array detector (DAD). An Ascentis® Express C18 (2.7 µm particle size, length× inner diameter (I.D.) 15 cm×4.6 mm) analytical column protected by a Phenomenex (AJ0-4287) C18 security guard cartridge (4× 3.0 mm) was used and the column temperature was set at 30°C. The flow rate of mobile phases was 0.8 mL/min with a 33 min elution gradient, composed of solvent (A) formic acid in water (1 %, v/v) and (B) acetonitrile. 50 µL filtrate sample was injected and mobile phase conditions (i) 0 min (A-B, 71:29, v/v); (ii) 21 min (A-B, 71:29, v/v); (iii) 24 min (A-B, 0:100, v/v); (iv) 27 min (A-B, 0:100, v/v); (v) 30 min (A-B, 71:29, v/v); (vi) 33 min (A-B, 71:29, v/v) were followed. Eluted *t*-res was monitored at 310 nm. Measurements were performed on triplicate samples.

2.3.5 Statistical analysis

All the data are reported as mean±standard deviation (SD). Results were analysed by one-way ANOVA using Minitab® 20.4 software. The level of statistical significance was defined by $p<0.05$.

2.4 Results and discussion

2.4.1 The physical characterization of liposomes, bilosomes, CH-coated and PGA/CH-coated bilosomes

2.4.1.1 Hydrodynamic diameter, polydispersity, and zeta potential

The D_H and ζ potential of the empty and *t*-res loaded liposomes are given in **Fig. 2.1** and **Fig. 2.2**, respectively. The average D_H of liposomes was 84.2±2.2 nm and 93.7±4.3 nm at pH 7.4 for empty liposomes and *t*-res loaded liposomes, respectively. The PDI was lower than 0.173 for all liposome samples and the ζ potential of liposomes ranged from -40.9±4.0 to -44.1±3.7 mV which is normally considered to make colloids highly stable. The D_H, PDI and ζ potential of loaded and unloaded liposomes did not change significantly with the pH change from 7.4 to 5.5 ($p>0.05$).

The characteristics of the empty and *t*-res loaded bilosomes are shown in **Fig. 2.1** and **Fig. 2.2**, respectively. The addition of NaC into the empty and *t*-res loaded bilosome formulations did not affect the D_H of bilosomes significantly ($p>0.05$). At pH 5.5, the D_H of B-5:1, B-7.5:1, and B-10:1 was 82.8±3.8 nm, 68.0±0.6 nm, and 96.5 ±0.5 nm, respectively. Additionally, the D_H of bilosomes was not affected significantly by the loading of *t*-res ($p>0.05$). These slight changes in the D_H of bilosomes with the addition of NaC are possibly connected with the disruption of phospholipid bilayers by bile salts. Changing the lipid/NaC ratio in the bilosome formulations alters their properties due to the powerful membranolytic activity of bile salts on phospholipid bilayers (Can et al., 2021). Previous research has shown that for ULVs, when the concentration of bile salt is lower than its CMC, bile salts first locate in the outer layer of the bilayer and then the inner layer. Bile salts bind to the monolayers and cause a pore formation which results in bilayer fluctuations, but they do not yield micelles. When bile salts saturate the liposome bilayer, the deformed bilayer begins to rupture, and the bilayer is converted to mixed micelles. For further increased bile salt concentration, the smaller-sized mixed micelles are yielded (Garidel et al., 2007; Lichtenberg et al., 2013). For the MLVs, the membranolytic activity of bile salts will be slower on MLVs than on ULVs because bile salts first locate on the outer bilayer and inner bilayers will expose the bile salts only after disruption of the outer bilayer (Lichtenberg et al., 2013).

Yang et al. studied the effect of NaDC on the properties of hyaluronic acid-coated bilosomes. Three different NaDC concentrations (1, 2, and 3 mg/mL) were used and D_H decreased from ~140 nm to ~90 nm and then increased to ~110 nm with an increased concentration of NaDC (H. Yang et al., 2019). Cyclosporine A-loaded bilosomes composed of SPC and NaDC were prepared by Guan et al. The D_H of the formulations prepared at SPC/NaDC ratios of 9:1, 5:1, and 3:1 was ~160 nm, ~70 nm,

and ~80 nm, respectively (Guan et al., 2011). After bile salts bind to the outer layer of the bilayer, if they cannot rapidly flip to the inner monolayer, they may induce positive outer monolayer curvature which may be the reason for the variations in the D_H (Elsayed & Cevc, 2011).

The PDI of empty and *t*-res loaded liposomes was around 0.170. For 5 mM and 7.5 mM NaC-containing formulations, the PDI increased significantly ($p<0.05$) and ranged from 0.201±0.029 to 0.250±0.008. The addition of 10 mM NaC resulted in a lower PDI between 0.041±0.002 and 0.100±0.013 ($p<0.05$). The ζ potential of empty and *t*-res bilosomes was highly stable, ranging from -43.1±1.1 mV to -47.9±2.9 mV, and not affected significantly by the addition of the negatively charged NaC into the liposome formulation ($p>0.05$). The ζ potential serves as a relative indicator of colloid stability. If the ζ potential falls below ±30 mV, it may lead to issues like aggregation, flocculation, or precipitation (Danaei et al., 2018). Additionally, loading the *t*-res into the liposomes and bilosomes did not significantly affect the ζ potential because *t*-res is a neutral phytochemical (Catalgol et al., 2012).

CH and PGA adsorption onto the surface of bilosomes was achieved using the electrostatic layer-by-layer approach **Fig. 2.1-2.2.** Based on optimization studies **(Fig. B.13-16)**, a NaC/CH ratio of 0.5 (w/w) and a CH/PGA ratio of 0.4 (w/w) were chosen as suitable ratios for the formation of the stable coating. CH was used as a first coating by electrostatic interaction between the negatively charged phosphate group ($-PO_4^{3-}$) of phospholipids and the positively charged amine group ($-NH_3^+$) of CH (Henriksen et al., 1994). 0.1 % TPP was also added as a crosslinker during CH coating. Anionic TPP interacts with the positively charged amine group (-NH3+) of CH through electrostatic interactions and enhances the stability of CH coating on the bilosome surface (Zhao & Wu, 2006). The CH coating increased the D_H significantly for all bilosome samples ($p<0.05$). After CH coating, D_H ranged from 304.9±7.3 nm to 326.2±7.8 nm for 5 mM and 7.5 mM NaC empty and *t*-res loaded bilosomes. The D_H of 10 mM NaC containing empty, and *t*-res loaded bilosomes was significantly higher and between 451.5±6.5 nm and 536.9±6.7 nm ($p<0.05$). The PDI of CH-coated bilosome samples decreased significantly ($p<0.05$) due to the CH coating and were more homogeneous with PDI<0.186±0.002 **(Fig. 2.1-2.2)**. The same D_H and PDI trends were also reported by Tai et al. who studied curcumin-loaded liposomes and the effect of CH coating on vesicle properties (Tai et al., 2020). After CH coating, while the D_H of vesicles increased significantly, the PDI decreased.

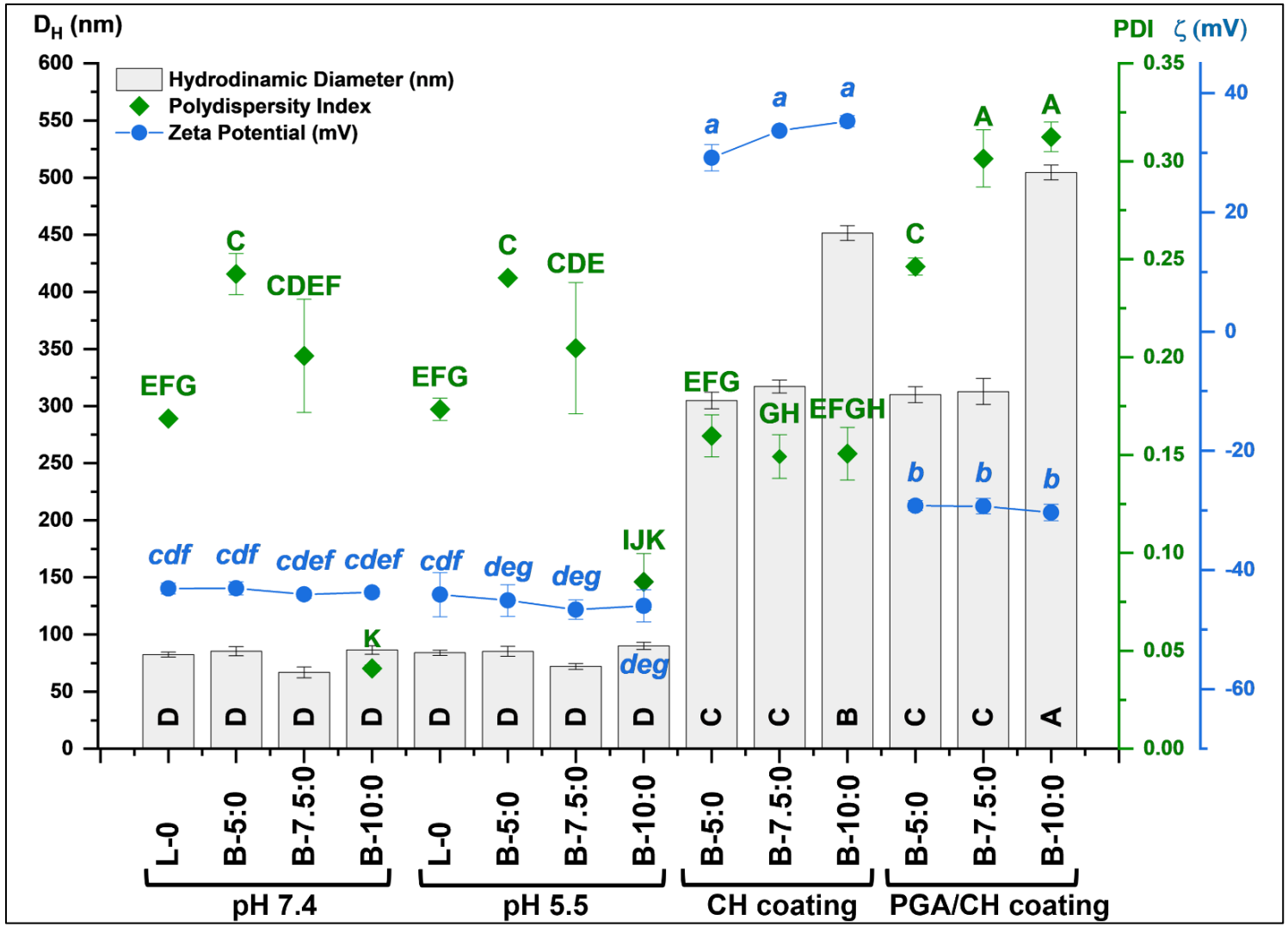

Figure 2.1 The D_H (▭), PDI (♦) and ζ potential (●) of empty liposomes, bilosomes, and CH-coated and PGA/CH-coated bilosomes. The data represent the mean±SD. Black capital letters represent significant differences in the D_H, green capital letters in the PDI, and blue lowercase letters in the ζ potential among the samples, respectively ($p < 0.05$).

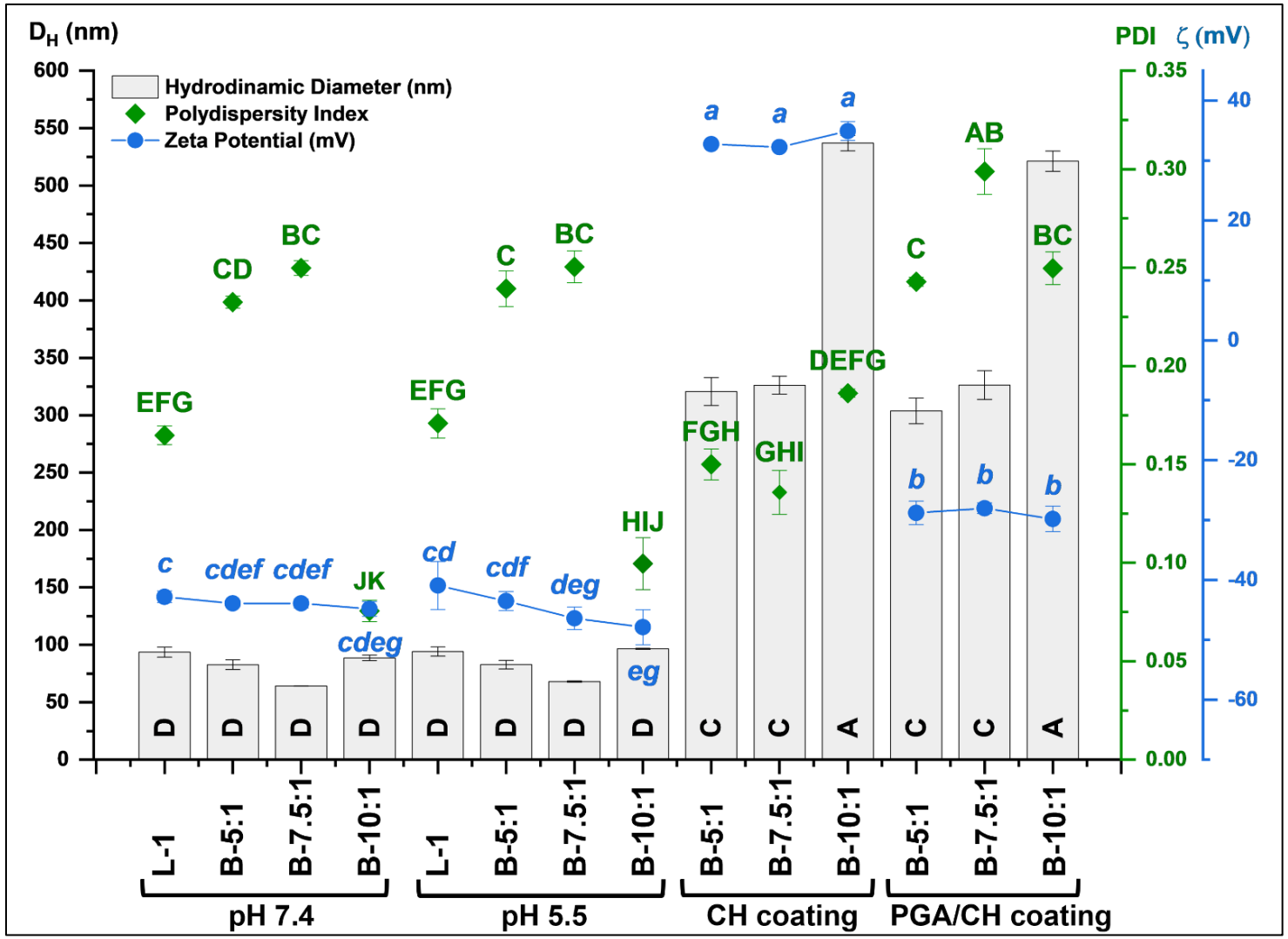

Figure 2.2 The D_H (▭), PDI (♦) and ζ potential (●) of *t*-res loaded liposomes, bilosomes, and CH-coated and PGA/CH-coated bilosomes. The data represent the mean±SD. Black capital letters represent significant differences in the D_H, green capital letters in the PDI, and blue lowercase letters in the ζ potential among the samples, respectively ($p < 0.05$).

The ζ potential turned from a negative to a positive (>30 mV) positive due to the adsorption of positively charged CH. The ζ potential of CH-B-5:1, CH-B-7.5:1, and CH-B-10:1 was 32.7±0.2 mV, 32.2±0.3mV and 34.9±1.6 mV, respectively. The ζ potential of CH-B-10:1 was significantly higher compared to ζ potential of CH-B-5:1 ($p<0.05$) **(Fig. 2.2)**. It has been reported that CH coating orders the phospholipid polar head groups and decreases the bilayer's membrane fluidity due to electrostatic interactions. This increases the rigidity of the bilayer and consequently enhances the stability against environmental stress (Tan et al., 2016). PGA was used as a second coating again achieved through electrostatic interaction between the positively charged amine group ($-NH_3^+$) of CH and the negatively charged carboxylate ion (-COO−) of PGA (Jeon et al., 2015). After PGA coating, there was some increase in the D_H, but it did not increase the D_H of CH-coated bilosomes significantly ($p>0.05$). This may be the result of stronger electrostatic interactions between the biopolymers deposited on the vesicles through polyelectrolyte interaction (Jeon et al., 2015). While D_H ranged from 303.8±11.2 nm to 326.3±12.4nm for 5 mM and 7.5 mM NaC containing empty and *t*-res loaded bilosomes, D_H of 10 mM NaC containing empty (504.4±6.6 nm), and *t*-res loaded bilosomes (521.2±8.8 nm) increased significantly ($p<0.05$). After PGA was coated on CH-coated bilosomes, PDI of B-5:0, B-5:1, and B7.5:0 samples increased significantly ($p<0.05$) but were still below 0.312. The ζ potential of CH-coated bilosomes turned from positive to negative, ranging from -28.0±0.9 mV to -30.3±1.4 mV **(Fig. 2.1-2.2)**. Alteration of ζ potential from negative to positive after the CH coating and positive to negative after the PGA coating verifies the success of the coating (Shishir et al., 2020).

2.4.1.2 Morphological behaviours

The size and shape of the empty liposomes and bilosomes were monitored by cryo-TEM and the structural properties of liposomes, bilosomes, CH-coated, and PGA/CH-coated bilosomes were investigated at 25 ºC by SANS and SAXS as the function of NaC concentration (5 mM, 7.5 mM, and 10 mM) at the constant lipid concentrations (10 mm POPC and 3.3 mM DOPG). The cryo-TEM micrographs show empty liposomes consisting of unilamellar, bilamellar, and trilamellar vesicles **(Fig. 2.3A).** The existence of a substantial population of MLVs after extrusion can result from using a relatively large pore size during extrusion, and working with zwitterionic phospholipids at the high ionic strength of the buffer (Scott et al., 2019). In order to decrease the lamellarity, the liposomes and bilosomes were already extruded through the small pore size (100 nm) and the negatively charged DOPG was used with POPC (zwitterionic) in the formulations to enhance the lamellar separation. However, the molarity of DOPG was less than neutral POPC by threefold in the formulations.

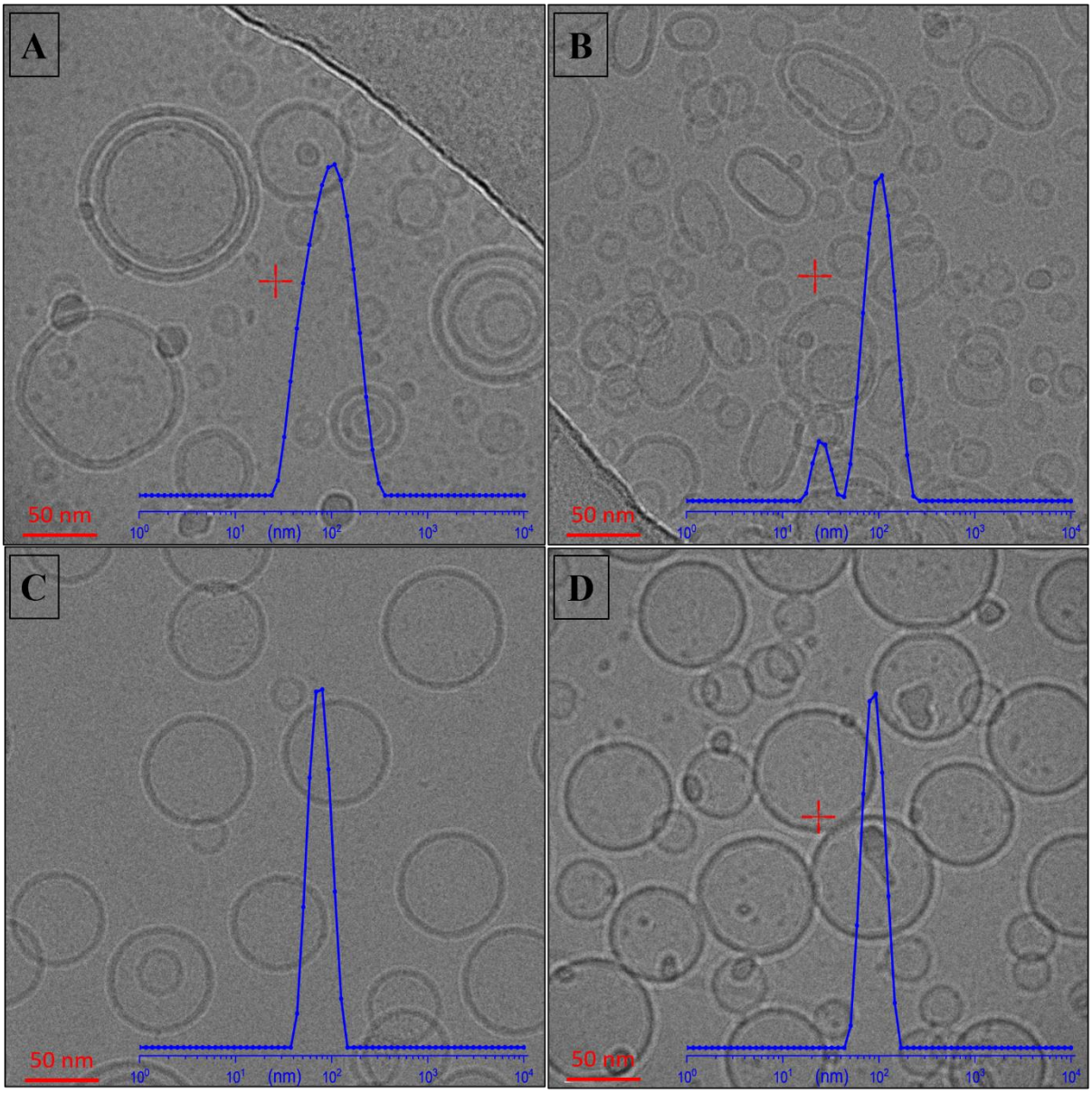

Figure 2.3 Cryo-TEM micrograph of **(A)** L-0, **(B)** B-5:0, **(C)** B-7.5:0, and **(D)** B-10:0. Scale bar: 50 nm. The insert is the corresponding particle size distribution (intensity (%) vs size (nm)) determined by DLS.

The SANS intensity (I) *vs* scattering vector (Q) of empty (L-0), and *t*-res loaded liposomes (L-1) at 25 ºC are given in **Fig. 2.4A**. Based on the cryo-TEM micrographs, a merged model combining uni-, bi- and trilamellar vesicles **(Appx. A.3.3)** were used for empty and *t*-res loaded liposomes and shell thickness (T_{shell}) was fixed to 40 Å because the T_{shell} of the phospholipid vesicles mainly depends on the molecular size of the lipids and is around 40 Å (Berti et al., 2011).

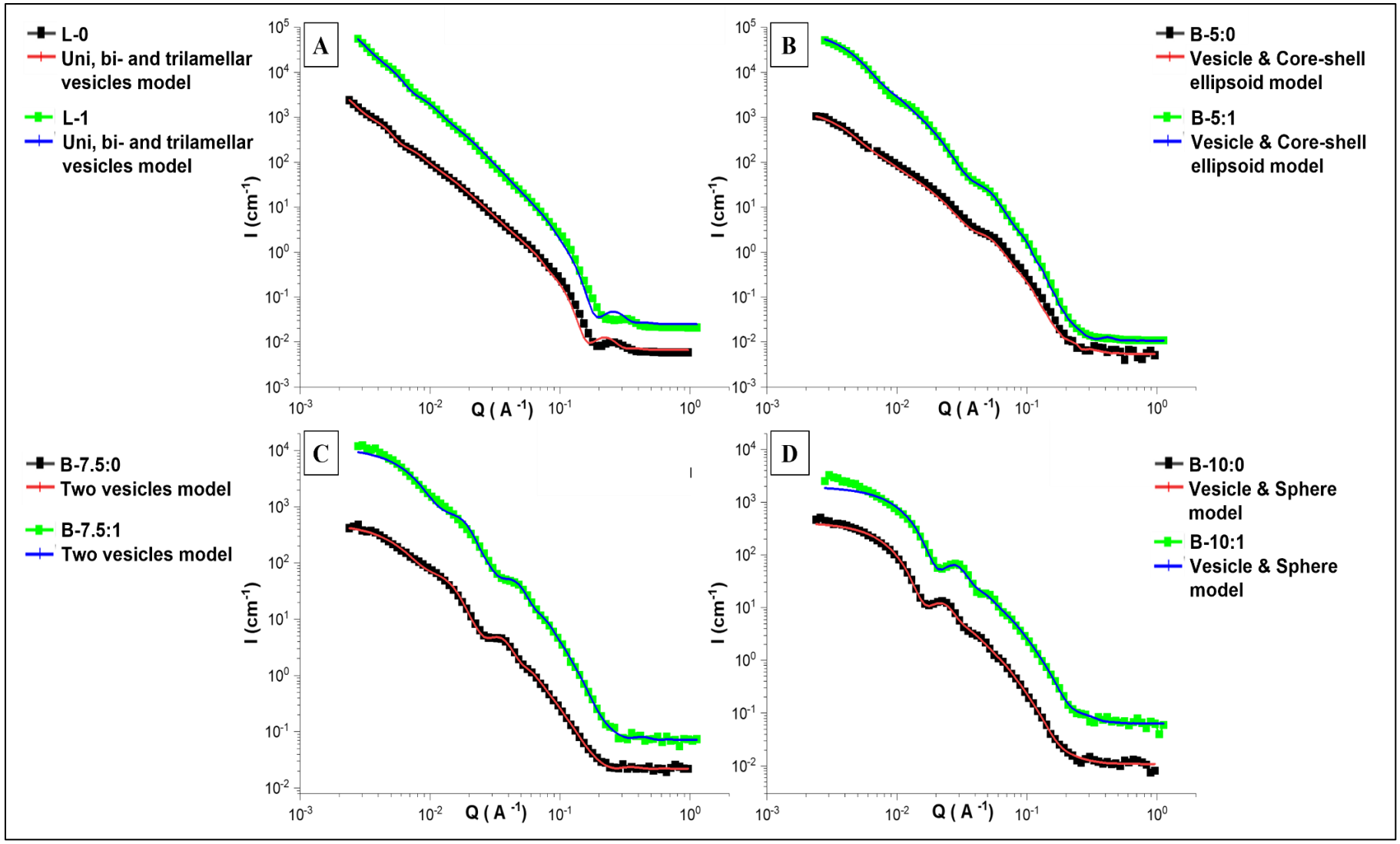

Figure 2.4 SANS profiles for empty and *t*-res loaded **(A)** L-0 and L-1, **(B)** B-5:0 and B-5:1, **(C)** B-7.5:0 and B-7.5:1 and **(D)** B-10:0 and B-10:1 at 25 °C. Data are plotted on a log−log scale. For clarity, SANS profiles are scaled on the y-axis.

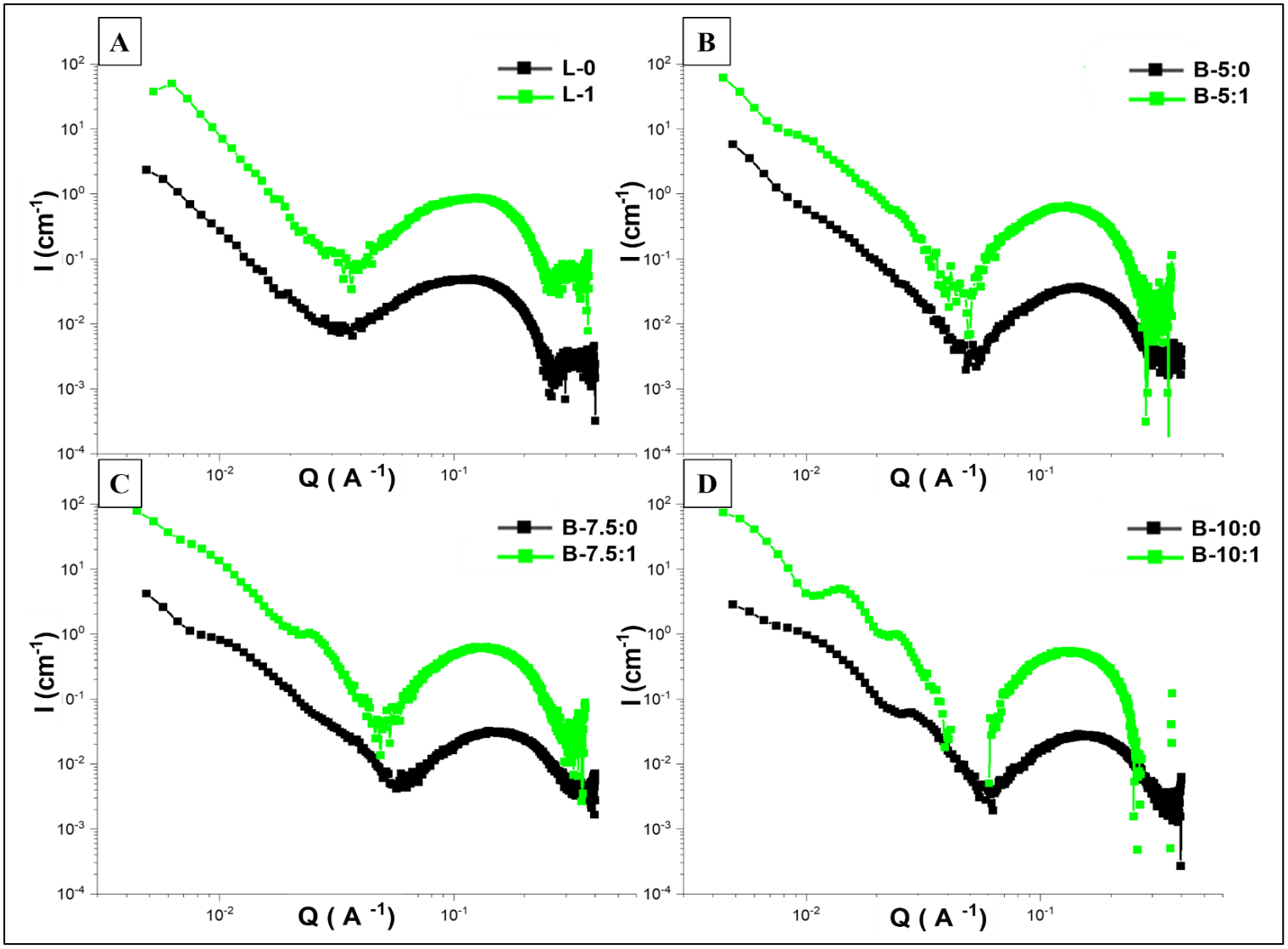

Figure 2.5 SAXS profiles for empty and *t*-res loaded **(A)** L-0 and L-1, **(B)** B-5:0 and B-5:1, **(C)** B-7.5:0 and B-7.5:1 and **(D)** B-10:0 and B-10:1 at 25 °C. Data are plotted on a log−log scale. For clarity, SAXS profiles are scaled on the y-axis.

Table 2.3 SANS data of empty and *t*-res loaded liposomes and bilosomes at 25 °C.

Sample	**Model**	**N_s**	**V_F**	**R_C (Å)**			**T_{shell} (Å)**	**PD**	**X^2**
L-0	uni-, bi- and trilamellar vesicles	1	0.0348±0.0002	385.3±1.1			40	0.469±0.004	42.5
		2	0.0004±0.0001	224.3±9.5			40	0.200±0.005	
		3	0.0047±0.0001	918.6±9.2			40	0.137±0.008	
L-1	uni-, bi- and trilamellar vesicles	1	0.0300±0.0001	393.0±0.5			40	0.371±0.008	47.0
		2	0.0007±0.0001	192.8±3.3			40	0.214±0.025	
		3	0.0039±0.0001	823.0±4.5			40	0.182±0.009	
Sample	**Model**	**Shape**	**V_F**	**R_C (Å)**			**T_{shell} (Å)**	**PD**	**X^2**
B-5:0	vesicle & core-shell ellipsoid	Vesicle	0.0045±0.0001	55.8±0.7			42.4±0.5	0.164±0.006	1.5
		Core-shell ellipsoid	0.017±0.0004	**R_{eq} (Å)**	**X_c**	**X_{ps}**	27.8±3.3	0	
				685.7±5.8	0.1± 0.00	1.2±0.2			
B-5:1	vesicle & core-shell ellipsoid	Vesicle	**V_F**	**R_C (Å)**			**T_{shell} (Å)**	**PD**	1.4
			0.004±0.0001	74.2±0.5			41.4±0.5	0.182±0.004	
		Core-shell ellipsoid	0.023±0.0005	**R_{eq} (Å)**	**X_c**	**X_{ps}**	32.3±2.8	0	
				597.1±6.5	0.2±0.00	0.9±0.1			
Sample	**Model**	**V_{no}**	**V_F**	**R_C (Å)**			**T_{shell} (Å)**	**PD**	**X^2**
B-7.5:0	Two vesicles	1	0.002±0.0001	276.3±1.5			42.4±0.8	0.200	14.6
		2	0.008±0.0001	102.7±0.2			24.6±0.3	0.200	
B-7.5:1	Two vesicles	1	0.003±0.0001	251.9±0.9			39.2±0.5	0.200	34.3
		2	0.007±0.0001	92.9±0.2			24.6±0.3	0.200	
Sample	**Model**	**Shape**	**V_F**	**R_C (Å)**			**T_{shell} (Å)**	**PD**	**X^2**
B-10:0	vesicle & sphere	Vesicle	0.007±0.0005	152.1±1.6			40.3±3.1	0.245±0.003	18.3
		Sphere	0.002±0.0005	19.5±1.6			-	0.003	
B-10:1	vesicle & sphere	Vesicle	0.009±0.0003	143.8±6.0			38.8±12.	0.228±0.006	40.8
		Sphere	0.002±0.0002	19.2±6.4			-	0.003	

N_S: shell number, V_{no}: vesicle no V_F: volume fraction of shell, R_C: core radius, T_{shell}: shell thickness, PD: Polydispersity, R_{eq}: Equatorial radius of core, X_c: axial ratio of core, X = r polar/r equatorial, X_{ps}: ratio of the thickness of shell at the pole to that at the equator, X^2: chi-square. The data represent the mean±SD.

Moreover, samples were prepared in Tris buffer that contain 150 mM NaCl which affects bending rigidity (K_c). The K_c is related to the energy necessary to change the membrane curvature of POPC and DOPG. According to the study on the Kc of POPC and POPC:(1-palmitoyl-2-oleoyl-sn-glycero-3-phosphoglycerol) POPG (1:1 molar ratio) as a function of the NaCl concentration, when the NaCl concentration was higher than 45 mM in the buffer, the Kc of POPC was higher than the Kc of POPC: POPG mixture (Faizi et al., 2019). Moreover, the presence of NaCl in the buffer also affected the electrostatic repulsion between the lipid bilayers due to the screening effect. As a result, using neutral POPC and NaCl may decrease the efficiency of preparation steps that produce ULVs because interlamellar repulsions (interlamellar hydration force, and electrostatic repulsion force) between layers, K_c of membranes, and membrane curvature are the determinants of the production of unilamellar and multilamellar structures (Jackman et al., 2014).

This model provided the best fit for the SANS data **(Table 2.3)** and showed that extruded L-0 and L-1 samples were mostly unilamellar, with a small subpopulation of bi- and tri-lamellar vesicles. The ULVs have the highest volume fraction (V_F) around 3.5% and 3% in the total vesicle population for L-0 and L-1 samples, respectively. For both samples, while the core radius (R_C) of ULVs was around 400 Å, the R_C of bi- and trilamellar vesicles was around 200 Å and 820-920 Å, respectively. According to the model, PD of the ULVs was ~0.470 and ~0.370 for L-0 and L-1 samples, respectively. For bi- and trilamellar vesicles, the PD was lower than 0.200. The high PD of the ULVs may have resulted from the multimodal size distribution. According to the DLS results, the hydrodynamic radius (R_H) of the L-0 and L-1 was ~420 Å and ~470 Å, respectively with similar PDI: ~0.172. The results from DLS and SANS are not comparable for these samples because samples have multiple size distributions and DLS gives the harmonic mean of D_H. However, if we consider ULVs were the majority due to the highest V_F, in the total vesicle population, their radius was close to the R_H which is slightly higher than the R_C because the D_H includes the hydrated shell (Kiselev et al., 2013).

The NaC is a bio-surfactant with a steroid nucleus that provides a rigid structure, so bile salts differ from more conventional surfactants. While the hydroxyl groups of the molecule are located on the concave side, methyl groups are located on the convex side (Moghimipour et al., 2015) and as a result, the CMC of NaC is not well defined. After the incorporation of 5 mM NaC into the liposome formulation, core-shell ellipsoidal structures appeared in addition to the spherical ULVs monitored by cryo-TEM **(Fig. 2.3B).** SANS data for 5 mM NaC-containing bilosomes (B-5:0 and B-5:1) were fitted merged model combined with the vesicle and core-shell ellipsoid model **(Appx. A.3.3)** which provides the best fit (**Fig. 2.4B**). According to modelled SANS

data **(Table 2.3),** while the V_F of ULV samples was ~0.4%, the V_F of core-shell ellipsoids in the B-5:0 and B-5:1 was 1.7% and 2.3%, respectively. The R_C of the vesicles of B-5:0 and B-5:1 was 55.8±0.7 Å and 74.2±0.5 Å respectively and T_{shell} was ~42 Å (PD: ~0.170) for both vesicle populations. When the T_{shell} and PD of core-shell ellipsoids of B-5:0 and B-5:1 was fitted in the model, it was observed that the T_{shell} values for the core-shell ellipsoids were reduced to around 10 Å, which is not feasible in a physical sense. To address this issue, the PD of the core-shell ellipsoids was set to zero, resulting in a more realistic T_{shell} value. Thus, the core-shell ellipsoid structures, as a majority in the system, had thinner T_{shell} (~30 Å) compared to ULVs according to the fitting. The R_H of the B-5:0 and B-5:1 was ~410 Å with PDI: ~0.240 according to the DLS measurement. The DLS calculates the D_H from the translational diffusion coefficient (D) by using the Stokes-Einstein equation with the assumption of a spherical particle and the D is inversely proportional to the D_H. However, in this system, the majority of the particles are ellipsoids, and their aspect ratio varies according to the cryo-TEM micrograph. Chen et al. studied the Brownian motion and D of the non-spherical microparticles and reported that the D was highly related to the anisotropy of the non-spherical particle. The D of the long axis of the ellipsoid are higher than the D of the short axis and the D was sensitive when the aspect ratio >2 (Chen et al., 2017).

When 7.5 mM NaC was added to the liposome formulation, the cryo-TEM micrograph showed that core-shell ellipsoidal structures returned to ULVs (**Fig. 2.3C).** According to the cryo-TEM micrograph, there are two vesicle populations in the B-7.5:0 and B-7.5:1 system at 25 ºC so the merged model combined with two vesicles **(Appx. A.3.3)** was used and provided the best fit (**Fig. 2.4C**). While smaller vesicles (R_C: ~100 Å and V_F: 0.75%) were dominant in both samples, the R_C of the bigger vesicles was ~250 Å with 0.25% of V_F **(Table 2.3).** The T_{shell} of the phospholipid vesicles mainly is around 40 Å (Berti et al., 2011). When the T_{shell} and PD were fitted in the model, the T_{shell} of both structures in the system was much lower than~40 Å, which is physically unrealistic, and PD was above 0.500. While phospholipids exhibit a highly organized bilayer (T_{shell}: 4-5 nm) arrangement in solid phases, the membrane undergoes a less organized and interdigitated structure in liquid phases. The terminal carboxyl group of the fatty acid chain can penetrate and overlap with the opposing bilayer because of several factors like temperature, osmotic pressure, or the introduction of hydrotropes, resulting in decreased T_{shell} (Battaglia & Ryan, 2005). Both POPC (16:0-18:1 PC) and DOPG (18:1(Δ9)/18:1(Δ9)) contain an unsaturated fatty acid as the lipophilic tails which are not anticipated to experience interdigitation (Polozova et al., 2005). In addition, there has been no observed interdigitation in POPC bilayers even at pressures of 5000 atmospheres (Chen et al., 2011). So, the PD of the systems was

fixed to 0.200 based on DLS results to get a realistic T_{shell} from the two-vesicle model. The T_{shell} of the smaller vesicles was 42.4±0.8 Å and 39.2±0.5 Å for B-7.5:0 and B-7.5:1, respectively. The T_{shell} of the bigger vesicles was around ~24 Å which does not represent the real T_{shell}. These low T_{shell} results might be because the bigger particles assumed as vesicles based on cryo-TEM in the systems were nonspherical. The core-shell ellipsoid structures were already observed in 5 mM NaC-containing bilosomes thus it is possible to have non-spherical structures, which affect the T_{shell} in the 5 mM NaC-containing bilosomes. In addition, the merged model did not fit well at low Q for the B-7.5:0 and B-7.5:1. This might also be because of non-spherical structures. According to the DLS results, the R_H of the samples was around 350 Å with ~0.225 of PDI. As has been mentioned before, because of the two-size distribution and the possibility of the existence of non-spherical structures, DLS and SANS results are not comparable.

Table 2.4 SANS and SAXS data of empty and *t*-res loaded CH-coated bilosomes (F4/F1:0.6) at 25 °C.

Sample	SANS				SAXS		
	Unified power-R_g model (Level:1)				Bilayer parameters		
	R_g (Å)	P_1	X^2	ρ:R_g /R_H	T_{shell} (Å)	T_{water} (Å)	d-spacing (Å)
CH-B-5:0	799.1±14.	2.499±0.00	2.1	0.52	38.0	15.8	53.8
CH-B-5:1	938.8±29.	2.568±0.01	2.7	0.59	38.0	15.6	53.6
CH-B-7.5:0	671.0±7.6	2.601±0.01	3.8	0.42	38.0	15.8	53.8
CH-B-7.5:1	691.2±9.2	2.575±0.01	2.1	0.42	37.6	15.8	53.4
CH-B-10:0	617.4±9.7	2.835±0.00	8.2	0.27	37.2	15.4	52.6
CH-B-10:1	601.2±7.0	2.749±0.00	8.8	0.22	37.2	15.0	52.2
R_g: radius of gyration, P_1: Power-law$_1$, X^2: chi-square, ρ: shape factor, R_H: hydrodynamic radius, T_{shell}: bilayer thickness, T_{water}: solvent thickness, d-spacing: the thickness of lipid plus water layer. The data represent the mean±SD.							

For 10 mM NaC-containing bilosomes (B-10:0 and B-10:1), the cryo-TEM graph **(Fig. 2.3D)** shows that vesicles were ULVs like the 7.5 mM NaC-containing bilosomes with higher PD and multi populations in the system. The merged model combining the vesicle and sphere model **(Appx. A.3.3)** provided the best fit of scattering data for B-10:0 and B-10:1 at 25 ºC given in **Fig. 2.4D**. The ULVs were the majority in the *t*-res loaded and empty 10 mM NaC containing bilosomes and have V_F: ~0.8% with T_{shell}: ~40 Å. Although the R_H and PDI of empty and *t*-res loaded samples were ~450 Å and ~0.100, their R_C, 3 times smaller than the DLS result, was around 150 Å with 0.230 of

PD according to SANS results **(Table 2.3).** The V_F of the spheres was 0.2% with ~20 Å of R_C. These small spherical structures were possibly mixed micelles of the lipid/bile salt because 10 mM NaC might be close to the range of the CMC of the NaC. When bile salts reach their solubilisation concentration, mixed micelles and monomers of the bile salts are yielded due to the disruption effect on lipid bilayers (Garidel et al., 2007). As seen in 7.5 mM NaC containing bilosomes, the merged model did not fit well at the low Q range of the B-10:0 and B-10:1. This system might still have some non-spherical structures or some aggregation in the system.

The SANS intensity (I) vs scattering vector (Q) of empty, and *t*-res loaded CH-coated bilosomes at 25ºC is given in **Fig. 2.6A-F**. The unified power-R_g (radius of gyration) model (Beaucage model) **(Appx. A.3.3)** which describes the different structures in the system was used to model SANS data of CH-coated bilosomes **(Table 2.4)**. While the R_g of the CH-B-5:0 and CH-B-5:1 was ~800 Å and ~940 Å respectively, the R_g of the other CH-coated samples was between ~600 Å to 700 Å. According to DLS, the R_H of the CH-coated bilosomes ranged from 1500 Å to 2500 Å. The R_H of the CH-coated samples was ~3 times bigger than their R_g because of the highly hydrated body and polymer chains of the CH. The shape factor ($\rho = R_g/R_H$) of the CH-coated samples decreased from 0.59 to 0.22 with an increasing concentration of NaC in the bilosomes. Low ρ values (from 0.59 to 0.22) of CH-coated bilosomes suggest that the CH around bilosomes was highly swollen, fuzzy, and polydisperse. In addition, the likely reason for the decreased ρ value with the increased concentration of NaC was the amount of CH used to coat 10 mM NaC-containing bilosomes was 2 times higher than the amount of CH used to coat 5 mM NaC-containing bilosomes. Because the ζ potential of bilosomes decreased with the increased NaC concentration in the system thus needing more biopolymer to coat the surface. The weak power-law$_1$ value of CH-coated bilosomes (~2.5) also supports the ρ values and shows that systems were highly swollen and polydisperse polymeric mass (Beaucage, 1996).

The data from the empty and *t*-res loaded CH-coated bilosomes obtained by the SAXS experiment are given in **Fig. 2.7A-F.** While there were no diffraction peaks in uncoated bilosomes, well-defined Bragg peaks were observed in the SAXS spectra of CH-coated bilosomes, which is an indication of lamellarity in the system. Both empty and *t*-res loaded CH-coated bilosomes presented first (Q: ~0.120 $Å^{-1}$), second (Q: ~0.240 $Å^{-1}$) and third order Bragg peaks (Q: ~0.360 $Å^{-1}$). The sequence of the Bragg peaks was 1:2:3 which shows the multilamellar structures and the intensity of the first-order Bragg peak increased as a function of the CH concentration.

The electron density profile (EDP) of CH-coated bilosomes obtained from the 3-peak model was calculated in **Table 2.5** according to **Appx. A.3.4.** The T_{shell}, water

thickness (T_{water}), and the thickness of lipid plus water layer (d-spacing=2π/Q) that corresponds to the thickness of the lipid plus water layer of CH-coated bilosomes are given. The EDP of the CH-coated bilosomes obtained from the 3-peak model is useful for understanding overall T_{shell} and T_{water} trends as a function of CH concentration but does not provide a precise determination **(Fig. 2.9A** and **Table 2.6)**. In addition, the Fourier artifacts and density fluctuations at the zero point of experimental data were detected. While the experimental EDPs of CH-coated bilosomes did not display the typical bilayers profile, the addition of the fourth-order diffraction peak can minimize Fourier artifacts (Rappolt, 2010). Thus, a theoretical EDP (4-peak method) was prepared with the addition of a forth-order Bragg peak (F4) for each CH-coated bilosomes. EDP which contains F4/F1 from 0.1 to 0.7 was plotted and the ratio which provided nearly flat CH_2 regions was chosen **(Fig. 2.8)**. According to the 4-peak method (F4/F1:0.6) in **(Fig. 2.9B** and **Table 2.6)**, the d-spacing of CH-coated bilosomes ranged from 52.2 Å to 53.8 Å. While the T_{shell} of the CH-coated samples ranged from 37.2 Å to 38 Å, T_{water} was between 15.8 Å and 15.0 Å. With increased CH concentration, both T_{shell} and T_{water} were reduced. The possible reason for the Bragg peaks and reduced d-spacing is that when bilosomes were added to the CH solution, the osmotic pressure of CH increased because of the increased salt concentration in the medium (Fernández-Nieves et al., 2003). The increased osmotic pressure of CH has been shown to dehydrate and push the structural order of the bilayer and turn ULVs into multilamellar structures (Amenitsch et al., 2004). In the liquid crystalline phase, T_{shell} of the POPC was reported as 37 Å (Kučerka et al., 2006).

In addition, the Bragg peaks became clearer with higher NaC concentrations, which require increased biopolymer for bilosome coating. Manconi et al. also reported an increased lamellarity after CH coating of empty and curcumin-loaded liposomes (Manconi et al., 2017). Bandara et al. investigated the structural changes on DOPC ULVs resulting from different hydrogel matrices such as PEG, poly(acrylamide) (PAM), gelatine, and alginate. After the addition of ULVs into the different hydrogels, while PEG and alginate showed significant and sharp first-order Bragg peaks, there was no peak after PAM coating. The Bragg peaks after gelatine coating were also significant but less sharp in the alginate- and PEG-coated samples. Different effects on liposome restructuring resulted from the formation mechanism of the hydrogels and their osmotic stress capability (Bandara et al., 2020). The peak (marked with green) in **Fig. 2.7E-F** emerged in the low Q region at 0.027 A^{-1} and 0.028 A^{-1} of the scattering curve of CH-B-10:0 and CH-B-10:1 respectively, indicating the aggregation of the system. In an aggregated system, the particles in the lattice touch each other. The radius of the aggregated vesicles was calculated as 134 Å (which compares well to the next nearest neighbour distance of 234 Å) and 130 Å (next nearest neighbour distance: 224 Å) for

CH-B-10:0 and CH-B-10:1, respectively. These results are matching with the R_C of B-10:0 (152.1±1.6 Å) and B-10:1 (143.8±6.0 Å) obtained from SANS data in **Table 2.3.**

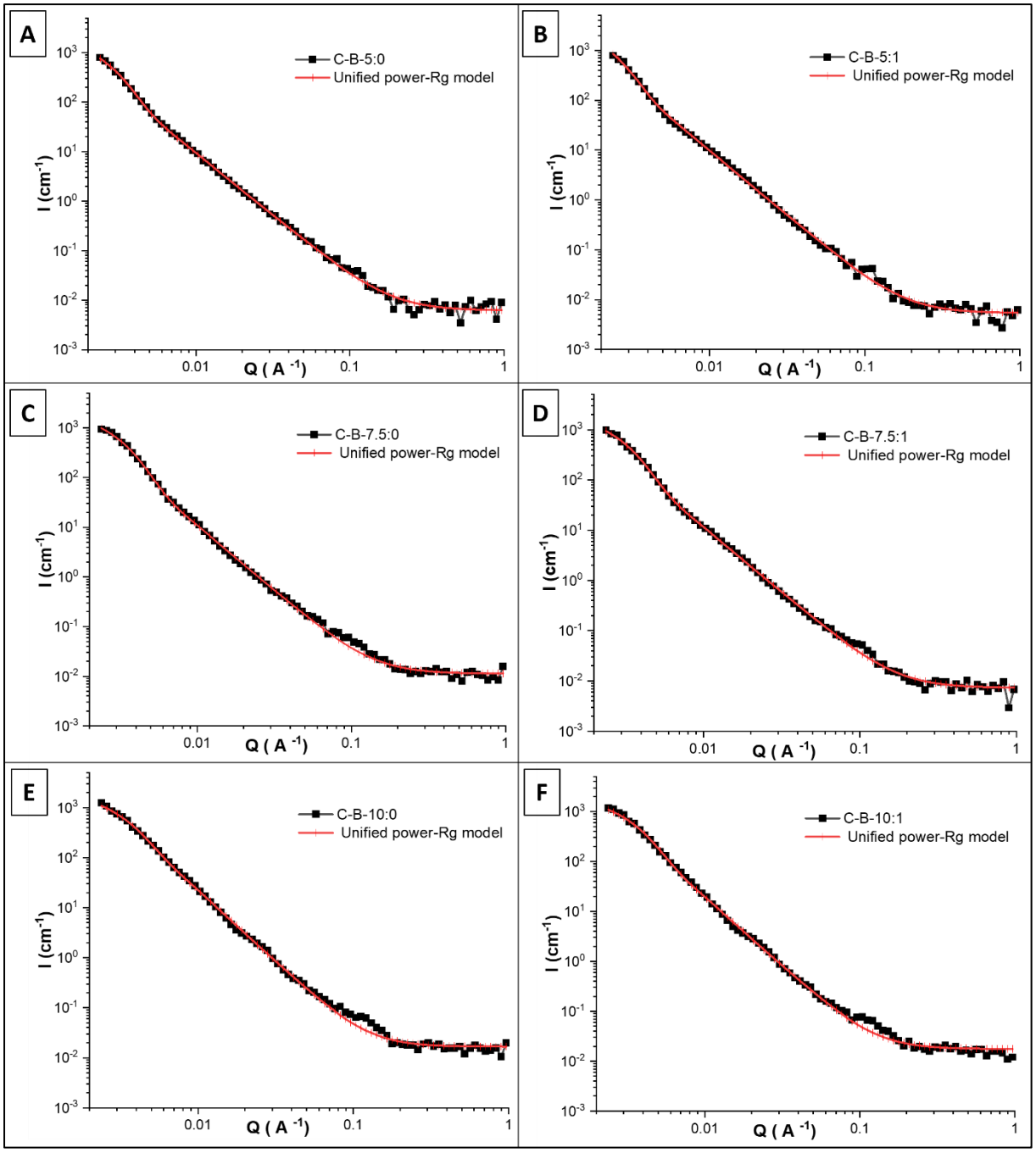

Figure 2.6 SANS profiles for empty and *t*-res loaded **(A)** CH-B-5:0, **(B)** CH-B-5:1, **(C)** CH-B-7.5:0, **(D)** CH-B-7.5:1, **(E)** CH-B-10:0, and **(F)** CH-B-10:1 at 25 °C.

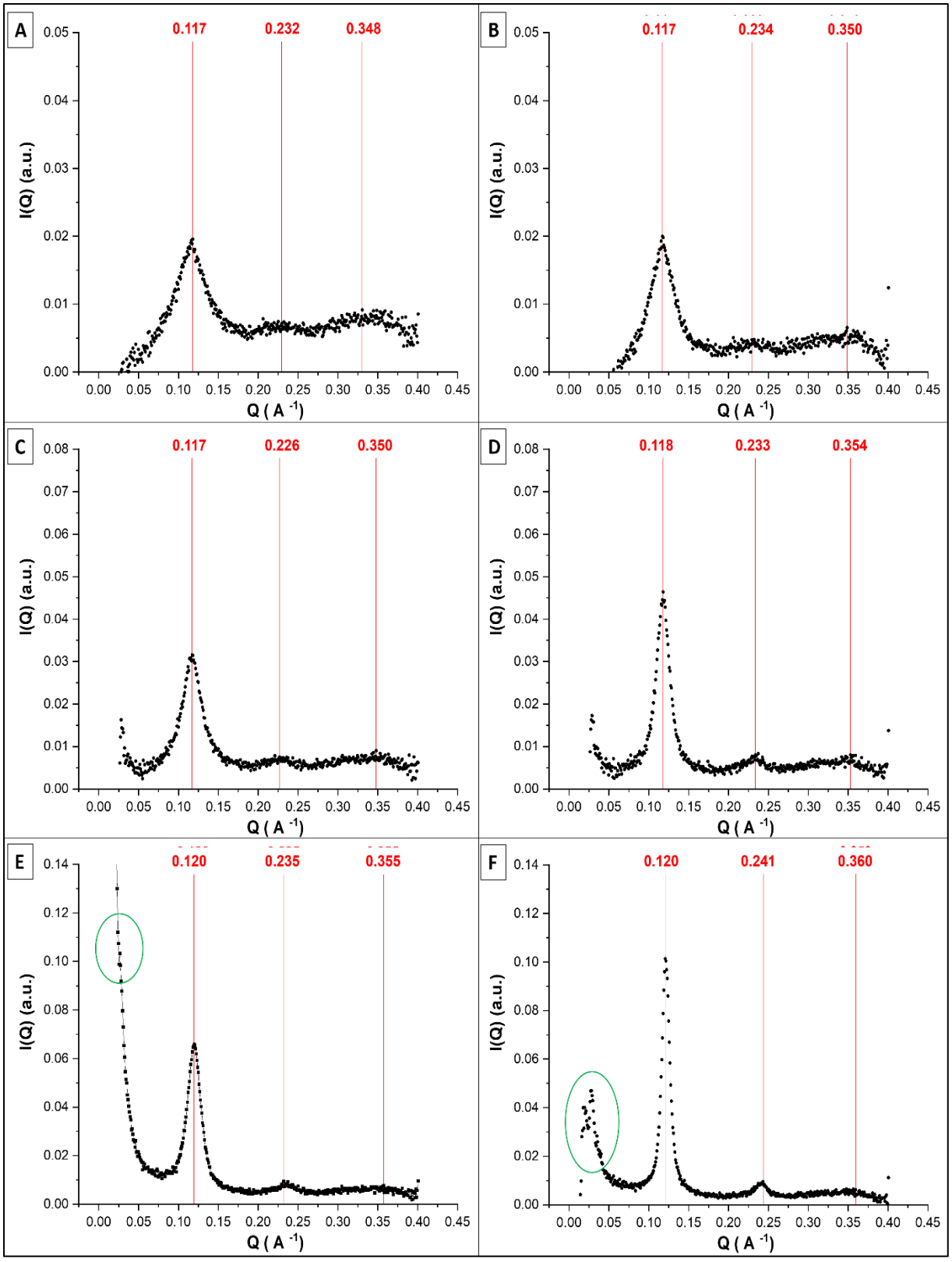

Figure 2.7 SAXS profiles for empty and *t*-res loaded **(A)** CH-B-5:0, **(B)** CH-B-5:1, **(C)** CH-B-7.5:0, **(D)** CH-B-7.5:1, **(E)** CH-B-10:0, and **(F)** CH-B-10:1 at 25 °C.

Table 2.5 Calculation of bilayer parameters of empty and t-res loaded CH-coated bilosomes measured by SAXS for 3-peak model and 4-peak method (F4/F1:0.6).

	h	XC	A	L_c: h^2.A	F(h):$\sqrt{Lc}$	F(h)/F(h:1)	d-spacing
CH-B-5-0	1	0.117	9.349	9.349	3.058	1.000	53.9
	2	0.232	0.951	3.804	1.950	0.638	54.1
	3	0.348	0.531	4.779	2.186	0.715	54.1
CH-B-5-1	1	0.117	9.092	9.092	3.015	1.000	53.5
	2	0.234	0.760	3.041	1.744	0.578	53.7
	3	0.350	0.503	4.524	2.127	0.705	53.8
CH-B-7.5-0	1	0.117	12.100	12.100	3.479	1.000	53.8
	2	0.226	1.618	6.471	2.544	0.731	55.6
	3	0.350	0.530	4.766	2.183	0.628	53.8
CH-B-7.5-1	1	0.118	12.800	12.800	3.578	1.000	53.3
	2	0.233	1.265	5.060	2.249	0.629	54.0
	3	0.354	0.938	8.439	2.905	0.812	53.2
CH-B-10-0	1	0.120	17.500	17.500	4.183	1.000	52.5
	2	0.235	1.566	6.264	2.503	0.598	53.4
	3	0.355	1.123	10.107	3.179	0.760	53.1
CH-B-10-1	1	0.120	17.300	17.300	4.159	1.000	52.2
	2	0.241	1.397	5.588	2.364	0.568	52.1
	3	0.360	0.612	5.505	2.346	0.564	52.3

h: order of Bragg`s peak, XC: centre of peak along x-axis, A: area, L_c: h^2.A, F(h):$\sqrt{Lc}$, d-spacing: the thickness of lipid plus water layer

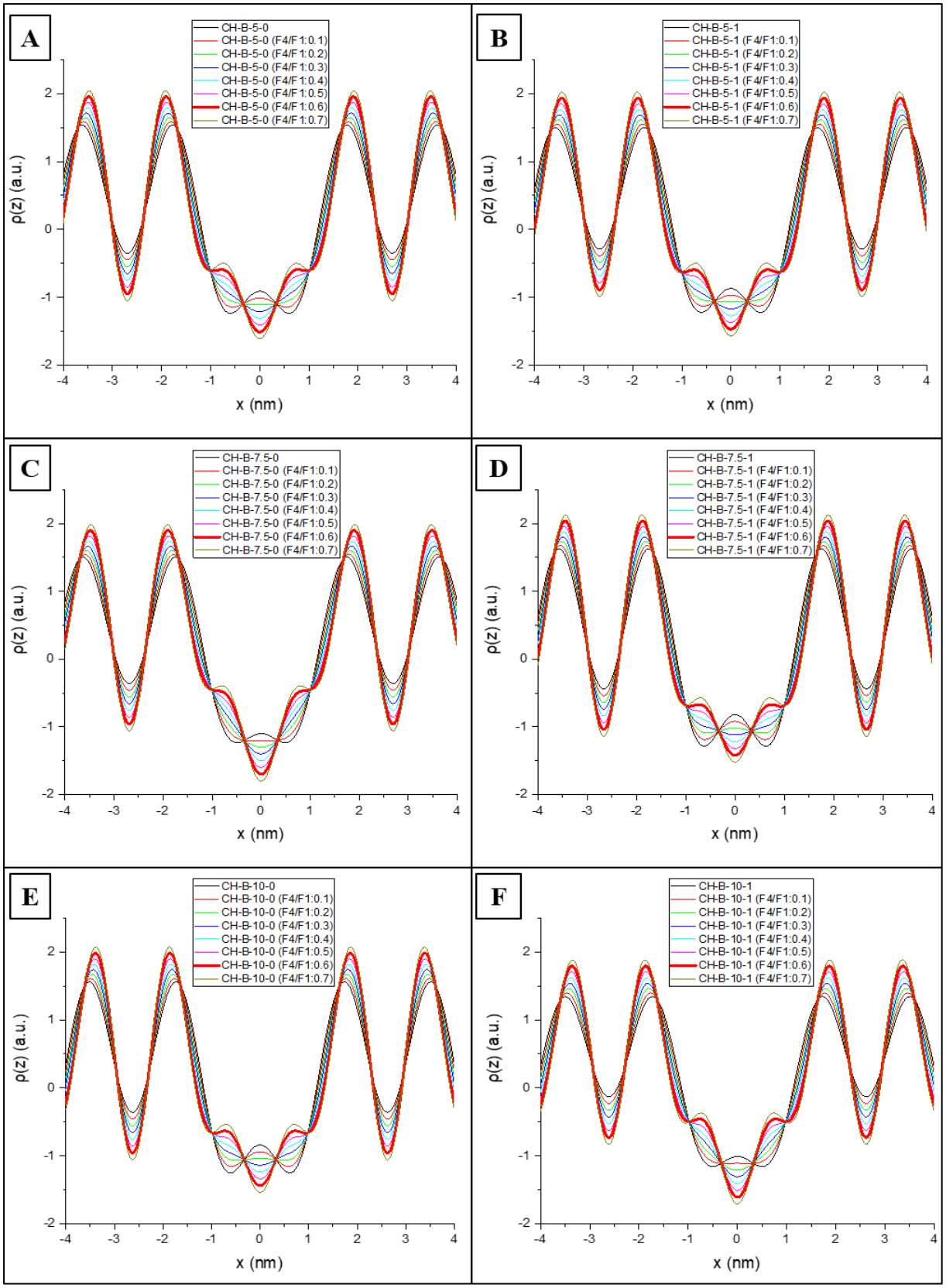

Figure 2.8 The EDP ρ(z) of bilayer obtained from the SAXS data for the first three diffraction orders and the theoretical electron density profile ρ(z) obtained from the refinement of the fourth-order amplitude (F4) from F4/F1:0.1 to 0.7 obtained by Fourier reconstruction with phases (-,-,+,-) for **(A)** CH-B-5:0, **(B)** CH-B-5:1, **(C)** CH-B-7.5:0, **(D)** CH-B-7.5:1, **(E)** CH-B-10:0, and **(F)** CH-B-10:1.

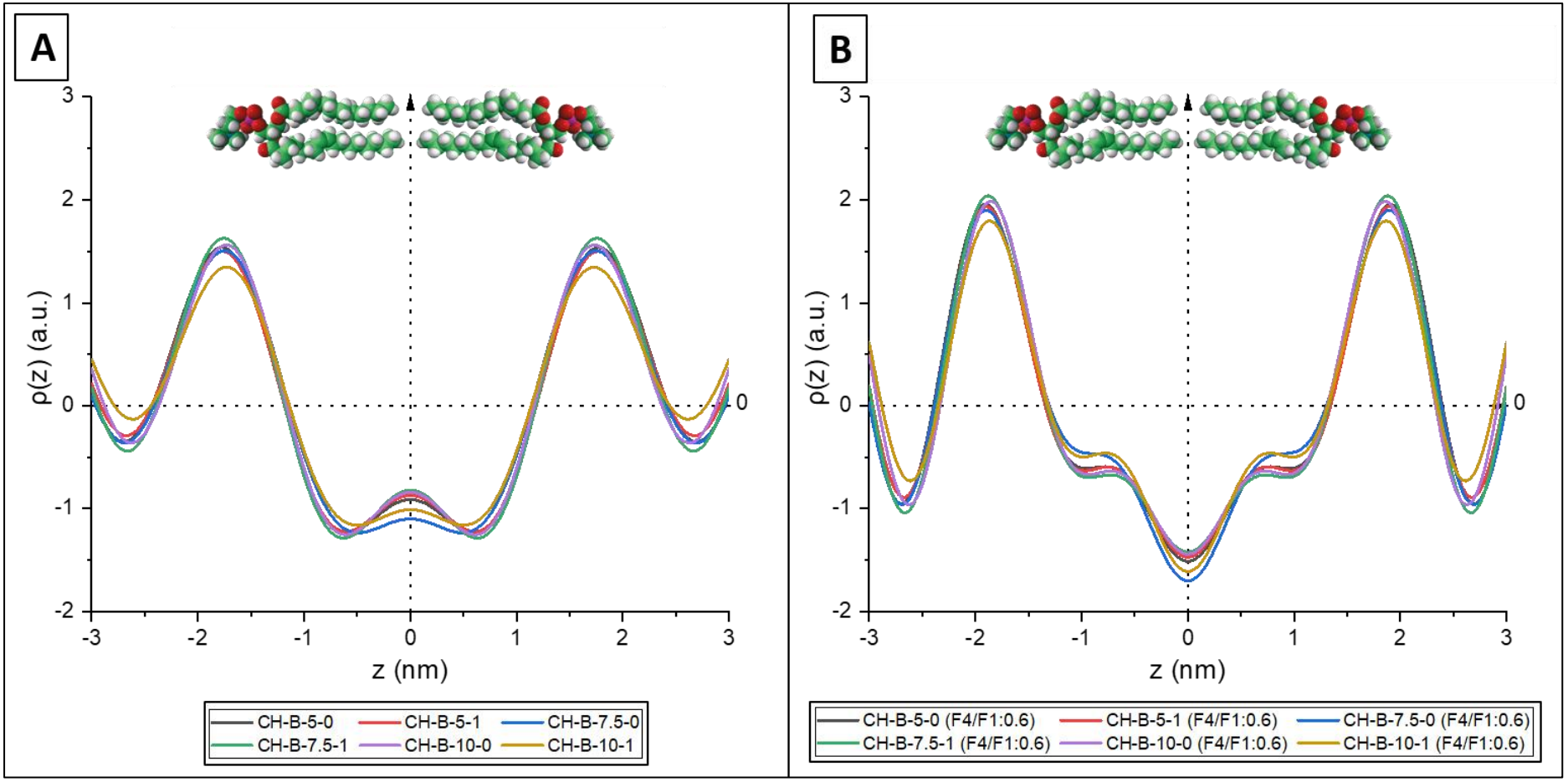

Figure 2.9 Bilayer electron density profile obtained from modelling the SAXS data of **(A)** empty and t-res loaded CH-coated bilosomes and **(B)** theoretical electron density profile ρ(z) of empty and t-res loaded CH-coated bilosomes (F4/F1:0.6) obtained by Fourier reconstruction with phases (-,-,+,-).

Table 2.6. Bilayer parameters of empty and t-res loaded CH-coated bilosomes measured by SAXS obtained from 3-peak model and 4-peak model (F4/F1:0.6).

3-peak method			4-peak method (F4/F1:0.6)		
T_{shell} (Å)	T_{water} (Å)	d-spacing	T_{shell} (Å)	Twater (Å)	d-spacing
35.6	18.4	54.0	38.0	15.8	53.8
35.2	18.2	53.4	38.0	15.6	53.6
34.8	19.0	53.8	38.0	15.8	53.8
35.2	18.2	53.4	37.6	15.8	53.4
34.8	17.8	52.6	37.2	15.4	52.6
34.4	17.8	52.2	37.2	15.0	52.2

SANS and SAXS scattering intensity (*I*) vs scattering vector (Q) of empty, and *t*-res loaded PGA/CH-coated bilosomes at 25 ºC are given in **Fig. 2.10- and Fig. 2.11**, respectively. Because it is common to see different structural levels for polymers in dilute solutions (mass-fractal scaling) (Beaucage, 2012), a unified power-R_g model **(Appx. A.3.3)** was used to model SANS data of PGA/CH-coated bilosomes **(Fig. 10A-F** and **Table 2.7)**. The model operates on the assumption that the levels consist of hierarchical formations (primary particles, aggregates, and agglomerates) that can be represented as mass fractals (Krzysko et al., 2020; Rai et al., 2012). A structure that exhibits self-similarity can be characterized by a fractal dimension (Colvin & Stapleton, 1985). CH and PGA are linear biopolymers. CH varies based on the differing quantities of attached glucosamine and N-acetyl-glucosamine residues. PGA is composed of galacturonic acid units arranged as a long polymer chain. Both CH and PGA are neither self-similar nor strictly random, but they are self-avoiding so can be characterized by fractal dimension (Colvin & Stapleton, 1985; Souza & Miller, 2011). The R_{g2} of the second level structure in the system ranged from 540±36 Å to 760±78 Å and the power law slopes decreased with increased concentration of PGA in the system. The ratio ρ for the second level structure in PGA/CH-coated samples was like the ρ of CH-coated bilosomes and between 0.50 and 0.21 which indicates a highly swollen and polydisperse polymeric fractal mass. The Rg_1 of first-level structures in the double-coated bilosomes ranged from 71.6±5.9 Å to 139.4±9.3 Å. While the power law (P_2) ranged from 1.6 to 2.5, The power law slope of the first structural (P_1) was between 2.6 and 3.5 for PGA/CH-coated bilosomes. When the power law slope is between 2<P<4, it is indicative of polymeric fractal mass. The first-level structures in the double-coated system might result from the salt-induced polyelectrolyte rearrangements caused by NaCl in the system. While the overall thickness of the shell appears to remain constant, the presence of salt may cause a breaking of the bonds

between oppositely charged polymers, local defects, and leakage of the small structures (Antipov et al., 2002).

In conclusion, the cryo-TEM, SANS, and SAXS data showed that varied sizes and shaped colloidal structures appeared with increasing NaC concentration. The demonstrated NaC-induced vesicle-to-micelle transition with increasing NaC concentration. After CH coating, systems were highly polydisperse, and swollen. The CH coating increased the structural order of the bilayer away from unilamellar structures and turned them into multilamellar structures due to osmotic pressure. After PGA coating, similar to CH coating, the systems were highly swollen, fuzzy, polydisperse and had multiple mode size distributions. The physicochemical properties of the bilayers can be modified with the addition of different concentrations of the bile salts depending on the desired structure and function. Moreover, the surface modification not only provided a difference on the surface but also in the bilayer properties.

Table 2.7 SANS data of empty and *t*-res loaded PGA/CH-coated bilosomes at 25 °C.

Sample	**Unified power-R_g model (Level:2)**					
	Level 1		**Level 2**		**X^2**	**ρ: R_{g1}/R_H**
	R_{g1} (Å)	**P_1**	**R_{g2} (Å)**	**P_2**		
PGA/CH-B-5:0	71.6±5.9	3.500±0.318	708.0±67.7	2.470±0.084	0.8	0.46
PGA/CH-B-5:1	85.3±7.8	2.982±0.223	756.5±78.1	2.437±0.095	1.1	0.50
PGA/CH-B-7.5:0	94.3±6.5	3.048±0.171	587.9±33.3	2.428±0.193	1.0	0.38
PGA/CH-B-7.5:1	90.8±11.7	2.922±0.224	541.4±35.5	2.473±0.182	1.3	0.33
PGA/CH-B-10:0	139.4±9.3	2.621±0.113	723.3±193.4	1.628±0.282	1.1	0.29
PGA/CH-B-10:1	125.3±0.2	2.799±0.145	555.8±104.0	1.623±0.413	1.4	0.21
R_g: radius of gyration, P_1: power-law$_1$, P_2: power-law$_2$, ρ: shape factor, R_H: hydrodynamic radius, X^2: chi-square. The data represent the mean ± SD.						

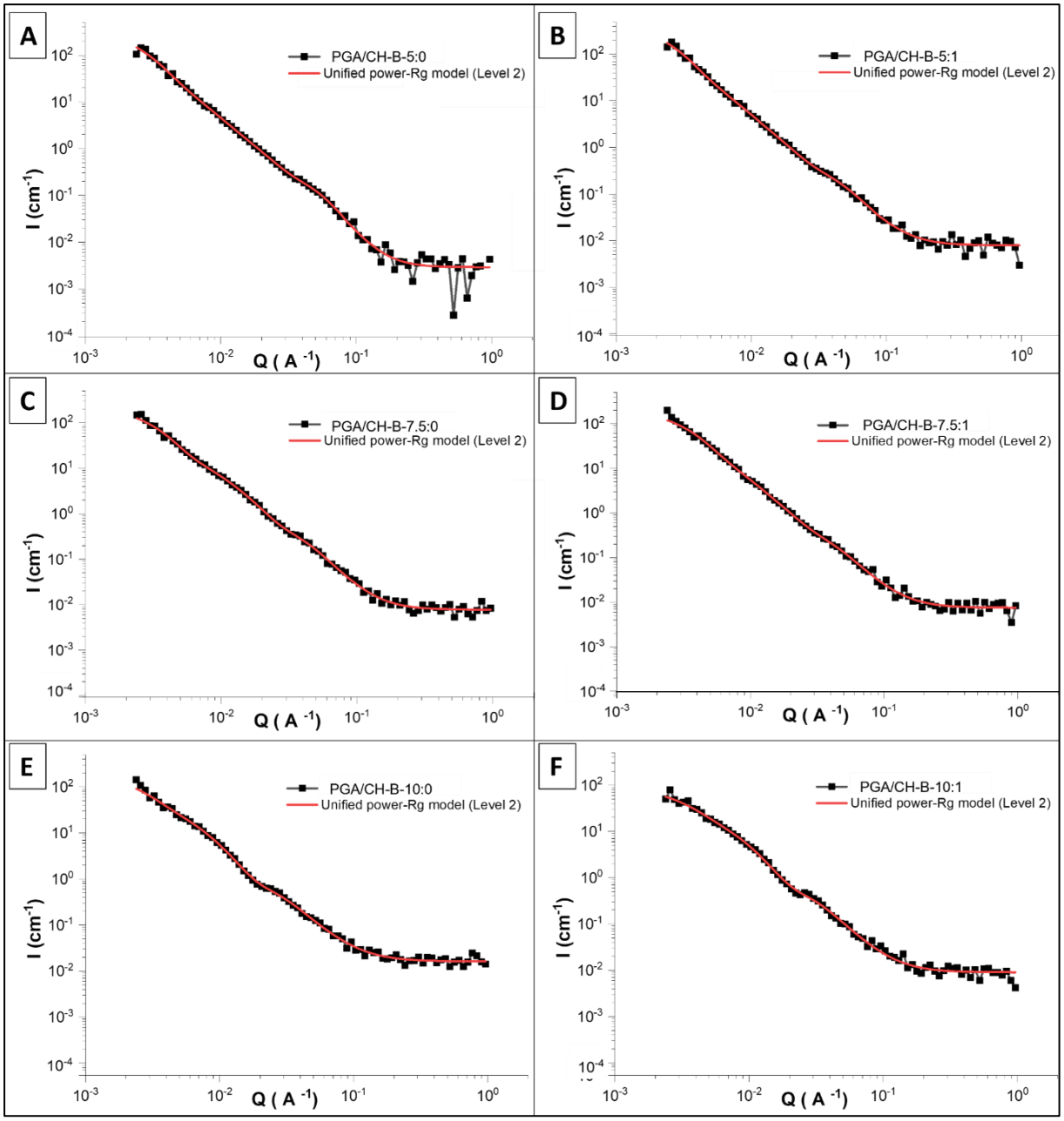

Figure 2.10 SANS profiles for empty and *t*-res loaded **(A)** PGA/CH-B-5:0, **(B)** PGA/CH-B-5:1, **(C)** PGA/CH-B-7.5:0, **(D)** PGA/CH-B-7.5:1, **(E)** PGA/CH-B-10:0, and **(F)** PGA/CH-B-10:1 at 25 °C.

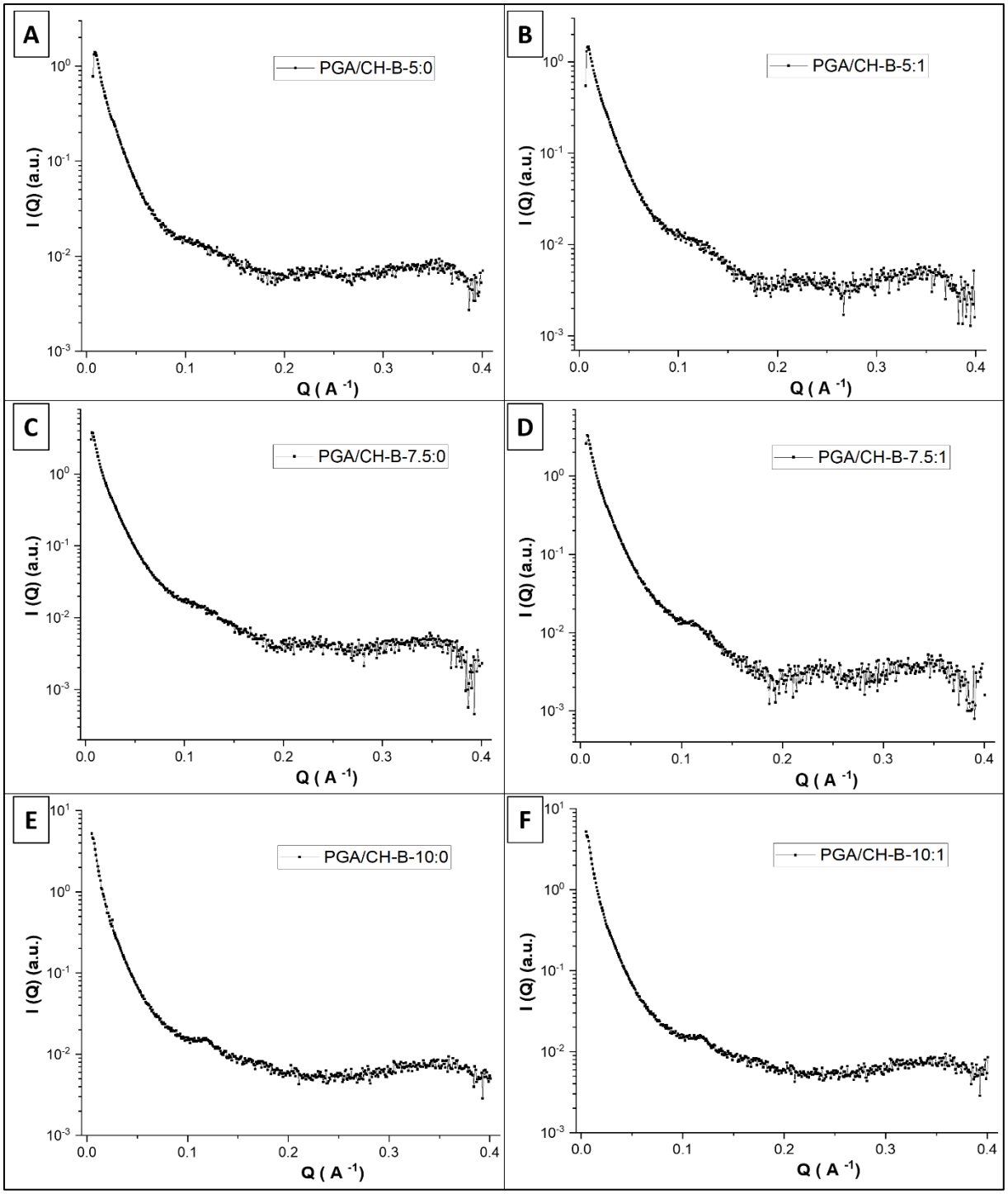

Figure 2.11 SAXS profiles for empty and *t*-res loaded **(A)** PGA/CH-B-5:0, **(B)** PGA/CH-B-5:1, **(C)** PGA/CH-B-7.5:0, **(D)** PGA/CH-B-7.5:1, **(E)** PGA/CH-B-10:0, and **(F)** PGA/CH-B-10:1 at 25 °C.

2.4.2 The chemical characterization of liposomes, bilosomes, CH-coated and PGA/CH-coated bilosomes

2.4.2.1 Fourier transform mid-infrared spectroscopy analysis

Adsorption of CH and PGA onto the bilosomes and the interactions of compounds in the formulations were analysed in the mid-infrared region (4000-550 cm^{-1}). Mid-IR can only penetrate a very shallow depth and identifies changes in major surface chemical functional groups (Roberts et al., 2018). IR spectra can be divided into two main regions as diagnostic region (>1500 cm^{-1}) and fingerprint region (<1500 cm^{-1}) which show the characteristics of the molecules. The major peaks in the diagnostic region for all compounds (POPC, DOPG, NaC, CH, PGA, and *t*-res) was -O-H stretching at 3390-3185 cm^{-1}, -CH and -CH_2 stretching at ~2900 cm^{-1}, and -C=O ester stretching at ~1770 cm^{-1}.

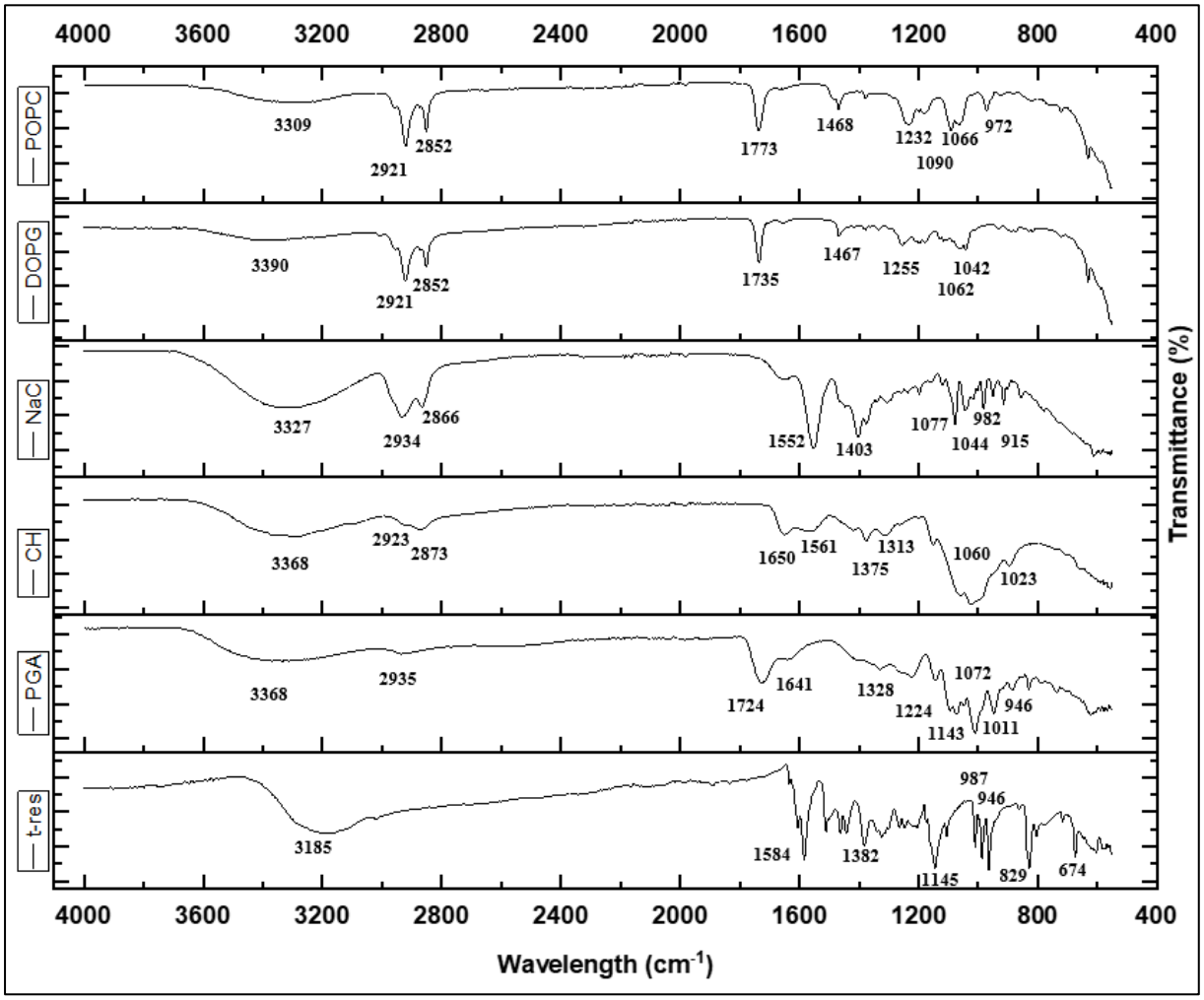

Figure 2.12 The FTIR spectrum of POPC, DOPG, NaC, CH, PGA, and *t*-res. For clarity, the FTIR profiles are scaled on the y-axis.

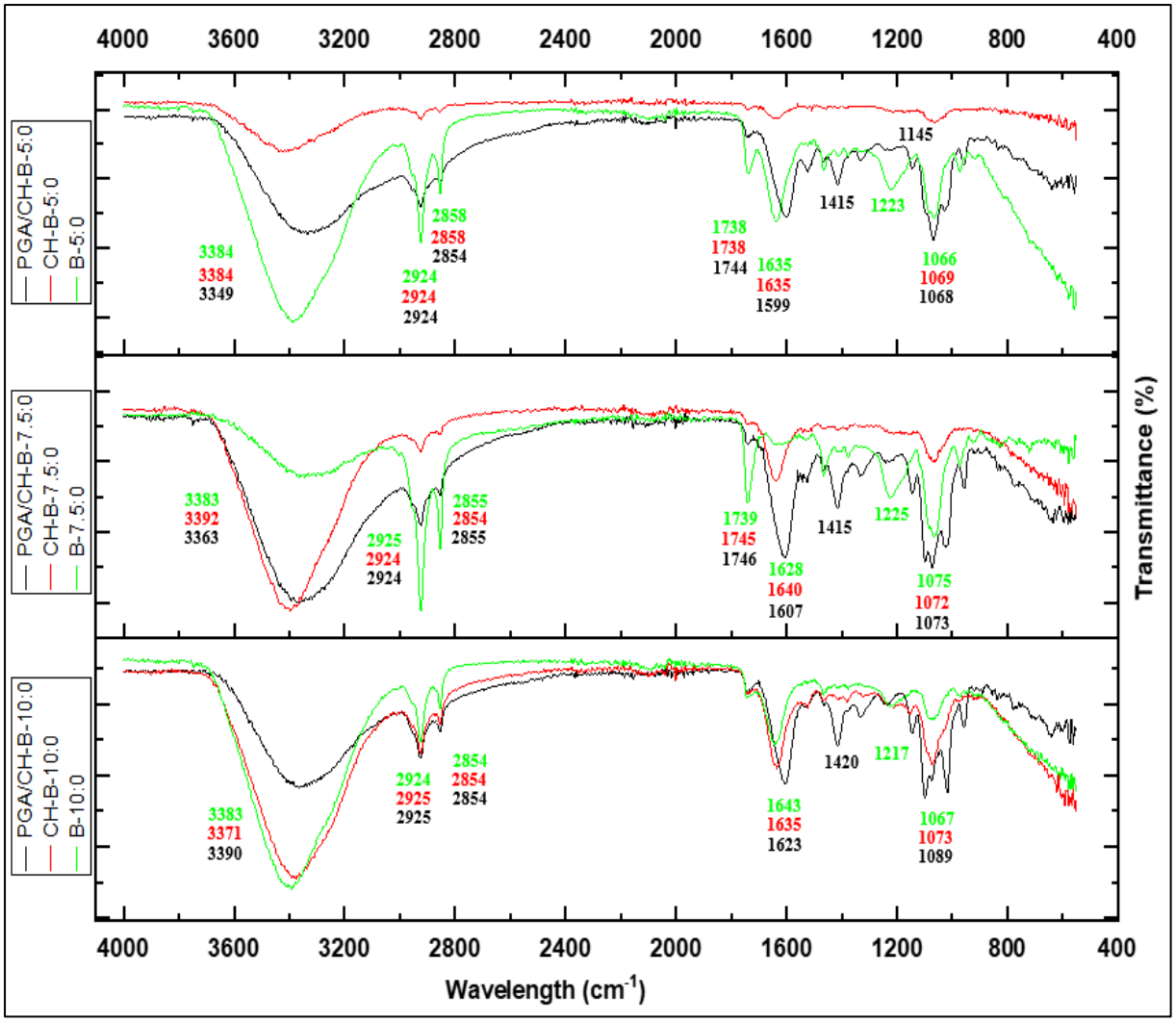

Figure 2.13 The FTIR spectrum of empty bilosomes, CH-coated and PGA/CH-coated bilosomes. For clarity, the FTIR profiles are scaled on the y-axis.

The major peaks of POPC in fingerprint region (**Fig 2.12**) were detected at 1468 cm^{-1} (C-H deformation) and 1232 cm^{-1} and 1090 cm^{-1} (PO^{2-} asymmetric and symmetric stretching) (Karim et al., 2020; Shishir et al., 2019). The same peaks slightly shifted were also observed for DOPG. Empty liposomes (L-0) have peaks that correspond to asymmetric and symmetric stretching of PO^{2-} between 1200 cm^{-1} to 1000 cm^{-1} band **(Fig. 2.14)**. The intensity of peaks at 1738 cm^{-1} and 1467 cm^{-1} for empty liposomes decreased or shifted after the addition of NaC into the liposomes, which might be related to the formation of new hydrogen bonds or the strengthening of hydrogen bonds (Cieślik-Boczula et al., 2012).

After CH coating, the main absorption peak of CH was slightly shifted from 1650 cm^{-1} (Amide I band) and the peaks for bilosomes at the 1210-1230 cm^{-1} band (PO^{2-} asymmetric and symmetric stretching) disappeared **(Fig 2.9-2.10).** Changes in this peak can result from the electrostatic interaction between the primary amine groups of CH and phosphate groups of bilosomes (Zhou et al., 2018). The absorption peaks

of PGA at 1724 cm^{-1} and 1641 cm^{-1} represent the C=O stretching of the methyl ester group ($COOCH_3$) and asymmetric C=O stretching of the COO^- group, respectively (Sene et al., 1994; Shishir et al., 2019). After PGA coating, the C-N amine II band of CH at 1561 cm^{-1} and asymmetric C=O stretching of the COO^- group of PGA (1724 cm^{-1}) were not observed after double coating possibly because of interaction between positively charged amine group ($-NH_3^+$) of CH and negatively charged carboxylate ion ($-COO^-$) of PGA **(Fig 2.9-2.10).** A peak at 1410-1420 cm^{-1} band to C-OH stretching of the carboxylic group was appeared after PGA coating (Rampino et al., 2016). The major peaks of *t*-res in the fingerprint region (**Fig 2.8**) were 1584 cm^{-1} (C=C alkene stretching), 1382 cm^{-1} (C-O stretching), 987 cm^{-1} and, 946 cm^{-1} (typical trans alkene stretching) and 829 cm^{-1} (deformational vibration of C-H group of benzene ring) (Schlich et al., 2020). The peaks of *t*-res in the fingerprint region **(Fig. 2.14)** were weakened after loading into lipid bilayers and the spectrum of empty and t-res loaded liposomes was similar.

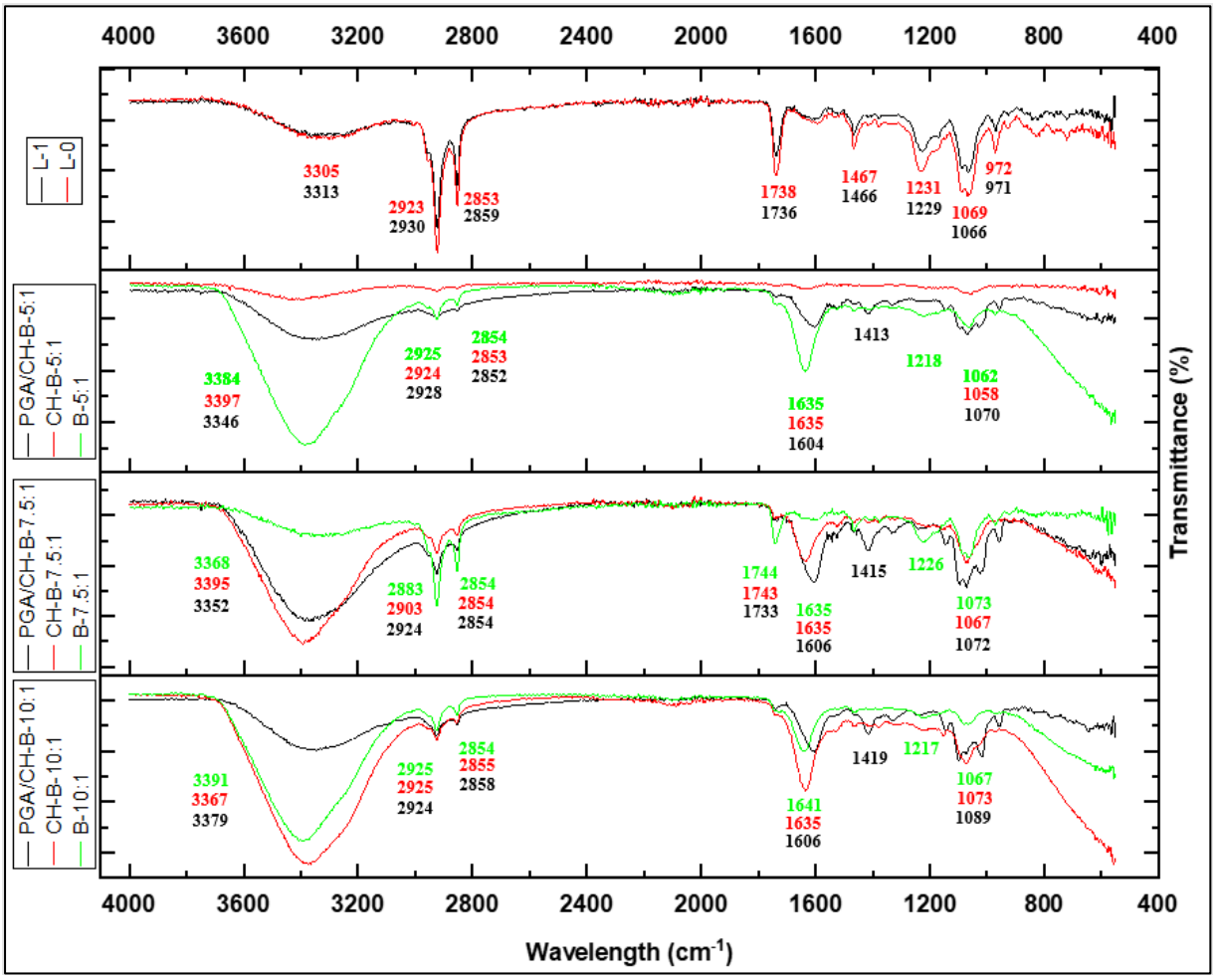

Figure 2.14 FT-IR spectrum of empty and *t*-res loaded liposomes, *t*-res loaded bilosomes, CH-coated and PGA/CH-coated bilosomes. For clarity, the FT-IR profiles are scaled on the y-axis.

The specific peak changes observed (such as the phosphate band of bilosomes, amine bands of CH, and carboxyl band of PGA) on FT-IR spectra after the application of biopolymer coatings indicate the successful coating of bilosomes with CH and PGA. Furthermore, the transformation of the ζ potential from negative to positive following the application of CH coating on bilosomes, and subsequently, the reversal of the ζ potential from positive to negative upon the introduction of PGA coating onto the bilosomes previously coated with CH, provide support for the successful deposition of the coatings.

2.4.2.2 Encapsulation efficiency and loading capacity

The EE and LC data of *t*-res loaded liposomes, bilosomes, CH-coated, and PGA/CH-coated bilosomes were obtained using HPLC (**Fig. 2.15**). The EE of liposomes was 86.0±4.7 % and the EE of bilosomes (90.6±1.7 % to 92.9 ±4.2 %) was not significantly higher than liposomes, ($p>0.05$). After coating bilosomes with CH and PGA, the EE of samples (87.0±5.0 % to 95.0±4.1 %) also did not change significantly ($p>0.05$). The high EE achieved for bilosomes compares well with previous studies. Huang et al. reported the EE of resveratrol was ~60% in the liposomes (Huang et al., 2019). Similarly, the EE of resveratrol in transfersomes composed of soy phospholipid and NaC was reported to be 72.32±3.45% (Arora et al., 2020). Abbas et al. prepared resveratrol-loaded liposomes (composed of Span 60, Chol, and NaDC), and CH-coated liposomes. The EE of resveratrol in liposomes was between 62.5±2.25 to 86.2±1.12. After coating the liposomes, EE (%) increased by around 85% (Abbas et al., 2021).

The initial *t*-res concentration was 0.23 mg/mL in all formulations. The LC of 2.3±0.1 % for liposomes was higher than all other samples. After adding NaC into the formulations, while the LC of *t*-res was slightly decreased for B-5 and B-7.5 ($p>0.05$), a significant decrease in LC of *t*-res was seen for B-10 formulations ($p<0.05$). There was a decrease in LC after the addition of NaC. Previous studies also reported similar LC of highly hydrophobic compounds in the liposomes. Cheng et al. prepared curcumin-loaded liposomes and rhamnolipids-modified liposomes. When the initial curcumin concentration was 0.2 mg/mL, LC was ~ 2% and EE was ~80% (Cheng et al., 2019). The LC and EE of the curcumin-loaded liposomes were reported as ~1.5% and 72%, respectively (Gómez-Mascaraque et al., 2017). The EE and LC of hydrophobic bioactive compounds are affected by the amount of solubilized compound in the hydrophobic domains of the bilayer and the LogP and chemical stability of the drugs (Peng et al., 2019). The location of resveratrol as a hydrophobic active compound is non-specific. Some studies report that resveratrol is embedded between the lipid bilayers of liposomes and bilosomes and is close to double bonds of fatty

acids (Koukoulitsa et al., 2011; Van Tran et al., 2019). Some other studies also reported the location of resveratrol between the head groups of phospholipids, stating that it penetrates the acyl chains but is close to the polar hydroxyl group in the head group (Brittes et al., 2010) and it changes the angle of the head groups thus decreasing the permeability of the bilayer (de Ghellinck et al., 2015). Overall, while EE of samples was above 86% and their LC was above 1.7%.

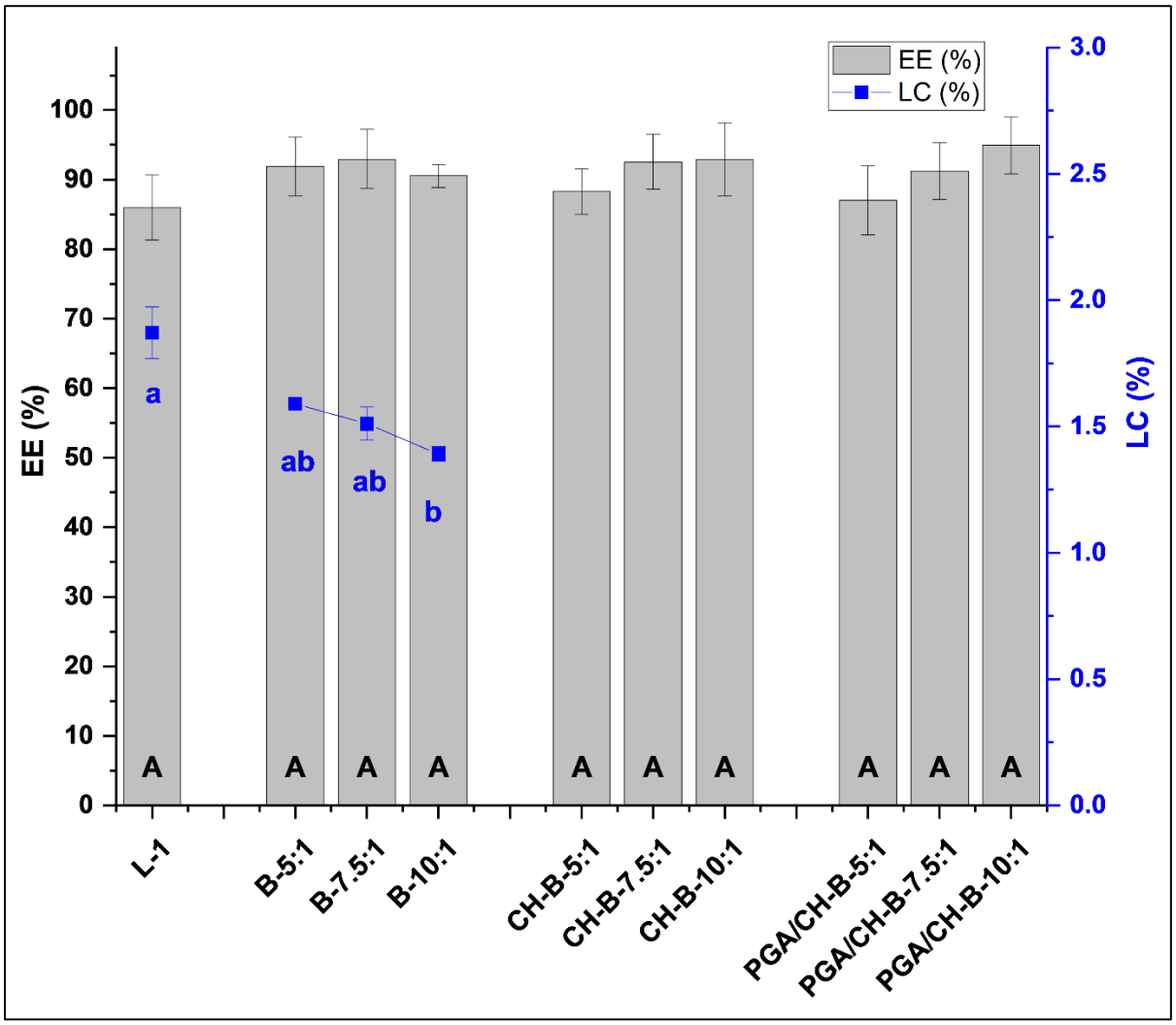

Figure 2.155 Encapsulation efficiency (EE %) (▭) of *t*-res loaded liposomes, bilosomes, and CH-coated and PGA/CH-coated bilosomes and loading capacity (LC %) (■) of *t*-res loaded liposomes, and bilosomes. The data represent the mean±SD. Black capital letters represent significant differences in EE, and blue lowercase letters in LC of the samples, respectively ($p < 0.05$).

2.5 Conclusion

This study seeks to contribute to understanding the effect of NaC on the POPC/DOPG bilayer properties and the effect of CH and PGA/CH coating on the surface properties of POPC/DOPG/NaC bilayers.

The physical properties of bilosomes as a function of NaC concentration in the vesicle-to-micelle transition and CH- and PGA/CH-coated bilosomes were characterised by a combination of dynamic and static light scattering (DLS, SANS, and SAXS) and electron microscopy (cryo-TEM). When NaC is incorporated into the lipid system, bile salts first locate in the outlet layer of the bilayer and then in the inner monolayer. Located bile salts cause a pore formation on the bilayer which results in bilayer fluctuations and the deformed bilayer begins to rupture and then the bilayer is converted to mixed micelles due to the powerful solubilisation effect of bile salts on phospholipid bilayers. The results show that the 5 mM NaC was incorporated in the lipid/bile salt system the shape of liposomes changed from ULVs with a subpopulation of bi- and tri-lamellar vesicles to vesicle and core-shell ellipsoid mixture. While the incorporation of the 7.5 mM NaC the liposomes turned into the ULVs with bimodal size distribution. For further increased NaC concentration (10 mM), the shape of the bilosomes was smaller-sized ULVs with bimodal size distribution with higher PD. In agreement with previous reports, the concentration of NaC in the lipid/bile salt system strongly affects bilayer interactions and the physical properties of the system.

FT-IR data showed that CH coating and PGA/CH coating onto the surface of bilosomes were successfully developed via electrostatic interaction. The effect of the biopolymer (CH and PGA) coating on the structure of the bilosomes was analysed by DLS, SANS and SAXS. SANS data did not provide information about the T_{shell} of the bilayer and thickness of CH coating because the scattering length density (SLD) of the lipids and CH is very close that layers in the structures were not visible. However, SANS data showed that CH-coated bilosomes were highly polydisperse which resulted in very swollen, and fuzzy structures. The Bragg peaks, an indication of multilamellarity, were observed in the SAXS spectra of the CH-coated bilosomes. The CH coating exerted an osmotic pressure and changed the structural order of the ULVs and turned them into multilamellar structures. As seen in CH-coated bilosomes, PGA/CH-coated bilosomes were also highly polydisperse and fuzzy and different structural levels of biopolymers were observed in the system. Furthermore, the biopolymer coating not only altered the surface properties but also impacted the bilayer properties.

Understanding the effect of bilayer and surface modification on the lipid bilayers and the characterization of their physical and chemical properties plays an essential role in controlling the fate of delivery systems in different environments such as the food matrix, the GIT, etc.

Chapter 3: The stability of *t*-res loaded liposomes, bilosomes, CH-coated and PGA/CH-coated bilosomes

3.1 Abstract

The degree of stability of the lipid bilayers during formulation or storage will significantly affect the physicochemical properties of the delivery vehicle and its application in food products. In this study, we investigated the effect of NaC addition on the physicochemical properties and stability of liposomes (bilosomes) and their further modification using biopolymers (CH and PGA). *t*-res was loaded into the systems as a model phenolic compound. Stability to different pH, during thermal treatment and storage were determined and the physicochemical properties (D_H, PDI, ζ potential, and DR) were measured. The results of this study indicate that liposomes and bilosomes showed good stability in different pH conditions (pH 3.0, 5.0, and 7.0), during thermal treatment (65℃ for 30 min), and storage conditions (4℃ and 20℃) for 28 days. Compared to liposomes, some changes in the physicochemical properties of the bilosomes were seen and bilosomes became more unstable with increasing concentrations of NaC in the system which causes increased bilayer fluidity. The CH-coated and PGA/CH-coated bilosomes were highly stable when the pH of the medium was far from the pKa of the biopolymer. After thermal treatment, the D_H of the biopolymer-coated bilosomes was significantly increased possibly because of increased swelling of the biopolymers with increased temperature. During storage, while sedimentation was seen for CH-coated bilosomes after 7 days, PGA/CH-coated bilosomes were highly stable in both storage conditions and seem to hinder the swelling and destabilisation of CH due to strong electrostatic interaction. The DR of all samples (~90%), was not affected significantly by the range of conditions used and protected the encapsulated *t*-res.

Keywords: bilosomes, resveratrol, chitosan, polygalacturonic acid, stability

3.2 Introduction

Bioactive compounds have a range of biological functions and health benefits such as antioxidant, anti-carcinogen, anti-tumoral, and anti-inflammatory activity when used alone or with other compounds (Amalraj et al., 2017; Mouhid et al., 2017). These biological functions and health benefits of bioactive compounds can be seen only when they reach the therapeutic concentration at the site of action. Recently bioactive-fortified functional foods have received remarkable attention due to their contribution to human health and growing consumer demand (Scarano et al., 2020). However, the

fortification of the food matrix with bioactive compounds can be problematic because of the poor solubility of some bioactive compounds. The incorporation of hydrophilic bioactive compounds into aqueous-based food products (beverages, sauces, dressings, soups, etc.) is easier because of their high aqueous solubility (McClements, 2015). Hydrophobic bioactive compounds such as well-known phenolic compounds resveratrol, quercetin, and curcumin, suffer from their very low solubility in aqueous media. The solubility of resveratrol is reported as <0.001 mol/L in aqueous media (Bonechi et al., 2012). The solubility of quercetin is ~1 µg/mL in water, 5.5 µg/mL in SGF, and 28.9 µg/mL in SIF (Aluani et al., 2016). Curcumin can dissolve only less than 0.6 µg/mL in pure water and 1 mg/mL in ethanol (Kurien et al., 2007). Thus, using some bioactive compounds as a powder can cause sedimentation in liquid products and undesired mouthfeel (Davidov-Pardo & McClements, 2014). Their utilization is also limited because of sensitivity to light, moisture, and heat and low chemical stability to oxidative degradation that can result in the generation of different free radicals (Chawda et al., 2017; Hu et al., 2018). In addition to their low solubility and sensitivity, interaction with other compounds and digestive conditions like fluctuation in pH, exposure to various enzymes, bile salts, and mucosal barriers in the GIT also cause low bioavailability of bioactive compounds (Mirafzali et al., 2014). These conditions affect shelf life, sensory characteristics, and consumer acceptability of the products fortified with bioactive compounds in a negative way (Ariyarathna et al., 2015).

Liposomes are one of the most commercialized delivery vehicles in the pharmaceutical field because of their biocompatibility, biodegradability, low toxicity, and achieving the desired bioactivity of the encapsulated compounds with reduced dose and controlled delivery (Pasarin et al., 2023; Sebaaly et al., 2021; Yu et al., 2021). The favourable outcomes from the use of liposomes in the pharmaceutical industry have led to liposomes being used in food and nutraceutical applications to provide protection during food processing, stability for extended shelf life, and controlled delivery for bioactive compounds suffering from sensitivity and low bioavailability. E- and C-loaded liposomes were prepared to fortify orange juices (Marsanasco et al., 2015) and chocolate milk (Marsanasco et al., 2016). After fortification using vitamin E- and vitamin C-loaded liposomes, both food samples were considered suitable for large-scale production. However, liposomes may suffer from instabilities during food processing at the industrial level (pH, thermal treatment, storage, light, etc.) and during gastrointestinal digestion (pH, enzymes, bile salts, etc.) (Pasarin et al., 2023; Zhou et al., 2021). The liposomes can undergo oxidation, hydrolysis, and aggregation during preparation or storage and show low physical and chemical stability (Yu et al., 2021). The body of liposomes is composed of phospholipids which may be susceptible to oxidation and hydrolysis. Unsaturated fatty acids of phospholipids are prone to

oxidation and the ester moieties can undergo hydrolysis. All these may cause structural changes or disruption of liposomes and drug leakage and consequently negatively affect the controlled release of active compounds and shortened shelf-life (Rideau et al., 2018). Moreover, during digestion, the acidic environment of the stomach can hydrolyse the ester moieties in the liposome body, and the intestinal enzymes and bile salts attack the bilayer to solubilise to micelles (Sebaaly et al., 2021). Thus, it is essential to check the stability of the liposomes in various conditions.

The physicochemical instability of liposomes can be improved in food processing and storage conditions and the environment of the GIT, by the addition of new compounds to modify the bilayer or coat their surface (Pasarin et al., 2023; Yu et al., 2021). While compounds such as Chol, surfactants (Liu et al., 2022), and bile salts (Tang et al., 2021) can change the bilayer properties like the membrane fluidity and packing capacity, a variety of polymers such as CH (Bang et al., 2011), PGA (Lopes et al., 2017) and alginate (Liu et al., 2013) can be used to modify the surface of the bilayer to decrease lipid oxidation (Panya et al., 2010), decrease the leakage of encapsulated compounds, control release properties of the particle (Refai et al., 2017) and enhance the stability against environmental stresses (Tai et al., 2020). Wechterbach et al. prepared vitamin C-loaded liposomes with/without Chol. Chol addition to the liposome formulation improved the thermal stability of vitamin C during short thermal treatment at 72°C (Wechtersbach et al., 2012). Resveratrol and EGCG-loaded liposomes were prepared, and liposomes were coated using LM-pectin. Orange juice was fortified using coated and uncoated liposomes. After pasteurization (65°C, for 30 min), coated liposomes showed higher stability and antioxidant activity compared to resveratrol, EGCG, and resveratrol/EGCG liposomes. Coated liposomes were also more stable in orange juice (Feng et al., 2019). A whey permeate drink was fortified using quercetin-loaded liposomes and whey protein isolate-coated liposomes. Coated liposomes provided improved physical stability against storage conditions (4°C, 20°C, and 40°C) and SGF compared to uncoated liposomes (Frenzel et al., 2015).

In this study, the effect of the modification of the lipid bilayer using bile salt (NaC) and the modification of the surface using biopolymers (CH and PGA) on the physicochemical properties and stability of the lipid/bile salt and biopolymer(s)-coated lipid/bile salt system was investigated. Liposomes and bilosomes were prepared and then bilosomes were coated with CH and PGA/CH polyelectrolyte complexes. *t*-res was used as a model hydrophobic phenolic compound. The pH stability, thermal stability, and storage stability were tested and the effect of the incorporation of NaC and the effect of CH- and PGA/CH-coating before, during, and after stability conditions was determined in terms of D_H, PDI and, ζ potential. The DR of the systems was measured.

3.3 Materials and methods

3.3.1 Materials

POPC (16:0-18:1 PC), and DOPG (18:1 (Δ9-Cis) PG) were purchased from Avanti Polar Lipids, USA. NaC hydrate (BioXtra, ≥99%), Tris base, (3,4′,5-Trihydroxy-trans-stilbene) (*t*-res), LMW-CH with 75-85% deacetylation, PGA with ≥85% (titration) from oranges, TPP, and Triton X-100 were purchased from Sigma Aldrich, UK. Chloroform, methanol, NaCl, and EDTA were purchased from Merck, UK.

3.3.2 Preparation of *t*-res loaded liposomes, bilosomes, CH-coated and PGA/CH-coated bilosomes

t-res loaded liposomes and bilosomes were prepared using thin-film hydration followed by the extrusion method with minor modifications reported by (Coreta-Gomes et al., 2015) **(Table 2.1).** Briefly, POPC: DOPG (10:3.3 molar ratio), NaC, and *t*-res were dissolved in a mixture of chloroform and methanol (80:20, v/v) and solvents were evaporated using a Genevac (EZ-2 plus) (Fisher Scientific Ltd, Leicestershire, UK) (25℃, Method: Very Low BP Mix) to obtain a dried lipid film. The lipid film was hydrated with Tris buffer (10 mM, pH 7.4) containing 150 mM NaCl and 1 mM EDTA and vortexed at RT for hydration. The hydrated suspension underwent 5 freeze-and-thaw cycles and then was sonicated using QSonica Sonicator (80% amplitude, 1s on, 2 s off for 5 min.) Samples were extruded (Avanti Polar Lipids, USA) through a 100 nm polycarbonate membrane (Nuclepore, Whatman Inc., UK) 21 times to obtain ULVs.

NaC/CH ratio (w/w) and CH/PGA ratio (w/w) were chosen at 0.5 and 0.4 respectively for the biopolymer coating of bilosomes according to the optimisation done previously **(Fig. B.13-16)**. For CH-coated samples, bilosomes (pH 5.5) were added dropwise into the CH solution (3 mg/mL, pH 5.5) under magnetic stirring (500 rpm) at RT. A 0.1% TPP (v/v) solution was used as a cross-linker. Samples were stirred overnight under magnetic stirring (500 rpm) at RT and were sonicated using QSonica Sonicator (35% amplitude, 1s on, 2s off for 10 min.). For PGA coating. CH-coated bilosomes (pH 5.5) were added dropwise into PGA solution (3 mg/mL, pH 5.5) under magnetic stirring (500 rpm) at RT. Samples were sonicated (35% amplitude, 1s on, 2 s off for 3 min.). Samples were filtered through a 1.5 µm nylon filter and finally were stored in a refrigerator at 4°C in the dark for further analysis. All liposomes, bilosomes and, biopolymer-coated bilosomes were prepared in triplicates.

3.3.3 Characterisation of *t*-res loaded liposomes, bilosomes, CH-coated and PGA/CH-coated bilosomes

3.3.3.1 Hydrodynamic diameter, polydispersity, and zeta potential

The D_H and PDI of samples were analysed by DLS using a Zetasizer Nano ZS series (Malvern Instruments, Malvern, UK) at 25 °C. The RI of liposomes used was 1.45, and the absorption coefficient was 0.001. The type of cuvette used was DTS0012. The ζ potential of samples was analysed by the Zetasizer Nano ZS series equipped with a 633 nm helium/neon laser at a detector angle of 90°. The type of cuvette used was DTS1070. Samples were diluted 50-fold using Millipore water to avoid multiple light scattering effects. Measurements were performed on triplicate samples.

3.3.3.2 Drug Retention

Free *t*-res separated from liposomes and bilosomes using a high-speed centrifuge (Beckman Coulter, Avanti Centrifuge J-30I) at 108800xg for 60 min at 4°C and from CH-coated and PGA/CH-coated samples using a centrifuge (Thermo Scientific, Fresco 21) at 21000xg for 60 min at 4°C. After centrifugation, supernatant and pellets were dried at 25°C using a Genevac (EZ-2 plus) (Fisher Scientific Ltd, Leicestershire, UK), and then dried samples were dissolved in methanol. Samples were filtered through a 0.20 µm polytetrafluoroethylene (PTFE) filter for HPLC. The HPLC method (Ares et al., 2015) was used to determine the free amount of *t*-res in the samples. Measurements were performed on triplicate samples. DR of samples was calculated by using the following equation (Eq. 3.1).

$$\text{DR (\%)} = \frac{\text{total tres (mg)-free tres (mg)}}{\text{total tres (mg)}} \text{x100} \qquad \textbf{Eq. 3.1}$$

3.3.4 Quantification of *t*-res using HPLC-DAD

The concentration of *t*-res in the filtrate was determined using the LS-MS (Shimadzu, Japan) system controlled by LabSolutions software (version 5.97) (Ares et al., 2015) with DAD. An Ascentis® Express C18 (2.7 µm particle size, length × I.D. 15 cm×4.6 mm) analytical column protected by a Phenomenex (AJ0-4287) C18 security guard cartridge (4× 3.0 mm) was used and the column temperature was set at 30°C. The flow rate of mobile phases was 0.8 mL/min with a 33 min elution gradient, composed of solvent (A) formic acid in water (1 %, v/v) and (B) acetonitrile. 50 µL filtrate sample was injected and mobile phase conditions (i) 0 min (A-B, 71:29, v/v); (ii) 21 min (A-B, 71:29, v/v); (iii) 24 min (A-B, 0:100, v/v); (iv) 27 min (A-B, 0:100, v/v); (v) 30 min (A-B, 71:29, v/v); (vi) 33 min (A-B, 71:29, v/v) were followed. Eluted *t*-res was monitored at 310 nm. Measurements were performed on triplicate samples.

3.3.5 Stability of liposomes, bilosomes, CH-coated and PGA/CH-coated bilosomes

3.3.5.1 pH stability

The pH of all the samples was adjusted to 3.0, 5.0, and 7.0 with HCl and sodium hydroxide (NaOH), respectively, and kept in dark condition for 24 h. Samples were collected at 0, 3, 6 and 24 h and were evaluated in terms of D_H, PDI, ζ potential and, DR.

3.3.5.2 Thermal stability

All the samples were kept at 65℃ for 30 min and in dark conditions and cooled immediately in an ice bath. Samples were collected and samples were evaluated in terms of D_H, PDI, ζ potential, and DR.

3.3.5.3 Storage stability

All the samples were stored at 4℃ and 20℃ for 28 days in dark conditions to evaluate the shelf life of the samples. Samples were collected at 0, 7, 14, 21 and 28 days and samples were evaluated in terms of D_H, PDI, ζ potential, and DR.

For the stability experiments measurements were performed on triplicate samples.

3.3.6 Statistical analysis

All the data were reported as mean±SD. Results were analysed by one-way ANOVA using Minitab® 20.4 software. The level of statistical significance was defined by $p<0.05$.

3.4 Results and discussion

3.4.1 The effect of the pH on the stability

Liposomes are commonly used in food products to protect bioactive compounds from environmental stress and improve their bioavailability during digestion. The liposome formulations are generally prepared at neutral pH conditions so incorporation of the liposomes into foods that have different pH conditions and passage through the GIT (the gastric phase (pH 3) and the intestinal phase (pH 7) (Brodkorb et al., 2019) can cause stability issues (Pasarin et al., 2023). Thus, the investigation of the physicochemical properties of the delivery system under different pH conditions provides information about the stability of the delivery system in foods and during passage through the GIT.

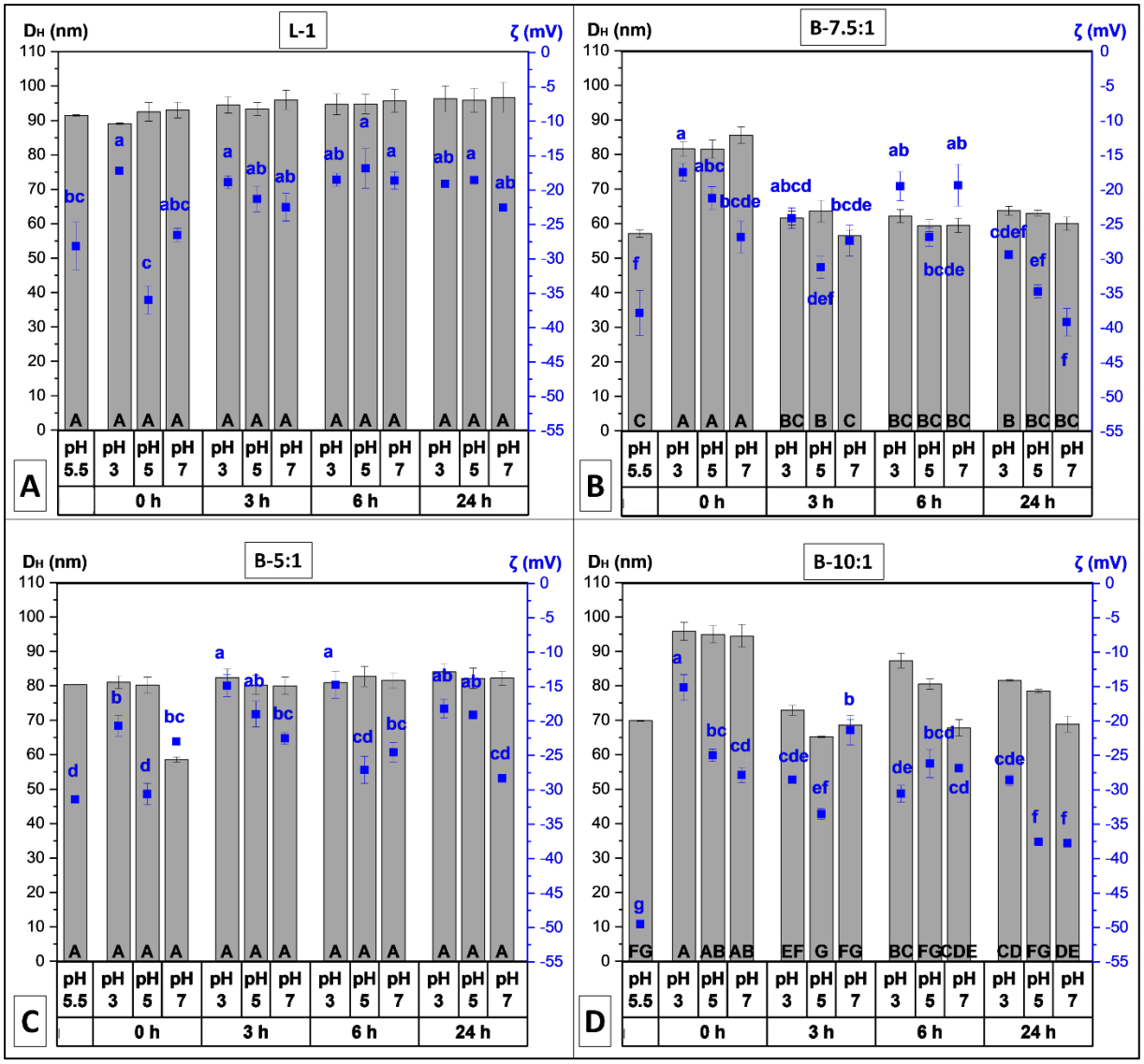

Figure 3.1 The D_H (nm) (▭) and ζ potential (mV) (■) of **(A)** L-5, **(B)** B-5:1, **(C)** B-7.5:1, and **(D)** B-10:1 in various pH conditions (pH 3.0, 5.0 and 7.0) for 24 h. The data represent the mean±SD. Black capital letters represent significant differences in the D_H and, blue lowercase letters in the ζ potential, respectively ($p < 0.05$).

The pH of *t*-res loaded liposomes, bilosomes, CH-coated and PGA/CH-coated bilosomes (pH 5.5) was adjusted to 3.0, 5.0, and 7.0 to represent different aqueous foods like orange juices (pH ~3), coffee (pH ~5) milk (pH ~7) and different GIT conditions like gastric phase (pH 3) and intestinal phase (pH 7) and kept in dark for 24 h. Samples were evaluated in terms of D_H, PDI, ζ potential, and DR.

For liposomes (L-1) and bilosomes (B-5:1, B-7.5:1, and B-10:1) **(Fig. 3.1**), while the D_H and PDI of L-1 and B-5:1 were not affected significantly by the pH changes during 24 h, the D_H of B-7.5:1 and B:10:1 increased significantly when the pH was adjusted to 3, 5 and 7 but then decreased to the initial D_H at 3 h. Although the PDIs of the liposomes and bilosomes were below 0.250 which shows a homogenous population

of phospholipid vesicles (Badran, 2014), the PDI of the B:10:1 increased up to 0.350±0.029 after 6 h at pH 3 ($p<0.05$). For further evaluation of the stability of samples, the ζ potential was determined. The initial ζ potential of the liposomes was around -28 mV at pH 5.5 which is moderately stable. Although slight fluctuations of ζ potential were observed at all pH conditions for 24 h, these fluctuations did not show an effect on DH and PDI. The initial ζ potential of bilosomes ranged from -31.4±2.3 mV to -49.5±2.3 mV (pH 5.5) suggesting that bilosomes should be highly stable (Bhattacharjee, 2016).

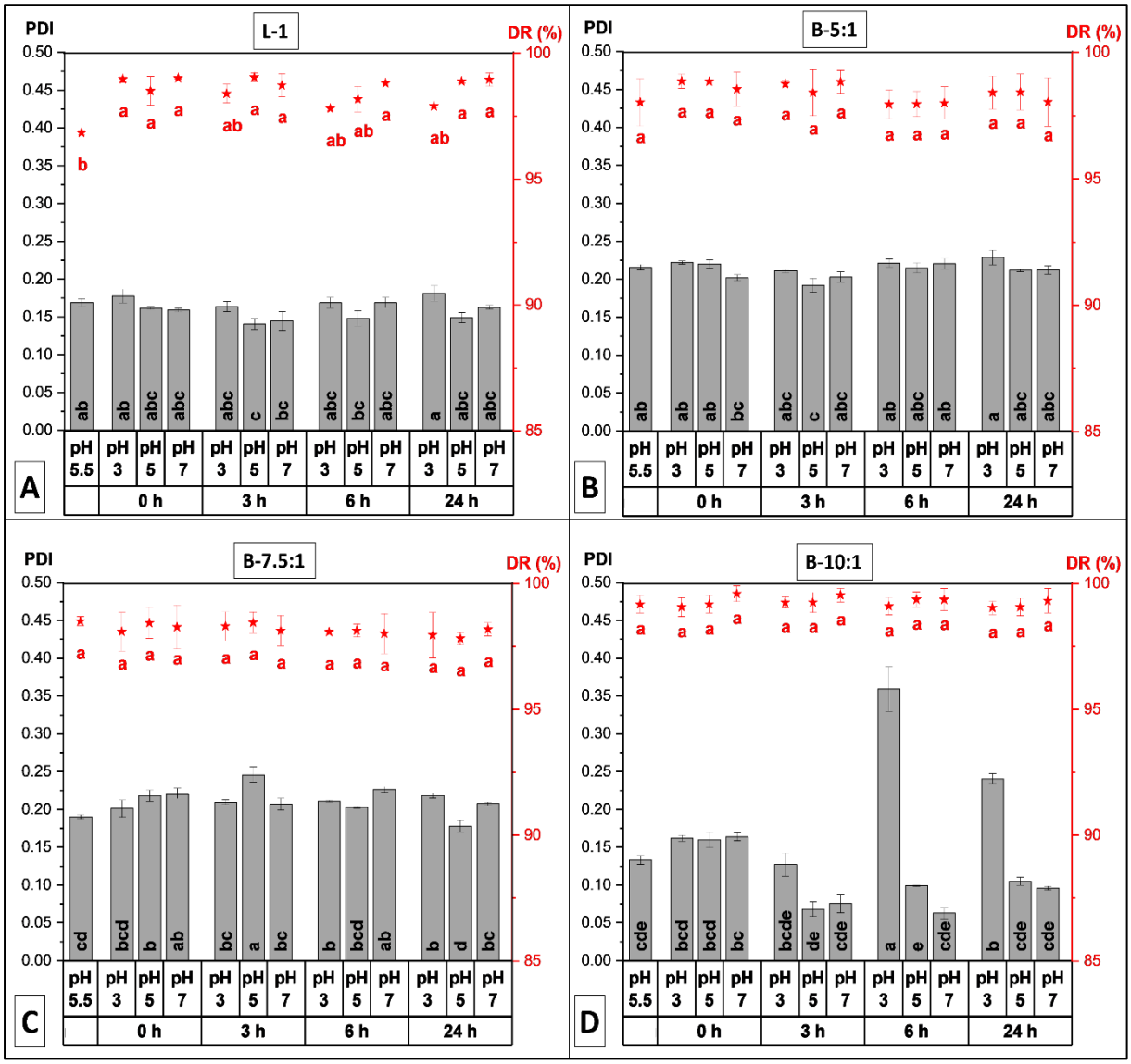

Figure 3.2 PDI (▭) and DR (★) of **(A)** L-5, **(B)** B-5:1, **(C)** B-7.5:1, and **(D)** B-10:1 in various pH conditions (pH 3.0, 5.0 and 7.0) for 24 h. The data represent the mean±SD. Black lowercase letters represent significant differences in the PDI, and red lowercase letters in the DR among the samples, respectively ($p < 0.05$).

After CH coating (**Fig. 3.3**) D_H and PDI increased because of the CH layer around the bilayer of bilosomes formed by electrostatic interaction between the negatively charged phosphate group ($-PO_4^{3-}$) of phospholipids and the positively charged amine group ($-NH_3^+$) of CH (Henriksen et al., 1994). For CH-coated bilosomes (CH-B-5:1, CH-B-7.5:1, and CH-B-10:1), while the D_H and PDI at pH 3 and pH 5 did not change for 24 h ($p>0.05$), they were significantly higher at pH 7 compared to the other pH conditions and sedimentation was observed immediately after pH adjustment. When bilosomes were coated with biopolymers, some sedimentation was seen at a neutral pH for CH (pKa: ~6.5) and at an acidic pH for PGA (pKa: ~2.9). Sedimentation primarily occurs due to a decrease in electrostatic repulsion between biopolymer-coated particles when the system's pH is close to the biopolymer's pKa. Electrostatic repulsion between particles is responsible for their uniform and stable dispersion in the colloidal system. When this repulsion weakens, particles undergo flocculation primarily caused by charge neutralization (Jiang et al., 2021). In addition, the interaction between CH and liposome weakened which resulted in increased D_H (Nguyen et al., 2014; Singla & Chawla, 2001). The ζ potential of the bilosomes was turned positive after positively charged CH coating. The ζ potential of CH-coated samples (initially ~25 mV) ranged from 21.2±1.4 mV to 27.6±1.1 mV during 24 h at pH 3 and pH 5 and samples were moderately stable. However, the ζ potential of the samples decreased to below 12.0±0.3 mV at pH 7 ($p<0.05$) because of the decrease in the protonation of amino groups of CH which ended in aggregation. Aggregation, flocculation, or precipitation problems can be seen when the ζ potential is lower than ±30 mV (Danaei et al., 2018) In addition, the ζ potential of CH-B-7.5:1 at pH 5 began to decrease significantly at 6 h and was around 15 mV, although there was no significant change in the D_H and PDI.

The initial DR of the *t*-res liposomes and bilosomes **(Fig. 3.2)** was above 95% and the DR of samples did not decrease significantly for any pH conditions for 24 h. When bilosomes were coated with CH, the initial DR decreased ($p>0.05$) and ranged from 88.9±4.2% to 90.8±3.8% for coated samples **(Fig. 3.4A-C)**. The decrease in DR might be related to the strong interaction between the lipid bilayer and CH. When CH coats the bilayer, due to the electrostatic interaction CH tightens the bilayer which might have resulted in losing some *t*-res from the bilayer (Bang et al., 2011). A similar decrease in DR was reported by (Refai et al., 2017) and (Bang et al., 2011). While the DR of liposomes was 89.68± 2.6%, it decreased to 72.24± 1.2% after CH coating (Refai et al., 2017). The DR of etofenprox- and α-cypermethrin-containing liposomes was decreased from ~90% to ~60% as CH concentration increased (0.1–0.5%, w/v) (Bang et al., 2011). The DR of all CH-coated bilosomes was above 88% during 24 h at all pH conditions.

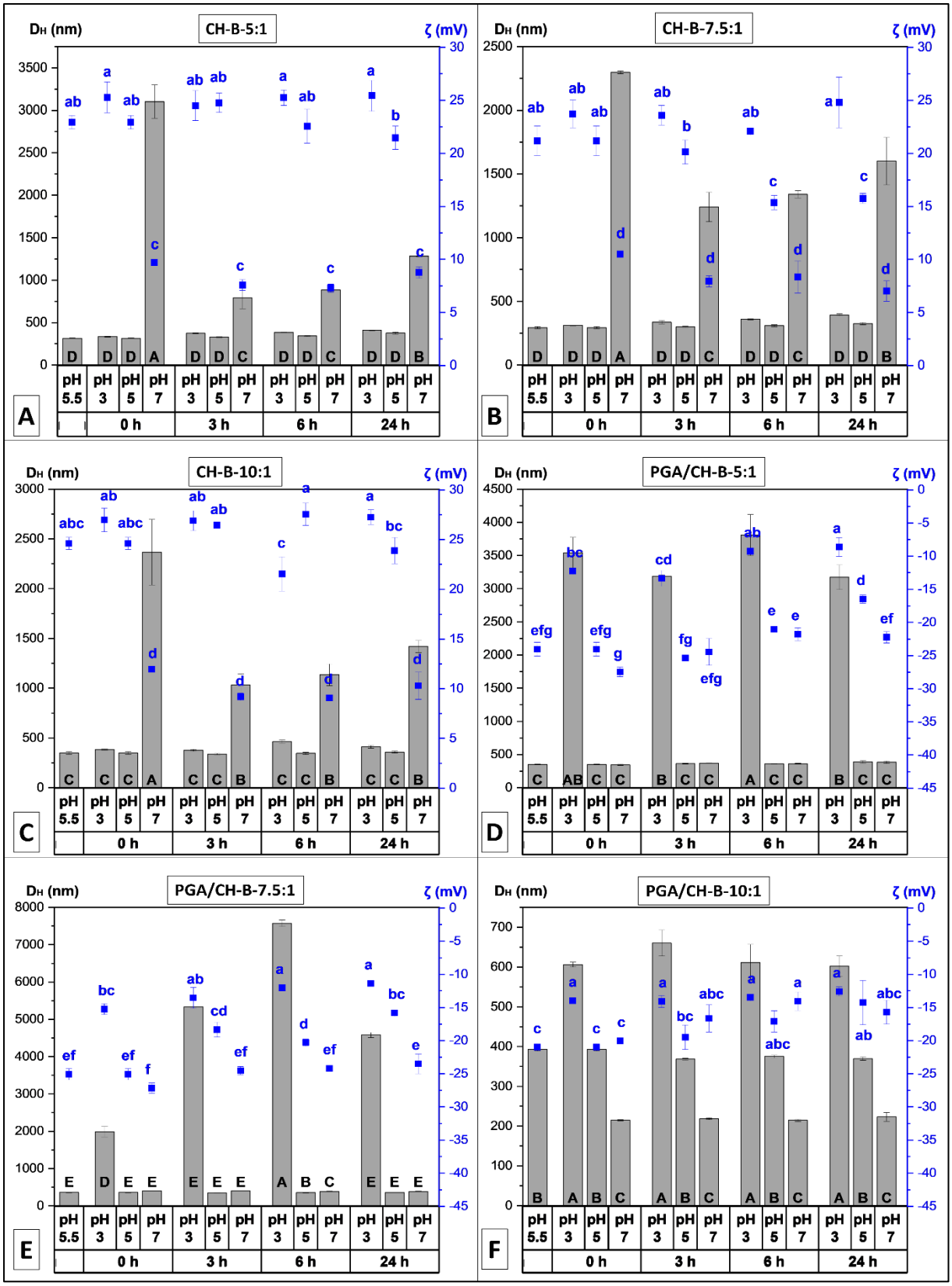

Figure 3.3 The D_H (nm) (▭) and ζ potential (mV) (■) of **(A)** CH-B-5:5, **(B)** CH-B-7.5:5, **(C)** CH-B-10:5 and PDI (▭) of **(D)** CH-B-5:5, **(E)**CH-B-7.5:5 and **(F)** CH-B-10:5 in various pH conditions (pH 3.0, 5.0 and 7.0) for 24 h. The data represent the mean±SD. Black capital letters represent significant differences in the D_H and, blue lowercase letters in the ζ potential, respectively ($p < 0.05$).

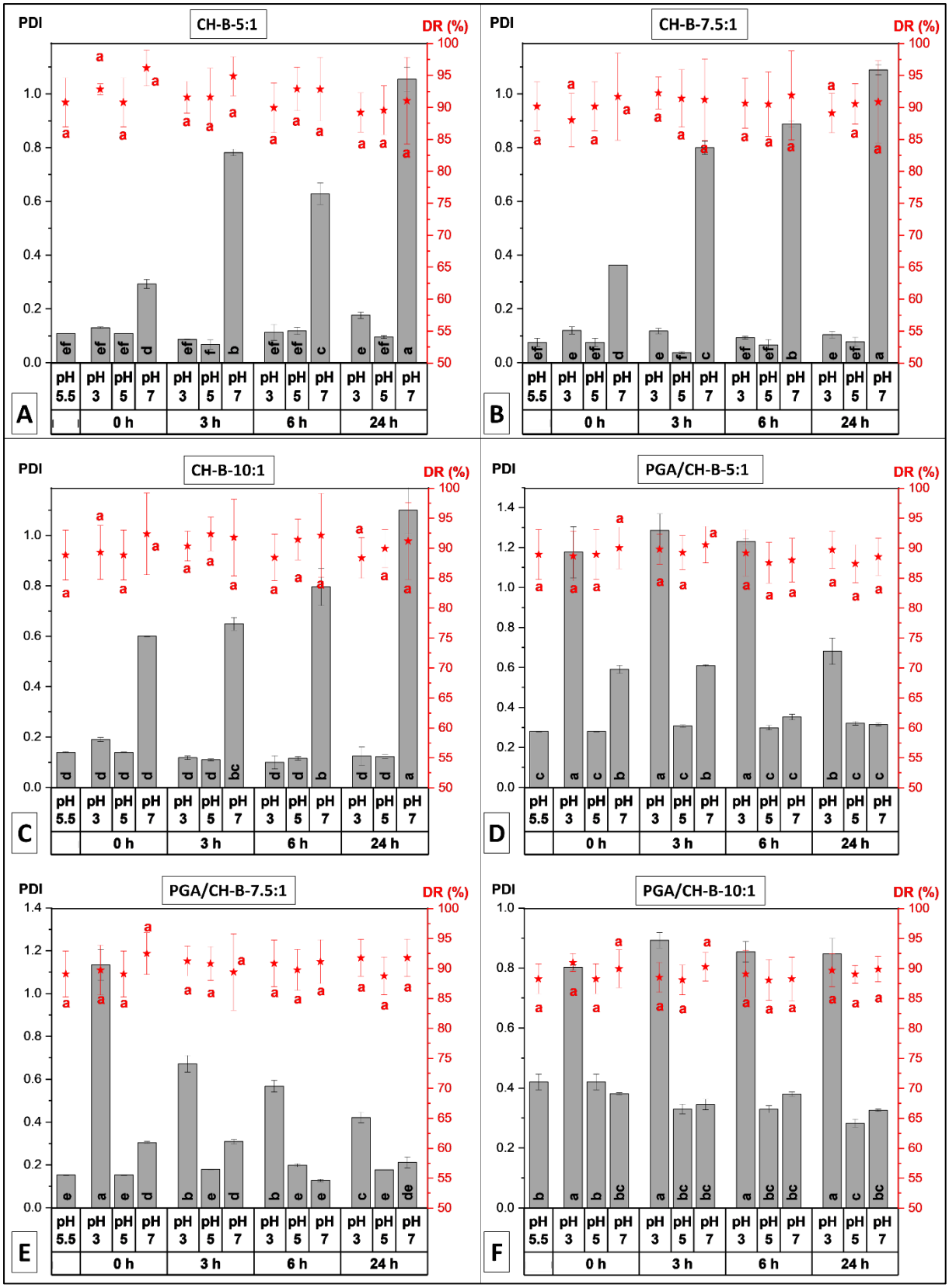

Figure 3.4 PDI (▭) and DR (★) of **(A)** CH-B-5:5, **(B)** CH-B-7.5:5, **(C)** CH-B-10:5 and PDI (▭) of **(D)** CH-B-5:5, **(E)** CH-B-7.5:5 and **(F)** CH-B-10:5 in various pH conditions (pH 3.0, 5.0 and 7.0) for 24 h. The data represent the mean±SD. Black lowercase letters represent significant differences in the PDI, and red lowercase letters in the DR among the samples, respectively ($p < 0.05$).

PGA as a second coating also did not affect the initial DR (from 88.3±2.5 to 89.1±3.8%) of the samples significantly **(Fig. 3.4D-F)**. For 24 h, DR of PGA/CH-coated samples was above 87% for all pH conditions. Many studies also report decreased DR after the CH coating of liposomes. Berberine hydrochloride-loaded liposomes and CH-coated liposomes were prepared by Nyugen et al. The DR of the liposomes was 83.2±0.4 and after CH coating DR decreased to 78.4±0.5% (Nguyen et al., 2014). The properties of eugenol-loaded liposomes and CH-coated liposomes were compared by (Sebaaly et al., 2022). While the DR of liposomes was 77.2±10.32 %, the DR of CH-coated liposomes was decreased and ranged from 68.8±3.06 to 78.4±6.11 %.

The pH has a significant effect on the size, charge, and consequently the stability of the system (Pasarin et al., 2023). Although liposomes are always mentioned as sensitive to pH changes, POPC/DOPC liposomes were stable during all pH conditions. Bilosomes also showed high stability to pH changes, however, when the NaC concentration increased in the system, some slight changes were seen. The possible reason for these changes is that when NaC is incorporated into the system it increases the membrane fluidity of the lipid bilayer, so the bilayer is not very strong and not stacked tightly (Can et al., 2021). When bilosomes were coated with biopolymers, some sedimentation was seen at a neutral pH for CH (pKa: ~6.5) and at an acidic pH for PGA (pKa: ~2.9). The main reason for the sedimentation is possibly that changing the pH resulted in decreasing the net charge of the systems. When the pH of the system is close to the pKa of the biopolymer, electrostatic repulsion between biopolymer-coated particles weakens, particles undergo flocculation caused by charge neutralization and then setteled (Jiang et al., 2021). Therefore, the stability of biopolymer-coated systems relies on pH which provides sufficient surface charges. The sedimentation was seen for biopolymer-coated samples when the pH of the medium was close to the pKa of biopolymers, but it did not affect the EE of the samples significantly. Because *t*-res is a highly hydrophobic bioactive compound and when it is encapsulated, it locates near the fatty acid chain of the lipids and is almost fully embedded (Koukoulitsa et al., 2011; Van Tran et al., 2019), thus the encapsulated amount of *t*-res might not be affected by losing the biopolymer layer or flocculation.

3.4.2 The effect of the thermal treatment on the stability

Thermal treatment is one of the most cost-effective processes to provide microbial safety and enzyme deactivation for food safety and extended shelf life for beverages (Petruzzi et al., 2017). While mild temperature-long time (<80 °C and >30 s) is the common thermal treatment for the preservation of fruit juices (pH 2.5-4.0) (Petruzzi et al., 2017), low temperatures-long time (~63°C and >30 min) is used for pasteurization of milk (pH ~6.8) (Dash et al., 2022). Thus, the investigation of the physicochemical

properties of the oral delivery system after thermal treatment provides information about the stability of the delivery system during food processing. The *t*-res loaded liposomes, bilosomes, CH-coated bilosomes, and PGA/CH-coated bilosomes were kept at 65℃ for 30 min and in dark conditions and cooled immediately in an ice bath. The D_H, PDI, ζ potential, and DR of samples were measured to investigate the effect of heating on the structure, stability, and *t*-res degradation.

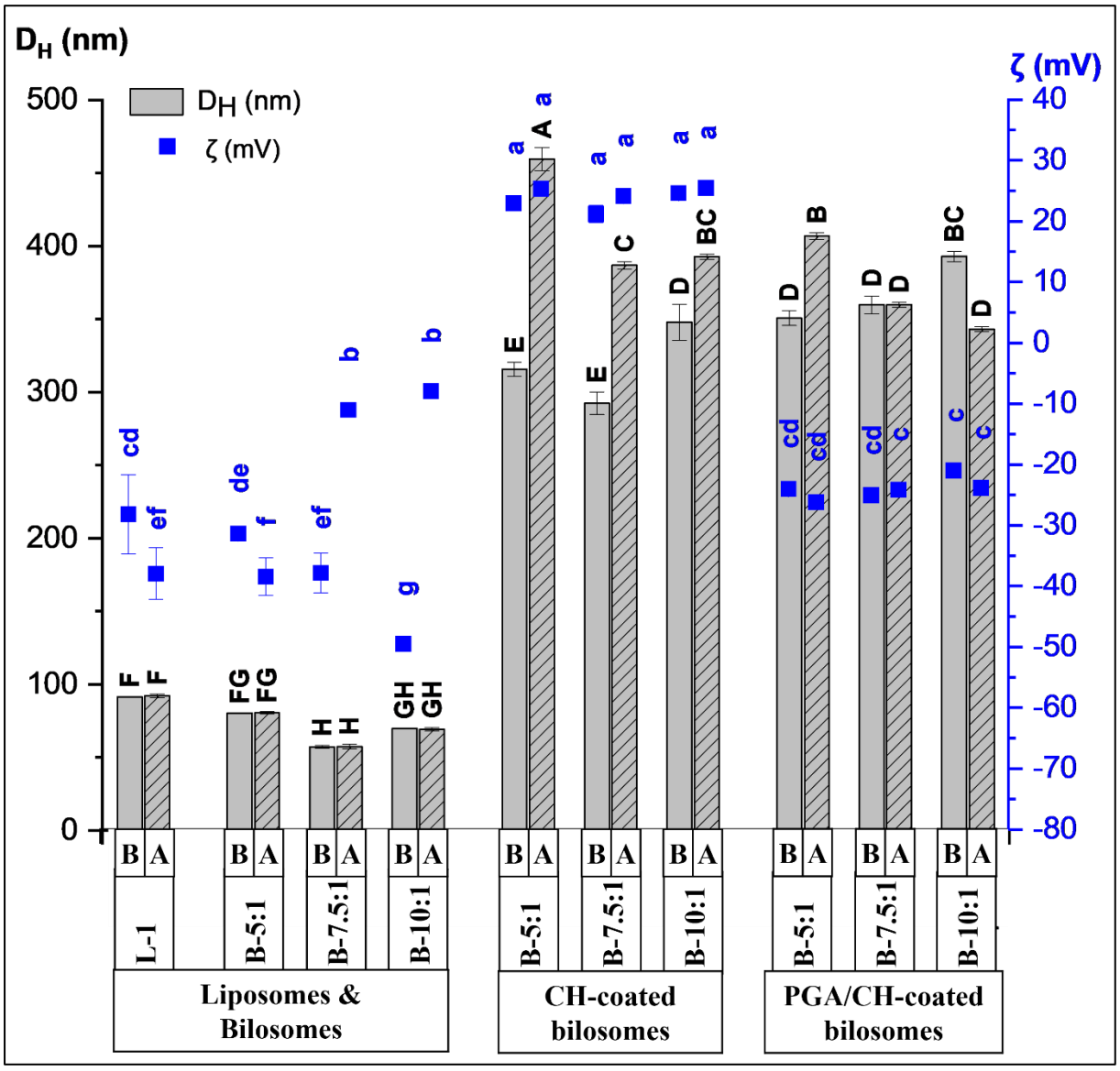

Figure 3.5 The physicochemical properties of *t*-res loaded liposomes, bilosomes, and CH-coated and PGA/CH-coated bilosomes. D_H (nm) (▭) and ζ potential (mV) (■) before (B) and after (A) thermal treatment (65℃ for 30 min). The data represent the mean±SD. Black capital letters represent significant differences in the D_H and, blue lowercase letters in the ζ potential, respectively ($p < 0.05$).

For the thermal stability of *t*-res loaded liposomes and bilosomes, the D_H and PDI of the liposomes and bilosomes did not change significantly after thermal treatment (D_H ≤92.2±0.9 nm and PDI≤0.220±0.001), the ζ potential of B-7.5:1 and B-10:1 increased up to -10 mV ($p<0.05$), but the D_H of these samples not affected by the increase in ζ potential **(Fig. 3.5-3.6)**. Temperature fluctuations may influence the physical attributes of membranes, including their fluidity and permeability. As the concentration of NaC in the system increases from 0 mM to 10 mM, the membrane fluidity of bilosomes also increases, as observed in the study (Hu et al., 2013).

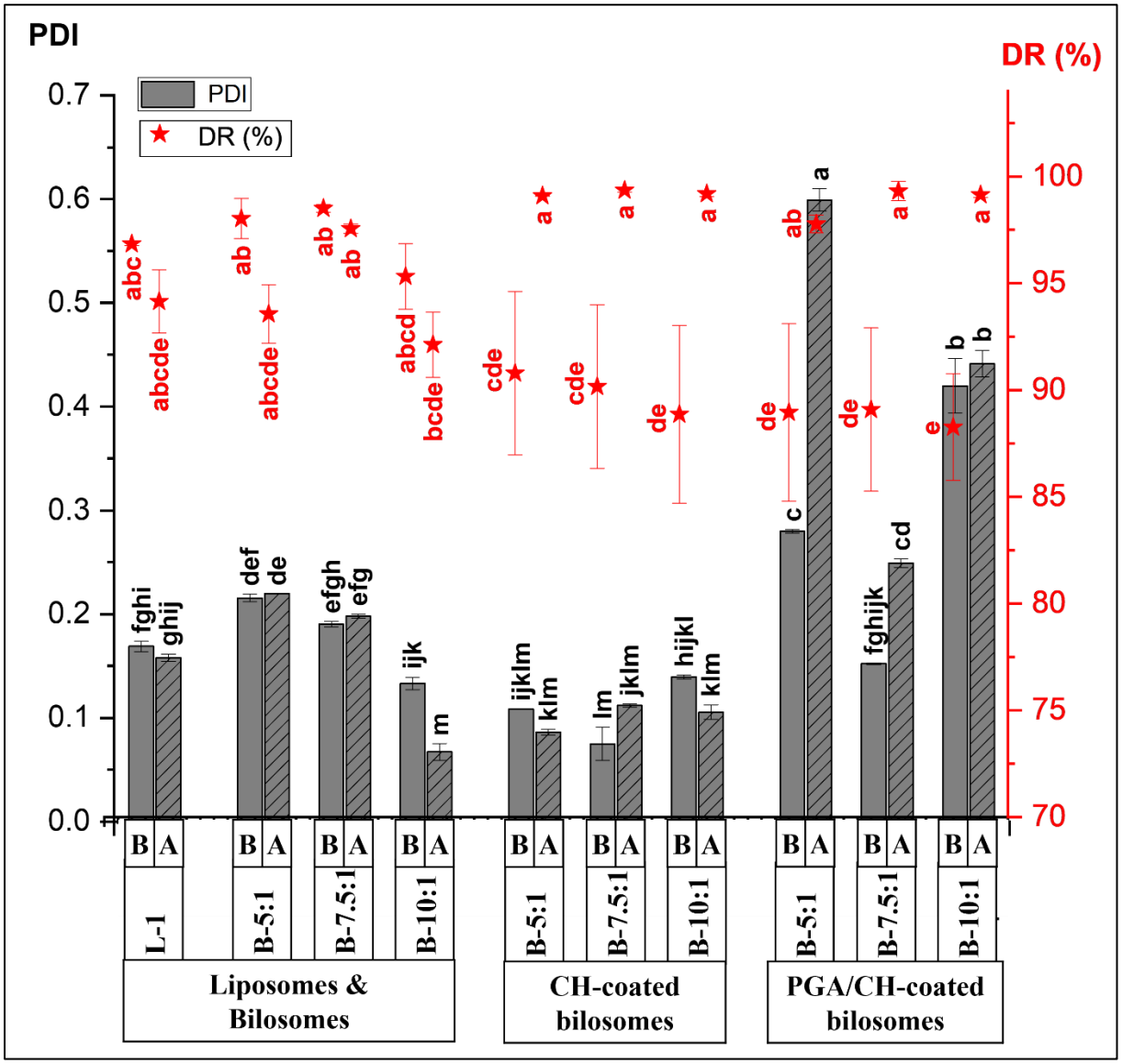

Figure 3.6 The physicochemical properties of *t*-res loaded liposomes, bilosomes, and CH-coated and PGA/CH-coated bilosomes. PDI (▭) and DR (%) (■) before (B) and after (A) thermal treatment (65℃ for 30 min). The data represent the mean±SD. Black lowercase letters represent significant differences in the PDI, and red lowercase letters in the DR among the samples, respectively ($p< 0.05$).

The heightened membrane fluidity, which has an adverse impact on bilayer stability, renders the bilayer more susceptible to the effects of heat treatment. Although liposomes and bilosomes are generally reported as sensitive to heat treatments, they were very stable and protected the encapsulated *t*-res, which was not affected by thermal treatment ($p>0.05$). Contrary to liposomes and bilosomes, the ζ potential of the biopolymer-coated samples **(Fig. 3.5)** was stable after thermal treatment and was around 25 mV and -25 mV for CH-coated and PGA/CH-coated bilosomes, respectively, the D_H of coated samples increased (up to 392.7±25.5 nm). These significant D_H increases may result from the swelling behaviour of the biopolymers. The heat treatment can weaken the interaction between the flexible polymer chains and can provide more space in the matrix for buffer (Rohindra et al., 2004). Although TPP was used as a crosslinker during CH coating, there were still uncrosslinked CH chains in the matrix. In previous work, the uncrosslinked and crosslinked CH hydrogels were prepared by Rohindra et al. to determine their swelling capacity depending on crosslinker concentration and temperature. While the uncrosslinked CH hydrogels had the highest swelling capacity, swelling capacity decreased with the increased crosslinker concentration. The swelling ratio of the uncrosslinked CH increased with increased temperature (25-45℃) (Rohindra et al., 2004).

The change of DR of liposomes and bilosomes was not significant after thermal treatment **(Fig. 3.6)**. Jash et al. prepared vitamin E-loaded liposomes from milk fat globule membrane and liposomes were exposed to the thermal treatment at three different temperatures (60, 75, and 90°C) for 30 min. DR of the untreated liposomes was not significantly different compared to the samples exposed to 60°C and 75°C. The DR decreased significantly after 90°C for 30 min thermal treatment (Jash et al., 2020). In order to improve the thermal stability of the vitamin E-loaded liposomes from milk fat globule membrane, liposomes were coated with a polymer (Eudragit S100). Coating the sample with polymer provided thermal stability of liposomes at 90°C for 30 min heat treatment (Jash & Rizvi, 2022). Thermal treatment is one of the challenging processes for liposomes which are composed of lipids with unsaturated double bonds acyl regions, which are prone to oxidation. Although liposomes and bilosomes were composed of lipids which have unsaturated double bounds (POPC and DOPG), they were mostly stable after heat treatment which might be because of using low temperature for heat treatment and encapsulation of the *t*-res which is an antioxidant and inhibits lipid oxidation (Panya et al., 2010). However, some significant increase in ζ potential after thermal treatment was seen depending on the increased bile salt concentration on the bilosomes. The increased ζ potential could be due to higher concentrations of NaC, which might be leading to increased membrane fluidity, which in turn adversely affects vesicle stability. A significant increase in the D_H was

observed for the biopolymer coating of bilosomes after thermal treatment. The thermal treatment can break the interaction between polymer chains and can change the swelling properties of the biopolymers. The DR of the *t*-res was above ~92% and protected after thermal treatment for all samples. In the literature, coating the liposomes improves the thermal stability but the stability of the liposomes is not only related to the surface modification but also the composition of the bilayer. Although there was no significant difference in DR of bilosomes and biopolymer-coated bilosomes, the application of higher temperatures than 65°C might show a significant protective effect of the biopolymer coating.

3.4.3 The effect of the storage on the stability

Processed foods have a specific and defined shelf life meaning the maximum time that the product can be stored without losing desired properties for consumption. The shelf life of the foods is mostly affected by temperature, moisture, and light. If the necessary storage conditions cannot be provided, food products deteriorate more rapidly, and they may lose their texture, flavour, colour, and nutritional composition consequently becoming unsafe to consume. Thus, the investigation of the physicochemical properties of the oral delivery system under different storage conditions provides information about the shelf life and the stability of the delivery system. The *t*-res loaded liposomes, bilosomes, CH-coated bilosomes, and PGA/CH-coated bilosomes were stored at 4℃ and 20℃ for 28 days to evaluate the shelf life of the samples. The D_H, PDI, ζ potential, and DR of samples were measured to investigate the size, stability, and *t*-res degradation during storage.

For L-1 (89.8±4.9 nm and 0.178±0.011, **Fig 3.7A-3.8A**) and B-5:1 (79.8±3.1 nm and 0.201±0.007, **Fig. 3.7B-3.8B**), the D_H and PDI did not change significantly during storage for both temperature conditions. While the ζ potential of the L-1 and B-5:1 (initial <-30 mV) showed an increase over 28 days and were finally around -20 mV and relatively stable. At 28 days for both 4ºC and 20ºC, although the D_H (<64.4±2.3) and the ζ potential (>-31.4±1.6) of B-7.5:1) were not significantly changed, an increase (~40%) was seen in the PDI ($p<0.05$) **(Fig. 3.7-3.8)**. Although ζ potential of the B-10:1 was <-35 mV and highly stable at 28 days, the D_H and PDI increased by ~30% (~70 nm) and ~100% (~0.280), respectively ($p<0.05$) (**Fig. 3.7D-3.8D)**. As also seen in the thermal stability experiments, with the increased bile salt concentration in the sample (from 0 mM to 10 mM NaC), bilosomes were less stable to the environmental stress resulting from increased membrane fluidity. The initial DR of liposomes and bilosomes were above ~88% and there were some slight changes during storage, but all samples kept the encapsulated *t*-res successfully ($p>0.05$) (**Fig 3.8)**.

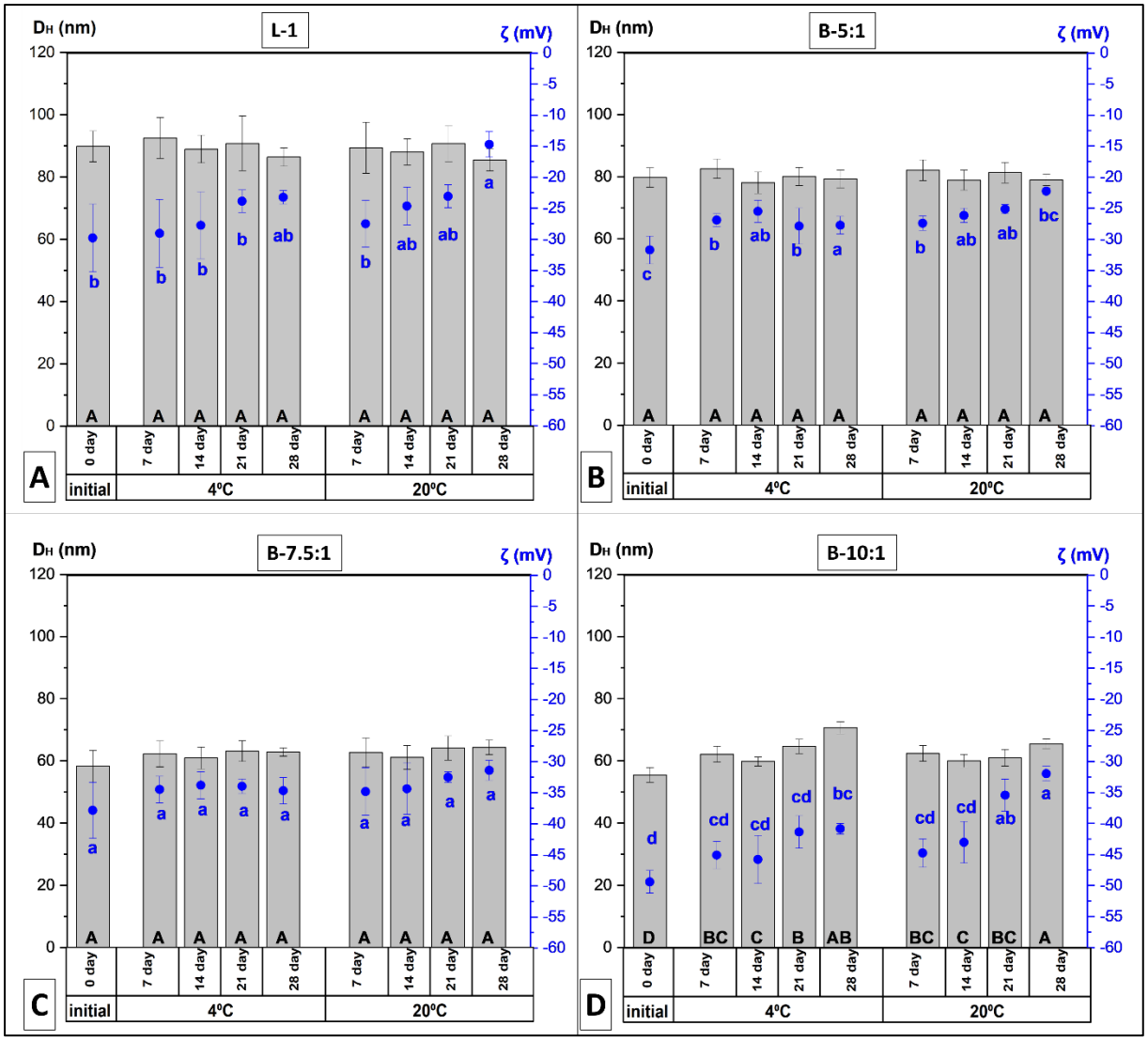

Figure 3.7 The D_H (nm) (▭) and ζ potential (mV) (■) of **(A)** L-5, **(B)** B-5:1, **(C)** B-7.5:1, and **(D)** B-10:1 in various storage conditions (4℃ and 20℃) for 28 days. The data represent the mean±SD. Black capital letters represent significant differences in the D_H and, blue lowercase letters in the ζ potential, respectively ($p < 0.05$).

The D_H and PDI of the CH-coated bilosomes increased and the magnitude of ζ potential decreased significantly during storage for 28 days for both temperature conditions. The size increase was more obvious for CH-coated samples stored at 20ºC compared to CH-coated samples stored at 4ºC. The initial D_H and PDI were 531.4±21.4 nm and 0.160±0.026 for CH-B-5:1 and 337.7±18.4 nm and 0.079±0.023 for CH-B-7.5:1, respectively **(Fig. 3.9A-B and Fig. 3.10A-B)**. However, sediment was observed at 7 days for both storage conditions and the D_H and PDI continued to increase until 28 days. The sedimentation might have resulted from using CH below and above the saturation concentration to coat the bilosomes. During sample optimisation, the amount of CH was determined according to NaC/CH ratio (w/w) because NaC provides the negative charge in the system. The samples might not be

fully covered because of the insufficient concentration of CH. Moreover, excessive concentration of CH might cause depletion flocculation resulting from the interaction between the extended CH segments (Laye et al., 2008; Li et al., 2015). The increase of D_H was not extreme for CH-B-10:1 as seen in CH-B-5:1 and CH-B-7.5:1 during storage. While the D_H was not changed during storage, PDI increased by ~190% at 4ºC, and the D_H and PDI increased by ~175% and ~115% respectively at 20ºC ($p<0.05$) **(Fig. 3.9C and Fig. 3.10C)**. The higher stability of CH-B-10:1 at 4ºC was possibly because of the low permeability of the CH coating at low temperatures consequently, keeping the structure more compact (Sebaaly et al., 2021).

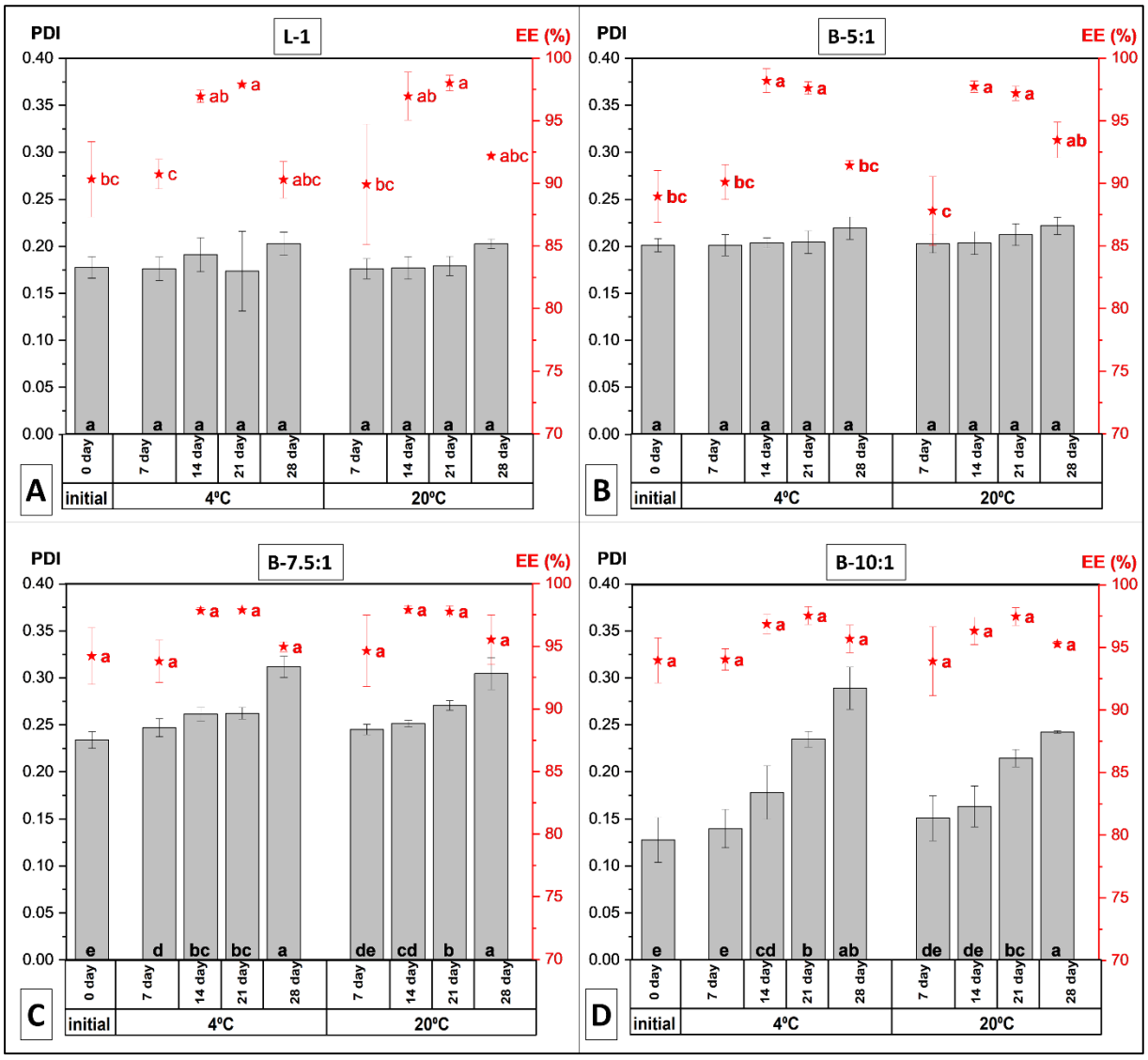

Figure 3.8 PDI (▭) and DR (★) of **(A)** L-5, **(B)** B-5:1, **(C)** B-7.5:1, and **(D)** B-10:1 in various storage conditions (4℃ and 20℃) for 28 days. The data represent the mean±SD. Black lowercase letters represent significant differences in the PDI, and red lowercase letters in the DR among the samples, respectively ($p < 0.05$).

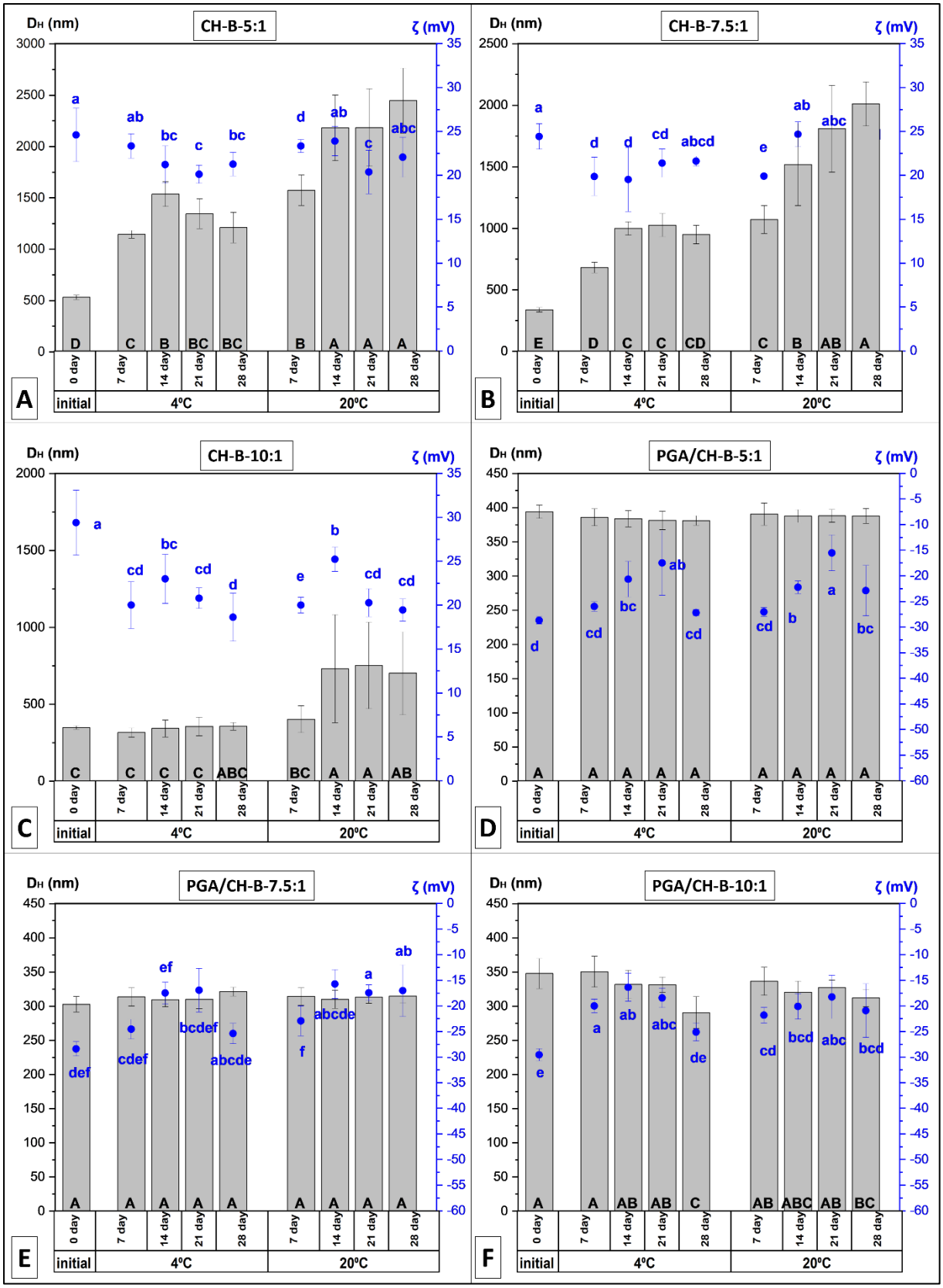

Figure 3.9 The D_H (nm) (▭) and ζ potential (mV) (■) of **(A)** CH-B-5:5, **(B)** CH-B-7.5:5, **(C)** CH-B-10:5 and PDI (▬) of **(D)** CH-B-5:5, **(E)**CH-B-7.5:5 and **(F)** CH-B-10:5 in various storage conditions (4℃ and 20℃) for 28 days. The data represent the mean±SD. Black capital letters represent significant differences in the D_H and, blue lowercase letters in the ζ potential, respectively ($p < 0.05$).

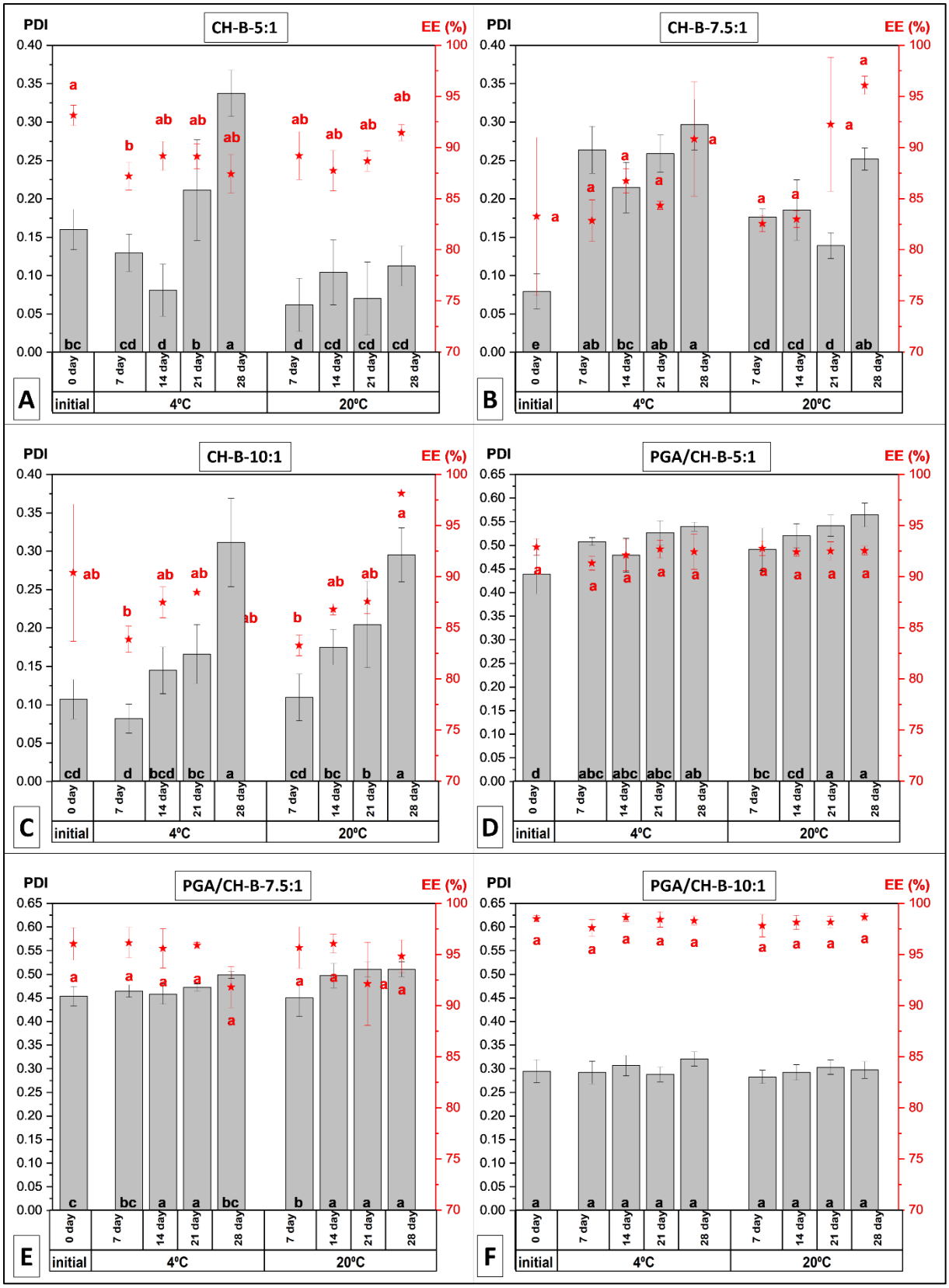

Figure 3.10 PDI (▭) and DR (★) of **(A)** CH-B-5:5, **(B)** CH-B-7.5:5, **(C)** CH-B-10:5 and PDI (▭) of **(D)** CH-B-5:5, **(E)** CH-B-7.5:5 and **(F)** CH-B-10:5 in various storage conditions (4℃ and 20℃) for 28 days. The data represent the mean±SD. Black lowercase letters represent significant differences in the PDI, and red lowercase letters in the DR among the samples, respectively ($p < 0.05$).

The initial DR of CH-coated bilosomes was above ~83%. Although CH-coated samples lost their stability after a week, the DR of CH-coated samples was not affected during storage ($p>0.05$) **(Fig. 3.10A-C)**. Because bilosomes already showed high stability and protected the *t*-res, which was embedded into the bilayer and *t*-res is a highly hydrophobic compound, which has a very low affinity toward the inner or outer aqueous regions of the bilayer (Refai et al., 2017). Compared to CH-coated samples, PGA/CH-coated samples (**Fig. 3.9D-F and Fig. 3.10-D-F**) were more stable. The D_H of the PGA-CH coated samples (except PGA/CH-B-10:1 at 28 days) did not change during the storage and the D_H of PGA/CH-B-10:1 (347.7±22.1 nm) was not significantly different until 28 days at both temperature conditions. Only the PDI of PGA/CH-B-7.5:1 (0.454±0.021) increased during storage by ~30% ($p<0.05$). The ζ potential of double-coated samples was slightly increased from -30 mV to around -25 mV at both storage conditions but systems were still relatively stable. The initial DR of double-coated samples was ~90% and there are some slight changes during storage, but all samples kept the encapsulated *t*-res successfully ($p>0.05$).

Conditions of storage have considerable effects on the stability of the samples. For liposomes and bilosomes, the storage temperature did not show any significant effect on the physicochemical properties of the samples. According to the literature, cold storage protects the samples more and slows their deterioration. However, liposomes and bilosomes already showed higher stability after heat treatment (65ºC) and encapsulation of *t*-res might be helpful to continue the stability during the storage period. The CH-coated samples lost their stability and sedimentation was observed. This instability problem might be because of either coalescence due to the insufficient concentration of CH or depletion flocculation due to the excessive concentration of CH in the system. Although there was instability of the CH-coated samples during storage, PGA, as a second coating, appeared to hinder the swelling of CH due to strong electrostatic interaction and provided more stable structures during storage. Although there were some instability issues, the DR of the *t*-res, which was embedded in the lipid bilayer was above ~80% and protected during storage for all samples.

3.5 Conclusion

The physicochemical properties of lipid bilayers are major factors that determine their stability, shelf life, and performance as oral delivery systems. The present study was designed to determine the effect of the bilayer modification using NaC and the surface modification using CH and PGA/CH on the physicochemical properties and stability of the lipid/bile salt and biopolymer(s)-coated lipid/bile salt system as carriers for oral delivery. The *t*-res loaded liposomes, bilosomes, CH- and PGA/CH-coated bilosomes were prepared and their stability in various stability conditions was investigated.

Liposomes showed high stability at different pH (pH 3.0, 5.0, and 7.0) over 24 h. The bilosomes were also stable against pH change but the physicochemical properties of the bilosomes were more unstable with increased concentration of NaC in the system, which might be because of increased bilayer fluidity due to increased NaC concentration. The CH-coated and PGA/CH-coated bilosomes were stable when the pH of the medium was far from the pKa of the coating material. While CH-coated bilosomes aggregated at pH 7.0, sedimentation was observed at pH 3 for PGA/CH-coated bilosomes due to the decreased net charge of the systems. The DR of all samples was not affected by pH change and was ~90%.

The D_H, PDI and ζ potential of the liposomes and bilosomes was not affected significantly during thermal treatment (65℃ for 30 min). However, there was a significant increase in the D_H for the CH-coated and PGA/CH-coated bilosomes, although the ζ potential of these samples was not changed after heat treatment. The possible reason for the increased D_H might be the increased swelling capacity of the biopolymers with increased temperature. The DR of all samples was ~90% and did not change possibly because *t*-res were embedded into the bilayer and although the biopolymer matrix was affected by heat treatment lipid bilayer effectively inhibited temperature-induced *t*-res degradation.

The liposomes and bilosomes showed high stability during storage at both storage conditions (4℃ and 20℃) for 28 days. The CH-coated bilosomes were more unstable at 20℃ compared to 4℃ and sedimentation was seen for CH-coated bilosomes after 7 days. The sedimentation could result from either using an insufficient concentration of CH in the system, leading to coalescence, or using an excessive concentration of CH in the system, resulting in depletion flocculation. Compared to the CH-coated bilosomes, double-coated bilosomes were highly stable in both storage conditions. Apparently, coating the bilosomes with PGA as a second layer prevented the loss of the stability of the CH. DR of all samples did not change significantly during storage and protected the encapsulated *t*-res.

The current findings add to a growing body of literature on the effect of bilayer modification using bile salts and surface modification using biopolymer(s) on the stability, shelf life, and performance of oral delivery systems. Compared to some industries like pharmaceutical, biomedical, or cosmetics, a very small number of food products containing lipid-based delivery systems are on the market due to the high cost of materials and production techniques. It is difficult to produce on a large scale for some carriers, and the low thermal stability of lipids adds to the challenge. The modification of lipid-based oral delivery systems for natural bioactive compounds is a promising strategy to enlarge their application in the food industry.

Chapter 4: *In vitro* gastrointestinal digestion and absorption of *t*-res loaded liposomes, bilosomes, CH-coated and PGA/CH-coated bilosomes

4.1 Abstract

The physical characteristics of oral delivery systems play a significant role in determining how well they perform in the GIT. Along with the physical characteristics, the influence of the selected food matrix is also essential since it has the potential to affect the stability, digestion profile, and absorption of the oral delivery system positively or adversely. Therefore, the present chapter investigated how the bilayer modification, surface modification, and food matrix impact the behaviour of lipid bilayers in the GIT and the effects on the bioaccessibility and bioavailability of *t*-res.

Bilosomes were prepared by adding NaC into the liposomes and then the bilosomes were coated with CH as the first coating and PGA as a second coating. Liposomes and bilosomes mostly maintained their stability during the oral and gastric phases of digestion and were digested in the intestinal phase. The encapsulation of *t*-res by the liposomes increased its bioaccessibility from ~40% to 70%, while the bioaccessibility of the *t*-res from bilosomes ranged from 83% to 90% and the incorporation of NaC into liposomes improved the bioaccessibility of *t*-res even more. The CH-coated (cross-linked with TPP) and PGA/CH-coated bilosomes were resistant to digestive enzymes and were stable during digestion, therefore, they protected lipid bilayers and retained the encapsulated *t*-res. The bioaccessibility of *t*-res from CH-coated and PGA/CH-coated bilosomes was ~20% and ~40%, respectively due to their resistance to the upper GIT. When these systems were mixed with OM (1:1 v/v), the initial properties of the lipid bilayer-OM mix and their behaviour during digestion looked mostly related to the properties of OM due to their low concentration in the mixture. When free *t*-res liposomes and bilosomes were digested with OM, the bioaccessibility of *t*-res increased significantly. The bioaccessible *t*-res increased by 5-10% for the coated bilosomes-OM mix. Similar to the bioaccessibility results, the tissue's accumulated *t*-res concentration was lower for samples digested with OM in comparison to those digested without OM. This reduction can be attributed to the presence of the micellar phase of OM. According to the absorption experiment, *t*-res concentration in the basolateral compartment at 2 h for free *t*-res, liposomes and bilosomes ranged from 0.379 µM to 0.487 µM. While the accumulated *t*-res in the intestinal tissue measured 0.400 µM for liposomes, the incorporation of NaC into the lipid bilayers resulted in an increased accumulation of *t*-res, consequently enhanced absorption. Specifically, the

levels were measured at 16.801 µM for 7.5 mM NaC-containing bilosomes and 3.345 µM for 10 mM NaC-containing bilosomes.

Overall, it can be concluded that while bilosomes could be a promising approach for enhancing the bioaccessibility and absorption of *t*-res as intestine-targeted oral drug delivery, CH-coated and PGA/CH-coated bilosomes can have potential as colon-targeted oral drug delivery. In addition, these findings highlight the crucial role of the food matrix in the bioaccessibility of *t*-res.

Keywords: bilosomes, resveratrol, biopolymer coating, oat milk, digestion, bioaccessibility, absorption.

4.2 Introduction

Phenolic compounds interact differently with physiological environments and their plasma concentrations differ because of their chemical structure, molecular size, solubility, and permeability (Chimento et al., 2019). Resveratrol is one of the well-studied phenolic compounds due to its biological activities such as antioxidant, anti-microbial, anti-inflammatory, and anti-carcinogenic activity. However, resveratrol suffers from poor aqueous solubility (<0.001 mol/L) (Biopharmaceutics Classification System class II drugs) and is quickly absorbed by the small intestine and undergoes metabolism into glucuronide and sulphate conjugates. Subsequently, both the unmetabolized resveratrol and its metabolites are eliminated from the bloodstream, preventing them from reaching sufficiently high concentrations to show their biological effects at the intended target location (Arzani et al., 2015; Bonechi et al., 2012; Wenzel & Somoza, 2005). Reabsorption of metabolites of resveratrol from enteric recirculation was also reported but overall, the oral bioavailability of resveratrol is less than 1% (G. K. Devi et al., 2019; Vaz-da-Silva et al., 2008; Wenzel & Somoza, 2005). Thus, when oral administration is aimed, encapsulation of resveratrol would be beneficial to enhance its bioavailability by improving the solubility of resveratrol, protecting it from chemical and enzymatic degradation, and controlling its release rate and release area.

Liposomes, LSAS, are suitable to encapsulate hydrophobic phenolic compounds. The low solubility issue of hydrophobic compounds can be improved with the encapsulation of the compound between the monolayers of liposomes (Faridi Esfanjani et al., 2018). With improved solubility, encapsulated compounds can be incorporated into foods and beverages. However, liposomes are rather unstable during digestion because of ionic strength and enzymes. In order to improve stability in the GIT, either modification of the bilayer or surface is the promising approach (Wang et al., 2017). The bilayer of liposomes can be modified by adding negatively charged bile salts as a surfactant. Bile salt-containing liposomes have been called bilosomes (H. Yang et al., 2019), ultra-

deformable liposomes (Barone et al., 2020), or elastic liposomes (Z. Wu et al., 2019) in the literature. The incorporation of bile salts induces membrane curvature of phospholipid bilayers in a concentration-dependent manner and results in a range of lipid structures, including ellipsoid shapes, rod-like formations, smaller vesicles, and micelles. Due to differences in the physicochemical properties, LC of these structures may differ, resulting in different bioaccessible concentrations (Lichtenberg et al., 2013; McClements, 2013). Moreover, bile salts can increase the elasticity of the bilayer and show a penetration-enhancing effect that facilitates the absorption and bioavailability of bilosomes (Aburahma, 2016; Hu et al., 2013; Tang et al., 2021). The modification of the surface of the liposomes can be accomplished by coating them with biopolymers (CH, pectin, etc.), which act as a barrier and stabilise the bilayer. Modifying the surface also can provide the desired properties like surface charge, size, and polarity that directly affect the behaviour of particles during digestion and absorption and controlled release of encapsulated compounds (Roger et al., 2010; Tan et al., 2016). CH is a biodegradable, biocompatible cationic biopolymer widely used for coating liposomes because it is mucoadhesive. The positively charged coated liposomes can interact with negatively charged mucosa and cell membranes and can open tight junctions of epithelial cells so CH-coating can enhance the bioavailability of the phenolic compounds (Chen et al., 2016). PGA is also biocompatible and biodegradable an anionic biopolymer, and a linear homopolymer linked by α-(1,4) glycosidic bonds (Müller et al., 2018). Both CH and PGA are digested by colonic microflora, and they show the potential to be carriers for colonic drug delivery (Yu et al., 2009).

The physicochemical properties of oral delivery systems have a major impact on the fate of delivery systems in different environments. Alongside physicochemical properties, the effect of the food matrix is also crucial because the physicochemical characteristics, stability, digestion profile, and absorption of the oral delivery system can all be positively or negatively impacted by the food matrix (Molet-Rodríguez et al., 2023). OM is a plant-based beverage that has recently attracted the attention of consumers following vegetarian/vegan diets and/or those who suffering from health issues such as lactose intolerance, cow's milk allergies, etc. OM is an aqueous extract of oat. The stability and nutritional value of the product are provided with the addition of some ingredients such as oil, plant-based proteins, sugar, vitamins, stabilizers, etc. (Martínez-Padilla et al., 2020). OM contains oil particles composed of triglyceride coated by a phospholipid/protein shell (Nikiforidis, 2019). Free *t*-res can be solubilized within the oil particles of OM thus bioaccessibility of *t*-res may be enhanced.

In this study, the effect of bilayer modification using bile salt (NaC), surface modification using biopolymers (CH and PGA), and the effect of food matrix (OM) on the behaviour of the *t*-res loaded lipid bilayers during GIT digestion and on the

bioaccessibility and absorption of *t*-res were investigated for the first time. The *t*-res was used as a model hydrophobic phenolic compound. Liposomes and bilosomes were prepared using the thin-film hydration followed by the sonication method and then bilosomes were coated with CH and PGA/CH polyelectrolyte complexes. The physical properties of the liposomes, bilosomes, and biopolymer-coated bilosomes were determined during static *in vitro* simulated digestion in terms of D_H, PDI, and ζ potential. The bioaccessible *t*-res, which was in a form available for absorption at the end of *in vitro* simulated GIT digestion was measured. The *ex vivo* intestinal permeability methodology using the Ussing chamber system was used to determine the absorption of *t*-res.

4.3 Materials and methods

4.3.1 Materials

POPC (16:0-18:1 PC), and DOPG (18:1 (Δ9-Cis) PG) were purchased from Avanti Polar Lipids, USA. NaC hydrate (BioXtra, ≥99%), Tris base, (3,4′,5-Trihydroxy-trans-stilbene) (*t*-res), LMW-CH with 75-85% deacetylation, PGA with ≥85% (titration) from oranges, TPP, Triton X-100, porcine pepsin (P7012), porcine pancreatin (P7545), bile bovine (B3883), Ammonium carbonate ($(NH_4)_2CO_3$), Pefabloc SC, D-mannitol and D-(+)-glucose were purchased from Sigma Aldrich, UK. Chloroform, methanol, NaCl, EDTA, Calcium chloride dihydrate ($CaCl_2.(H_2O)_2$), NaOH, Potassium chloride (KCl), Sodium bicarbonate ($NaHCO_3$) and Magnesium chloride ($MgCl_2(H_2O)_6$) were purchased from Merck, UK. HCl and Potassium dihydrogen orthophosphate (KH_2PO_4) were purchased from J.T. Baker. Agar was purchased from VWR International. OM (Alpro, whole, 3.5% fat in **Table 4.1**) was purchased from a local grocery store (Tesco, Leeds, UK).

Table 4.1 Nutritional composition of the oat milk (Alpro) as given on the package labelling.

Ingredients	Oat base (Water, Oat (8.7%)), Sunflower oil, Soluble corn fibre, Sugar, Pea protein, Calcium (Calcium carbonate), Acidity regulator (Potassium phosphates), Flavourings, Sea salt, Stabiliser (Gellan gum), Potassium Iodide, Vitamin D_2.
Nutritional information (per 100ml)	Energy: 260 kJ / 62 kcal, Fat: 3.5 g (Saturated: 0.4 g, mono-unsaturated: 1 g and polyunsaturated: 2.1 g), Carbohydrate: 6.4 g (Sugars: 1.2 g), Fibre: 1 g, Protein: 0.7 g, Salt:0.12 g, Vitamin D: 0.75 µg, Calcium: 120 mg

4.3.2 Preparation of *t*-res loaded liposomes, bilosomes, CH coated and PGA/CH coated bilosomes

The *t*-res loaded liposomes, bilosomes, CH-coated and PGA/CH-coated bilosomes **(Table 4.2)** were prepared according to methods described in **Chapter 2** using thin-film hydration followed by sonication with minor modifications reported by (Coreta-Gomes et al., 2015).

Table 4.2 Composition of liposomes, bilosomes, and CH-coated and PGA/CH-coated bilosomes with *t*-res.

System	POPC (mM)	DOPG (mM)	NaC (mM)	*t*-res (mM)	NaC/CH (w/w)	C/PGA (w/w)
L-5	10	3.3	-	5	-	-
B-5:5	10	3.3	5	5	-	-
B-7.5:5	10	3.3	7.5	5	-	-
B-10:5	10	3.3	10	5	-	-
CH-B-5:5	10	3.3	5	5	0.5	-
CH-B-7.5:5	10	3.3	7.5	5	0.5	-
CH-B-10:5	10	3.3	10	5	0.5	-
PGA/CH-B-5:5	10	3.3	5	5	0.5	0.4
PGA/CH-B-7.5:5	10	3.3	7.5	5	0.5	0.4
PGA/CH-B-10:5	10	3.3	10	5	0.5	0.4

POPC: 2-oleoyl-1-palmitoyl-sn-glycero-3-phosphocholine, DOPG: 1,2-dioleoyl-sn-glycero-3-phospho-(1'-rac-glycerol) (sodium salt), NaC: Sodium cholate, *t*-res: trans-resveratrol, CH: Chitosan, PGA: Polygalacturonic acid

Briefly, POPC: DOPG (10:3.3 molar ratio), NaC, and *t*-res were dissolved in a mixture of chloroform and methanol (80:20, v/v) and solvents were evaporated using Genevac (EZ-2 plus) (Fisher Scientific Ltd, Leicestershire, UK) (25℃, Method: Very Low BP Mix) to obtain dried lipid films. Lipid film hydrated with Tris buffer (10 mM, pH 7.4) containing 150 mM NaCl and 1 mM EDTA and vortexed at RT for hydration. Hydrated suspension underwent five freeze-and-thaw cycles and then was sonicated using QSonica Sonicator (80% amplitude, 1s on, 2 s off for 10 min).

The CH- and PGA/CH-coated bilosomes were prepared according to ratios (NaC/CH ratio (w/w): 0.5 and CH/PGA ratio (w/w): 0.4) in **(Fig. B.13-16)**. CH coating and PGA/CH coating onto the surface of bilosomes were successfully developed via electrostatic interaction. All liposomes, bilosomes and, biopolymer-coated bilosomes were prepared in triplicates.

4.3.3 Characterization of t-res loaded liposomes, bilosomes, CH-coated and PGA/CH-coated bilosomes

4.3.3.1 Hydrodynamic diameter, polydispersity Index, and zeta potential

The D_H and PDI of samples were determined by DLS using a Zetasizer Nano (ZS series, Malvern Instruments, Malvern, UK) at 25°C. The RI of liposomes used was 1.45, and the absorption coefficient was 0.001. The type of cuvette used was DTS0012. Samples from the intestinal phase were centrifuged at 1000xg for 5 min to remove insoluble materials from the sample for DLS measurements. The ζ potential of samples was analysed by the Zetasizer Nano ZS series equipped with a 633 nm helium/neon laser at a detector angle of 90°. The type of cuvette used was DTS1070. Samples were diluted 50-fold using Millipore water to avoid multiple light scattering effects. Measurements were performed on triplicate samples.

4.3.3.2 Encapsulation efficiency and loading capacity

Free *t*-res was separated from samples by centrifugation of 0.5 mL liposome and bilosome samples using a high-speed centrifuge (Beckman Coulter, Avanti Centrifuge J-30I) at 108800 x g for 60 min at 4°C and 1.5 mL coated bilosome samples (Thermo Scientific, Fresco 21) at 21000 x g for 60 min at 4°C. The supernatants were collected, supernatants and pellets were mixed with Triton X-100 to disrupt the lipid bilayer and then were dried using a Genevac (EZ-2 plus) (Fisher Scientific Ltd, Leicestershire, UK) (25℃, Method: Aqueous). The dried samples were dissolved in methanol and were filtered through a 0.20 µm PTFE filter for HPLC. The HPLC method (Ares et al., 2015) described below determined the free *t*-res and the amount of *t*-res loaded in formulations. Measurements were performed on triplicate samples. EE and LC of samples were calculated by using the following equations (Eq. 2.1 and 2.2).

4.3.3.3 Quantification of t-res

The *t*-res was quantified using the HPLC-DAD method was used to determine the free amount of *t*-res in the samples (Ares et al., 2015). The concentration of *t*-res in the filtrate was determined using the HPLC (Shimadzu, Japan) system controlled by LabSolutions software (version 5.97) with DAD. An Ascentis® Express C18 (2.7 µm particle size, length×I.D.15 cm×4.6 mm) analytical column protected by a Phenomenex (AJ0-4287) C18 security guard cartridge (4× 3.0 mm) was used and the column temperature was set at 30°C. The flow rate of mobile phases was 0.8 mL/min with a 33 min elution gradient, composed of solvent (A) formic acid in water (1 %, v/v) and (B) acetonitrile. A 50 µL filtrate sample was injected and mobile phase conditions (i) 0 min (A-B, 75:25, v/v); (ii) 21 min (A-B, 75:25, v/v); (iii) 24 min (A-B, 0:100, v/v); (iv) 27 min (A-B, 0:100, v/v); (v) 30 min (A-B, 75:25, v/v); (vi) 33 min (A-B, 75:25, v/v) were

followed. Eluted *t*-res was monitored at 310 nm. Measurements were performed on triplicate samples.

4.3.4 Static *in vitro* simulated gastrointestinal digestion with INFOGEST protocol

A three-stage *in vitro* simulated GIT digestion model reported by (Brodkorb et al., 2019) was performed to monitor and compare the fate of empty and *t*-res loaded liposomes, bilosomes as well as CH- and PGA/CH-coated bilosomes during digestion. For investigation of the effect of the food matrix on the behaviour of the samples during digestion, samples were mixed with OM (pH 7.64 and fat: 3.5%) (1:1 v/v) to mimic food fortified with samples and three phases of static *in vitro* simulated GIT model were repeated. Simulated salivary fluid (SSF, pH 7), SGF (pH 3), and SIF (pH 7) were prepared according to **Table 4.3** and enzyme activity assays were performed according to the supplementary data 1 and 2 of INFOGEST protocol (Brodkorb et al., 2019). All electrolyte stock solutions of digestion fluids were warmed to 37°C and enzymes and bile solution were prepared immediately before digestion steps.

Oral Phase: The sample was mixed first with SSF 5:4 (v/v) and then mixed with $CaCl_2.(H2O)_2$ (final concentration: 1.5 mM). $CaCl_2.(H2O)_2$ was added immediately before the digestion experiment to avoid precipitation during incubation. Deionized water was added to make the final sample to SSF ratio 1:1 (v/v) and then incubated in a shaking incubator (SciQuip Incu-Shake MAXI) at 37°C, 100 rpm for 2 min. After the oral phase, the sample was taken.

Gastric phase: Oral bolus was mixed with pre-warmed SGF 5:4 (v/v). Later on, the porcine pepsin solution was prepared in water (final activity: 2000 U/mL) and $CaCl_2.(H2O)_2$ (final concentration: 1.5 mM) were added, respectively. $CaCl_2.(H2O)_2$ was added immediately before the digestion experiment to avoid precipitation during incubation. The pH of the mixture was adjusted to pH 3 with 1 M HCl solution and the final volume was completed with deionized water to make the oral bolus to SGF ratio 1:1 (v/v). The mixture was incubated in a shaking incubator at 37°C, 100 rpm for 2 h. The samples were taken during and after the gastric phase and 1 M $NaHCO_3$ was added to the samples to stop the pepsin activity.

Intestinal phase: Gastric chyme was mixed with pre-warmed SIF 2.35:1 (v/v). Bile solution (final concentration: 10 mM) and porcine pancreatin solution (final trypsin activity, 100 U/mL) prepared in SIF were added, respectively. Finally, $CaCl_2.(H2O)_2$ (final concentration: 0.6 mM) was added to the mixture and the pH of the mixture was adjusted to pH 7 with 1 M NaOH solution. $CaCl_2.(H2O)_2$ was added immediately before the digestion experiment to avoid precipitation during incubation. The samples were taken during and after the intestinal phase and Pefabloc (Final concentration: 5 mM)

was added to the samples to stop the trypsin activity. The final volume was completed with deionized water to make the gastric chyme to SIF ratio 1:1 (v/v) and the mixture was incubated in a shaking incubator at 37°C, 100 rpm for 2 h. The samples were taken during and after the intestinal phase.

All samples taken from the static *in vitro* simulated digestion experiment were flash freeze with liquid nitrogen and then stored at -80 °C until further analysis. Measurements were performed on triplicate samples.

Table 4.3 Volumes of electrolyte stock solutions of digestion fluids for a volume of 400 mL diluted with water (1.25× concentrations) (Brodkorb et al., 2019; Minekus et al., 2014).

Salt solution added	Stock concentrations		SSF (pH 7)		SGF (pH 3)		SIF (pH 7)	
			Stock added to prepare 0.4 L (1.25×)	Final salt concentration in SSF	Stock added to prepare 0.4 L (1.25×)	Final salt concentration in SGF	Stock added to prepare 0.4 L (1.25×)	Final salt concentration in SIF
	(g/L)	(M)	(mL)	(mM)	(mL)	(mM)	(mL)	(mM)
KCl	37.3	0.5	15.1	15.1	6.9	6.9	6.8	6.8
KH_2PO_4	68	0.5	3.7	3.7	0.9	0.9	0.8	0.8
$NaHCO3^a$	84	1	6.8	13.6	12.5	25	42.5	85
NaCl	117	2	-	-	11.8	47.2	9.6	38.4
$MgCl_2(H_2O)_6$	30.5	0.15	0.5	0.15	0.4	0.12	1.1	0.33
$(NH_4)_2CO_3^*$	48	0.5	0.06	0.06	0.5	0.5	-	-
HCl		6	0.09	1.1	1.3	15.6	0.7	8.4
$CaCl_2(H_2O)_2^b$	44.1	0.3	0.025	1.5	0.005	0.15	0.04	0.6

SSF: Simulated salivary fluid, SGF: Simulated gastric fluid, and SIF: Simulated intestinal fluid. [a] The use of carbonate salts in the electrolyte solutions requires the use of sealed containers with limited headspace, [b] $CaCl_2(H_2O)_2$ should be added immediately before the digestion experiment to avoid precipitation during incubation. Volumes in **Table 4.3** are indicated for a typical experiment of 5 mL of SSF. The addition of enzymes, bile salts, Ca^{2+} solution etc. and water will result in the correct electrolyte concentration in the final digestion mixture.

4.3.5 Bioaccessibility assessment

The amount of released *t*-res at the end of *in vitro* simulated GIT digestion was determined as described previously (Niaz et al., 2021) with slight modifications. The raw digesta was collected and centrifuged using a high-speed centrifuge (Beckman Coulter, Avanti Centrifuge J-30I) at 108800xg for 60 min at 4°C. The supernatant was

collected and dried using a Genevac (EZ-2 plus) (Fisher Scientific Ltd, Leicestershire, UK) (25℃, Method: Aqueous). The dried samples were dissolved in methanol and were filtered through a 0.20 µm PTFE filter for quantification of *t*-res using HPLC-DAD. Measurements were performed on triplicate samples. The bioaccessibility of *t*-res was calculated using the following equations:

$$\text{Bioaccessibility (\%)} = \frac{\text{tres in raw digesta (mg)}}{\text{initial tres (mg)}} \text{x}100 \qquad \textbf{Eq. 4.1}$$

4.3.6 Using chamber system for intestinal permeability of the *t*-res

To assess the intestinal permeability of free *t*-res and *t*-res loaded in liposomes and bilosomes, the Ussing chamber method outlined by Mackie et al. was followed (Mackie et al., 2019).

Setup of Using chamber: Before preparing the intestinal tissue, salt bridges (2% agar and 0.9% NaCl) were inserted into the Ussing chambers. The compartments of the Ussing chambers were then filled with Ringer solution, consisting of NaCl (120 mM), KCl (3 mM), $MgCl_2.6H_2O$ (0.5 mM), $CaCl_2.2H_2O$ (1.25 mM), and $NaHCO_3$ (23 mM). The chamber temperature was maintained to 37°C throughout the experiment by circulating water bath and a continuous supply of oxygen was ensured by using a carbogen gas (5% CO_2/95% O_2) cylinder connected to the Ussing chamber. The current and fluid resistance was adjusted to zero from the epithelial voltage clamps (EC-825A, Warner instruments) and the system was left for 10 min for stabilisation.

Tissue preparation and mounting: Intestinal samples from C57BL/5 mice were collected. The collected intestines were flushed twice with ice-cold Krebs–Ringer bicarbonate (KRB) solution and placed into ice-cold 10 mM glucose solution. We selected a segment of the duodenum because it is the primary site for fat digestion in the upper small intestine and for nutrient absorption. The dissected mouse intestine was longitudinally opened using fine forceps and dissection scissors, after which the serosa and muscularis layers were carefully removed using fine forceps. The prepared intestinal tissue was then mounted onto a tissue slider/insert (with an exposed tissue area of 0.25 cm^2 (P2404, Physiologic Instruments, San Diego, USA), compatible with Ussing chamber system (EM-CSYS-4 with a low-volume P2400 chamber). Throughout the preparation and mounting processes, the tissue was consistently rinsed with a solution of 10 mmol/L glucose. Subsequently, the prepared slide was inserted into the stabilised Ussing chamber for the experiment.

Ussing chambers experiment: Upon insertion of the slide of intestinal tissue into the Ussing chamber, the apical compartment was filled with 1 mL of Ringer's solution containing 10 mM mannitol, while the basolateral compartment was filled with 1 mL of

Ringer's solution containing 10 mM glucose to balance both sides osmotically. The inserted tissue was equilibrated for 30 min before the addition of the sample into the apical side of the chamber **(Fig. 4.1).**

After 30 min of tissue equilibrium, 500 µL of buffer was removed from the apical side of the Ussing chambers and replaced with 500 µL of the sample (which had been centrifuged 280x g, for 5 min at 4 °C). After regular intervals (60min and 120min), 300 µL samples were taken from both the apical and basolateral sides of the Ussing chamber. Subsequently, the volumes were completed back to 1 mL by adding an equal amount of fresh buffers. At the end of the experiment (120 min), both the apical and basolateral solutions (1 mL) were collected for the quantification of *t*-res absorption. Additionally, intestinal tissue was collected to assess the accumulated *t*-res within the tissue.

For tissue viability, the open circuit potential difference (P.D.) was continuously monitored during the experiment using silver-silver chloride electrodes and salt bridges. Data of the short circuit current (Isc) and P.D. were collected every 15 min and resistance and the transepithelial electrical resistance (TEER) of the mounted tissue were calculated through Ohm's law, as outlined below. Tissue with TEER value more than 20 $\Omega \cdot cm^2$ was considered from the experiment.

$$\text{Resistance} = \frac{\text{P.D. (mV)}}{\text{Isc (mAmp)}} \qquad \textbf{Eq. 4.2}$$

$$\text{TEER} = \text{Resistance } (\Omega) \text{ x area}(cm^2) \qquad \textbf{Eq. 4.3}$$

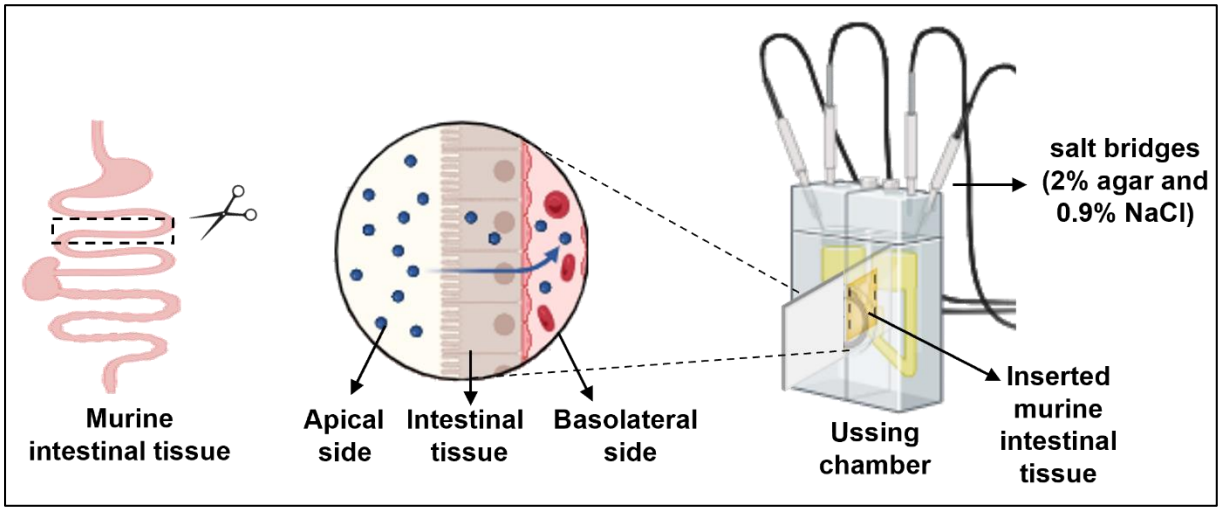

Figure 4.1 Schematic representation of murine intestinal tissue and the Ussing chamber.

4.3.7 Statistical analysis

All the data were reported as mean±SD. Results were analysed by one-way ANOVA) using Minitab® 20.4 software. The level of statistical significance was defined by $p<0.05$.

4.4 Results and discussion

4.4.1 Initial properties of liposomes, bilosomes, CH-coated and PGA/CH-coated bilosomes and their mix with oat milk

4.4.1.1 Liposomes, bilosomes, CH-coated and PGA/CH-coated bilosomes;

The physical properties (D_H, PDI, and ζ potential) of *t*-res loaded liposomes, bilosomes, CH-coated and PGA/CH-coated bilosomes, and properties before and after mixing with OM were monitored. The initial D_H of *t*-res loaded liposomes and bilosomes were between 263.0±2.1 nm to 428.8±2.7 nm with a PDI of ~0.250 and the ζ potential was between -40.9±4.0 mV to -47.9±2.9 mV **(Fig. 4.2)**. When negatively charged NaC (Garidel et al., 2007) was incorporated to the liposome formulation, the D_H of the bilosomes increased and ζ potential decreased significantly but different concentrations of NaC did not affect the D_H and ζ potential of the bilosomes. When the NaC concentration is lower than its critical micelle concentration (CMC), it can still disturb and cause pore formation on the bilayer, but their concentration is not enough to convert the bilayer to mixed micelles (Garidel et al., 2007). Because 5 mM t-res loaded liposomes and bilosomes prepared for digestion experiments were only sonicated and not extruded through a 100 nm polycarbonate membrane, they have multilamellar structures. The destabilisation effect of bile salts on the multilamellar structures will be slower than the unilamellar structures presented in 1 mM t-res loaded liposomes and bilosomes. Because bile salts first locate on the outermost bilayer, and only when the outer bilayer has been disrupted or some pores are formed by them, bile salt molecules can begin to locate the next bilayers (Lichtenberg et al., 2013).

Bilosomes were first coated with CH by electrostatic interaction between the negatively charged phosphate group ($-PO_4^{3-}$) of phospholipids and the positively charged amine group ($-NH_3^+$) of CH (Henriksen et al., 1994). The anionic TPP was also added as a cross-linker during CH coating which interacts with the positively charged amine group (-NH3+) of CH through electrostatic interactions to enhance the stability of the coating (Zhao & Wu, 2006). After CH coating **(Fig. 4.2)**, ζ potential of bilosomes was turned from negative (around -45 mV) to positive (around +20 mV) ($p<0.05$). The D_H of the CH-coated bilosomes was between 375.9±4.4 nm and 460.7±21.0 nm with PDI: ~0.170. Although the CH coating did not increase the D_H significantly for bilosome

samples except (CH-B-10:5), the positive surface charge of the coated samples shows that the coating was successful.

Moreover, the significant increase in D_H could be because of the osmotic pressure effect of CH, which can dehydrate and change the structural order of the bilayers under the coating (Amenitsch et al., 2004). For CH-B-10:5, the significant increase in the D_H of B-10:5 after CH coating may have resulted from the concentration of CH. The increased concentration of NaC in the bilosome formulations turns the ζ potential more negative thus needing more CH to coat the surface. So higher concentration of CH might have provided a thicker shell compared to the other bilosome samples.

The CH-coated bilosomes were coated using negatively charged PGA by electrostatic interaction between the amine group ($-NH_3^+$) of CH and the carboxylate ion ($-COO^-$) of PGA (Jeon et al., 2015). For the PGA/CH-coated bilosomes, ζ potential of samples turned from positive (around +20 mV) to negative (around -20 mV) ($p<0.05$) **(Fig. 4.2)**. The initial D_H of PGA/CH-coated samples ranged from 349.2±7.4 to 668.7±22.0 nm with a high polydispersity (PDI: ~0.400) ($p<0.05$). The second biopolymer coating significantly increased the D_H of the samples compared to the CH-coated bilosomes (except PGA/CH-10-5:5). When combined with the change in ζ potential, PGA was successfully deposited on the CH-coated bilosomes. For PGA/CH-B-5:5, compared to other PGA/CH-coated samples, a lower PGA concentration was needed to coat the surface because of its lower ζ potential so the D_H may not have increased significantly.

The bilayer of the liposomes was first modified with the addition of NaC and then the surface of the bilosomes was modified with CH coating and PGA/CH coating. These changes induced the following interactions; hydrophobic interactions between *t*-res/phospholipids, cross-linking between CH and TPP, and electrostatic interaction between bilosomes/CH and CH/PGA (Balanč et al., 2015; Yu et al., 2009). Understanding the interactions and impact of bilayer and surface modification on the lipid bilayers as a drug delivery system is essential to control the behaviours during digestion.

The EE and LC data of 5 mM *t*-res loaded liposomes, bilosomes, CH-coated and PGA/CH-coated bilosomes were obtained using HPLC **(Fig. 4.3).** The EE of liposomes was 25.3±0.2% with 2.5% of LC. The EE of bilosomes was significantly higher than the EE of liposomes and ranged from 41.4±0.4% to 45.4±3.5%. The incorporation of NaC into lipid bilayers increased the EE. An increased EE could be because the addition of bile salts altered the packing of the molecules within the hydrophobic domains of the lipid bilayers. As a result, *t*-res molecules might more readily integrate into these lipid bilayers (Cheng et al., 2019).

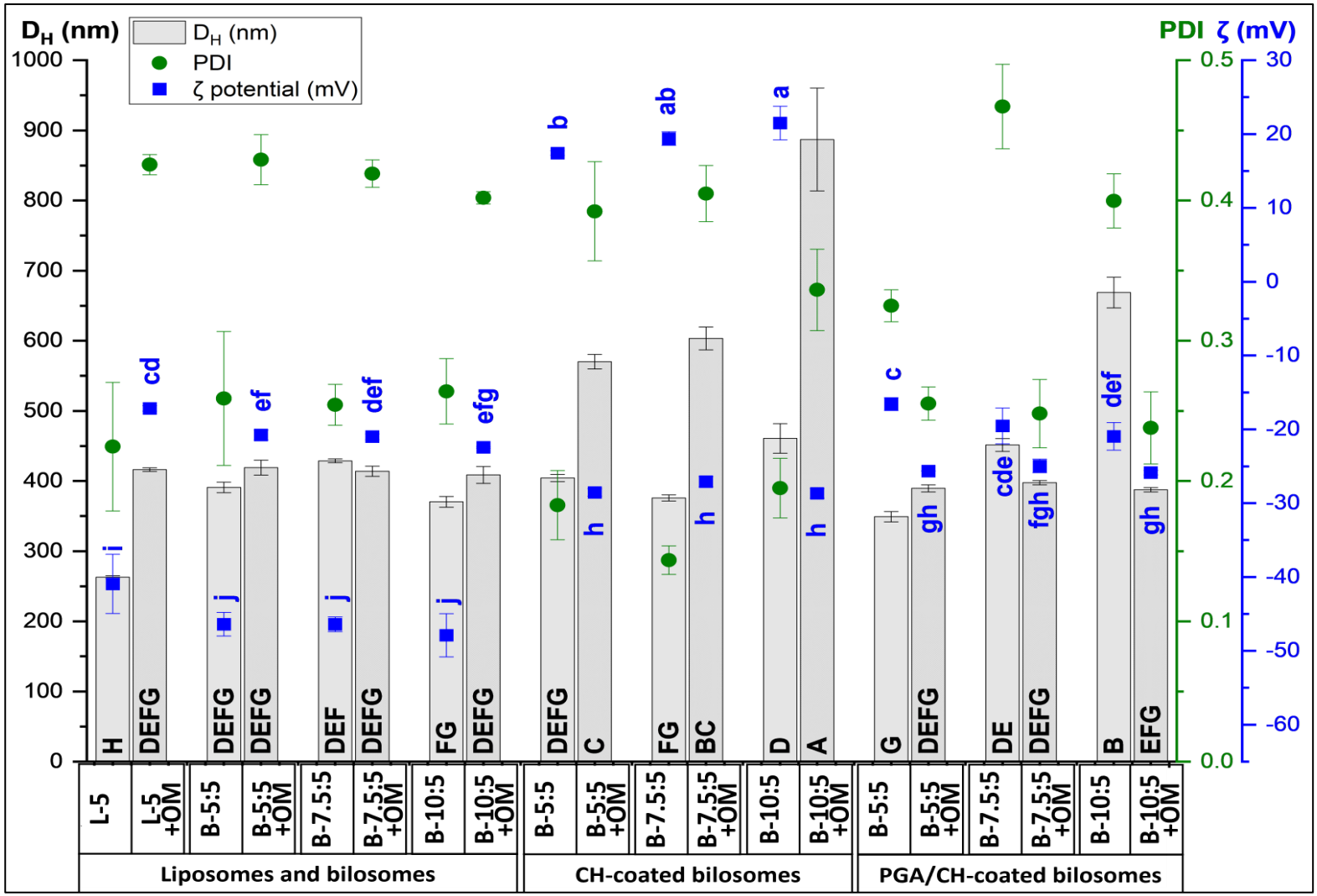

Figure 4.2 The D_H (nm) (▭), PDI (●) and ζ potential (mV) (■) of liposomes, bilosomes, CH-coated and PGA/CH-coated bilosomes without (▭) and with OM (▨). The data represent the mean±SD. Black capital letters represent significant differences in the D_H, and blue lowercase letters in the ζ potential among the samples, respectively ($p < 0.05$).

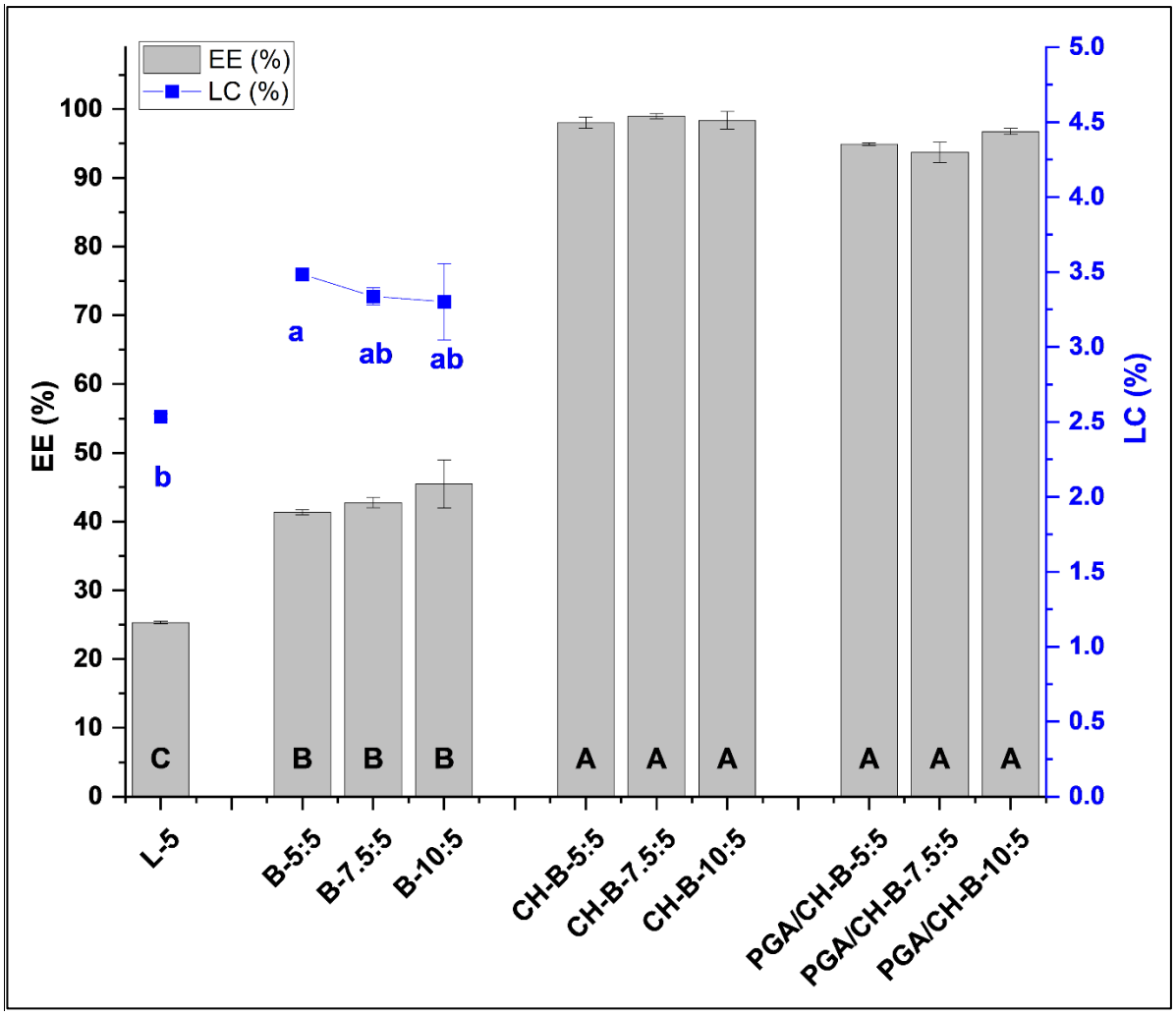

Figure 4.3 Encapsulation efficiency (EE%) (▭) of *t*-res loaded liposomes, bilosomes, and CH-coated and PGA/CH-coated bilosomes and loading capacity (LC%) (■) of *t*-res loaded liposomes, and bilosomes. The data represent the mean±SD. Black capital letters represent significant differences in the EE, and blue lowercase letters in the LC potential among the samples, respectively ($p < 0.05$).

EE of EGCG-loaded liposomes and bilosomes were reported as 74.4±1.3% and 85.9±1.4% respectively (L. Wang et al., 2021). Biopolymer coating increased the percentage of encapsulated the *t*-res. While the EE of the CH-coated samples was around 98%, the EE of the double-coated samples was ~95%. This could be attributed to the fact that CH and PGA cover the surface of lipid bilayers, creating a protective shield that prevents the leakage of *t*-res from lipid bilayers. The increased EE after biopolymer coating compares well with previous studies. The EE of cinnamaldehyde-loaded liposomes and CH-coated liposomes was determined by Wang et al. The EE of the uncoated liposomes was around 40%, while the EE of the coated samples did not change significantly up to 1 mg/mL CH. However, the EE increased significantly to approximately 55% when 3 mg/mL of CH was used (X. Wang et al., 2021). The EE of curcumin-loaded liposomes increased from 41.42±3.03% to 52.80±3.23% after CH

coating (Y. Liu et al., 2015). Lycopene-loaded liposomes and canthaxanthin-loaded liposomes prepared by Tan et al. The EE of the lycopene-loaded liposomes and canthaxanthin-loaded liposomes was reported as 87% and 58%, respectively. After CH coating (1.5 mg/mL) EE values increased by ~10% (Tan et al., 2016). While the EE of curcumin-loaded liposomes was 73.8%, exhibited an increase to a range of 84.0%–99.8% following the CH coating of 0.1%–0.5% (Chen et al., 2022).

While LC of liposomes was ~2.5%, the LC of the bilosomes was around 3.4% **(Fig. 4.3)**. The LC of the CH-coated bilosomes was higher than liposomes and bilosomes due to their EE and The LC decreased from 6.3% to 4.6% with increased CH concentration in the system. The LC of the PGA/CH-coated bilosomes ranged from 3.8% to 2.4% which was lower than the LC of CH-coated samples due to the addition of PGA into the system. Previous researchers have studied the EE and LC of hydrophobic bioactive compounds. LC capacity of resveratrol-loaded liposomes was ~3.1% (Soo et al., 2016). Curcumin-loaded liposomes modified with rhamnolipids, as reported by Chen et al. achieved EE exceeding 90% and LC higher than 3.5% (Chen et al., 2022).

4.4.1.2 Liposomes, bilosomes, CH-coated and PGA/CH-coated bilosomes mixed with oat milk;

The D_H, PDI and ζ potential of the OM was determined as 390.3±11.2 nm, 0.398±0.008 and -22.5±0.7 mV, respectively **(Fig. 4.4)**. OM (pH 7.64) is basically a colloidal system which contains oil droplets composed of a triglyceride core covered by a phospholipid/protein shell (Nikiforidis, 2019). However, as a commercial product, OM **(Table 4.1)** contains several ingredients such as sunflower oil, pea proteins, and fibres besides oat and water to provide stability to the products and to meet customer expectations. The phospholipid/protein monolayer on the oil droplets improves the dispersion of the oil consequently providing stability to the OM. The OM used in this study contained pea proteins (pKa ~4.5) which are negatively charged at the neutral pH and provide charge to the system and stability due to the electrostatic repulsive forces (Wei et al., 2020).

When liposomes or bilosomes (pH 5.5) were mixed with OM, while the D_H of L-5 was 263.0±2.1 nm, the DH of L-5+OM mix was 416.4±2.6 nm ($p<0.05$). However, there was no significant difference between the D_H of the bilosome and D_H of the bilosome OM mix **(Fig. 4.2)**. However, the D_H and PDI of the OM were already 390.3±11.2 nm and 0.398±0.008, respectively. Similar properties of OM and lipid bilayer-OM mix may be related to low concentration of liposomes or bilosomes in the mixture. As a result, the properties of the lipid bilayer-OM mix were mostly related to the properties of OM. The several types of interactions such as electrostatic binding or repulsion,

hydrophobic interaction, and adsorption can form due to the different components in the lipid bilayer-OM mix. Phospholipids (POPC and DOPG) are surface-active compounds and behave differently depending on their head group and fatty acid chains at the oil/water interface. Proteins (pea proteins and proteins from oat base) are also amphiphilic molecules that behave differently at the oil/water interface because of their molecular structure and conformations (He et al., 2008). This complex system is a mixed phospholipid/protein complex with the associated interactions and behaviours of the compounds.

The final pH of the lipid bilayer-OM mixture was ~7.35 after liposomes or bilosomes (pH 5.5) were mixed with OM (pH 7.64). The ζ potential of both liposomes and bilosomes was approximately -45 mV. However, upon combining the samples with OM, the ζ potential of the resulting liposomes-OM mixture and bilosomes-OM mixture increased to about -20 mV **(Fig. 4.2)**. The increased D_H of the liposome or bilosome dispersion after mixing with OM might be also related to flocculation because of the decreased magnitude of the ζ potential resulting in weakened electrostatic repulsion between negatively charged lipid bilayers and negatively charged lipid droplets of the OM (Brooksbank et al., 1993). Moreover, in this mixed system, phospholipids and proteins can displace each other from the water/oil interface by synergetic or competitive adsorption. For synergetic adsorption, which occurs at low phospholipid concentration, both phospholipids and proteins can absorb together onto the interface. During competitive adsorption firstly rapid diffusion and distribution of the phospholipids at the interface and then the displacement of the proteins take place (Shen et al., 2023).

When CH-coated bilosomes were mixed with OM, the D_H and PDI of the CH-coated bilosomes-OM mix were significantly higher compared to CH-coated bilosomes and ranged from 570.2±10.3 nm to 887.0±24.0 nm and from 0.336±0.029 to 0.405±0.020 respectively ($p<0.05$) **(Fig. 4.2)**. While the ζ potential of the CH-coated bilosomes was positive, the ζ potential of the CH-coated bilosomes-OM mix was negative (around -28 mV) ($p<0.05$). CH-coated bilosomes have positive ζ potential whereas the surface charge of the phospholipid/protein monolayer shell on the oil droplets was negative. The negatively charged oil droplets within OM or proteins displaced from the water/oil interface might have neutralized the positive charges of CH-coated bilosomes and reduced the electrostatic repulsion between particles resulting in flocculation (Zhao et al., 2021). As a result, the mixed system ended up with increased D_H and PDI and decreased magnitude of the ζ potential.

While the properties of PGA/CH-B-5:5 and PGA/CH-B-7.5:5 were not significantly different than their mix with OM, the D_H of PGA/CH-B-10:5-OM mix (387.5±3.1 nm) was significantly lower than the D_H of PGA/CH-B-10:5 (668.7±22.0

nm). The ζ potential and PDI of samples were around -25 mV ($p<0.05$) and ~0.250, respectively. As seen in the properties of liposomes or bilosomes-OM mix, the properties of the PGA/CH-coated bilosomes-OM mix also looked mostly predominated by the properties of OM possibly due to the low concentration of double-coated bilosomes **(Fig 4.2)**. The food matrix can show beneficial or adverse impacts on the physicochemical properties, stability, digestion profile, and absorption of the drug delivery system (Molet-Rodríguez et al., 2023). Therefore, understanding the formed interactions after the incorporation of lipid bilayers into the food matrix is crucial for oral delivery systems.

4.4.2 *In vitro* digestion characteristics of the fate of free *t*-res, liposomes, bilosomes, CH-coated and PGA/CH-coated bilosomes and systems digested with oat milk

The potential behaviour of free *t*-res, *t*-res loaded liposomes, bilosomes, and CH-coated and PGA/CH-coated bilosomes with and without OM was investigated during a static *in vitro* simulated digestion.

4.4.2.1 Free *t*-res;

When free *t*-res **(Fig. 4.4** and **Table 4.4)** was exposed to SSF, the D_H measured as ~1200 nm with PDI: ~0.800. Because of the low solubility of *t*-res at neutral pH, its crystals were suspended in the buffer. The ζ potential of *t*-res was determined around -3 mV. In the gastric phase, the D_H of free *t*-res decreased to ~250 nm ($p<0.05$). The ζ potential of gastric chyme of free *t*-res became more negative to around -6 mV at the end of the gastric phase. When gastric chyme of free *t*-res was exposed to the intestinal phase, the D_H of SIF was ~350 nm and the ζ potential of SIF of free *t*-res became even more negative to around -12 mV at the end of the intestinal phase ($p<0.05$). The changes in properties were possibly related to the formation of mixed micelles that included negatively charged bile salts. Up to 30% of dietary lipids are digested by gastric lipase during digestion (Wilde & Chu, 2011). Gastric lipase was not used in the *in vitro* digestion experiments, so lipid digestion was expected to begin with pancreatic lipases with the cooperation of bile salts in the intestinal phase for free *t*-res. When *t*-res are exposed to intestinal fluid and bile, the content of bile which are bile salts, phospholipids, and Chol solubilises *t*-res in mixed micelles. Mixed micelles carry the solubilised *t*-res to the intestinal mucosa for absorption (Mackie & Macierzanka, 2010; Wilde & Chu, 2011).

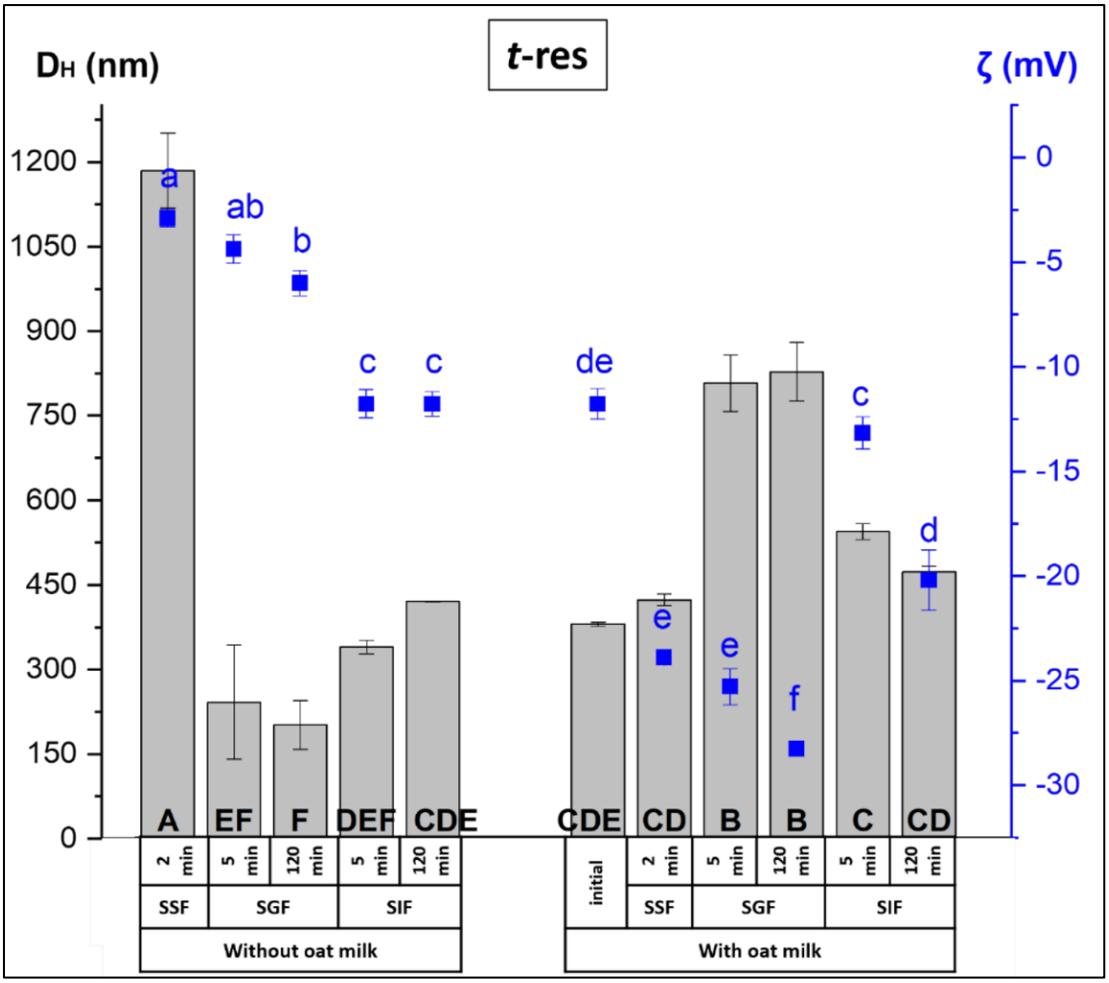

Figure 4.4 The effect of exposure to different phases of the static *in vitro* simulated digestion model on the D_H (nm) (▭) and ζ potential (mV) (■) of free *t*-res without and with OM. The data represent the mean±SD. Black capital letters represent significant differences in the DH, and blue lowercase letters in the ζ potential, respectively ($p < 0.05$).

4.4.2.2 Liposomes and bilosomes;

When the liposomes **(Fig. 4.5A)** and bilosomes **(Fig. 4.5B-D)** were exposed to SSF, the ζ potential increased from around -35 mV to around -10 mV and their D_H decreased significantly (between 72.9±2.8 and 137.8±6.1 nm) ($p<0.05$). The increase in the ζ potential could be attributed to the screening effect of salts in SSF. Also due to the pH of the SSF (pH 7), the head group of phospholipids was slightly deprotonated which caused a reduction in its charge and steric size (Zidovska et al., 2009). These significant decreases in the D_H could have been caused by several factors. When liposomes and bilosomes are mixed with SSF, the bilayers can be dehydrated by the osmotic pressure created by the cationic ions (K^+, Na^+, and Ca^{2+}) in the oral phase, and osmotic pressure induces an osmotic shrinking, consequently reduction in the D_H. Also, these ions can be adsorbed to the bilayers and alter the membrane curvature consequently altering shape and lamellarity (Hupfeld et al., 2010; Sabın et al., 2006).

The D_H, PDI, and ζ potential in the oral bolus of liposomes and bilosomes were not changed significantly after exposure to the gastric phase **(Fig 4.5** and **Table 4.4)**. There was a slight changes in the ζ potential which may be linked to the high ionic strength and acidic pH of the gastric phase which affects the ionisation state and charge distribution of the head groups of phospholipids (Toro-Uribe et al., 2018). Liposomes and bilosomes remained unchanged during the gastric phase basically, showing their stability. These results agree with Hui and Huang who reported no significant change in D_H but slight changes in ζ potential of liposomes during the gastric phase (Hui & Huang, 2021).

When the gastric chyme of liposomes and bilosomes was exposed to the SIF, the D_H increased significantly up to ~300 nm and did not change until the end of the intestinal phase. The D_H of SIF of liposomes and bilosomes looked mostly related to the properties of porcine pancreatin and bile in SIF because the D_H of the SIF of free *t*-res was also 261.0± 12.3 nm with PDI: ~0.250. The ζ potential of SIF of samples was more negative (around -15 mV) at the intestinal phase compared to the gastric phase (around -5 mV, $p<0.05$) **(Fig 4.5** and **Table 4.4)**. The composition of the intestinal phase (pancreatin, bile salts, and ions) affects the stability of lipid bilayers. As mentioned before, bile salts have a solubilisation effect on the lipid bilayer and work cooperatively with pancreatic enzymes in the intestinal phase. Bile salts facilitate the adsorption of lipase and co-lipase and help to solubilise the lipolysis products. Bile salts displace the hydrolysed lipids from the interface and transport them as mixed micelles for absorption and provide accessibility to lipase for further hydrolysis (Chu et al., 2010; Labourdenne et al., 1997; Wilde & Chu, 2011). At the end of the intestinal phase, there was no noticeable difference between the D_H and PDI of the SIF of liposomes and bilosomes. However, the D_H of SIF of bilosomes was slightly higher than liposomes, and ζ potential of the intestinal phase was getting more negative with increased concentration of NaC in the system. The interactions between positively charged ions and negatively charged lipid systems may reduce membrane curvature and result in swelling and size expansion of the bilayers (Toro-Uribe et al., 2018).

Table 4.4 The effect of exposure to different phases of the static *in vitro* gastrointestinal digestion model on the PDI of t-res loaded samples digested without and with OM. The data represent the mean±SD. Lowercase letters indicate the significant differences between columns (in PDI of the samples during digestion) ($p<0.05$).

Sample	Without oat milk						With oat milk					
	initial	SSF	SGF		SIF		initial	SSF	SGF		SIF	
		2 min	5 min	120 min	5 min	120 min		2 min	5 min	120 min	5 min	120 min
***t*-res**	-	0.794 ±0.007 a	0.277 ±0.029 bcd	0.207 ±0.019 d	0.269 ±0.009 cd	0.332 ±0.009 bc	0.300 ±0.011 b	0.093 ±0.053 e	0.816 ±0.024 a	0.916 ±0.041 a	0.221 ±0.006 cd	0.236 ±.004 cd
L-5	0.225 ±0.046 c	0.202 ±.006 c	0.242 ±.012 bc	0.239 ±0.015 c	0.251 ±0.022 bc	0.233 ±0.004 c	0.426 ±0.007 a	0.133 ±0.069 c	0.169 ±0.031 c	0.154 ±0.079 c	0.377 ±0.045 ab	0.269 ±0.021 bc
B-5:5	0.259 ±0.048 bc	0.291 ±0.003 bc	0.348 ±0.032 ab	0.354 ±0.040 ab	0.255 ±0.004 bc	0.226 ±0.013 cd	0.429 ±0.018 a	0.116 ±0.058 de	0.051 ±0.020 e	0.112 ±0.023 de	0.305 ±0.024 bc	0.216 ±0.041 cd
B-7.5:5	0.254 ±0.015 bcde	0.291 ±0.002 abcd	0.381 ±0.050 abc	0.399 ±0.055 ab	0.242 ±0.012 cde	0.226 ±0.004 de	0.419 ±0.010 a	0.109 ±0.087 e	0.234 ±0.025 cde	0.111 ±0.078 e	0.303 ±0.023 abcd	0.250 ±0.008 bcde
B-10:5	0.264 ±0.023 b	0.128 ±0.040 de	0.229 ±0.013 bcd	0.248 ±0.003 bc	0.227 ±0.005 bcd	0.265 ±0.016 b	0.402 ±0.004 a	0.157 ±0.031 cde	0.280 ±0.065 b	0.060 ±0.027 e	0.318 ±0.029 ab	0.230 ±0.018 bcd

Table 4.4 The effect of exposure to different phases of the static *in vitro* gastrointestinal digestion model on the PDI of t-res loaded samples digested without and with OM. The data represent the mean±SD. Lowercase letters indicate the significant differences between columns (in PDI of the samples during digestion) ($p<0.05$) (*continued*).

Sample	Without oat milk						With oat milk					
	initial	SSF	SGF		SIF		initial	SSF	SGF		SIF	
		2 min	5 min	120 min	5 min	120 min		2 min	5 min	120 min	5 min	120 min
CH-B-5:5	0.183 ±0.025 cde	0.572 ±0.071 a	0.306 ±0.020 bc	0.292 ±0.006 bc	0.368 ±0.012 b	0.296 ±0.018 bc	0.392 ±0.035 b	0.265 ±0.028 bcd	0.090 ±0.064 e	0.114 ±0.028 de	0.296 ±0.043 bc	0.239 ±.001 cd
CH-B-7.5:5	0.144 ±0.010 c	0.445 ±0.096 a	0.304 ±0.033 ab	0.301 ±0.018 ab	0.361 ±0.016 a	0.307 ±0.006 ab	0.405 ±0.020 a	0.296 ±0.056 abc	0.286 ±0.081 abc	0.136 ±0.024 bc	0.292 ±0.018 abc	0.305 ±0.026 ab
CH-B-10:5	0.195 ±0.021 de	0.666 ±0.022 a	0.336 ±0.011 c	0.305 ±0.020 c	0.308 ±0.010 c	0.339 ±0.034 c	0.336 ±0.029 c	0.462 ±0.007 b	0.191 ±0.058 e	0.139 ±0.044 e	0.298 ±0.003 cd	0.302 ±0.029 c
PGA/CH-B-5:5	0.325 ±0.011 cd	0.654 ±0.049 a	0.292 ±0.004 cd	0.325 ±0.029 cd	0.310 ±0.021 cd	0.269 ±0.013 cd	0.255 ±0.012 d	0.365 ±0.018 bcd	0.408 ±0.080 bc	0.474 ±0.073 b	0.280 ±0.026 cd	0.241 ±0.019 d
PGA/CH-B-7.5:5	0.467 ±0.030 abc	0.469 ±0.023 ab	0.358 ±0.008 bcd	0.308 ±0.027 d	0.336 ±0.009 d	0.281 ±0.015 d	0.248 ±0.024 d	0.371 ±0.020 bcd	0.588 ±0.018 a	0.591 ±0.057 a	0.340 ±0.059 cd	0.244 ±0.032 d
PGA/CH-B-10:5	0.400 ±.019 c	0.748 ±0.039 a	0.227 ±0.011 e	0.242 ±0.013 e	0.358 ±0.042 cd	0.303 ±0.029 cde	0.238 ±0.026 e	0.388 ±0.026 c	0.630 ±0.020 b	0.737 ±0.035 ab	0.271 ±0.036 de	0.244 ±0.001 e

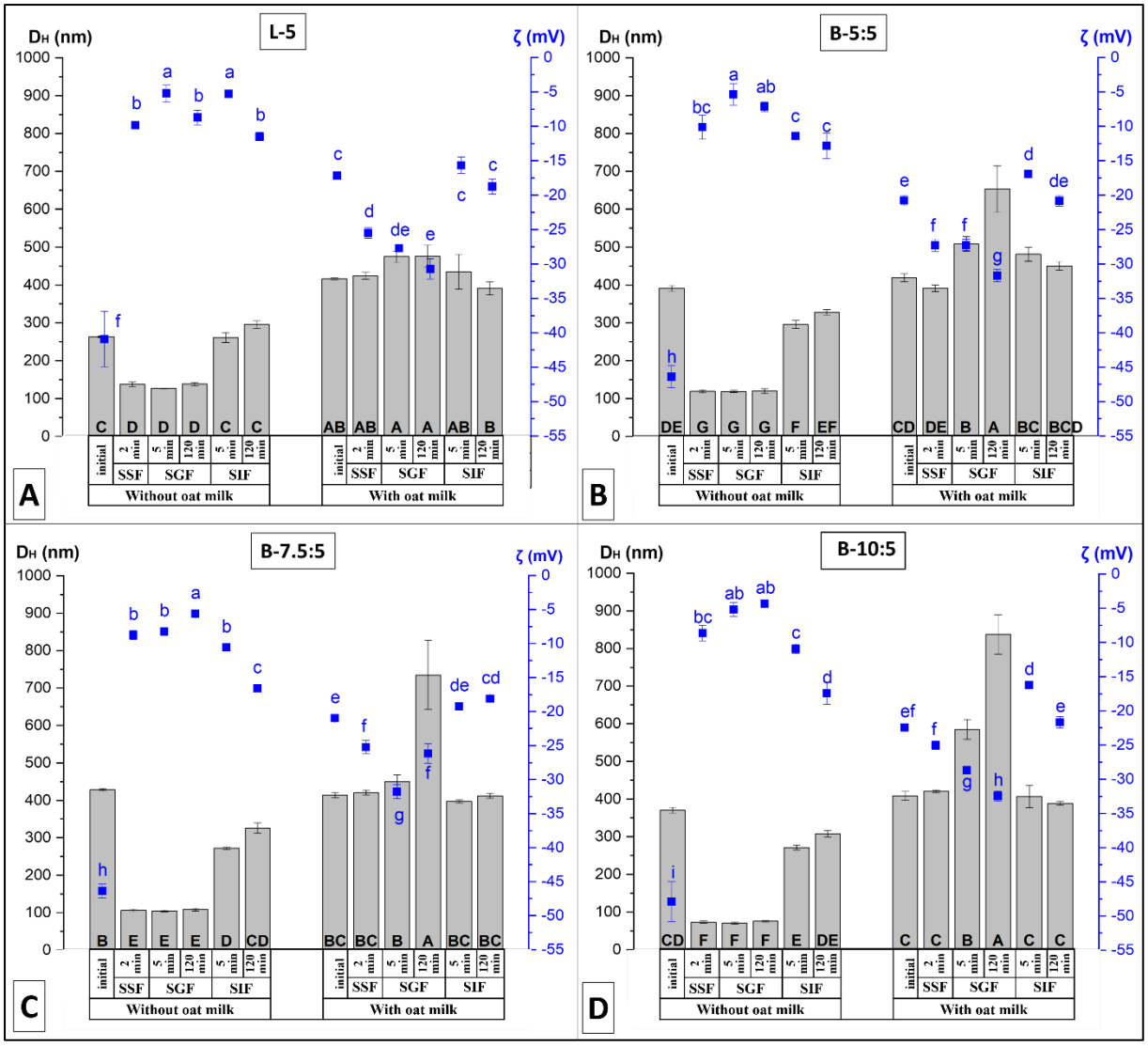

Figure 4.5 The effect of exposure to different phases of the static *in vitro* simulated digestion model on the D_H (nm) (▭) and ζ potential (mV) (■) of **(A)** L-5, **(B)** B-5:5, **(C)** B-7.5:5, and **(D)** B-10:5 without and with OM. The data represent the mean ± SD. Black capital letters represent significant differences in the DH, and blue lowercase letters in the ζ potential, respectively ($p < 0.05$).

4.4.2.3 CH-coated bilosomes;

When CH-coated bilosomes **(Fig. 4.6A-C** and **Table 4.4)** were exposed to the SSF, aggregation was observed. A possible explanation of the aggregation is the deprotonation of the CH (pKa: ~6.5) due to the pH of the oral phase (pH 7). This caused the reduction of the ζ potential of CH-coated bilosomes from ~20 mV to around -3 mV thus promoting the flocculation of the system (Espinal-Ruiz et al., 2014). The D_H and PDI decreased to ~130 nm and ~0.300 respectively ($p<0.05$) and these parameters remained unchanged during the gastric phase. The unchanged properties of SGF of CH-coated bilosomes during the gastric phase could be because the coating could protect the liposomes and loaded compounds from pancreatic enzymes (Hua et

al., 2021). Similar to the bilosomes, unchanged properties during the gastric phase demonstrate the stability of CH-coated bilosomes (Hui & Huang, 2021). When the gastric chyme of the CH-coated samples was exposed to the SIF, the D_H of SIF was ~350 nm and ζ potential was around -11 mV ($p<0.05$). The significant increase in the D_H of SIF compared to the D_H of SGF is mostly related to the effect of pH and the ionic strength of the SIF on the CH. The CH functions as a protective layer for the lipid bilayers, minimizing the interaction between pancreatic lipase and the lipid bilayers and effectively reducing damage to the liposomes (Hui & Huang, 2021). The pH of the SIF (pH 7) is close to the pKa of the CH. When CH-coated bilosomes were exposed to the SIF after SGF, the amine groups of CH would have become deprotonated and uncharged which resulted in the formation of a bigger and insoluble biopolymer network. The slight changes in the properties continued during the intestinal phase could have possibly resulted from the weakened interaction between TPP ions and the amino group of the CH caused by the pH of the intestinal phase (Gokce et al., 2014). The CH is resistant to hydrolysis by the digestive enzymes secreted by the upper GIT (the oral, stomach, and intestine). The digestion of CH has been reported in the colon by lysozymes, nonspecific cellulases, and enzymes secreted by colonic microflora (Kim et al., 2016).

4.4.2.4 PGA/CH-coated bilosomes;

The initial D_H, PDI, and ζ potential of double-coated bilosomes and properties after exposure to the SSF was mostly similar **(Fig. 4.6D-F** and **Table 4.4)** When oral bolus was exposed to the SGF, the D_H, and PDI of SGF were ~140 nm and 0.300 respectively and ζ potential was less negative (around -8 mV) at 5 min of gastric phase compared to SSF ($p<0.05$). The decrease in the D_H at pH 3 is possibly because both the amine group ($-NH_3^+$) of CH (pKa: ~6.5) and the carboxyl group ($-COO^-$) of PGA (pKa ~2.9-3.5) are protonated (Liu et al., 2016; Morel et al., 1987). The dominating impact of the protonated carboxyl groups in pectin has been shown to cause the deswelling of the pectin network (Yu et al., 2009). The D_H, PDI and ζ potential of SGF of double-coated samples remained constant through the gastric phase. When the gastric chyme of double-coated samples was exposed to the SIF, while the D_H of SIF was ~330 nm, ζ potential was around -13 mV ($p<0.05$). The ζ potential continued to decrease during intestinal digestion and reached around -18 mV possibly because of the deprotonation of the PGA or the production of free fatty acids.

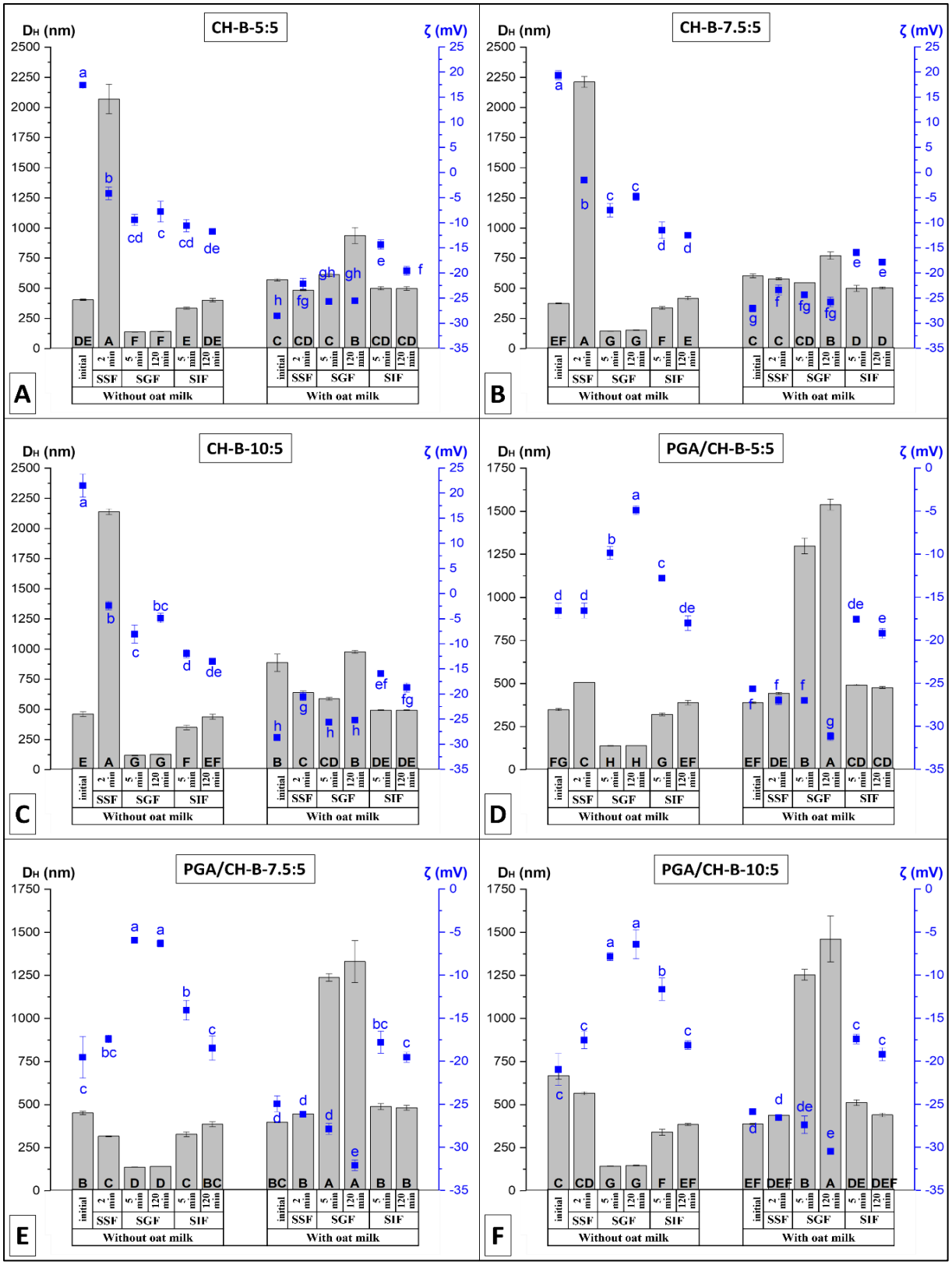

Figure 4.6 The effect of exposure to different phases of the static *in vitro* simulated digestion model on the D_H (nm) (▭) and ζ potential (mV) (■) of **(A)** CH-B-5:5, **(B)** CH-B-7.5:5, **(C)** CH-B-10:5, **(D)** PGA/CH-B-5:5, **(E)** PGA/CH-B-7.5:5, **(F)** PGA/CH-B-10:5 without and with OM. The data represent the mean±SD. Black capital letters represent significant differences in the DH, and blue lowercase letters in the ζ potential, respectively ($p < 0.05$).

When the double-coated samples passed from SGF to SIF, the concentration of the deprotonated carboxylate groups would have increased causing repulsion between the PGA chains and consequently resulting in swelled biopolymer shell (Yu et al., 2009). A similar decrease in ζ potential and increase in D_H was also reported by Liu et al. who investigated the behaviour of alginate/CH-coated liposomes during *in vitro* digestion. The ζ potential of double-coated samples was around -7.5 mV respectively after the gastric phase and decreased to around -20 mV when the sample was exposed to the intestinal phase and the decrease continued to around -55 mV during the intestinal phase. The D_H of alginate/CH-coated liposome increased from ~330 nm to ~530 nm during the intestinal phase (Liu et al., 2013). PGA is also resistant to enzymes secreted by upper GIT but can be digested by pectate lyase and pectate hydrolase secreted by colonic microflora (Matsuura, 1991).

4.4.2.5 Free *t*-res digested with oat milk;

As a control, free *t*-res was digested with OM **(Fig. 4.4** and **Table 4.4)** to see the effect of OM as a food matrix on the behaviour of *t*-res during digestion. The examination of the particle properties of *t*-res suspension (crystals in water) was not done due to the difficulty of obtaining representative samples. The D_H and PDI of the OM were 390.3±11.2 nm and 0.398±0.008 respectively so the D_H and PDI of the *t*-res-OM mix (pH: 7.35, D_H: 380±3.4 nm and PDI: 0.300±0.011) was mostly related to the properties of OM. While the ζ potential of the t-res was -22.5±0.7 mV, it was -11.8±0.7 mV for t-res-OM mix. When *t*-res-OM mix was exposed to SSF, the D_H of the SSF of the *t*-res-OM mix was not significantly different from the initial sample. The ζ potential decreased to -23.9±0.2 mV. Mucin and amylase were not used in the SSF so the change in ζ potential was possibly due to the weakened screening effect of the medium resulting from decreased ionic strength. When the oral bolus of *t*-res-OM mix was exposed to SGF, the D_H and PDI of SGF were ~800 nm and 0.800, respectively. Proteins are hydrolysed by proteases (pepsin, pancreatic trypsin, chymotrypsin, etc.). In the gastric phase, the chemical digestion of proteins by pepsin starts. Pepsin breaks polypeptide chains into smaller peptides by cleaving peptide bonds (Jahan-Mihan et al., 2011). When the pea protein on the lipid particles begins to be digested to polypeptides by pepsin, oil droplets may begin to destabilise, which can result in coalescence (Mackie & Macierzanka, 2010; Zheng et al., 2021) consequently increasing D_H. During the gastric phase, the D_H and PDI of SGF continued to increase and ζ potential decreased from around -25 to around -28 mV ($p<0.05$). The D_H and PDI of gastric chyme decreased to ~550 nm and 0.220 after 5 min of intestinal phase digestion and did not change during the intestinal phase. The ζ potential of SIF first increased to around -13 mV and decreased to around -20 at the end of the intestinal phase ($p<0.05$) due to the negatively charged fatty acids.

After the gastric phase, as mentioned before, lipase, colipase, and bile salts work cooperatively and digest the triglycerides which were hydrolysed in the intestinal phase into fatty acids and monoglycerides. Produced fatty acids and monoglycerides are transported as mixed micelles for absorption (Wilde & Chu, 2011). The digestion of proteins is continued in the intestine by pancreatic trypsin and chymotrypsin which break the polypeptides into peptides. Although bile salts mostly are associated with lipid digestion, they also show effects on protein digestion. Bile salts can denature proteins digested by pepsin and make them more vulnerable to pancreatic protein digestion (Gass et al., 2007). Moreover, bile salts can displace any remaining proteins from the water/oil interface in the intestinal phase (Mackie & Macierzanka, 2010).

4.4.2.6 Liposomes and bilosomes digested with oat milk;

When the liposomes-OM mix **(Fig. 4.5A** and **Table 4.4)** and the bilosomes-OM mix **(Fig. 4.5B-D** and **Table 4.4)** were exposed to SSF, the D_H of the SSF of the samples was not significantly different from the initial properties of the samples. Contrary to liposomes and bilosomes, the ζ potential of the SSF of the samples-OM mix became more negative (around -25 mV) and PDI decreased to ~0.150 after exposure to the oral phase ($p<0.05$). As mentioned before, decreased ζ potential might be related to the weakened screening effect of ions in the medium. The D_H, PDI and ζ potential of SSF and SGF of the liposomes-OM mix was similar during the oral and gastric phases. There was a significant increase in D_H of SGF (up to 730 nm) and a decrease in PDI of SGF (~0.100) by the end of the gastric phase. The ζ potential of SGF was also decreased during the gastric phase (around -31 mV). As mentioned before the increase in the D_H of SGF during the gastric phase can be attributed to protein digestion by pepsin that can lead to the formation of larger oil droplets due to the coalescence (Mackie & Macierzanka, 2010; Zheng et al., 2021). Large protein-oil complexes and numerous free oil droplets are present in undigested OM (Wang et al., 2022). A similar mean particle diameter increase during the gastric phase was also reported by Zhen et al. who investigated the digestion of plant-based milks such as oat, almond, coconut, and cashew (Zheng et al., 2021). In the gastric phase, while proteins are digesting, liposomes and bilosomes may interact with digested proteins and oil droplets because gastric mucosa secretes phospholipids in human digestion and several interactions between secreted phospholipids and protein emulsions which affect the digestion of proteins reported (Mackie & Macierzanka, 2010). The phospholipid bilayers may interact with partially digested and/or undigested proteins. Moreno et al. reported that the molten globule state (between native structure and unfolded chain) of proteins induced by the acidic pH of the gastric phase can attach to the phospholipid bilayer and digestion of attached proteins can be prevented (Moreno et al., 2005). Moreover, secreted phospholipids may displace the proteins absorbed

on the surface of the oil particles. The acidic pH can weaken the arrangement of proteins therefore proteins may end up becoming vulnerable to the displacement effect of phospholipids (Dupont et al., 2010). When the gastric chyme of the liposomes-OM mix was exposed to the SIF, no significant change was observed between the D_H, PDI, and ζ potential of SIF and SGF. The D_H and ζ potential of the SIF of bilosomes-OM mix was ~450 nm and -17 mV, respectively ($p<0.05$) and then they were not changed significantly by the end of the intestinal phase.

4.4.2.7 CH-coated bilosomes digested with oat milk;

When CH-coated bilosomes were mixed with OM **(Fig. 4.6A-C** and **Table 4.4)**, contrary to the CH coating of bilosomes, coated samples-OM mixture did not aggregate when exposed to the SSF. The ζ potential of the particles in the medium might have been affected by several conditions. The pH of the SSF (pH 7) is close to the pKa of the CH therefore CH might be expected to have a nearly neutral charge and be aggregated. When the oral bolus of the samples was exposed to the SGF, the ζ potential of the SGF of the samples was lower and the D_H of the SGF of samples was higher than the SSF ($p<0.05$). The D_H of the SGF of the CH-coated bilosomes-OM mix was ~770-970 nm at the end of the gastric phase. These results show similarity to the D_H of the SGF of bilosomes-OM mixture at the end of the gastric phase (D_H: ~650-850 nm). As mentioned before, the increased D_H after the gastric phase possibly results from the digestion of proteins which were absorbed by the oil droplets within OM followed by the coalescence of oil droplets. For the gastric chyme of coated samples-OM mix, their D_H decreased to ~500 nm with PDI: 0.300 and their ζ potential increased to around -15 mV at 5 min of intestinal phase ($p<0.05$). Slight changes were seen but the properties of the CH-coated bilosomes-OM mix did not change significantly during the intestinal phase.

4.4.2.8 PGA/CH-coated bilosomes digested with oat milk;

After the oral phase, there was no significant difference between the D_H and ζ potential of SSF and the initial samples **(Fig. 4.6D-F** and **Table 4.4)**. When the oral bolus of PGA/CH-coated bilosomes-OM mix was exposed to SGF, although there was no significant change in ζ potential (around -27 mV), the D_H and PDI of SGF were ~1300 nm and 0.600 respectively ($p<0.05$). During the gastric phase, D_H and PDI of SGF continued to increase and ζ potential of SGF reached around ~31 mV. As mentioned before, the oil particles within OM begin to coalesce due to destabilisation caused by protein hydrolysis by gastric pepsin. These oil droplets have a positive surface charge due to the pH of the gastric phase which is lower than the pKa:~5 (Wang et al., 2019). High values of D_H might have resulted from the interaction of negatively charged PGA-coated bilosomes with positively charged oil droplets. The D_H and PDI of SIF were

~500 nm and 0.300 respectively and ζ potential of SIF was around ~ 18 mV at the 5 min of the intestinal phase. These parameters did not change significantly during the intestinal phase.

4.4.3 The bioaccessibility of *t*-res

After *in vitro* digestion of the liposomes, bilosomes, CH-coated and PGA/CH-coated bilosomes, the concentration of *t*-res which was present within the mixed micelle phase of digesta and in a form available for absorption was measured **(Fig. 4.7)**. As a control, *t*-res suspended in tris buffer was also tested for comparison. The effect of OM on the bioaccessibility of *t*-res was also investigated.

4.4.3.1 Liposomes, bilosomes, CH-coated and PGA/CH-coated bilosomes;

When *t*-res was encapsulated into the liposomes, its bioaccessibility increased from 39.0±0.1% to 70.9±0.4% ($p<0.05$). Similar to our results, the bioaccessibility of catechin and epicatechin from cocoa extract-loaded liposomes was improved 2.3-fold and 2.2-fold respectively, when they were encapsulated into the liposomes (Toro-Uribe et al., 2018). Encapsulation of the bioactive compounds into the lipid bilayers can improve the solubility and stability of the compounds and can prevent rapid degradation by controlling their release thus encapsulation can provide improved bioaccessibility of the bioactive compounds (McClements, 2020). Compared to the liposomes, the incorporation of NaC improved the bioaccessibility of the *t*-res which ranged from 83.6±1.8 to 90.3±0.3% ($p<0.05$). Wang et al. investigated the effect of the type of nanocarriers (liposomes, niosomes, and bilosomes) on the bioaccessibility of EGCG. Results showed that, while the bioaccessibility of free EGCG was 3.1±0.4%, encapsulation of the EGCG improved its bioaccessibility to 24.0± 3.9%, 55.7± 6.9% and 71.7±4.1% respectively for liposomes, niosomes, and bilosomes (L. Wang et al., 2021). The improved bioaccessibility after incorporating NaC into the system compared to liposomes may be associated with the incorporation of bile salts which leads to the disruption of the lipid bilayer and induces membrane curvature in a concentration-dependent manner. These changes give rise to a range of lipid structures, including ellipsoid shapes, rod-like formations, smaller vesicles, and micelles. Due to differences in the physicochemical properties, LC of these structures may differ, resulting in different bioaccessible *t*-res concentrations (Lichtenberg et al., 2013; McClements, 2013). Although CH-coated bilosomes **(Fig. 4.6A-C)** showed responses like swelling or deswelling to the pH and ionic strength changes during digestion, they retained around ~85% of the encapsulated *t*-res and the bioaccessibility of t-res from CH-coated bilosomes was ranging from 15.1±0.6% to 19.8±0.5%. The decreased bioaccessibility of *t*-res after CH coating of bilosomes could be due to the ability of the layer of CH cross-linked with TPP to protect lipid

bilayers against digestive enzymes, bile salts, and pH changes. So, CH coating could provide protection and reduce the release rate of *t*-res (Hua et al., 2021). In addition, with increased CH concentration in the system, the bioaccessibility of *t*-res decreased. Decreased release with increased CH concentration in the system might be because of the thicker shell, which released fewer *t*-res. When the target absorption area of the encapsulated compounds is the colon, it is crucial to retain the encapsulated compounds until colonic fermentation can release the compounds in the colon.

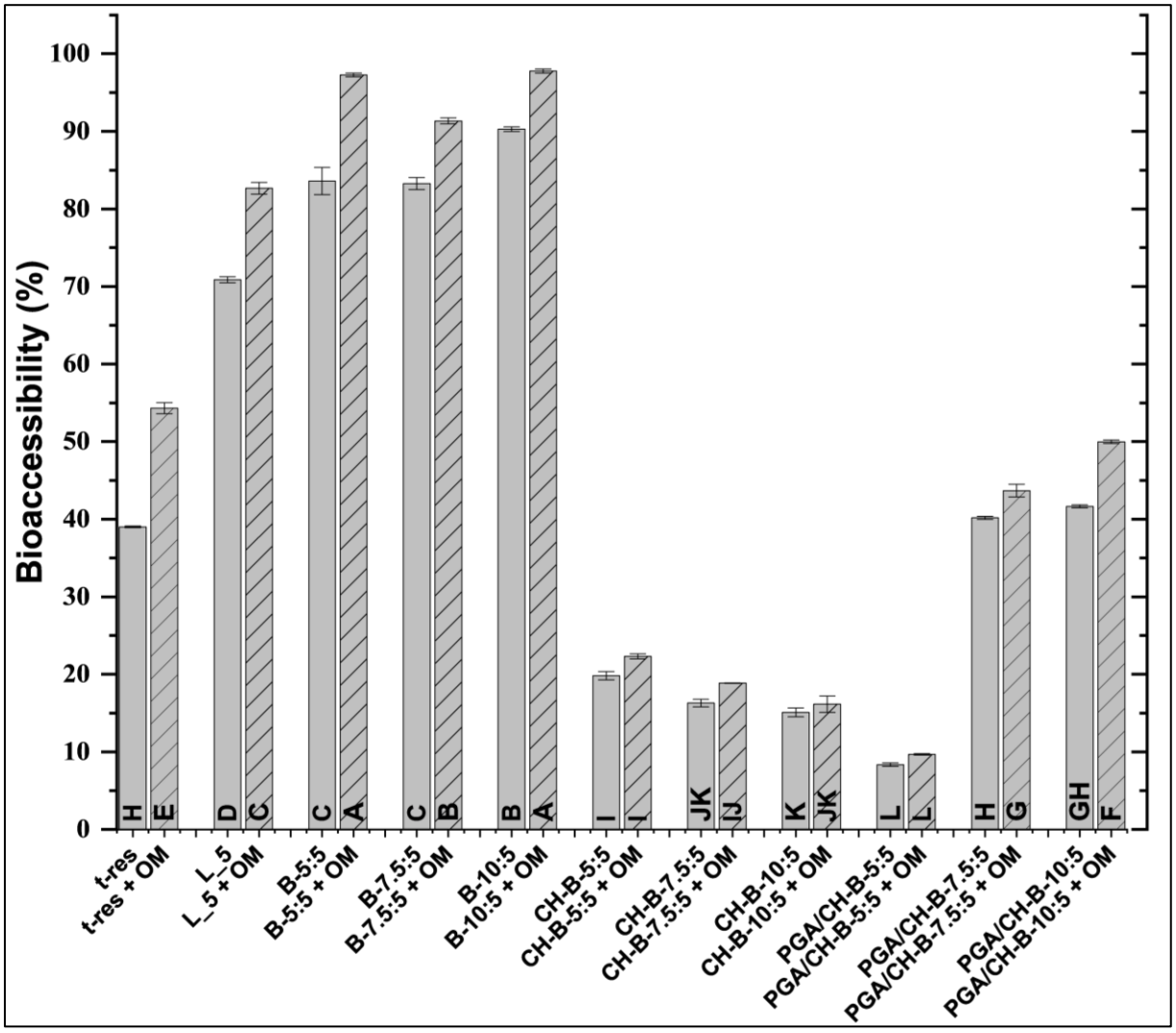

Figure 4.7 The bioaccessibility (%) of free-tres, *t*-res from liposomes, bilosomes, CH-coated and PGA/CH-coated bilosomes without ( ) and with OM ( ). The data represent the mean±SD. Capital letters indicate the significant differences between in bioaccessibility of *t*-res from the samples ($p<0.05$).

Resveratrol-PEG-loaded pectin-CH polyelectrolyte complex was prepared by Andishmand et al. to control the release of resveratrol until colonic digestion and the system only released 33% of resveratrol in SGF and SSF (Andishmand et al., 2016). 5-aminosalicylic acid loaded polymer (Eudragit S100)/CH-coated liposomes for colon-

targeted delivery was prepared by Barea et al. While CH-coated liposomes (without cross-linker) released their content by 60%, Eudragit S100/CH-coated liposomes retained the loaded compound by ~90% at the end of the intestinal phase (Barea et al., 2012). The bioaccessibility of *t*-res released from PGA/CH-B-5:5 (8.4±0.2%), was much lower than CH-coated bilosomes because of the protective effect of the PGA as a second layer onto the CH-coated bilosomes. However, the bioaccessibility increased sharply to ~40% for PGA/CH-B-7.5:5 and PGA/CH-B-10:5. The excess polymer concentration generates a difference in osmotic pressure which might begin to disrupt the lipid bilayer, leading to the leakage of the encapsulated compounds (Laye et al., 2008; Tan et al., 2021).

4.4.3.2 Liposomes, bilosomes, CH-coated and PGA/CH-coated bilosomes digested with oat milk;

The bioaccessibility of the free and *t*-res encapsulated in liposomes, bilosomes, and biopolymer-coated bilosomes was slightly improved when free-res and *t*-res loaded nanocarriers were digested with OM **(Fig. 4.7)**. The bioaccessibility of *t*-res increased from 39.0±0.1% to 54.3±0.7 when *t*-res was digested with OM. Moreover, the presence of OM during digestion increased the bioaccessibility of *t*-res, which was encapsulated in liposomes and bilosomes significantly, which is consistent with previous results. Improved bioaccessibility of hydrophobic bioactive compounds was also reported by Zheng et al. The bioaccessibility of the curcumin increased from ~2% to 60-67% when the compound was digested with plant-based milk (almond, cashew, coconut, and OM) (Zheng et al., 2021). The improved bioaccessibility of free *t*-res could be due to the triacylglycerol-rich core of oil droplets within OM. Triacylglycerols would have been hydrolysed during lipid lipolysis by pancreatin and produced mixed micelles that could solubilize *t*-res in the intestinal phase (Zheng et al., 2021). Niaz et al. reported that the bioaccessibility of carvacrol loaded into the CH/bovine serum albumin-based core-shell nanocarriers was improved from 80±3.1% to 91±4.9% when nanocarriers were digested with skimmed milk (Niaz et al., 2021). This shows that not only the fat in the milk facilitates the micellar phase but also other components like metabolites from protein digestion or interactions resulting in protection of the bioactive compound from degradation may provide improved bioaccessibility (Chen et al., 2018; Niaz et al., 2021).

There was no significant difference in the bioaccessibility of *t*-res when the CH-coated bilosomes and PGA/CH-B-5:5 was digested with OM. When CH-coated bilosomes and PGA/CH-B-5:5 was digested without OM, the release of the *t*-res was already lower than 20%. This shows the stability of these systems against pH differences, digestive enzymes, and bile salts during digestion. Because the percentage of released *t*-res

was already low, the addition of OM during digestion might have not shown an enhanced effect. The bioaccessibility of *t*-res increased by ~ 3% and ~8% for PGA/CH-B-7.5:5 and PGA/CH-B-10:5 respectively when they were digested with OM ($p<0.05$).

4.4.4 Absorption of *t*-res through murine intestinal tissue

Within the scope of this study, free *t*-res, *t*-res loaded liposomes, bilosomes, and *t*-res loaded samples digested with OM were exposed to murine intestinal tissue within this study to assess their fate **(Fig 4.8-4.9).** The centrifuged digesta sample following *in vitro* digestion was added to the apical compartment of Ussing chambers containing murine intestinal tissue. The transportation and absorption of *t*-res in both the apical and basolateral chambers were monitored over time to ascertain the final location of *t*-res. Furthermore, the experiment involved the collection of intestinal tissue for the detection of any accumulated *t*-res within the tissue by the end of the experiment.

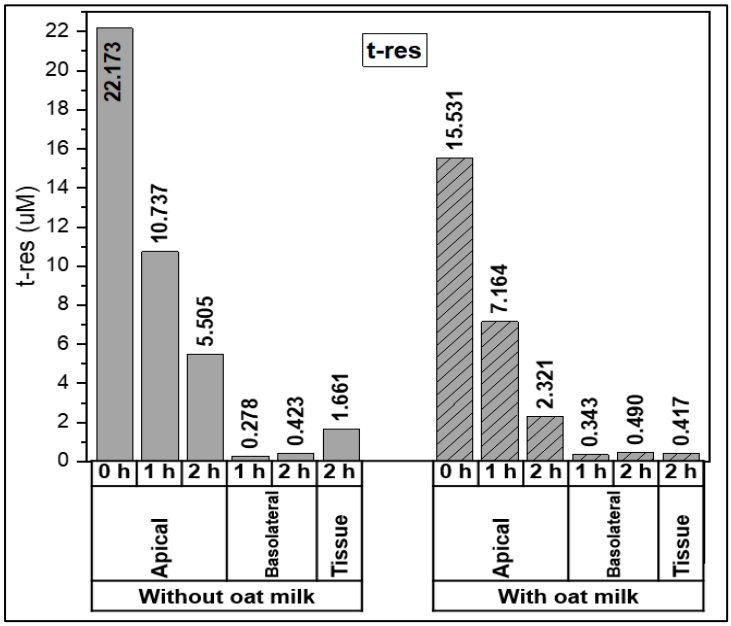

Figure 4.8 The concentration changes of free *t*-res ( ) and *t*-res digested with OM ( ) in the apical and basolateral chamber after exposure to the murine intestinal mucosa and the concentration of accumulated *t*-res in the tissue.

The initial concentration of *t*-res within the apical compartment differed among samples, despite the initial *t*-res concentration being the same. Because, as shown in **Fig. 4.7**, the bioaccessible *t*-res that was present within the mixed micelle phase of the digesta and in a form available for absorption is different for each sample. Furthermore, *t*-res is susceptible to degradation by environmental factors like air, light, and temperature, all of which were encountered during the sample preparation, digestion, and absorption processes. *t*-res might convert to *c*-res because of the exposure to light (Vian et al., 2005) or undergo auto-oxidation resulting in hydrogen peroxide (Yang et al., 2010).

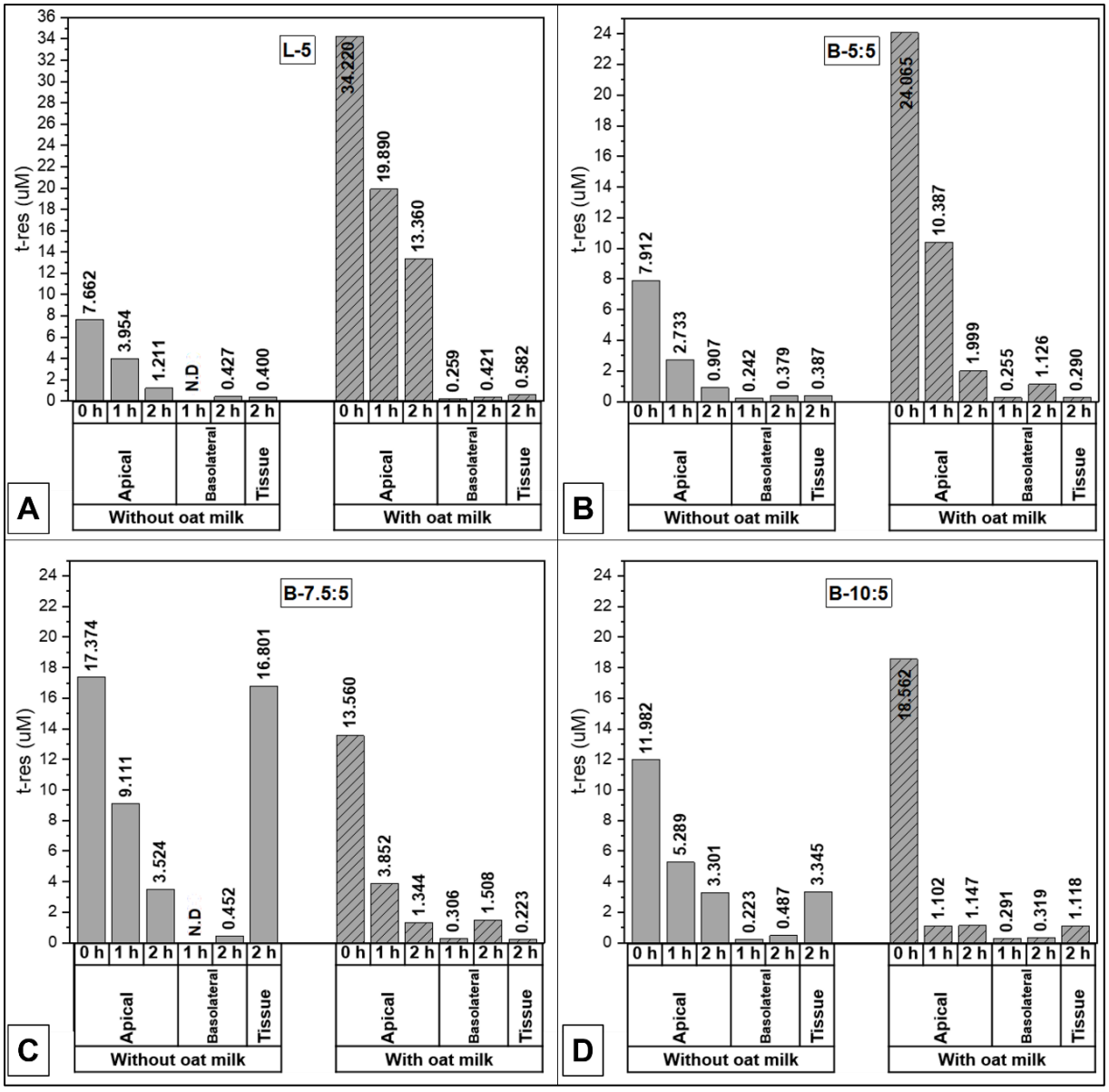

Figure 4.9 The concentration changes of free *t*-res (▭) and *t*-res digested with OM (▨) in the apical and basolateral chamber after exposure to the murine intestinal mucosa and the concentration of accumulated *t*-res in the tissue for **(A)** L-5, **(B)** B-5:5, **(C)** B-7.5:5, and **(C)** B-10:5.

A progressive decrease in the concentration of *t*-res within the apical chamber was observed over 120 min for all samples digested with/without milk. Throughout the experiment, an increase in *t*-res concentration was observed within the basolateral compartment, except for L-5 and B-7.5:5. The concentration of *t*-res in the basolateral compartment at 1 h was not detected for L-5 and B-7.5:5 because values were below the limit of detection **(Fig 4.9A,C).** The *t*-res concentration in the basolateral compartment at 2 h for free *t*-res, liposomes, and bilosomes ranged from 0.379 µM to 0.487 µM. Compared to the free *t*-res, liposomes, and bilosomes, *t*-res concentration in the basolateral compartment at 2 h was slightly higher for samples digested with

OM and reached 1.126 µM for B-5:5 and 1.508 µM for B-7.5:5-OM **(Fig 4.9B,C)**. Enhanced absorption could potentially be attributed to the presence of fat in the OM, which could facilitate the formation of a micellar phase leading to the solubilisation of the hydrophobic bioactive compound. This, in turn, might contribute to improved absorption of *t*-res (Chen et al., 2018; Niaz et al., 2021). Any *t*-res that has accumulated within the murine intestinal tissue is poised for more systemic dispersion. However, due to the 2-h duration of the experiment and the limited viability of murine intestinal tissue (typically ranging from 1 to 3 h), the tissue loses its integrity and viability close to the end experiment (Mackie et al., 2020). TEER value of various murine intestinal tissue during 120 min exposed to different samples was given in **Fig 4.10**. As seen in the graph, the TEER value of the intestinal tissues from different mice showed different decreasing trends during the 120 min absorption experiment. While the tissue exposed to B-5:5-OM lost its viability at the end of 120 min, other tissues were still viable although their TEER values were close to zero. While accumulated *t*-res in the intestinal tissue was 0.400 µM for liposomes **(Fig 4.9A)**, it increased to 16.801 µM for B-7.5:5 and 3.345 µM for B-10:5 **(Fig 4.9C,D)**.

Similarly, Song et al. reported an increase in the absorption of salmon calcitonin, with enhancements of 10.8-fold through Caco-2 cell experiments and 7.1-fold through intra-duodenal administration to rats due to the incorporation of NaTDC into the pro-liposome formulation (Song et al., 2005). The pharmacokinetic results in rats demonstrated enhanced absorption of hydrophobic cyclosporine A in SPC/NaDC liposomes (120.3%) compared to SPC/Chol (98.6%) liposomes (Guan et al., 2011) variations in the accumulated *t*-res concentrations within the intestinal tissue can be associated with the concentration of NaC incorporated in the lipid bilayer. The incorporation of bile salts leads to the disruption of the lipid bilayer and induces membrane curvature in a concentration-dependent manner. These changes give rise to a range of lipid structures, including ellipsoid shapes, rod-like formations, smaller vesicles, and micelles. Due to differences in size, structure, and surface properties, these diverse lipid structures are likely to exhibit distinct absorption kinetics (Lichtenberg et al., 2013; McClements, 2013). In addition, the accumulated *t*-res in the tissue was lower for samples digested with OM compared to the samples digested without OM due to OM providing a higher micellar phase. The accumulated concentration of *t*-res in the intestinal tissue was 1.661 µM and 0.417 µM for *t*-res and *t*-res-OM, respectively **(Fig 4.8)**. As a result, in comparison to the absorption of free *t*-res and *t*-res loaded liposomes, the absorption of *t*-res loaded bilosomes (B-7.5:5 and B-10:5) demonstrated an enhanced *t*-res absorption, attributed to the introduction of bile salts into the lipid bilayers.

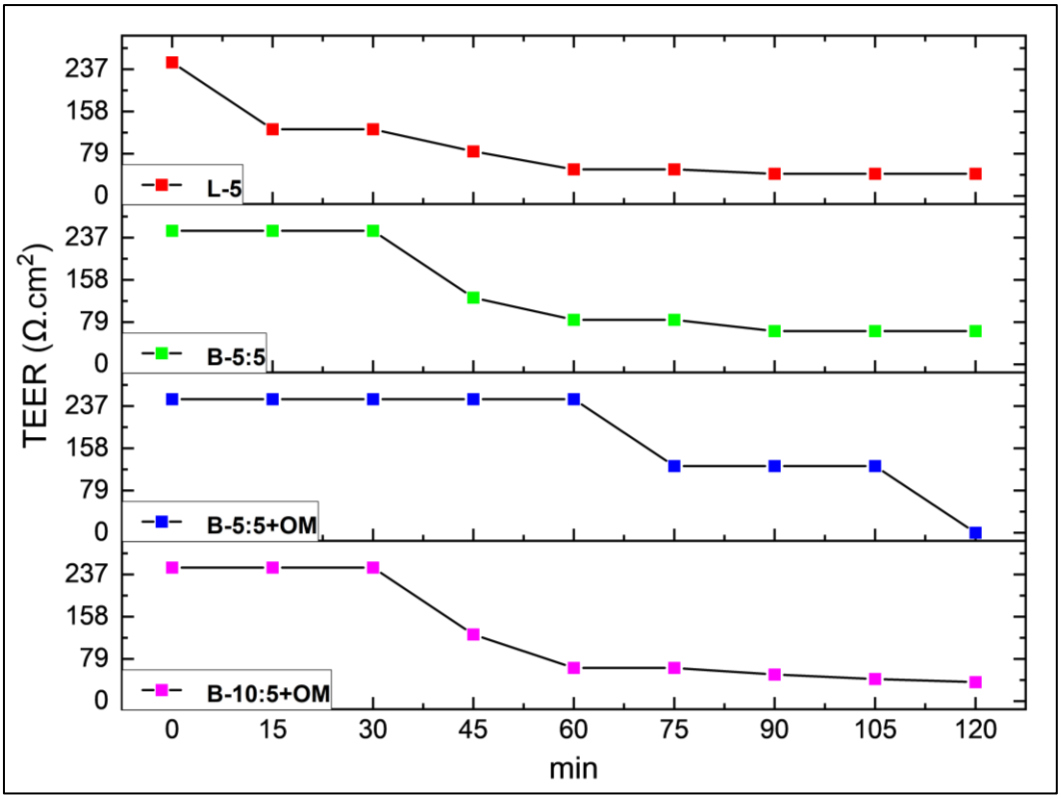

Figure 4.10 TEER value of murine intestinal tissue during 120 min exposed to L-5 (■), B-5:5 (■), B-5:5+OM (■) and B-10:5+OM (■).

4.5 Conclusion

In this study, the effect of bilayer modification, surface modification, and the effect of a food matrix on the behaviour of the *t*-res loaded lipid bilayers during *in vitro* digestion and on the bioaccessibility and absorption of *t*-res was investigated.

The *t*-res loaded liposomes, bilosomes, CH-coated bilosomes, and PGA/CH-coated bilosomes were prepared and initial physical properties (D_H, PDI, and ζ potential) and properties after mixing with OM were investigated. When lipid bilayers were modified with NaC, a decrease in ζ potential was observed due to the incorporation of negatively charged bile salts. An increase in D_H and changes in surface charge after oppositely charged biopolymer coating showed the surface of the lipid bilayers was successfully coated. When liposomes and bilosomes were mixed with OM (1:1 v/v), the properties of the lipid bilayer-OM mix looked mostly related to the properties of OM due to the low concentration of liposomes or bilosomes in the mixture. The ζ potential of the liposomes and bilosomes increased from around -45 mV to around -20 mV after mixing with OM possibly due to the pH difference and protonated proteins. The ζ potential of the CH-coated bilosomes turned negative after mixing with OM and a significant increase in D_H was observed. This negative surface charge could be related to the

deprotonation of CH and the interaction between CH and proteins in the mix. Similar to liposome-OM and the bilosomes-OM mix, the properties of PGA/CH-coated bilosomes-OM mix were mostly related to the properties of OM.

The potential behaviour of free *t*-res, *t*-res loaded liposomes, bilosomes, and CH-coated and PGA/CH-coated bilosomes was investigated during a static *in vitro* simulated digestion model, and bioaccessibility of *t*-res was determined. In order to see the effect of OM as a food matrix on the behaviours of mentioned systems during digestion and on the bioaccessibility of *t*-res, samples were digested with OM.

Free t-res are expected to be solubilized by mixed micelles composed of bile salts, phospholipids, and Chol and transported for absorption. Liposomes and bilosomes were maintained unchanged during the gastric phase basically, showing their stability. At the end of the intestinal phase, the D_H of bilosomes was higher and ζ potential was more negative compared to liposomes possibly due to the externally added bile salts into lipid bilayers. Like free *t*-res, liposomes, and bilosomes were also digested in the intestinal phase. The CH-coated bilosomes were resistant to digestive enzymes and were stable during the gastric and intestinal phase possibly due to the usage of TPP which reduce the porosity of the CH network and leakage of bilayers and loaded *t*-res. PGA/CH-coated bilosomes were also resistant to digestive enzymes and the pH difference between digestion phases.

When *t*-res was encapsulated into the liposomes, its bioaccessibility increased from ~40% to 70% because liposomes can improve the solubility of *t*-res and can prevent its degradation. Compared to the liposomes, the incorporation of NaC improved to bioaccessibility of the *t*-res which ranged from 83% to 90%. The improved bioaccessibility of t-res may be associated with different structures of lipid bilayers resulting from the different concentrations of NaC. Due to differences in the physicochemical properties, LC of these structures may differ, resulting in different bioaccessible concentrations. The bioaccessibility of *t*-res from CH-coated bilosomes was only ~20%. CH coating protected the *t*-res-loaded lipid bilayers and did not leak possibly CH coating cross-linked with TPP was resistant to enzymes and conditions of digestion. Low bioaccessibility of *t*-res was also expected after double coating of lipid bilayers but the bioaccessible *t*-res was ~40%.

OM is a colloidal system containing oil particles stabilised by phospholipid/protein monolayer. When free *t*-res are digested with OM, *t*-res were expected to solubilise within the oil particles thus the characteristics observed during digestion of *t*-res-OM mix were mostly related to the behaviour of OM during digestion. Although interactions between phospholipids and protein during the gastric and intestinal phases were reported, the behaviours of liposomes and bilosomes were not expected to be affected

significantly when they were digested with OM. As mentioned before, CH and PGA were expected to not be digested during the digestion experiment because of their resistance to the enzymes used in the study. The properties of the CH-coated bilosomes-OM mix and the PGA/CH-coated bilosomes-OM mix were mostly related to the behaviour of OM during digestion.

When free *t*-res, *t*-res loaded liposomes and bilosomes were digested with OM the bioaccessibility of *t*-res increased by ~15%. After digesting with OM, the increase in bioaccessible *t*-res was not significant for CH-coated bilosomes whereas the bioaccessible *t*-res increased by 5-10% for double-coated bilosomes. The improved bioaccessibility of free *t*-res due to the OM is if lipid bilayers and/or biopolymer coating were partly damaged during the oral and gastric phase and leaked the loaded *t*-res, *t*-res can be solubilized by oil particles within OM and carried to the intestinal phase.

Throughout the *ex vivo* intestinal permeability experiment using Ussing chambers, there was an observed progressive decrease in *t*-res concentration within the apical chamber, coupled with an increase within the basolateral chamber for all samples digested with/without milk. *t*-res concentration in the basolateral compartment at 2 h for free *t*-res, liposomes, and bilosomes ranged from 0.379 µM to 0.487 µM. While the accumulated concentration of *t*-res within the liposomes remained at 0.400 µM in the intestinal tissue, the incorporation of NaC into the lipid bilayers resulted in a notable increase and the accumulation reached 16.801 µM for B-7.5:5 and 3.345 µM for B-10:5. The variations in accumulated *t*-res concentrations within the intestinal tissue can be linked to the concentration of NaC embedded in the lipid bilayer, which induces membrane curvature and may lead to various lipid structures exhibiting different absorption kinetics. Furthermore, it was observed that the presence of OM during digestion led to a reduction in accumulated *t*-res within the tissue, in comparison to samples digested without OM. This effect was attributed to the higher micellar phase concentration provided by OM.

According to all findings, bilosomes have the potential for intestine-targeted oral drug delivery due to having the ability to improve the bioaccessibility and absorption of *t*-res. Due to their release profile and resistance to enzymes secreted in the upper GIT, CH-coated and PGA/CH-coated bilosomes could be promising as colon-targeted oral drug delivery. In addition, whole OM as a food matrix showed an enhancing effect on the bioaccessibility of *t*-res due to its oil content, which could solubilize *t*-res.

Chapter 5: General discussion

Phenolic compounds have gained significant attention and thorough comprehensive research for their biological activities, including antimicrobial, antioxidant, anti-carcinogenic, and anti-aging effects (Mouhid et al., 2017; Shishir et al., 2018). However, achieving these benefits depends on the compounds reaching enough plasma concentrations, which is challenged by limitations such as solubility and permeability, as well as environmental stressors including factors like food composition, storage conditions, processing methods, and the GIT. Consequently, these factors reduce their bioavailability, preventing them from achieving enough concentrations for the desired biological effects (Arzani et al., 2015; Bonechi et al., 2012; Tønnesen et al., 2002; Wenzel & Somoza, 2005).

Bilosomes (bile salts containing liposomes) are promising vehicles for the oral administration of encapsulated phenolic compounds to improve their bioavailability due to (i) enhancing the solubility and permeability (Abbas et al., 2022), (ii) protecting encapsulated compounds from chemical and enzymatic degradation due to the repulsion between externally added bile salts and the bile salts within the intestine (Liu et al., 2022), and (iii) controlling their release rate and target area.

However, a knowledge gap exists in the literature regarding the (i) comprehensive structural analysis of the impact of bile salts and biopolymers on lipid bilayers, (ii) the food application of phenolic compound-loaded bilosomes, (iii) their behaviours in the food matrix, (iv) their behaviours during GIT, their bioaccessibility and absorption when they digest with food matrix. Therefore, the overall objective of this thesis was to explore the use of bilosomes as carriers for the delivery of *t*-res as a model phenolic compound. This project hypothesises that the incorporation of bile salts into the self-assembled vesicles can enhance the bioavailability of phenolic compounds.

With our overall objective in mind, the impact of bilayer modification using bile salts and surface modification using biopolymers on the physicochemical properties, behaviour, and bioavailability of LSAS across various environments were reviewed **in Chapter 1**, drawing from existing literature.

In **Chapter 2**, empty and *t*-res loaded POPC (10 mM)/DOPG (3.3 mM) liposomes were prepared, and the *t*-res (1 mM) was used as a model hydrophobic phenolic compound. The lipid bilayers were modified by the addition of NaC, a typical bile salt, at three different concentrations (5 mM, 7.5 mM, and 10 mM). CH as a positively charged biopolymer and PGA as a negatively charged biopolymer were chosen for surface modification. Anionic TPP was used to enhance the stability of CH coating on the bilosome surface (Zhao & Wu, 2006). Utilizing data from the optimization experiments,

the ideal ratios of NaC/CH (w/w) at 0.5 for CH coating and CH/PGA (w/w) at 0.4 for PGA coating were selected. These ratios were then applied to form a coating onto the surface of bilosomes, with CH as the initial coating, followed by PGA as the second layer, formed via electrostatic interaction. The physical characteristics of bilosomes were analysed in relation to the concentration of NaC highlighting the transition from vesicles to micelles, as well as in the context of bilosomes coated with CH and PGA/CH. The samples were characterised using a combination of dynamic and static scattering techniques (DLS, SANS, and SAXS), along with cryo-TEM.

The D_H of the liposomes and bilosomes ranged from ~70 nm to 100 nm with <~0.250 of PDI and the incorporation of NaC into the lipid bilayers did not result in any significant difference in D_H. The ζ potential of the bilosomes (-43.1±1.1 mV to -47.9±2.9 mV) was more negative than the liposomes (around -40 mV) due to the incorporation of negatively charged NaC. Changing the lipid/NaC ratio in the bilosome formulations alters their properties due to the powerful membranolytic activity of bile salts on phospholipid bilayers (Can et al., 2021). Similarly, bile salts induced physical properties change in terms of shape, D_H, PDI, and ζ potential were also reported for hyaluronic acid-coated NaDC-bilosomes (H. Yang et al., 2019) and cyclosporine A-loaded NaDC-bilosomes (Guan et al., 2011). After CH coating, the D_H of the lipid bilayers increased significantly and ranging from 304.9±7.3 nm to 536.9±6.7 nm with <0.200 of PDI. The CH coating increased the D_H significantly for all bilosome samples ($p<0.05$). The D_H of the double-coated bilosomes was similar to CH-coated bilosomes with a slightly higher PDI (~0.300). The ζ potential of bilosomes transitioned from a negative charge to a positive charge after being coated with CH (~32 mV), and subsequently shifted to a negative charge of around -30 mV following the PGA coating. A similar increase in D_H, decrease in PDI and shift of ζ potential from negative to positive after CH coating were also reported for curcumin-loaded CH-coated liposomes ((Tai et al., 2020).

According to the cryo-TEM micrographs and SANS data, liposomes were mostly unilamellar, with a small subpopulation of bi- and tri-lamellar vesicles. Although specific preparation steps such as freezing-thawing, sonication, and extrusion were applied to decrease the lamellarity of the lipid bilayers, interlamellar repulsions between layers, K_c of membranes, and membrane curvature are the determinants of the production of unilamellar and multilamellar structures (Jackman et al., 2014). The findings demonstrated that at a concentration of 5 mM NaC in the bilosomes, the morphology of the liposomes shifted from predominantly ULVs to a mixture of vesicles and core-shell ellipsoids. With the addition of 7.5 mM NaC into the lipid formulation, the liposomes reverted to ULVs with a bimodal size distribution. Further increase of NaC concentration (10 mM) resulted in a bimodal size distribution (smaller-sized ULVs

and spherical structures) with higher PD. After the incorporation of NaC into the lipid system, incorporated bile salts disrupted the bilayer, leading to fluctuations in the bilayer structure. The perturbed bilayer underwent deformation, ultimately resulting in rupture and transformation into mixed micelles by bile salts in a concentration-dependent manner (Lichtenberg et al., 2013). Various sizes and shapes of DPPC structures such as ellipsoidal vesicles, ribbon-like structures, and spherical mixed micelles induced as a function of the NaDC concentration have also been reported (Kiselev et al., 2013).

The impact of biopolymer (CH and PGA) coating on the bilosome structure was assessed using SANS and SAXS. In the SAXS scattering patterns of the CH-coated bilosomes, Bragg peaks were observed, which are indications of multilamellarity. In addition, with increased CH concentration in the system, T_{shell} of lipid bilayers was reduced. This suggests that the CH coating induced osmotic pressure, which dehydrates the bilayer, increasing the structural order of the bilayer and leading to a transformation of the structural arrangement of the initial ULVs into multilamellar structures (Amenitsch et al., 2004; Fernández-Nieves et al., 2003). The structural changes in the lipid bilayers due to the osmotic pressure were also reported for empty and curcumin-loaded liposomes after CH coating (Manconi et al., 2017) and DOPC-liposomes after different coating such as PEG, PAM, gelatine and alginate (Bandara et al., 2020). The SANS data did reveal that CH-coated bilosomes exhibited high PD, resulting in structures that were notably swollen and diffuse.

The unified power-R_g model, which provides a measure of understanding in complicated and varied systems through uncomplicated parameters and operates on the assumption that the levels consist of hierarchical formations, (Beaucage, 2012; Krzysko et al., 2020; Rai et al., 2012) was applied to model SANS data of PGA/CH-coated bilosomes. PGA/CH-coated bilosomes displayed a high degree of PD and fuzziness. Two power-law decays were determined from SANS data of PGA/CH-coated bilosomes. While the R_g of the secondary structures was between 540±36 Å and 760±78 Å, the R_g of the primary structures ranged from 71.6±5.9 Å to 139.4±9.3 Å. The first structures in the double-coated system might result from the NaCl-induced polyelectrolyte rearrangements resulting in a breaking of the bounds between oppositely charged polymers, local defects, and leakage of the lipid bilayers and encapsulated compounds (Antipov et al., 2002).

The interactions between compounds in liposomes, bilosomes, CH-coated bilosomes, and PGA/CH-coated bilosomes were examined using FT-IR. The FT-IR spectra indicated complete encapsulation of *t*-res within the bilayers, confirming the successful development of CH-coated and PGA/CH-coated bilosomes through electrostatic

interactions. Lastly, the EE and LC were quantified. The samples exhibited EE values exceeding 87%. The LC of the bilosomes was 1.7%. Although the LC was low, previous studies also reported similar LC for highly hydrophobic compounds-loaded liposomes such as curcumin-loaded liposomes with ~2% of LC (Cheng et al., 2019) and 1.5% of LC (Gómez-Mascaraque et al., 2017).

After comprehensive characterisation (**Chapter 2**) of *t*-res loaded liposomes, bilosomes and CH-coated bilosomes, and PGA-coated bilosomes the stability of *t*-res loaded samples was investigated to determine how modifying bilayers with NaC and modifying surface using CH and PGA could affect the physicochemical properties under various experimental stability conditions in **Chapter 3**.

The pH of samples was adjusted to 3, 5, and 7 to mimic the different aqueous foods like orange juices (pH ~3), coffee (pH ~5), milk (pH ~7), and different GIT conditions like gastric phase (pH 3) and intestinal phase (pH 7) (Brodkorb et al., 2019). Liposomes and bilosomes exhibited remarkable stability over 24 h under varying pH conditions (pH 3, 5, and 7). However, some fluctuations in the properties of bilosomes were seen which might be because of increased bilayer fluidity due to the NaC (Can et al., 2021). CH- and PGA/CH-coated bilosomes remained stable when the medium's pH was far from the coating material's pKa. Nonetheless, CH-coated bilosomes aggregated at pH 7.0, while PGA/CH-coated bilosomes displayed aggregation at pH 3, attributable to reduced net charge (Nguyen et al., 2014; Singla & Chawla, 2001). The DR% of all samples remained unaffected by pH difference and was around 90%.

To examine the thermal stability, samples were treated by heating at 65°C for 30 min in the dark and cooled immediately in an ice bath, which is the common thermal treatment for the preservation of fruit juices and milk (Dash et al., 2022; Petruzzi et al., 2017). Thus, the investigation of the physicochemical properties of the oral delivery system after thermal treatment can provide information about the stability of the delivery system for food processing. The liposomes and bilosomes exhibited minimal alterations in their physical properties in terms of D_H, PDI, and ζ potential after thermal treatment. Although liposomes and bilosomes were composed of unsaturated POPC and DOPG, they were mostly stable after thermal treatment which might be because of using low temperature and encapsulation of the *t*-res which is an antioxidant and inhibits lipid oxidation (Panya et al., 2010). However, the D_H of CH-coated bilosomes and PGA/CH-coated bilosomes which crosslinked using TPP increased significantly ($p<0.05$). This increase might be attributed to the increased swelling capacity of the biopolymers at increased temperatures. Although TPP was used as a crosslinker during CH coating, there were still uncrosslinked CH chains in the matrix. The heat treatment can weaken the interaction between the flexible polymer chains and can

provide more space in the matrix for buffer (Rohindra et al., 2004). Rohindra et al. reported that while the swelling capacity of CH hydrogels decreased with increased crosslinker concentration, it increased with increased temperature (25-45°C) (Rohindra et al., 2004). The DR% was ~90%, presumably due to *t*-res being embedded into the bilayer, which effectively shielded them from temperature-induced degradation. While the DR of vitamin E-loaded liposomes did not change after exposure to thermal treatments at 60°C and 75°C for 30 min, the DR decreased significantly after exposure to thermal treatment at 90°C for 30 min. The biopolymer coating provided stability for the samples which were exposed at 90°C for 30 min (Jash & Rizvi, 2022).

As a final stability condition, samples were stored at 4°C and 20°C for 28 days to evaluate the shelf life. If the necessary storage conditions cannot be provided, food products deteriorate more rapidly and end up becoming unsafe to consume. Liposomes and bilosomes exhibited stability in both storage conditions. Curcumin-loaded liposomes were stable for 40 days at 4 °C and 23 °C (Y. Liu et al., 2015). In the first week of storage, sedimentation was observed for CH-coated bilosomes. This might be attributed to either coalescence due to the insufficient concentration of CH or depletion flocculation due to the excessive concentration of CH in the system (Laye et al., 2008, Li et al., 2015). PGA/CH-coated bilosomes remained highly stable under both storage conditions. PGA seems to have hindered the swelling of CH due to strong electrostatic interaction and provided more stable structures during storage. The initial DR of double-coated samples was ~90% and there were some slight changes during storage, but all samples kept the encapsulated *t*-res successfully.

After the physicochemical properties of prepared samples had been investigated under various experimental stability conditions in **Chapter 3**, in **Chapter 4**, the influence of modifying bilayers with NaC, modifying surfaces with CH and PGA, and the presence of a food matrix on the behaviour of *t*-res loaded bilosomes during simulated *in vitro* digestion, as well as on the bioaccessibility and absorption of *t*-res was examined. Firstly, *t*-res (1 mM) loaded samples prepared in **Chapter 2** were used for the simulated *in vitro* digestion experiment but because the *t*-res concentration was too low for detection for the absorption experiment due to the dilutions during static *in vitro* simulated digestion experiment, the initial *t*-res concentration was increased to 5 mM and the extrusion step was removed from preparation.

The initial D_H of *t*-res (5 mM) loaded liposomes and bilosomes were between 263.0±2.1 nm to 428.8±2.7 nm with a PDI of ~0.250 and the ζ potential was between -40.9±4.0 mV to -47.9±2.9 mV. The initial D_H and PDI of 5 mM t-res loaded liposomes and bilosomes were higher because the extrusion step was excluded during their

preparation. Even though the extrusion step was employed for 1 mM t-res loaded liposomes and bilosomes, some multilamellarity was still observed in Cryo-TEM images. Consequently, exclusion of the extrusion step from the preparation of 5 mM t-res loaded liposomes and bilosomes would likely result in the presence of multilamellarity in these samples. The destabilisation effect of bile salts on the multilamellar structures will be slower than on the unilamellar structures. Because bile salts first locate on the outermost bilayer, and only when the outer bilayer has been disrupted or some pores are formed by them can bile salt molecules begin to locate into the next bilayers (Lichtenberg et al., 2013). While the D_H of the CH-coated bilosomes was between 375.9±4.4 nm and 460.7±21.0 nm with PDI: ~0.170, the initial D_H of PGA/CH-coated samples ranged from 349.2±7.4 to 668.7±22.0 nm with a high polydispersity (PDI: ~0.400). The EE of liposomes was 25.3±0.2% with 2.5% of LC. The EE of bilosomes was significantly higher than the EE of liposomes and ranged from 41% to 45% with 3.4% of LC. An increased EE could be because the addition of bile salts altered the packing of the molecules within the hydrophobic domains of the lipid bilayers resulting in more readily integration of *t*-res into these lipid bilayers (Cheng et al., 2019). Wang et al. also reported the increased EE of EGCG in the bilosomes (85.9±1.4%) compared to the liposomes (74.4±1.3%) (L. Wang et al., 2021). While the EE of the CH-coated samples was around 98% (from 6.3% to 4.6% of LC), the EE of the double-coated samples was ~95% (from 3.8% to 2.4% of LC). This could be attributed to the fact that CH and PGA cover the surface of lipid bilayers, creating a protective shield that prevents the leakage of *t*-res from lipid bilayers. The protective effect of biopolymer coating was also reported for cinnamaldehyde-loaded CH-coated liposomes by Wang et al, curcumin-loaded CH-coated liposomes by Liu et al., and lycopene-loaded CH-coated liposomes and canthaxanthin-loaded CH-coated liposomes by Tan et al. (Y. Liu et al., 2015; Tan et al., 2016; X. Wang et al., 2021).

The food matrix can show beneficial or adverse impacts on the physicochemical properties, stability, digestion profile, and absorption of the delivery system (Molet-Rodríguez et al., 2023). So, samples were mixed with OM (pH 7.64 and fat: 3.5%) (1:1 v/v) to mimic food fortified with *t*-res loaded samples, for the investigation of the effect of the food matrix on the behaviour of the samples during digestion. When liposomes, bilosomes, and PGA-coated bilosomes were mixed with OM (1:1 v/v), the characteristics of the lipid bilayer-OM mixture appeared to be predominantly influenced by the properties of OM. This might be mainly due to the relatively low concentration of liposomes or bilosomes present in the mixture. Following the mixing of CH-coated bilosomes with OM, their ζ potential became negatively charged, accompanied by a noticeable rise in D_H. This shift in surface charge could be attributed

to the deprotonation of CH and the interaction between CH and negatively charged compounds within the OM (Zhao et al., 2021).

According to the results of the static *in vitro* simulated digestion experiment, when the liposomes and bilosomes were exposed to SSF, their ζ potential increased and their D_H decreased significantly. The increase in the ζ potential could be attributed to the screening effect of the presence of salts in SSF and the deprotonated head group of phospholipids at pH 7 (Zidovska et al., 2009). The decreased D_H might be attributed to the dehydrated bilayer due to the osmotic pressure created by the ions in SSF and absorption of ions to the bilayers, resulting in altering the shape and lamellarity of the bilayer (Hupfeld et al., 2010; Sabın et al., 2006). All samples remained unchanged throughout the gastric phase, demonstrating their stability. Stable liposomes during the gastric phase were also reported by (Hui & Huang, 2021). In order to determine the D_H change at the end of the intestinal phase, samples were centrifuged at 280 x g for 5 min. Although mostly insoluble materials were separated with centrifugation, the D_H of samples taken at the end of digestion was predominantly influenced by the pancreatin. When CH-coated bilosomes were exposed to the SSF, aggregation was observed possibly due to the deprotonation of the CH (pKa: ~6.5) at pH 7 (Espinal-Ruiz et al., 2014). CH-coated bilosomes (cross-linked with TPP) remained stable throughout the gastric phase. TPP has been shown to provide protection for CH-coated bilosomes against the acidic stomach phase compared to CH coating without a cross-linker (Hua et al., 2021). CH-coated samples were also stable during the intestinal phase because the CH is resistant to hydrolysis by the digestive enzymes secreted by the upper GIT. The digestion of CH has been reported in the colon by lysozymes, nonspecific cellulases, and enzymes secreted by colonic microflora (Kim et al., 2016). Slight changes in PGA/CH-coated bilosomes were observed when they were exposed to SSF and SGF, but they were stable. The increase in D_H was observed during the intestinal phase which might be because the concentration of the deprotonated carboxylate groups would have increased causing repulsion between the PGA chains and consequently resulting in a swelled biopolymer shell (Yu et al., 2009). Swelling of alginate/CH-coated liposomes in SIF was also reported by (Liu et al., 2013). In addition, like the CH, PGA is resistant to enzymes secreted by upper GIT but can be digested by pectate lyase and pectate hydrolase secreted by colonic microflora (Matsuura, 1991).

When samples were digested with OM, the properties of the samples observed during the different phases of digestion mostly related to the behaviour of OM during digestion. For all samples, when they were mixed with OM and exposed to SSF, the properties were not significantly different from the initial samples. When the samples mixed with OM were exposed to SGF, D_H, and PDI increased significantly. OM is

basically a colloidal system that contains oil droplets composed of a triglyceride core covered by a phospholipid/protein shell (Nikiforidis, 2019). When the proteins that cover the lipid particles begin to be digested into polypeptides by pepsin, oil droplets may begin to destabilise, which can result in flocculation, coalescence, or phase separation consequently increasing D_H (Mackie & Macierzanka, 2010; Zheng et al., 2021). During the gastric phase, while the proteins in OM were digested, the liposomes, bilosomes, and coated samples were not expected to be affected much according to their digestion experiments without OM. After the gastric phase, lipase, colipase, and bile salts work cooperatively and digest the triglycerides, which are hydrolysed in the intestinal phase into fatty acids and monoglycerides (Wilde & Chu, 2011). The digestion of proteins is continued in the intestine by pancreatic trypsin and chymotrypsin that break the polypeptides into peptides (Gass et al., 2007). Produced fatty acids and monoglycerides are transported with mixed micelles for absorption (Wilde & Chu, 2011). During the intestinal phase, while the digestion of proteins and oil within the OM begins, the digestion of liposomes and bilosomes by lipases is also expected to begin. Digestion of biopolymer-coated samples is not expected due to their resistance to the enzymes used in the experiment and the inability of enzymes to penetrate the coating.

When *t*-res was encapsulated within liposomes, its bioaccessibility increased from around 40% to 70%. This enhancement could be attributed to the liposomes' ability to enhance the solubility of *t*-res and protect it from degradation. The bioaccessibility of catechin and epicatechin increased 2.3-fold and 2.2-fold respectively due to the encapsulation into the liposomes (Toro-Uribe et al., 2018). Comparatively, with the incorporation of NaC, the bioaccessibility of *t*-res further improved, ranging between 83% and 90%. The enhanced bioaccessibility of *t*-res might be linked to the electrostatic repulsion between externally added bile salts and the bile salts within the SIF. This electrostatic repulsion could lead to prolonged retention of lipid bilayers of bilosomes in the intestinal phase as compared to liposomes. As a result, bilosomes could effectively preserve the loaded bioactive compound, minimizing its alteration and degradation (Elnaggar et al., 2019). Increased bioaccessibility of hydrophobic EGCG from 24.0± 3.9% to 71.7±4.1% was reported by (L. Wang et al., 2021) when the bile salts were introduced into the lipid bilayer. The bioaccessibility of *t*-res from CH-coated bilosomes was approximately 20%. The decreased bioaccessibility of *t*-res after CH coating could be due to the protective effect of enzyme-resistant CH coating crosslinked with TPP and the modified release of *t*-res due to the biopolymer coating (Hua et al., 2021). Similar bioaccessibility results were also expected for double-coated bilosomes. However, the bioaccessible *t*-res from PGA/CH coated bilosomes was ~40%. The excess polymer concentration generates a difference in osmotic

pressure which might begin to disrupt the lipid bilayer, leading to the leakage of the encapsulated compounds (Laye et al., 2008; Tan et al., 2021).

Digesting samples with OM increased the bioaccessibility of *t*-res significantly for the free *t*-res, liposomes, and bilosomes. The enhanced bioaccessibility of *t*-res can be attributed to oil bodies within the OM which can solubilize the free *t*-res leaked from the partially damaged samples during digestion (Zheng et al., 2021). Improved bioaccessibility of curcumin was reported when curcumin was digested with plant-based milk (almond, cashew, coconut, and OM) (Zheng et al., 2021).

Following static *in vitro* simulated digestion, free *t*-res, *t*-res loaded liposomes, bilosomes, and *t*-res loaded samples digested with OM were exposed to murine intestinal tissue to assess the absorption of *t*-res. Biopolymer-coated samples were excluded from the absorption experiment due to their low bioaccessibility which would result in values that are below the limit of detection of HPLC. During the *ex vivo* intestinal permeability experiment using Ussing chambers, a gradual decline in *t*-res concentration within the apical chamber was accompanied by an increase in the basolateral chamber for all samples, whether digested with or without OM. *t*-res concentration in the basolateral compartment at 2 h for free *t*-res, liposomes, and bilosomes ranged from 0.379 µM to 0.487 µM. Accumulated *t*-res was detected in the intestinal tissue which was collected at the end of the experiment. Any *t*-res that has accumulated within the murine intestinal tissue is poised for absorption. However, due to the 2-h duration of the experiment and the limited viability of murine intestinal tissue (typically ranging from 1 to 3 h), the tissue mostly loses its integrity and viability close to the end experiment before the transition of accumulated t-res in the tissue to the basolateral chamber (Mackie et al., 2020). While the accumulated *t*-res concentration in intestinal tissue exposed to *t*-res loaded liposomes was 0.400 µM, *t*-res concentration in the intestinal tissue notably increased to 16.801 µM for tissue exposed to B-7.5:5 and for tissue exposed to 3.345 µM for B-10:5. Consequently, compared to the absorption of free *t*-res and *t*-res loaded liposomes, *t*-res loaded bilosomes (B-7.5:5 and B-10:5) exhibited an enhanced absorption for *t*-res. The enhancement and variations in accumulated *t*-res levels within the intestinal tissue can be attributed to the incorporation of NaC in the lipid bilayer, which induces membrane curvature, resulting in various lipid structures that may exhibit different kinetics of absorption (Lichtenberg et al., 2013; McClements, 2013). Increased absorption of salmon calcitonin through Caco-2 cells (10.8-fold) and through intra-duodenal administration to rats (7.1-fold) due to the incorporation of NaTDC into the pro-liposomes (Song et al., 2005) and increased absorption of hydrophobic cyclosporine A (from 98.6% to 120.3%) in rats with the addition of NaDC into liposomes (Guan et al., 2011) were reported. Additionally, the presence of OM led to reduced accumulation

of *t*-res in the tissue compared to samples without OM, owing to the higher micellar phase facilitated by OM (Chen et al., 2018; Niaz et al., 2021).

According to all findings, this thesis provides a comprehensive characterization of modified lipid bilayers using bile salts and biopolymers and knowledge of the stability of modified bilayers during food applications. Most importantly, the evidence about enhanced bioaccessibility and absorption of *t*-res, indicates the validity of the hypothesis that the bioavailability of the phenolic compounds can be enhanced with the addition of bile salts into the lipid bilayers. In conclusion, bilosomes have the potential for intestine-targeted oral delivery due to having the ability to improve the bioavailability of *t*-res as a model phenolic compound. Due to their bioaccessibility and resistance to enzymes secreted by the upper GIT, CH-coated and PGA/CH-coated bilosomes can be promising as colon-targeted oral delivery.

5.1 Conclusion

With our hypothesis and objectives in mind, this thesis demonstrated how modifying bilayers with bile salts (NaC) and modifying surfaces using biopolymers (CH and PGA) could affect (i) the physicochemical properties of lipid bilayers, (ii) the stability of lipid bilayers under various experimental stability conditions, (iii) the behaviour of lipid bilayers during GIT with/without a food matrix (OM), (iv) the bioaccessibility and absorption of encapsulated *t*-res as a model phenolic compound, with/without a food matrix (OM).

According to the compressive structural investigation, the incorporation of NaC into the lipid bilayers strongly affects the interactions between POPC/DOPG lipid bilayers and the physical properties of the system in a concentration-dependent manner. Complementary cryo-TEM images and SANS analysis demonstrated the transition of structures of POPC/DOPG lipid bilayers from ULVs with a subpopulation of bi- and tri-lamellar vesicles to vesicle and core-shell ellipsoid mixture (5 mM NaC), then ULVs with a bimodal size distribution (7.5 mM NaC), and lastly smaller-sized ULVs with spherical structures (10 mM NaC), with the increased concentration of NaC. The CH coating, as an initial biopolymer layer, generates osmotic pressure that changes the structural order of the ULVs and turns them into multilamellar structures. The addition of a second biopolymer layer, PGA coating, led to different structural levels of biopolymers in the system. In general, biopolymer-coated bilosomes were highly polydisperse which resulted in very swollen, and fuzzy structures. Liposomes, bilosomes, and biopolymer-coated bilosomes provided efficient encapsulation for *t*-res which was above 87%.

The stability of liposomes, bilosomes, and biopolymer-coated bilosomes was investigated under various experimental stability conditions (pH, thermal, and storage) to gain insight into future food applications. Liposomes and bilosomes showed high stability at different pH (pH 3.0, 5.0, and 7.0) over 24 h and during storage (at 4℃ and 20℃) for 28 days. In addition, the physical properties of liposomes and bilosomes were not affected by thermal treatment (65℃ for 30 min). The physicochemical properties of the bilosomes became more unstable with the increased concentration of NaC in the system. This might be attributed to the increased bilayer fluidity resulting from the increased NaC concentration. The CH-coated and PGA/CH-coated bilosomes were stable when the pH of the medium was far from the pKa of the coating material. However, after thermal treatment, a significant increase in D_H was observed for biopolymer-coated samples which might be because of increased swelling capacity of the biopolymers with increased temperature. For storage stability, the sedimentation which could result from either using an insufficient or excessive concentration of CH in the system, was seen for CH-coated bilosomes after 7 days. PGA/CH-coated bilosomes remained highly stable under both storage conditions and PGA coating appeared to hinder the instability of CH-coating.

According to the results of the static *in vitro* simulated digestion experiment, when liposomes and bilosomes were exposed to SSF, the D_H of the samples decreased significantly. This decrease could be related to changes in the shape and lamellarity of the bilayer resulting from the absorption of ions and the dehydration of the bilayer is caused by the osmotic pressure created by the ions in SSF. While the D_H of CH-coated bilosomes increased significantly when they were exposed to SSF, the D_H of the double-coated samples did not change. The increase in D_H of CH-coated samples possibly resulted from the pH of SSF (pH 7) which causes deprotonation of the CH (pKa:~6.5), promoting the flocculation of the system. All samples remained unchanged throughout the gastric phase, demonstrating their stability. After samples were exposed to SIF, the D_H of the centrifuged digesta was mostly related to pancreatin. In the intestinal phase, the expected process is the solubilisation of free *t*-res by mixed micelles and the digestion of liposomes and bilosomes by lipases and bile salts work cooperatively. Digestion of biopolymer-coated samples in the gastric or intestinal phase was not expected because of their resistance to the enzymes and the inability of enzymes to penetrate the biopolymer coating. In addition, the physical properties of the samples-OM mix were predominantly influenced by the OM during digestion.

While encapsulation of *t*-res into the POPC/DOPG lipid bilayers increased its bioaccessibility from ~40% to 70%, incorporation of NaC into the bilayer improved the bioaccessibility of *t*-res further which ranged from 83% to 90%. This improved bioaccessibility was attributed to firstly the improved solubility of *t*-res due to the lipid

bilayers. Thereafter, bilosomes might stay stable longer than liposomes in the intestine due to the electrostatic repulsion between externally added bile salts and intestinal bile salts, consequently, bilosomes might retain the loaded bioactive compound and reduce the transformation and degradation of encapsulated *t*-res. While the bioaccessibility of *t*-res which encapsulated into the CH-coated bilosomes was ~20%, it increased to ~40% for PGA/CH-coated bilosomes. Low bioaccessibility of *t*-res from biopolymer-coated bilosomes can be associated with the usage of TPP which strengthens the CH coating, the resistance of CH and PGA to the enzymes secreted by upper GIT and the inability of enzymes to penetrate the coating. The bioaccessibility of *t*-res increased significantly when t-res, liposomes, and bilosomes were digested with oat milk. Enhanced bioaccessibility can be related to the solubilisation of *t*-res which leaked from partly damaged bilayers during the oral and gastric phase, by oil particles within OM and carried to the intestinal phase.

The absorption of free *t*-res, *t*-res loaded liposomes, and bilosomes whether digested with or without OM through murine intestinal tissue was investigated using Ussing chamber. A decrease in the concentration of *t*-res in the apical chamber was observed along with an increase in the basolateral chamber for all samples. *t*-res concentration in the basolateral chamber at 2 h for free *t*-res, liposomes, and bilosomes ranged from 0.379 µM to 0.487 µM. A notable concentration of *t*-res accumulated in the murine intestinal tissue. Accumulated *t*-res is ready for absorption, but the analysis time was limited for the transition of accumulated *t*-res to the basolateral chamber, because of the tissue integrity and viability. The accumulated *t*-res in the tissue was 0.400 µM for liposomes. With the incorporation of NaC into the lipid bilayers, the accumulated *t*-res increased remarkably and reached 16.801 µM for B-7.5:5 and 3.345 µM for B-10:5. Consequently, compared to free *t*-res and liposomes, bilosomes (B-7.5:5 and B-10:5) enhanced the absorption of *t*-res.

Based on all of the findings, bilosomes provided stability to the encapsulated *t*-res and enhanced bioaccessibility and absorption of *t*-res, consequently increasing bioavailability, compared to the liposomes. In conclusion, for future food application, while bilosomes show potential for intestine-targeted oral delivery of phenolic compounds, CH-coated and PGA/CH-coated bilosomes can be promising as colon-targeted oral delivery.

5.2 Limitations and future directions

This research has shown that by adjusting the concentration of bile salts within the system and modifying surface characteristics using biopolymers, it is possible to manage the physicochemical attributes, stability, and behaviours of bilosomes throughout the GIT. As a result, this also influences what happens to the encapsulated bioactive compound(s). The key suggestions for potential future research are outlined below.

Formulation: In this research, we utilized NaC, the simplest form of bile salts. However, it would be valuable to explore incorporating various types of bile salts, including non-conjugated and conjugated forms with taurine or glycine into the lipid bilayers to understand how the chemical structure of bile salts influences the physicochemical properties and behaviours of lipid bilayers in various environment.

The lipids used in this study, namely POPC, and DOPG, are synthetic lipids known for their high purity. Nonetheless, their production cost is considerably elevated compared to natural phospholipids due to the synthesis process. In future investigations, natural lipids like soybean PC and egg PC could be considered for more cost-effective large-scale production.

For surface modification, the introduction of various biopolymers like dextran, alginate, and cellulose could provide information on their impacts on the lipid bilayer structure. Additionally, exploring how different biopolymers and their various layers affect the behaviour of lipid bilayers during the GIT holds significance for enhancing the targeted absorption of encapsulated compounds.

Physicochemical characterization: The improved bioavailability of bioactive compounds is crucial to reach sufficient concentrations in systemic circulation for observing biological activities. Nevertheless, conducting *in vitro* studies to assess the biological activities of the encapsulated compound(s) is also significant. Consequently, evaluating the antioxidant activity of prepared samples could provide insight into how modification in lipid bilayers impact the biological activity of encapsulated bioactive compound(s).

Stability and food processing: In this research, the stability of the *t*-res-loaded systems was examined in terms of storage, thermal conditions, and pH variations. Additionally, it is important to note that *t*-res is sensitive to light. When exposed to light, *t*-res transforms into *c*-res, which exhibits lower bioactivity compared to *t*-res. Consequently, assessing the light stability of *t*-res loaded samples becomes essential in order to investigate the protective effect of the prepared samples against light-induced degradation.

To ensure long-term stability, drying techniques can be employed on the prepared samples. Dried samples would also facilitate the investigation of the effects within low-moisture foods, such as cereal products and chocolate, serving as food matrices.

Food application: Because the target is oral administration, sensory analysis of the food(s) fortified with prepared bilosomes and biopolymer-coated bilosomes could be useful to determine how the sensory profile (texture, flavour, taste, appearance, smell, etc.) of the food is affected after fortification.

Digestion: During the *in vitro* GIT digestion, mucin, and α-amylase for the oral phase, as well as gastric lipase for gastric digestion, were not used. However, incorporating mucin could potentially influence the behaviours of CH-coated bilosomes during GIT due to the expected interaction between negatively charged mucin and positively charged CH. While the majority of lipids are typically digested by pancreatic lipases with the cooperation of bile salts during the intestinal phase, the inclusion of gastric lipase might impact lipid digestion. Thus, the incorporation of mucin, α-amylase, and gastric lipase could mimic the complexity of *in vivo* digestion better and provide more information about the fate of samples.

CH-coated and PGA/CH-coated bilosomes have the potential for colon-targeted oral drug delivery because both CH and PGA resist hydrolysis by the digestive enzymes secreted in the upper GIT (oral, stomach, and intestine), and they are digested by enzymes secreted by colonic microflora. In future studies, bioactive compounds such as anthocyanins, which are absorbed in the colon, could be encapsulated, and the performance of CH-coated and PGA/CH-coated bilosomes could be investigated.

In this study, the static *in vitro* simulated digestion was employed to investigate the physical properties of samples during GIT, the effect of the OM on the behaviour of the samples, and the bioaccessibility of *t*-res. However, the static *in vitro* simulated digestion model does not adequately mimic the complexity of *in vivo* digestion. This is because the digestive fluids, pH levels, and enzymes are set at the beginning of each digestion phase, and the system cannot provide the dynamic aspects of digestion. Therefore, using a semi-dynamic *in vitro* digestion model could enhance the digestion process by introducing gradual pH changes, enzyme and digestive fluid secretion, and gastric emptying.

While *in vitro* digestion experiments offer insights into the behaviour of samples during the GIT, they cannot fully replicate the complex digestion environments. Therefore, *in vivo* digestion models could be utilized to validate the bioavailability of *t*-res from the prepared samples.

Toxicity: Bile salts become cytotoxic at abnormally high concentrations. Although NaC does not exhibit cytotoxicity, it can become cytotoxic at very high concentrations. Therefore, determining the *in vitro* cytotoxicity of *t*-res loaded samples using the 3-(4,5-dimethylthiazol-2-yl)-2,5-diphenyl-2H-tetrazolium bromide (MTT) assay with human colon adenocarcinoma cells (Caco-2) could be a crucial method to assess the suitability of various bile salts and their concentrations.

Appendix A - Methods

A.1 Dynamic Light Scattering

The D_H obtained through dynamic light scattering (DLS) represents the size of a hypothetical hard sphere that diffuses at the same speed as the particle being studied. The hydrodynamic diameter is calculated using the Stokes-Einstein equation, which defines the velocity of Brownian motion in terms of the translational diffusion coefficient (Bhattacharjee, 2016; Pecora, 2008).

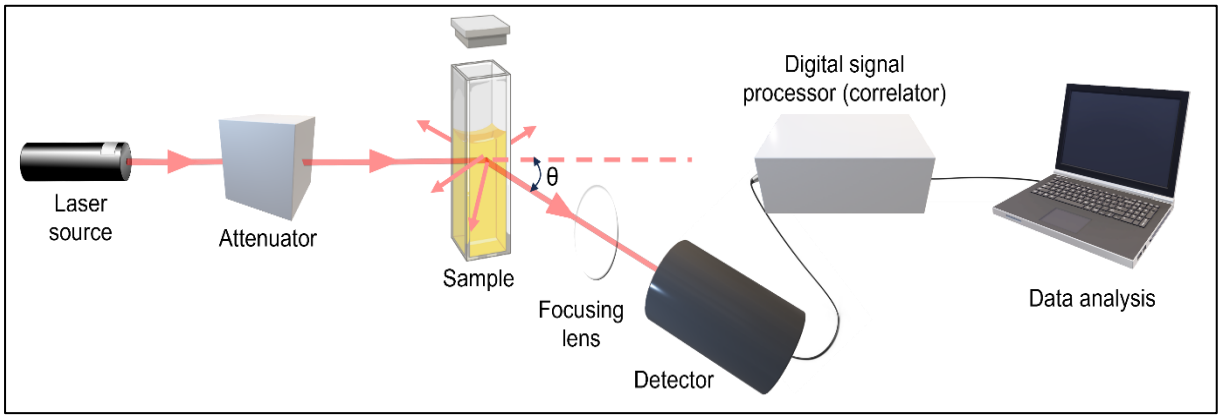

Figure A.1 Schematic representation of instrumentation of dynamic light scattering. Adapted from (Bhattacharjee, 2016).

In DLS the fluctuation of intensity in scattered light is correlated against delay time and the intensity autocorrelation function is obtained through the mono-exponential equation for samples with purely monodisperse particles.

$$G(\tau) = 1 + b.\, e^{-2.D.q^2\tau} \qquad \textbf{Eq. A1.1}$$

$$|q| = \frac{4.\pi.n_0}{\lambda_0.\sin\frac{\theta}{2}} \qquad \textbf{Eq. A1.2}$$

The intensity autocorrelation function is expressed as a function of the field correlation function:

$$G2(\tau) = 1 + G1(\tau)^2 \qquad \textbf{Eq. A1.3}$$

In DLS, a correlogram is generated where the raw correlation function is plotted against delay time:

$$\text{Raw correlation function} = G2(\tau) - 1 = G1(\tau)^2 \qquad \textbf{Eq. A1.4}$$

τ: delay time,

b: constant dependent upon the instrument and settings of optics,

D: translational diffusion coefficient,

Q: scattering vector,

n_o: refractive index of the solvent,

λ_o: wavelength in vacuum,

θ: scattering angle,

G1(τ): field correlation function,

G2(τ): the intensity autocorrelation function.

The autocorrelation functions [G2(τ) or G2(τ) – 1] are calculated by data fitting and then the D is calculated using the Stokes-Einstein equation:

$$D_H = \frac{k_B.T}{3.\pi.\eta.D} \quad \textbf{Eq. A1.5}$$

D_H: the hydrodynamic diameter (m),

k_B: the Boltzmann constant (1.381×10^{-23} $J.K^{-1}$),

T: temperature (K),

η: the zero-shear viscosity of the medium (Pa.s),

D: the translational diffusion coefficient ($m^2.s^{-1}$).

Analysis of the autocorrelation function allows us to determine the actual distribution of particle sizes, and the z-average value can be determined as the intensity-weighted average hydrodynamic diameter of the particles. The polydispersity index, a measure of the width of the particle size distribution, can also be calculated.

$$PDI = \left(\frac{SD}{D_H}\right)^2 \quad \textbf{Eq. A1.6}$$

SD: the standard deviation,

D_H: Hydrodynamic diameter.

A.2 Zeta (ζ) potential

The ζ potential of a particle cannot be measured directly; instead, it is inferred from the assessment of the electrophoretic mobility when an electric field is applied. Electrophoretic mobility is defined as the particle's velocity in response to the strength of the applied electric field (Delgado et al., 2007).

$$\mu_e = \frac{V_p}{E} \quad \textbf{Eq. A1.7}$$

μ_e: the electrophoretic mobility,

E: the magnitude of the electric field strength ($V.m^{-1}$),

V_p: the electrophoretic velocity of a particle ($m.s^{-1}$).

From the obtained electrophoretic mobility, the ζ potential can be calculated using the Henry's equation:

$$\mu_e = \frac{2.\varepsilon_r.\varepsilon_0.\zeta.f(kR_H)}{3.\eta}$$ **Eq. A1.8**

ε_r: the relative permittivity/dielectric constant,

ε_0: the permittivity of vacuum,

ζ: zeta potential (V),

η: the viscosity of the medium (Pa.s),

$f(kR_H)$: Henry's function which refers to the ratio of the particle radius (R_H (m)) to the Debye length (k (m^{-1})).

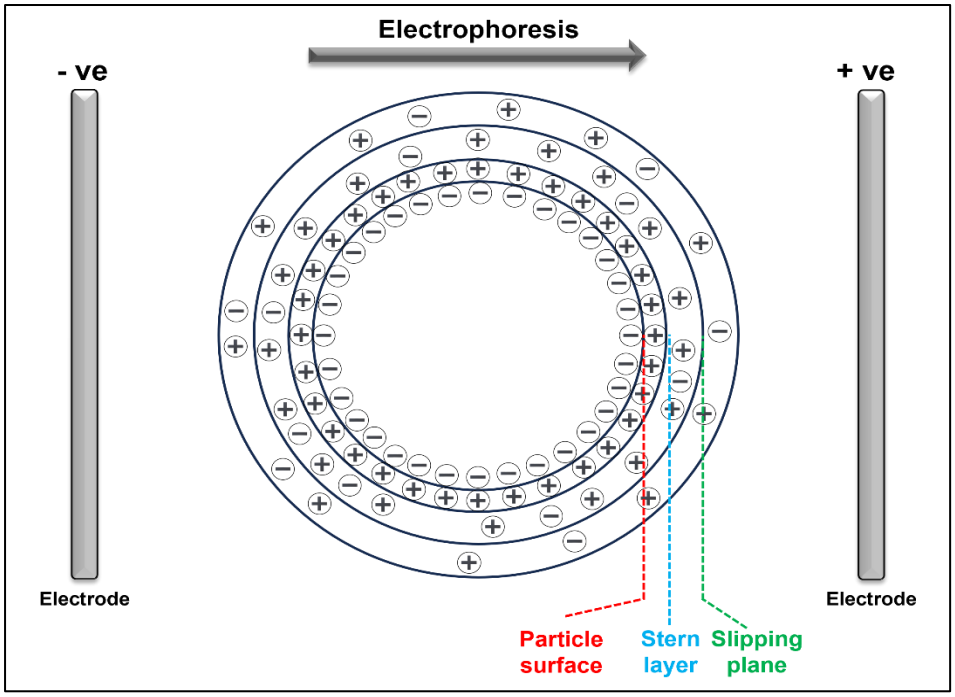

Figure A.2 Schematic representation of negatively charged particle surface, strongly adhered stern layer with positive charges, and slipping plane with both negative and positive charges. During electrophoresis, the particles move toward the oppositely charged electrode, and the slipping plane becomes the interface between the mobile particles and the medium. The ζ potential is the electrokinetic potential at this slipping plane. Adapted from (Bhattacharjee, 2016).

The Debye length is approximated to equal 1 for small particles in low ε media and Henry's equation can be modified as the Hückel equation:

$$\mu_e = \frac{2.\varepsilon_r.\varepsilon_0.\zeta}{3.\eta}$$ **Eq. A1.9**

The Debye length is approximated to equal 1.5 for larger particles (> 0.2 μm) in the more concentrated electrolyte solution and Henry's equation then modifies into the Helmholtz-Smoluchowski equation:

$$\mu_e = \frac{\varepsilon_r.\varepsilon_0.\zeta}{\eta}$$ **Eq. A1.10**

A.3 Small-Angle Scattering

A.3.1 Theoretical background

Small-angle scattering enables the characterisation of the object`s size and shape (through the determination of their volume, radius of gyration, dimension, and specific area), and their organisation in a continuous medium.

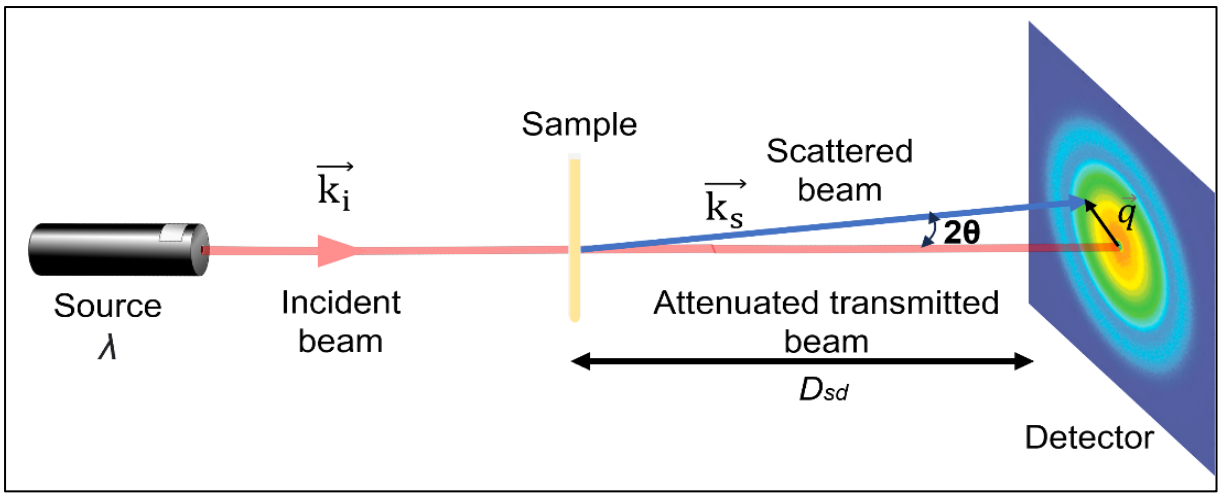

Figure A.3 Schematic representation of small-angle scattering. Adapted from (Grillo, 2008).

An incident (neutron or X-ray) beam of wavelength is directed at a sample and partially transmitted, absorbed, and scattered, as a result of its interaction with the material. A detector, positioned at a distance and covering a scattering angle from the sample, records the intensity of scattered radiation as a function of the modulus of the scattering vector. The incident beam can be described as a planar monochromatic wave characterised by an incident and scattered wave vector. The difference between these two vectors corresponds to the scattering vector whose modulus is defined as follows:

$$q = |\vec{q}| = \left|\overrightarrow{k_s} - \overrightarrow{k_i}\right| = \frac{4.\pi.\sin\theta}{\lambda} \qquad \textbf{Eq. A1.11}$$

In crystalline materials, Bragg's law of diffraction is given by the following equation (Singh, 2017):

$$x = \frac{n.\lambda}{2} = d.\sin\theta \qquad \textbf{Eq. A1.12}$$

$$q = \frac{2.\pi}{d} \qquad \textbf{Eq. A1.13}$$

$$q = \frac{4.\pi.\sin\theta}{n.\lambda} \qquad \textbf{Eq. A1.14}$$

$$s = n/d \qquad \textbf{Eq. A1.15}$$

$\overrightarrow{k_s}$: scattered wave vector,

$\overrightarrow{k_i}$: incident wave vector,

λ: wavelength of an incident beam,

D_{sd}: sample-to-detector distance,

2θ: scattering angle, (note, incoming and outgoing angles add up to 2θ),

I(q): the intensity of scattered radiation,

n: integer (1, 2, 3..) describing the order of the diffraction peak,

q: scattering vector (reciprocal space),

d: distance in the sample (real space), lattice spacing, bilayer thickness.

For small angles, sin θ ≈ θ and therefore, the scattering angle 2θ is indirectly proportional to the lattice spacing, d, i.e. the scattering pattern is plotted in the reciprocal space. (Li et al., 2017).

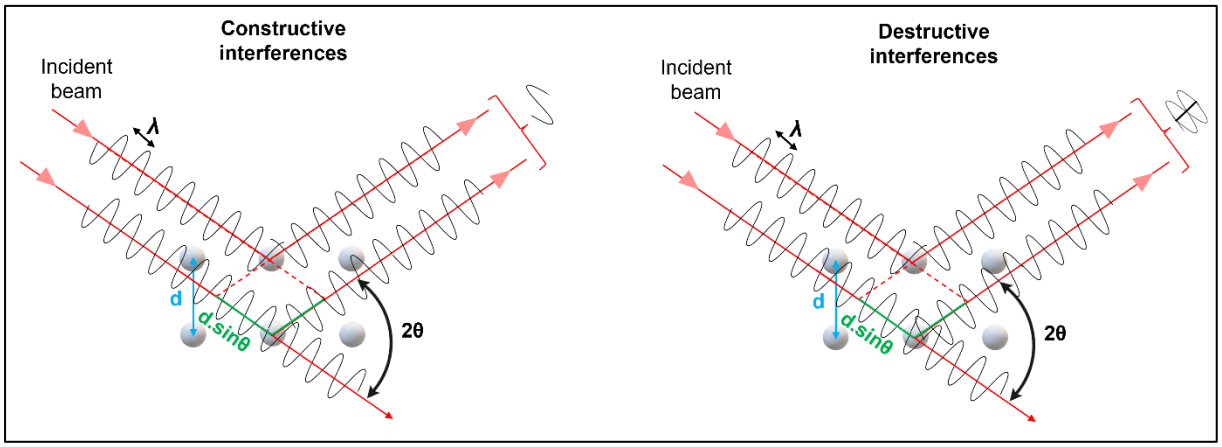

Figure A.4 Schematic representation of incident beam and scattered beam. Scattered waves can interfere either constructively (enhancing each other) or destructively (cancelling each other out) when they interact with the nucleus (for neutrons) or the electronic cloud (for X-rays). Constructive interference happens when waves from adjacent atomic planes align in phase, which occurs when the difference in their travelled distances is an integral multiple of the wavelength. The figure shows that the second wave travels an extra distance (2dsinθ). When that distance is set equal to nλ, the result is Bragg's Law nλ = 2dsinθ. In the case of destructive interferences, both signals are cancelled. Adapted from (Pynn, 2009).

$$n.\lambda = 2d.\sin\theta = 2d.\theta \qquad \textbf{Eq. A1.12}$$

for small θ, $\frac{n.\lambda}{d} = 2\theta$ **Eq. A1.16**

In general, the expression of scattering intensity, I(q);

$$I(q) = \varphi.V^2.\Delta\rho^2.P(q).S(q) + background \qquad \textbf{Eq. A1.17}$$

Φ: the particle number density of scattering particle,

V: the volume of the particle,

$\Delta\rho = \rho_{shell} - \rho_{solvent}$: the contrast factor,

P(q): form factor,

S(q): structure factor.

A.3.2 Data Analysis

Data analysis of samples was performed with SasView (5.0.6) (SasView, 2022), DAWN (2.25.0), and OriginPro (2020) software considering the formed structures below.

SANS-Liposomes (L-0 and L-1); the intensity I(q) scattered from empty, and *t*-res loaded liposomes was fitted using the uni-bi-tri-lamellar vesicles model. Fixed parameters were scale: 1, SLD: 0.5x10^{-6}Å^{-2}, SLD solvent: 6.36x10^{-6}Å^{-2} and thick solvent: 10 Å, T_{shell}: 40 Å.

SANS-5 mM NaC-containing bilosomes (B-5:0 and B-5:1); the intensity I(q) scattered from empty, and *t*-res loaded bilosomes was fitted using a merged model combined with the vesicle and core-shell ellipsoid model: Fixed parameters were SLD: 0.5x10^{-6}Å^{-2}, SLD solvent: 6.36x10^{-6}Å^{-2} and PD of the core-shell ellipsoids: 0.

SANS-7.5 mM NaC-containing bilosomes (B-7.5:0 and B-7.5:1); the intensity I(q) scattered from empty, and *t*-res loaded bilosomes was fitted using a merged model combined with the two vesicles model. Fixed parameters were SLD: 0.5x10^{-6}Å^{-2}, SLD solvent: 6.36x10^{-6}Å^{-2}, and PD of the vesicles: 0.200.

SANS-10 mM NaC-containing bilosomes (B-10:0 and B-10:1); the intensity I(q) scattered from empty, and *t*-res loaded bilosomes was fitted to a merged model combined with the vesicle and sphere model. Fixed parameters were SLD: 0.5x10^{-6}Å^{-2} and SLD solvent: 6.36x10^{-6}Å^{-2}.

SANS-CH-coated bilosomes; the intensity I(q) scattered from empty, and *t*-res loaded CH-coated bilosomes was fitted using the unified power-R_g (Beaucage) model (Level 1).

SAXS-CH-coated bilosomes; the intensity I(q) scattered from empty, and *t*-res loaded CH-coated bilosomes was fitted using a nonlinear least-squares routine for the Lorentz fit. The *d-spacing* was calculated from the position of the Bragg peak *(*d = 2π/q*).* The value of *q* was determined by fitting a Lorentz function to the peak.

SANS-PGA/CH-coated bilosomes; the intensity I(q) scattered from empty, and *t*-res loaded CH-coated bilosomes was fitted using the unified power-R_g (Beaucage) model (Level 2).

A.3.3 Small-angle neutron scattering models

A.3.3.1 Multilayer vesicles model

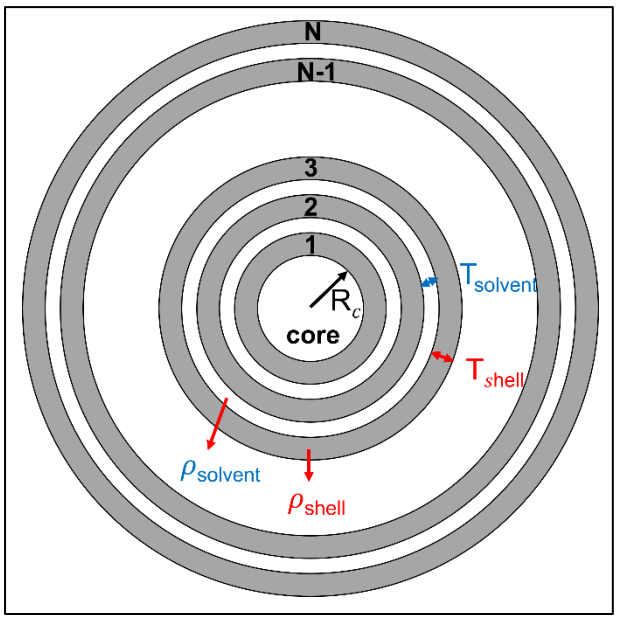

Figure A.5 Schematic representation of multilayer vesicles model. Adapted from (SasView, 2022).

This model represents the core-shell sphere concept, featuring a core filled with a solvent and surrounded by N layers of material, with N-1 intervening layers of solvent. The 1D scattering intensity is calculated below (Guinier & Fournet, 1955) (SasView, 2022).

$$P(q) = \text{scale}.\frac{V_F}{V(R_N)}F^2(q) + \text{background} \qquad \textbf{Eq. A1.18}$$

where

$$F(q) = (\rho_{shell} - \rho_{solvent})\sum_{i=1}^{N}\left[3V(r_i)\frac{\sin(qr_i) - qr_i\cos(qr_i)}{(qr_i)^3} - 3V(R_i)\frac{\sin(qR_i) - qR_i\cos(qR_i)}{(qR_i)^3}\right] \qquad \textbf{Eq. A1.19}$$

for

$$r_i = R_c + (i-1)(T_{shell} + T_{solvent}) \quad \text{solvent radius before shell } i \qquad \textbf{Eq. A1.20}$$

$$R_i = r_i + T_{shell} \quad \text{shell radius for shell } i \qquad \textbf{Eq. A1.21}$$

P(q): form factor,

R_N: the outer-most shell radius,

F(q): Bessel function,

V_F: the volume fraction of particles,

V(r): the volume of a sphere of radius r,

R_c: the radius of the core,

T_{shell}: the thickness of the shell,

$T_{solvent}$: the thickness of the solvent layer between the shells,

ρ_{shell}: the SLD of a shell

$\rho_{solvent}$: the SLD of the solvent.

A.3.3.2 Vesicle model

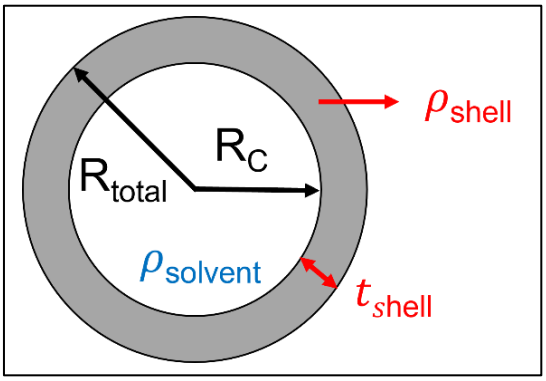

Figure A.6 Schematic representation of vesicle model. Adapted from (SasView, 2022).

This model provides the form factor for an unilamellar vesicle and normalizes the form factor by the volume of the shell. The 1D scattering intensity is calculated below (Guinier & Fournet, 1955; SasView, 2022).

$$P(q) = \frac{V_{Fshell}}{V_{shell}}\left[\frac{3V_{core}(\rho_{solvent}-\rho_{shell})j_1(qR_C)}{qR_C} + \frac{3V_{total}(\rho_{shell}-\rho_{solvent})j_1(qR_{total})}{qR_{total}}\right]^2 + background \qquad \textbf{Eq. A1.22}$$

$$T_{shell} = R_{total} - R_C \qquad \textbf{Eq. A1.23}$$

The background is a flat background level (due for example to incoherent scattering in the case of neutrons),

$$j_1 = \frac{\sin(q)-q\cos(q)}{q^2} \qquad \textbf{Eq. A1.24}$$

P(q): form factor,

V_{Fshell}: the volume fraction of shell material,

V_{shell}: the volume of the shell,

V_{core}: the volume of the core,

V_{total}: the total volume,

R_C: the radius of the core,

R_{total}: the outer radius of the shell,

$\rho_{solvent}$: the SLD of the solvent (which is the same as for the core in this case),

ρ_{shell}: the SLD of the shell,

j_1: the spherical Bessel function.

A.3.3.3 Sphere model

The 1D scattering intensity is calculated in the following way (Guinier & Fournet, 1955) (SasView, 2022).

$$I(q) = \frac{scale}{V_s}.\left[3V(\Delta\rho).\frac{\sin(qR_s)-qr\cos(qR_s)}{(qR_s)^3}\right]^2 + background \quad \textbf{Eq. A1.25}$$

Scale: volume fraction,

V_s: the volume of the sphere,

R_s: the radius of the sphere,

$\Delta\rho$: $\rho_{shell} - \rho_{solvent}$: the contrast factor.

A.3.3.4 Core-shell ellipsoid model

The core axial ratio and shell thickness are parameters for the core-shell ellipsoid model. These parameters can enhance the model's performance, especially when dealing with polydispersity, as compared to the four independent radii used in the model's original parameterization (Berr, 1987; Kotlarchyk & Chen, 1983; SasView, 2022).

When $X_c<1$ the core is oblate; when $X_c>1$ it is prolate. $X_c= 1$ is a spherical core.

For a fixed T_{shell}, $X_{polarshell}=1$, to scale the T_{shell} pro-rata with the radius set or constrain $X_{polarshell}=X_c$

The calculation of intensity follows that for the solid ellipsoid, but with separate terms for the core-shell and shell-solvent boundaries.

$$P(q,\alpha) = \frac{scale}{V}F^2(q,\alpha) + background \quad \textbf{Eq. A1.26}$$

where

$$F(q,\alpha) = f(q,R_e,R_e.X_{core},\alpha) + f\left(q,R_e + T_{thickshell},R_e.X_c + T_{thickshell}.X_p,\alpha\right) \quad \textbf{Eq. A1.27}$$

where

$$f\left(q,R_e,R_p,\alpha\right) = \frac{3\Delta\rho V\left(\sin[qr(R_p,R_e,\alpha)]-\cos[qr(R_p,R_e,\alpha)]\right)}{[qr(R_p,R_e,\alpha)]^3} \quad \textbf{Eq. A1.28}$$

and

$r(R_e, R_p, \alpha) = [R_e{}^2 \sin^2\alpha + R_p{}^2 \cos^2\alpha]^{1/2}$ α): Form factor **Eq. A1.29**

X_c: the core axial ratio,

T_{shell}: shell thickness,

α: the angle between the axis of the ellipsoid,

$\vec{q}, V = \frac{4}{3}\pi R_p R_e^2$: the volume of the ellipsoid,

R_p: the polar radius along the rotational axis of the ellipsoid,

R_e: the equatorial radius perpendicular to the rotational axis of the ellipsoid,

$\Delta\rho$: the contrast factor, either ($\rho_{core} - \rho_{shell}$) or ($\rho_{shell} - \rho_{solvent}$).

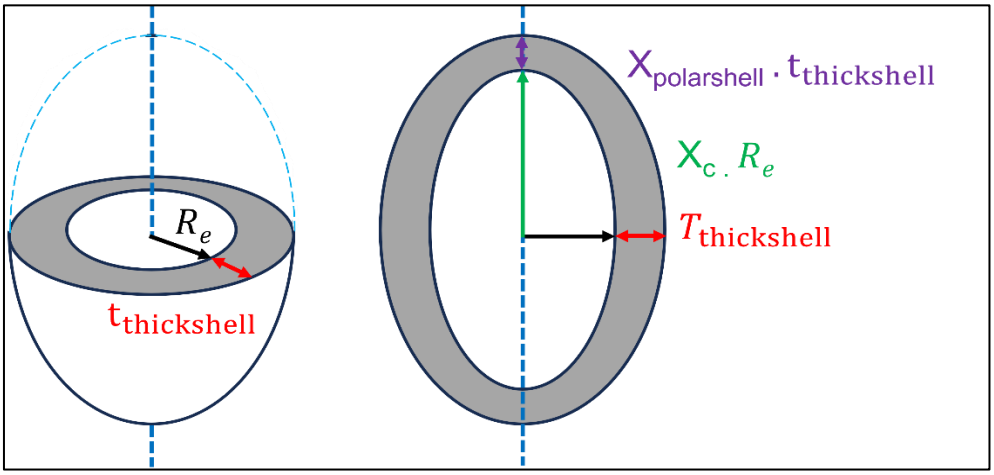

Figure A.7 Schematic representation of core-shell ellipsoid model. Adapted from (SasView, 2022).

A.3.3.5 The unified power R_g model

This model employs the empirical multiple-level unified Exponential/Power-law fit method developed by Beaucage. Four functions are included so that 1, 2, 3, or 4 levels can be used. In addition, a 0 level has been added which simply calculates (Beaucage, 1995, 1996; Hammouda, 2010; SasView, 2022):

$$I(q) = \frac{scale}{q} + background \qquad \textbf{Eq. A1.30}$$

The Beaucage method can reasonably approximate the scattering from many different types of particles, including fractal clusters, random coils (Debye equation), ellipsoidal particles, etc.

The model works best for mass fractal systems characterized by Porod exponents between 5/3 and 3. It should not be used for surface fractal systems. Hammouda (2010) has pointed out a deficiency in the way this model manages the transitioning between the Guinier and Porod regimes and which can create artifacts that appear as kinks in the fitted model function. The empirical fit function is:

$$I(q) = \text{background} + \sum_{i=1}^{N}\left[G_i \exp\left(-\frac{q^2 R^2_{gi}}{3}\right) + B_i \exp\left(-\frac{q^2 R^2_{g(i+1)}}{3}\right)\left(\frac{1}{q_i^*}\right)^{P_1}\right]$$ **Eq. A1.31**

where

$$q_i^* = q\left[\text{erf}\left(\frac{qR_{gi}}{\sqrt{6}}\right)\right]^{-3}$$ **Eq. A1.32**

N: structural level.

For each level, the four parameters Gi, Rgi, Bi, and Pi must be chosen. Beaucage has an additional factor k in the definition of q_i^* which is ignored here.

A.3.4 Electron Density Profile (EDP)

in order to obtain the EDP (Li et al., 2017),

1) the reflection intensities must be adjusted by the so-called Lorentz correction.

The Lorentz correction is a geometrical correction factor that accounts for the relative differences in the diffraction probabilities of different crystal planes, and usually also considers the given geometry of the instrumental set-up.

2) all amplitudes, F_n, which are directly proportional to the probed electron density contrasts need to be calculated from the corrected intensities, (I_h n_2), by taking their square root.

3) Fourier transform in order to obtain the EDP in the radial direction of our MLVs;

$$\rho(z) = \sum_{n=1}^{n_{max}} \alpha_n F_n \cos(2\pi s_n z) = \sum_{n=1}^{n_{max}} \alpha_n F_n \cos\left(\frac{2\pi n z}{d}\right)$$ **Eq. A1.33**

F_h: experimentally derived amplitudes (form factors)

S_h: the peak positions

n: the peak order (also known as Miller index)

α_h: the phase factors of the given amplitudes F_h

z: the distance in real space.

Appendix B - Supporting information of Chapter 2

B.1 Preparation of POPC-liposomes and POPC-bilosomes

B.1.1 Methods

Preparation of NaC solutions, empty and *t*-res loaded POPC-bilosomes: The empty and *t*-res loaded POPC-liposomes and POPC-bilosomes **(Table A.1)** were prepared according to methods described in **Chapter 2, Section 2.3.2** using thin-film hydration followed by sonication with minor modifications reported by Coreta-Gomes et al. (2015).

Preparation of CH and PGA solutions and optimisation of CH and PGA coating: The stock solution of CH (3 mg/mL) and PGA (3 mg/mL) was prepared and bilosomes were coated with CH and PGA/CH polyelectrolyte complex according to methods described in **Chapter 2, Section 2.3.3.**

Evaluation of storage stability: The stability of POPC-liposomes and POPC-bilosomes formulations was evaluated during storage stored at 4°C and 20°C for 4 weeks and the method described in **Chapter 3, Section 3.3.5.3.**

Characterization of empty and *t*-res loaded bilosomes, CH-coated and PGA/CH-coated bilosomes: The D_H, PDI, and ζ potential were analysed according to methods described in **Chapter 2, Section 2.3.4.1.**

SANS: The SANS experiments were performed at ISIS Neutron and Muon Source at the STFC Rutherford Appleton Laboratory (Oxfordshire, UK) and methods described in **Chapter 2, Section 2.3.4.4.**

Quantification of *t*-res: The *t*-res was quantified using the HPLC-DAD method, which was described in **Chapter 2, Section 2.3.4.7** was used to determine the free amount of *t*-res in the samples (Ares et al., 2015).

Statistical analysis: All the data were reported as mean±SD. Results were analysed by one-way ANOVA and General Linear Model (ANOVA) using Minitab® 20.4 software. The level of statistical significance was defined by $p<0.05$.

B.1.2 Results and Discussion

B.1.2.1 Schematic phase diagram of NaC solutions, POPC-liposomes and POPC-bilosomes

A phase diagram of POPC (mM) vs NaC (mM) was prepared using the phase diagram prepared by (Garidel et al., 2007). D_H, PDI and ζ potential of the formulations of NaC

solutions, POPC-liposomes, and POPC-bilosomes were shown in the diagram at 20°C **(Fig. B1**).

According to DLS measurements, the D_H of NaC solutions (40-125 mM) was determined within the range of 2.2±0.1 nm to 3.7±0.9 nm. The D_H of 10 mM POPC liposomes was 102.9±4.5 nm, while for 100 mM POPC liposomes, it was 120.7±11.7 nm. The addition of NaC to the liposome formulations and the variation in molarity and POPC/NaC molar ratio within the formulations significantly influenced the sample properties.

For 10 mM POPC liposomes, the D_H of NaC-containing liposomes was approximately 100 nm up to a 1:1 POPC/NaC molar ratio. With an increase in NaC molarity from 10 mM to 12.5 mM, the D_H decreased from approximately 100 nm to 66.8±0.5 nm. Despite having the same POPC/NaC ratio, the D_H of 10 mM POPC-10 mM NaC was 98.9±4.6 nm, whereas for 20 mM POPC-20 mM NaC, it decreased to 16.4±0.1 nm.

The 20 mM POPC-20 mM NaC formulation was positioned between the saturation and solubilisation line on the phase diagram, likely indicating partial solubilisation due to the higher NaC molarity. As the NaC concentration increased to 40 mM, the sample moved beyond the solubilisation line, leading to a D_H reduction to 6.9±0.5 nm. This decrease in D_H of NaC-liposomes could potentially be attributed to the disruptive effects of bile salts on phospholipid bilayers. When bile salts saturate the liposome bilayer, the bilayer becomes distorted and eventually ruptures, resulting in the formation of mixed micelles. As the bile salt concentration increases further, smaller-sized mixed micelles are formed (Garidel et al., 2007; Lichtenberg et al., 2013).

It has been reported that treating phospholipids with bile salts results in a sudden decrease in the D_H of liposomes due to reaching the saturation point (Hildebrand, 2004). NaC-induced vesicle-to-micelle transition of DPPC, 1,2-dipalmitoyl-sn-glycero-3-phosphatidylglycerol (DPPG), and DPPC/DPPG systems (molar ratios 3:1 and 1:1) were studied by (Hildebrand, 2004). The initial D_H of samples ranged from 60 to 20 nm. Upon titration of the samples with a 100 mM NaC solution, the D_H of all formulations prominently decreased below 5 nm when saturation was reached.

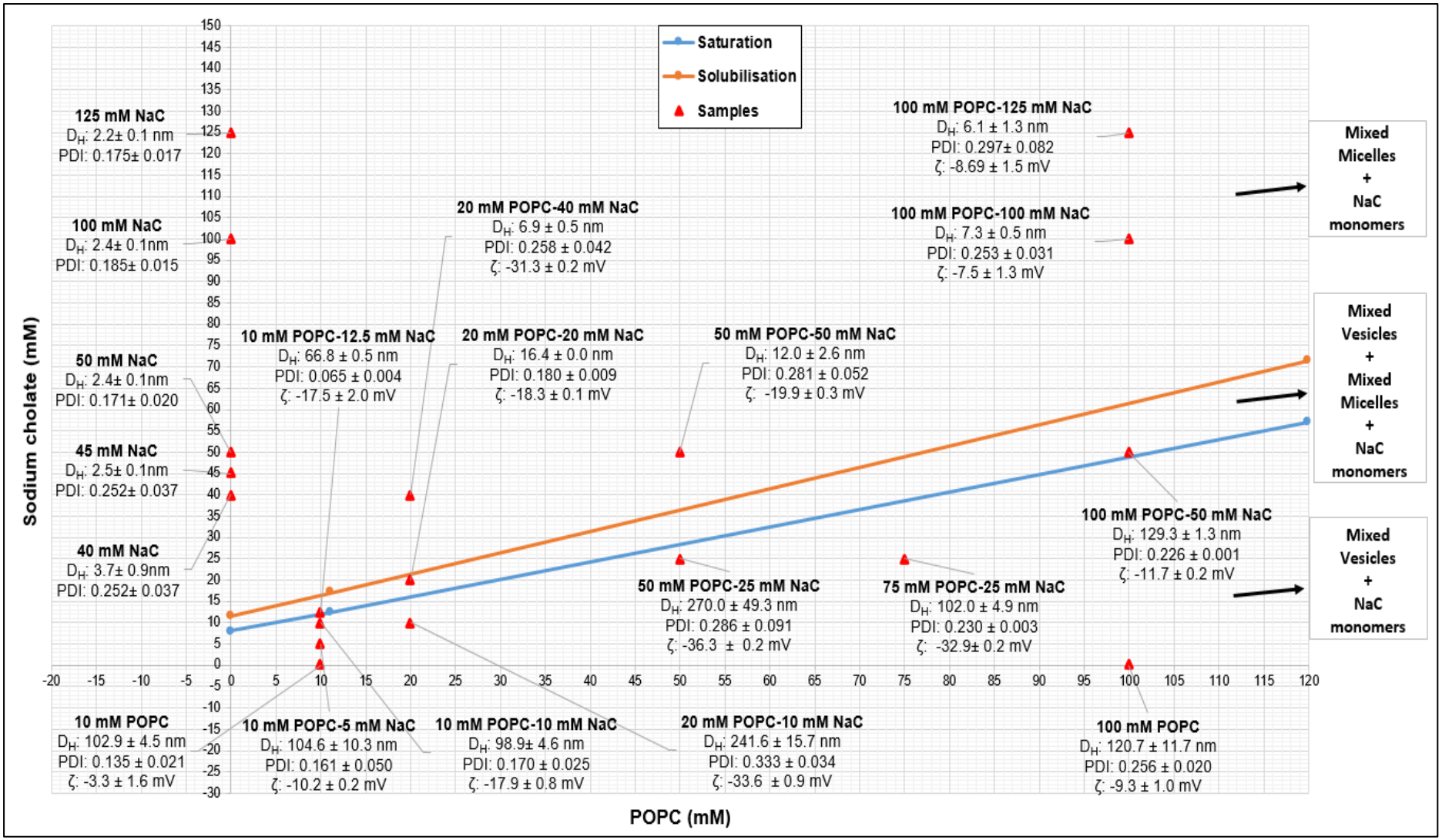

Figure B.1 Schematic phase diagram of POPC/NaC mixtures. The blue (saturation) and red (solubilisation) lines indicate the phase boundaries at 20°C. Adapted from (Garidel et al., 2007). Sample (▲), saturation (—●—) and (—●—) solubilisation.

B.1.2.2 Small-Angle Neutron Scattering

The morphology of bilosomes and phase transitions as a function of bile salts concentration plays an essential role in controlling colloidal stability and phytochemical loading and consequently, in the bioavailability of phytochemicals (Zhang & Wang, 2016). The shape and size of POPC liposomes and POPC bilosomes were investigated as a function of NaC concentration (0-10 mM) at the constant POPC concentration (10 mM). SANS data on Sans2D **(Fig. B2)** and data analysis show that pure lipid extruded liposomes are mostly unilamellar, with a small subpopulation of bi- and tri-lamellar vesicles. Upon incorporation of NaC, different colloidal structures appear, such as pure unilamellar spherical vesicles, to ellipsoidal vesicles coexisting with spherical vesicles in a concentration-dependent manner.

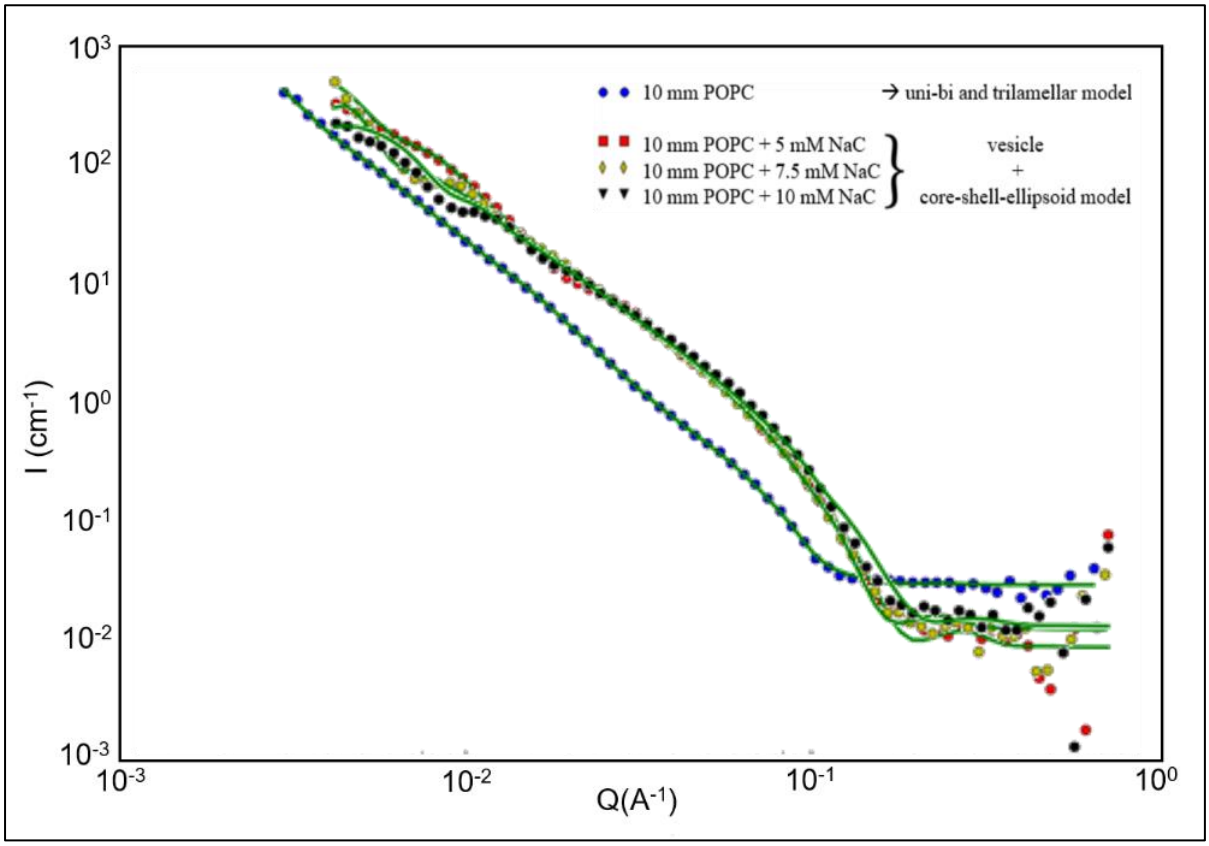

Figure B.2 SANS data of POPC and POPC-bilosomes prepared with three different NaC concentration, at 25°C.

B.1.2.3 Storage stability

The samples were stored at 4℃ and 20℃ for 28 days in dark conditions to evaluate the shelf life of the samples **(Table B1).** Samples were collected at 0, 7, 14, 21, and 28 days and samples were evaluated in terms of D_H, PDI, and ζ potential.

According to the initial properties of samples in **Fig. B3**, the D_H of both pure POPC liposomes and NaC-liposomes were within the range of 60 nm to 100 nm, with PDI<0.2

for all samples. When considering the same POPC/NaC molar ratio, there was a slight decrease in D_H and the PDI of the samples showed no significant change with the loading of *t*-res ($p>0.05$). Within the same POPC/*t*-res molar ratio, increasing NaC concentration from 5 mM to 7.5 mM did not lead to a significant difference in D_H, but it did result in a significant decrease in PDI ($p<0.05$). However, when the NaC concentration was further increased from 7.5 mM to 10 mM, D_H showed a significant increase, while the higher NaC molarity had no impact on the PDI of the samples. According to the general linear model, although *t*-res did not exhibit a significant effect on D_H (p: 0.067) and PDI (p: 0.952), the molarities of NaC had a significant effect on both D_H (p: 0.002) and PDI (p: 0.005).

According to ζ potential results **(Fig. B3)** ζ potential of pure POPC liposomes was -2.3±0.1 mV. This formulation tends to agglomerate because samples with ζ potential are lower than ±30 mV. Aggregation, flocculation, or precipitation problems can be seen during storage with the decrease of the magnitude of the ζ potential below ±30 mV (Danaei et al., 2018). The ζ potential of POPC-bilosomes had a greater negative surface charge density because of the incorporation of negatively charged NaC into the formulation. POPC bilosomes look delicate dispersion due to their ζ potential ranging from -16.4±1.7 to -25.7±0.9 mV ($p>0.05$). According to the general linear model, while *t*-res were not shown an effect on ζ potential (p: 0.154), molarities of NaC have a significant effect (p: 0.002).

Table B.1 Composition of POPC-liposome and POPC-bilosome formulations.

System		**POPC (mM)**	**NaC (mM)**	***t*-res (mM)**
POPC	L-0	10	-	-
	B-5:0	10	5	-
	B-5:0.1	10	5	0.1
	B-5:0.133	10	5	0.133
	B-7.5:0	10	7.5	-
	B-7.5:0.1	10	7.5	0.1
	B-7.5:0.133	10	7.5	0.133
	B-10:0	10	10	-
	B-10:0.1	10	10	0.1
	B-10:0.133	10	10	0.133
POPC: 2-oleoyl-1-palmitoyl-sn-glycero-3-phosphocholine, NaC: sodium cholate, *t*-res: trans-resveratrol, CH: chitosan, PGA: polygalacturonic acid				

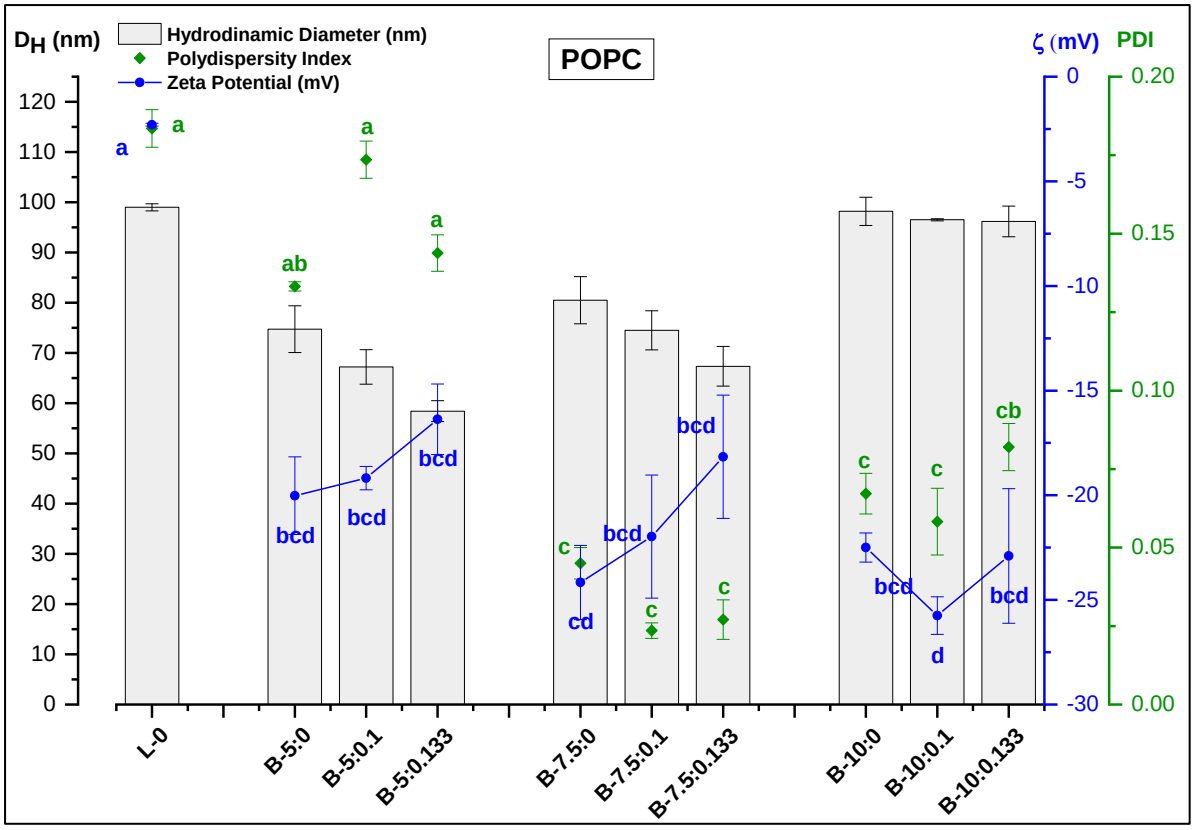

Figure B.3 The D_H (nm) (▭), PDI (●) and ζ potential (mV) (■) of POPC-bilosomes (B-5:0) for different NaC/CH (w/w) ratios. The data represent the mean±SD. Capital letters indicate the significant differences between in D_H of the samples during different GIT phases ($p<0.05$). The blue lowercase letters and green lowercase letters indicate the significant differences between ζ potential and PDI of the samples, respectively ($p<0.05$).

For general linear model analysis *t*-res (0.00 mM, 0.10 mM, and 0.13 mM), time (0, 1, 2, 3, and 4 week), and NaC (5 mM, 7.5 mM, and 10 mM) was chosen as an independent variable and their effect on D_H, PDI and ζ potential was analysed for NaC-liposomes stored at 4°C and 20°C.

D_H of Pure POPC liposomes were similar during storage for both storage conditions. However, their PDI increased from ~0.200 to ~0.250. The D_H of 5 mM POPC-bilosomes **(Fig. B4, B7)** increased slightly during storage but the D_H of 7.5 mM POPC-bilosomes **(Fig. B5, B8)** and 10 mM POPC-bilosomes **(Fig. B6, B9)** increased significantly after the first week of storage. For both storage condition, all variables (time, NaC concentration, and *t*-res concentration) had a significant effect on the D_H of samples ($p<0.001$) and time*NaC interactions was also significant ($p<0.001$).

PDI of all POPC-bilosomes stored at 4°C was lower than 0.200 **(Fig. B4-B6)**. While time (p: 0.006) and NaC ($p<0.001$) had a significant effect on the PDI of samples, *t*-res did not affect D_H (p: 0.759). For POPC-bilosomes stored at 20°C **(Fig. B7-B9)**; PDI of 5 mM and 7.5 mM POPC-bilosomes was lower than 0.200. However, the PDI of 10

mM POPC-bilosomes was increased from ~0.06 to ~0.25 during storage. While time ($p<0.001$) and NaC ($p<0.001$) had a significant effect on the PDI of samples, *t*-res did not affect D_H (p: 0.267). Same as D_H, the binary interaction of time*NaC variables was also significant for storage at 4°C ($p<0.001$) and 20°C (p: 0.014).

The ζ potential of POPC-bilosomes stored at 4°C were ranging from -25 mV to -5 mV **(Fig. B4-B6)**. The ζ potential of samples was increased during storage. According to the general linear model, time (p: 0.013) and NaC (p: 0.001) had a significant effect on the ζ potential of samples. However binary interaction of independent variables was not significant ($p>0.05$). The ζ potential of POPC-bilosomes stored at 20°C was between -25 mV to -3 mV **(Fig. B7-B9)**. According to the general linear model, time (p: 0.001) and NaC (p: 0.012) had a significant effect on the ζ potential of samples. Compared to samples stored at 4°C, the binary interaction of *t*-res*time (p: 0.014) and time*NaC (p: 0.005) showed a significant effect on the ζ potential of samples.

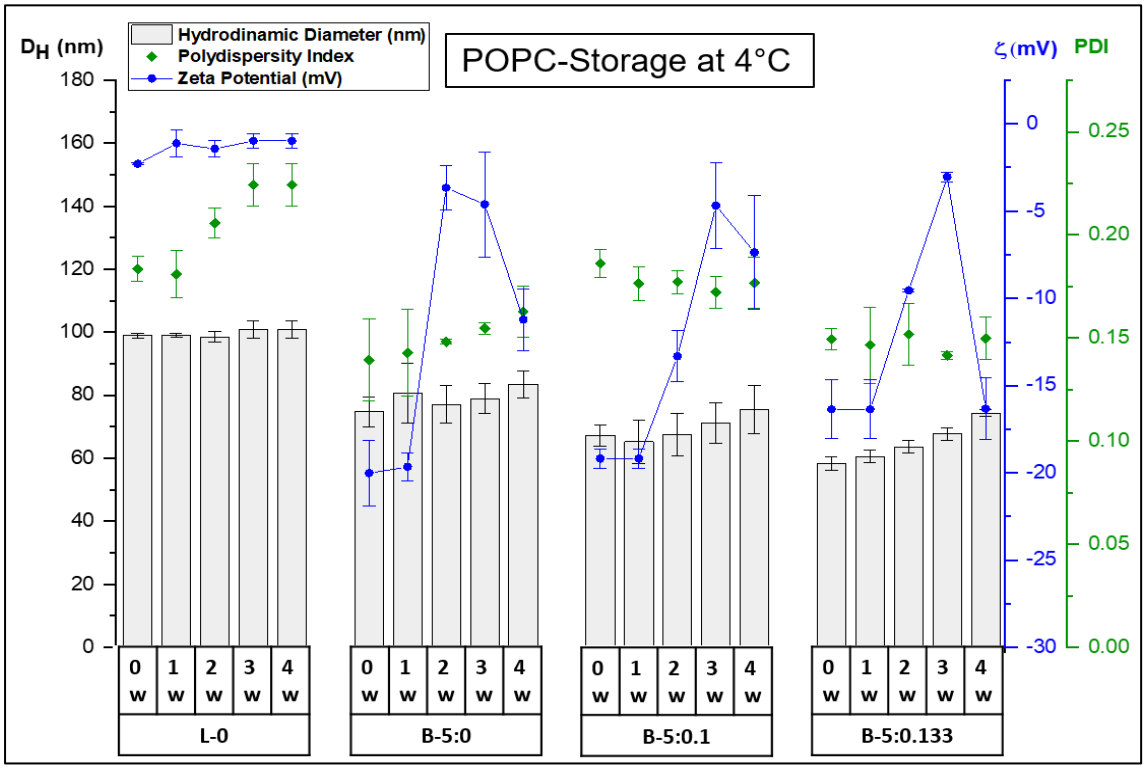

Figure B.4 The D_H (nm) (▭), PDI (●) and ζ potential (mV) (■) of POPC-liposomes and POPC-bilosomes stored at 4ºC for 4 weeks. The data represent the mean±SD.

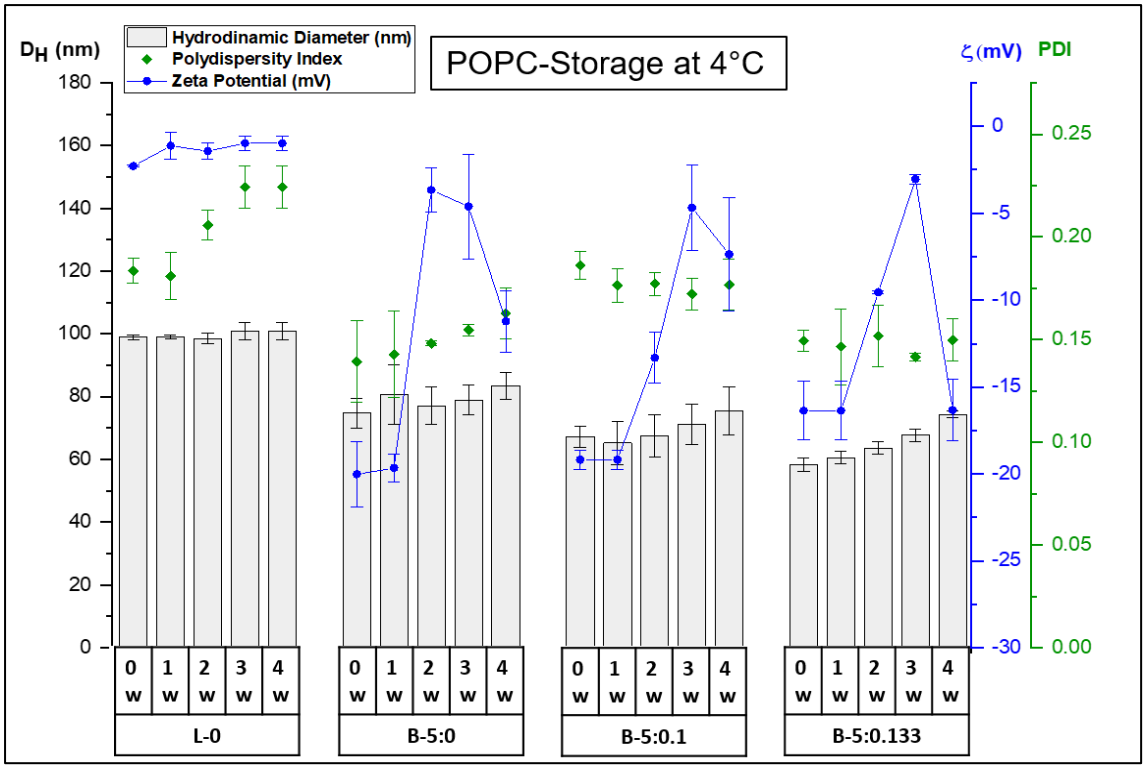

Figure B.5 The D_H (nm) (▬), PDI (●) and ζ potential (mV) (■) of POPC-liposomes and POPC-bilosomes stored at 4ºC for 4 weeks. The data represent the mean±SD.

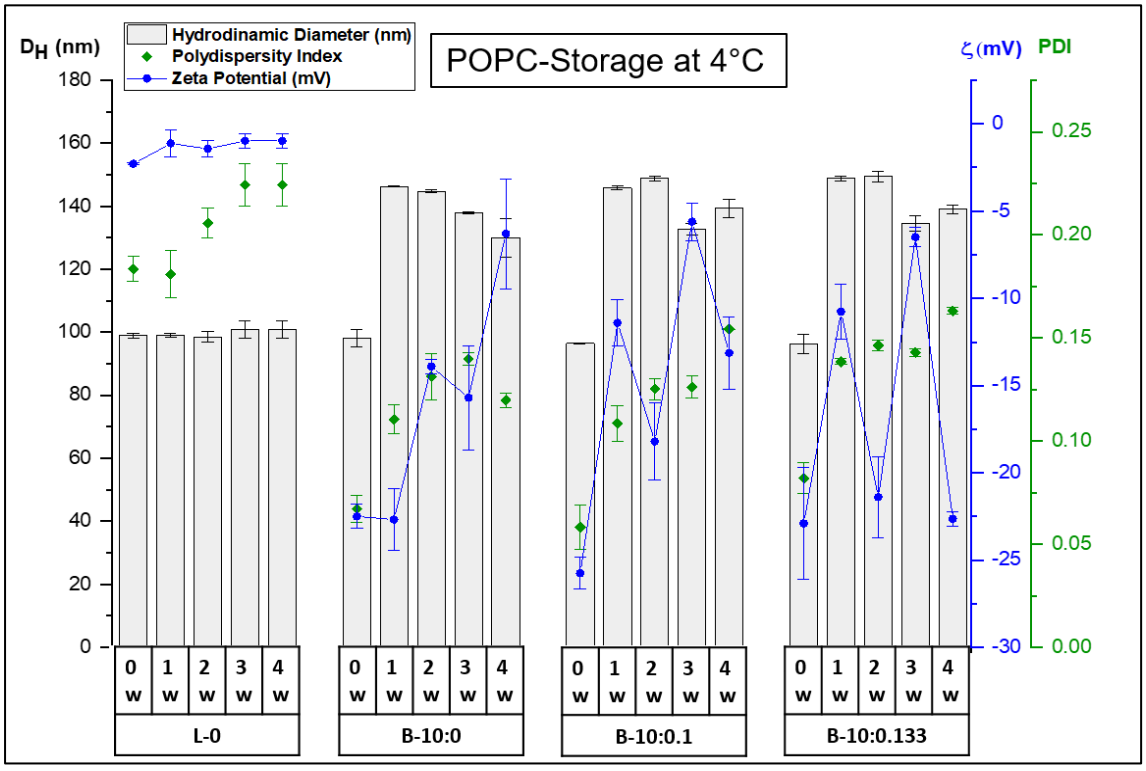

Figure B.6 The D_H (nm) (▬), PDI (●) and ζ potential (mV) (■) of POPC-liposomes and POPC-bilosomes stored at 4ºC for 4 weeks. The data represent the mean±SD.

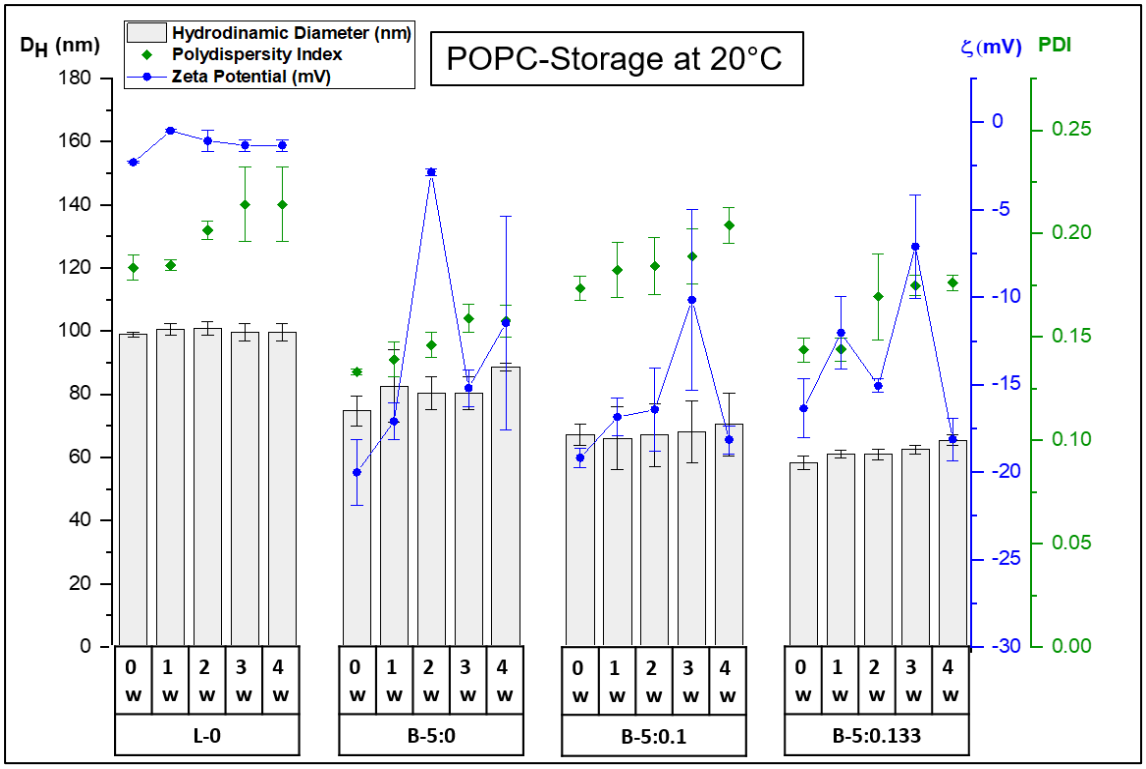

Figure B.7 The D_H (nm) (▬), PDI (●) and ζ potential (mV) (■) of POPC-liposomes and POPC-bilosomes stored at 20ºC for 4 weeks. The data represent the mean±SD.

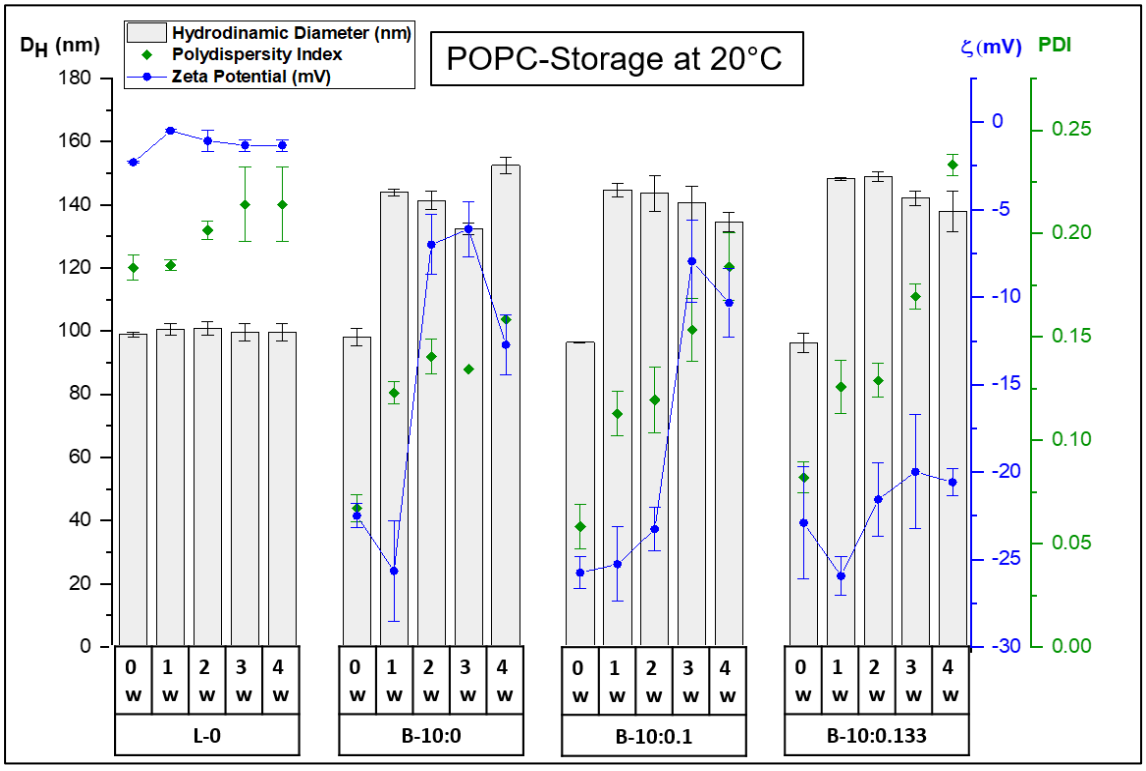

Figure B.8 The D_H (nm) (▬), PDI (●) and ζ potential (mV) (■) of POPC-liposomes and POPC-bilosomes stored at 20ºC for 4 weeks. The data represent the mean±SD.

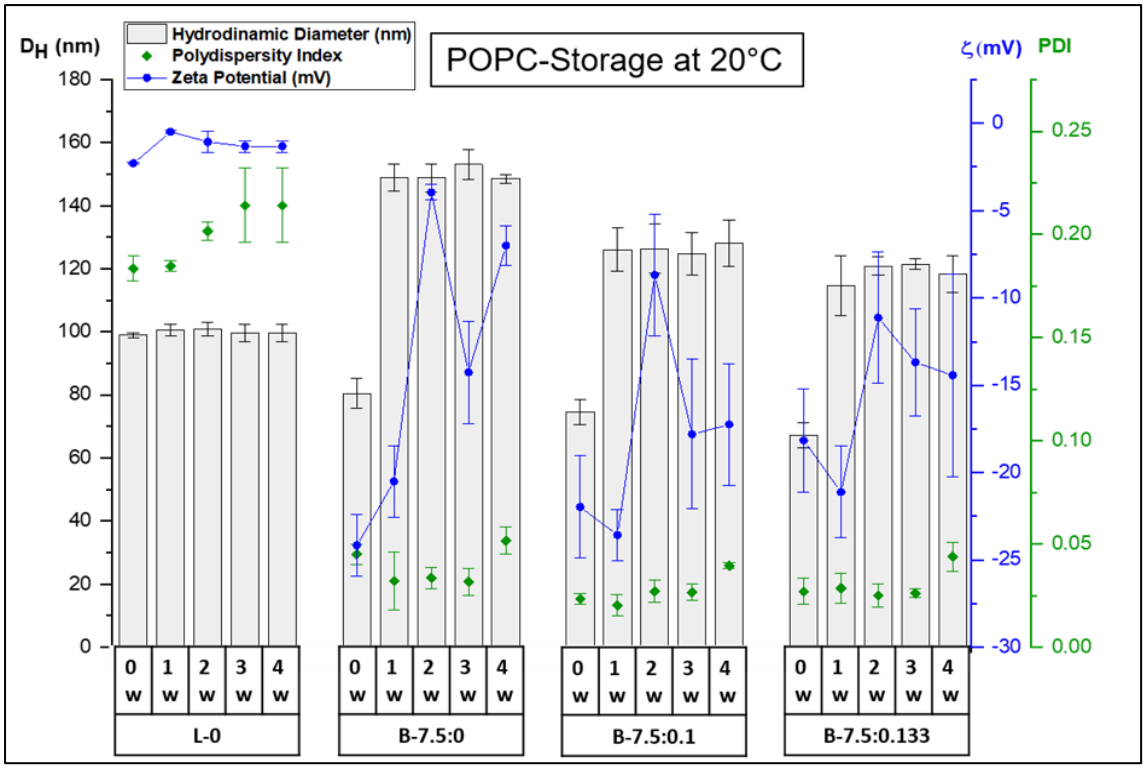

Figure B.9 The D_H (nm) (▭), PDI (●) and ζ potential (mV) (■) of POPC-liposomes and POPC-bilosomes stored at 20ºC for 4 weeks. The data represent the mean±SD.

B.1.2.4 Optimisation of CH coating and PGA coating of POPC/DOPG-bilosomes

For the surface modification, POPC-bilosomes were first coated with CH and Then PGA as a second biopolymer coating. To form a stable CH coating, bilosomes were added into the increased volume of CH solution (1 mg/mL) until the ζ potential shifted entirely from negative to positive, and the D_H of CH-coated bilosomes closed the original D_H of bilosomes. To assess the impact of CH concentration, the D_H, PDI, and the ζ potential of the POPC-bilosomes-CH mix were measured. The optimal NaC/CH ratio (w/w) was determined as 1.7 based on the physical properties. For the PGA coating, CH-coated POPC-bilosomes were added to an increased volume of PGA solution (1 mg/mL) to achieve the formation of stable PGA/CH-coated bilosomes. This progression persisted until the ζ potential transitioned entirely from positive to negative and the D_H of the CH-coated POPC-bilosomes was close to their original size. The optimal CH/PGA ratio (w/w) was determined as 0.4 based on the D_H, PDI, and ζ potential measurements.

Based on the results obtained, the D_H of the 5 mM NaC containing POPC-bilosomes was approximately 65 nm, accompanied by a ζ potential of around -25 mV. Upon CH coating, the D_H of the CH-coated POPC-bilosomes remained similar to the initial D_H of

the uncoated POPC-bilosomes. The ζ potential of the CH-coated POPC-bilosomes ranged from ~20 mV to ~25 mV.

For the 7.5 mM NaC containing POPC-bilosomes, the D_H showed a slight decrease from around 165 nm to 150 nm, and the ζ potential shifted from about -25 mV to ~20 mV. Although the ζ potential (~20 mV) was similar to that of other NaC concentrations, the D_H of the POPC-bilosomes containing 10 mM NaC increased significantly, from approximately 130 nm to a higher range of D_H which was from around 500 nm to 1000 nm, with a PDI of approximately 0.600.

After CH coating, a secondary coating of PGA was applied. For the 5 mM and 7.5 NaC containing POPC-bilosomes, the D_H ranged from approximately 200 nm to 300 nm, with a ζ potential of around -25 mV. Similar to the CH coating, the D_H of the PGA-coated bilosomes exhibited variability for the 10 mM NaC-containing POPC-bilosomes, with the only distinction being the different concentrations of *t*-res.

Due to the instability of bilosome coatings and the inability to achieve a sufficient surface charge (>±30 mV) with the NaC/CH (w/w) ratio of 1.7 and the CH/PGA (w/w) ratio of 0.4, the incorporation of DOPG, a negatively charged lipid, was introduced into the bilosome formulations to enhance the stability and coating effectiveness of the bilosomes.

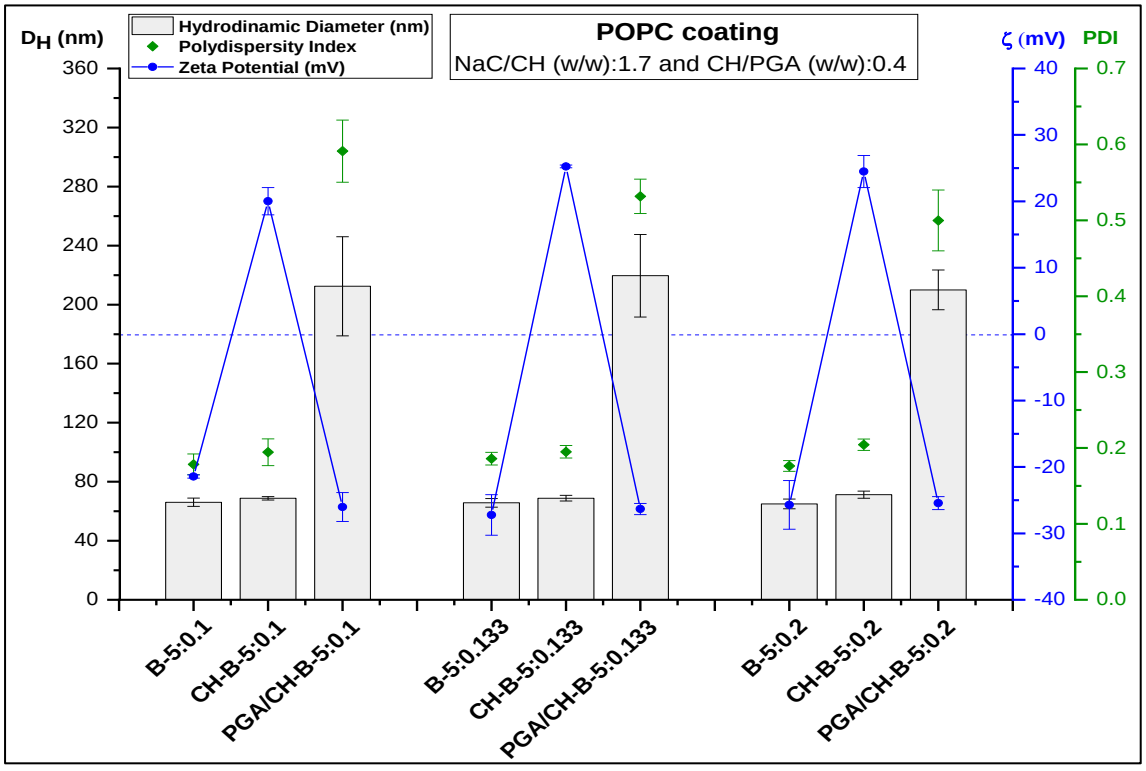

Figure B.10 The D_H (nm) (▭), PDI (●) and ζ potential (mV) (■) of POPC-bilosomes, CH-coated and PGA/CH coated bilosomes. The data represent the mean±SD.

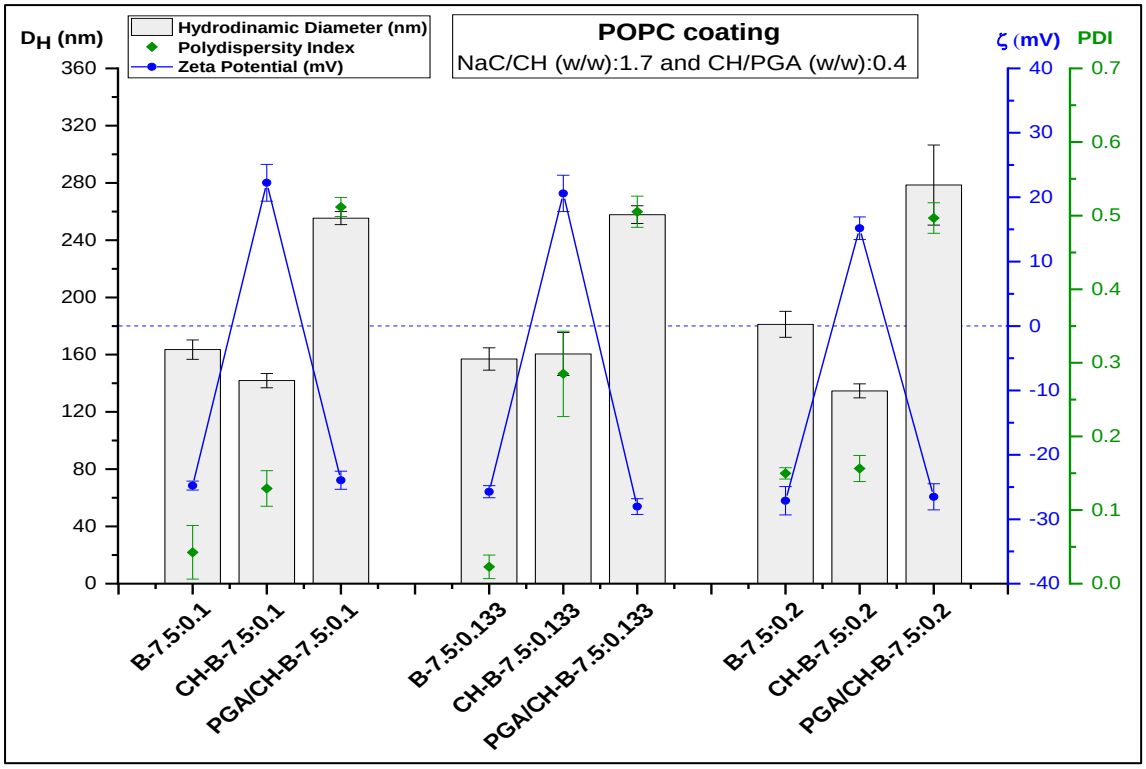

Figure B.11 The D_H (nm) (▬), PDI (●) and ζ potential (mV) (■) of POPC-bilosomes, CH-coated and PGA/CH coated bilosomes. The data represent the mean±SD.

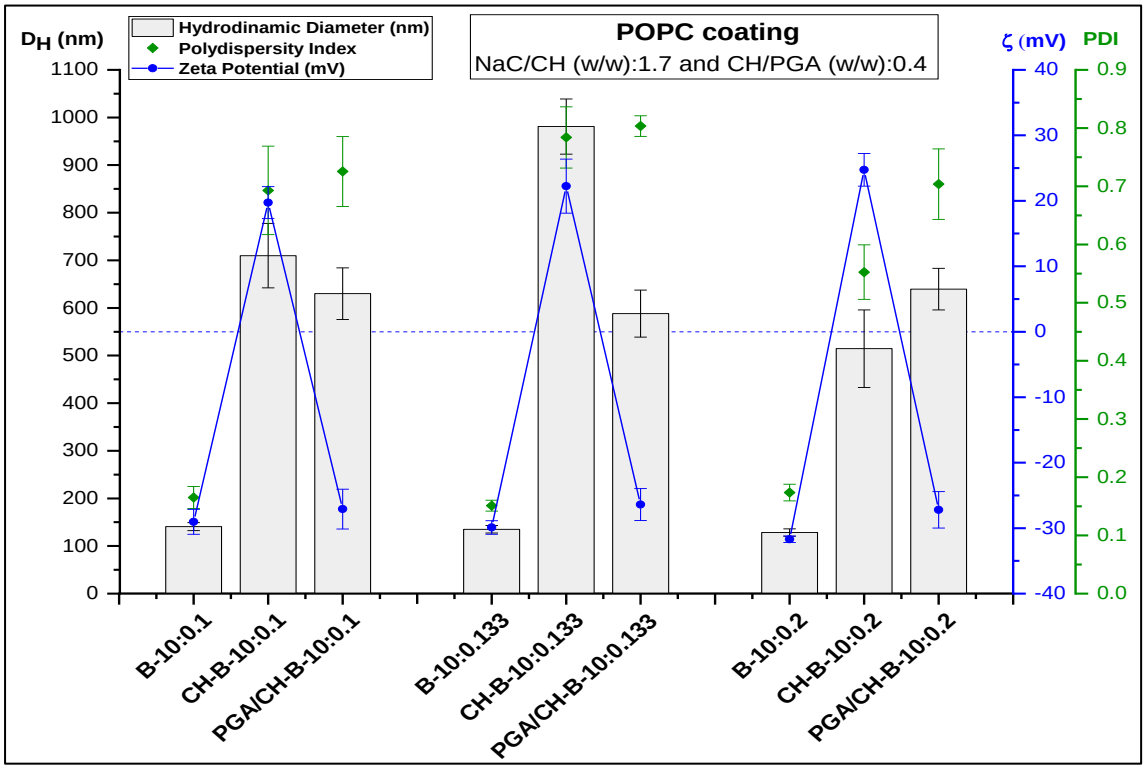

Figure B.12 The D_H (nm) (▬), PDI (●) and ζ potential (mV) (■) of POPC-bilosomes, CH-coated and PGA/CH coated bilosomes. The data represent the mean±SD.

B.2 Preparation of POPC/DOPG-liposomes and POPC/DOPG-bilosomes

B.2.1 Methods

Preparation of NaC solutions, empty and *t*-res loaded POPC-bilosomes: The empty and *t*-res loaded POPC-liposomes and POPC-bilosomes **(Table A.1)** were prepared according to methods described in **Chapter 2, Section 2.3.2** using thin-film hydration followed by sonication with minor modifications reported by Coreta-Gomes et al. (2015).

Preparation of CH and PGA solutions and optimisation of CH and PGA coating: The stock solution of CH (3 mg/mL) and PGA (3 mg/mL) was prepared and bilosomes were coated with CH and PGA/CH polyelectrolyte complex according to methods described in **Chapter 2, Section 2.3.3.**

Characterization of empty bilosomes, CH-coated and PGA/CH-coated bilosomes: The D_H, PDI, and ζ potential were analysed according to methods described in **Chapter 2, Section 2.3.4.1.**

B.2.2 Results and Discussion

B.2.2.1 Optimisation of CH coating and PGA coating of POPC/DOPG-bilosomes

To form stable CH-coated bilosomes, bilosomes were added to increasing volumes of CH solution until the ζ potential turned fully from negative to positive, and the D_H of CH-coated bilosomes was close to the initial D_H of bilosomes. In order to monitor the effect of increased CH concentration in the system, the physical properties of the system were measured in terms of D_H, PDI, and the ζ potential **(Fig. B13-15).** The D_H and PDI of the bilosomes-CH mix increased sharply due to the aggregation resulting from predominate attractive forces between partly covered bilosomes when the Z potential was close to zero. However, once the surface of the bilosomes was entirely covered, the Z potential became more positive, resulting in dominant repulsive forces among the CH-coated bilosomes. This ended up with the CH-coated bilosomes reverting to their initial D_H and exhibiting lower PDI values. As a result, the optimum NaC/CH ratio (w/w) was identified as 0.5 according to the physical properties of the samples. These conditions guarantee the complete coating of bilosomes with CH.

After CH coating, CH-coated bilosomes were coated with PGA as a second coating. CH-coated bilosomes were gradually introduced into an increased volume of PGA solution to form stable PGA/CH-coated bilosomes. This process continued until the ζ potential completely shifted from positive to negative, and the D_H of the CH-coated

bilosomes approached the initial D_H of the CH-coated bilosomes **(Fig. B16).** The optimum CH/PGA ratio (w/w) was identified as 0.4 according to the D_H, PDI, and ζ potential of the samples.

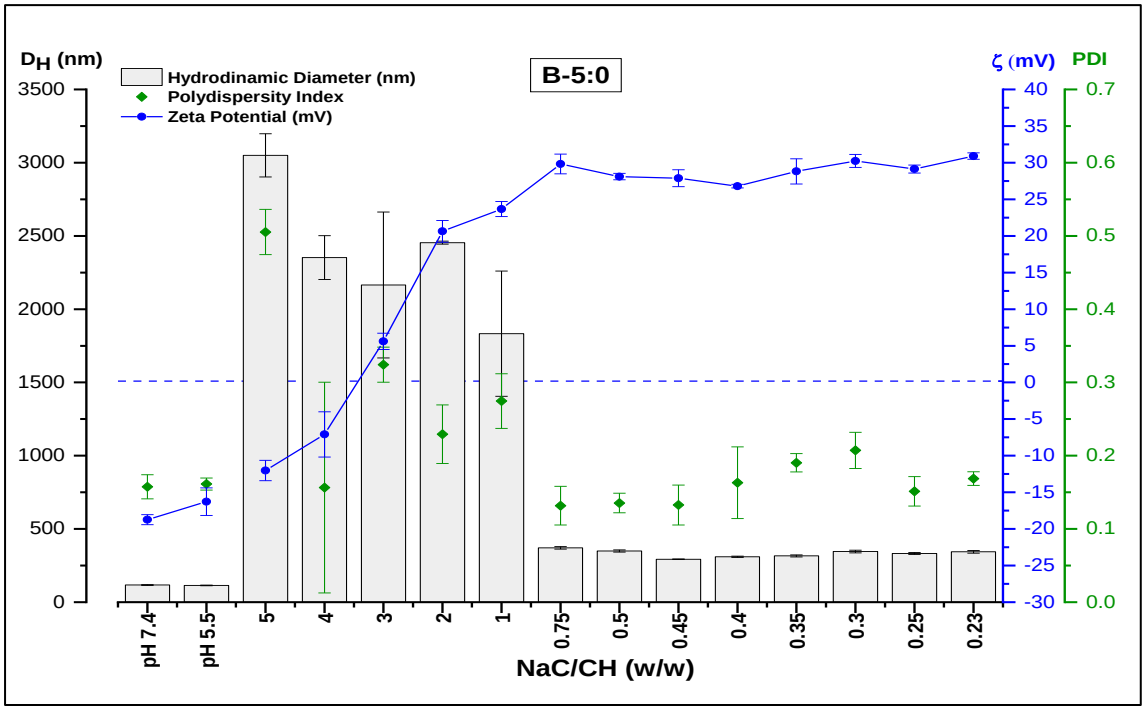

Figure B.13 The D_H (nm) (▬), PDI (●) and ζ potential (mV) (■) of POPC/DOPG-bilosomes (B-5:0) for different NaC/CH (w/w) ratios. The data represent the mean±SD.

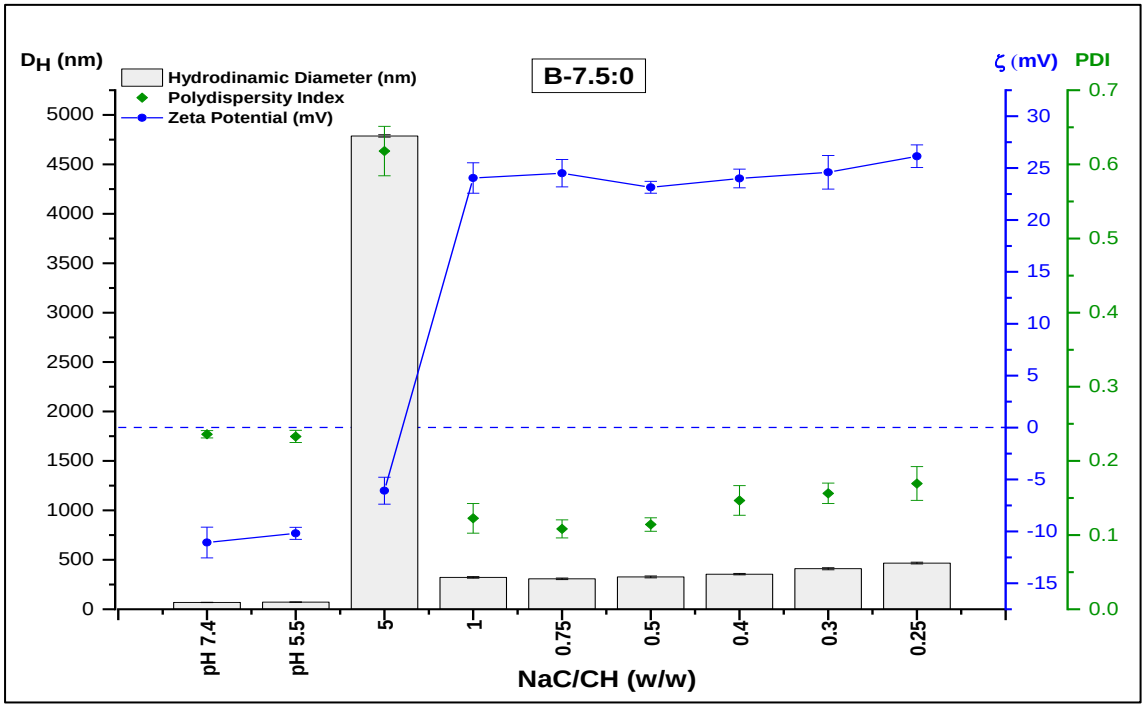

Figure B.14 The D_H (nm) (▬), PDI (●) and ζ potential (mV) (■) of POPC/DOPG-bilosomes (B-7.5:0) for different NaC/CH (w/w) ratios. The data represent the mean±SD.

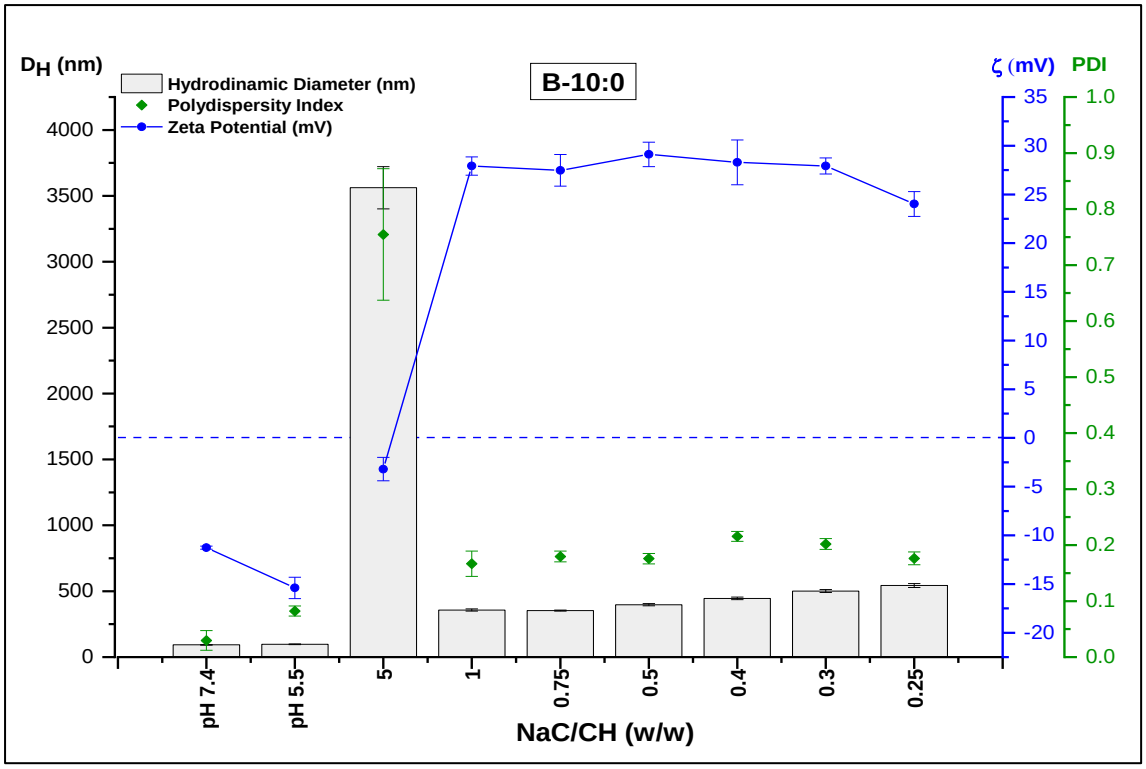

Figure B.15 The D_H (nm) (▭), PDI (●) and ζ potential (mV) (■) of POPC/DOPG-bilosomes (B-10:0) for different NaC/CH (w/w) ratios. The data represent the mean±SD.

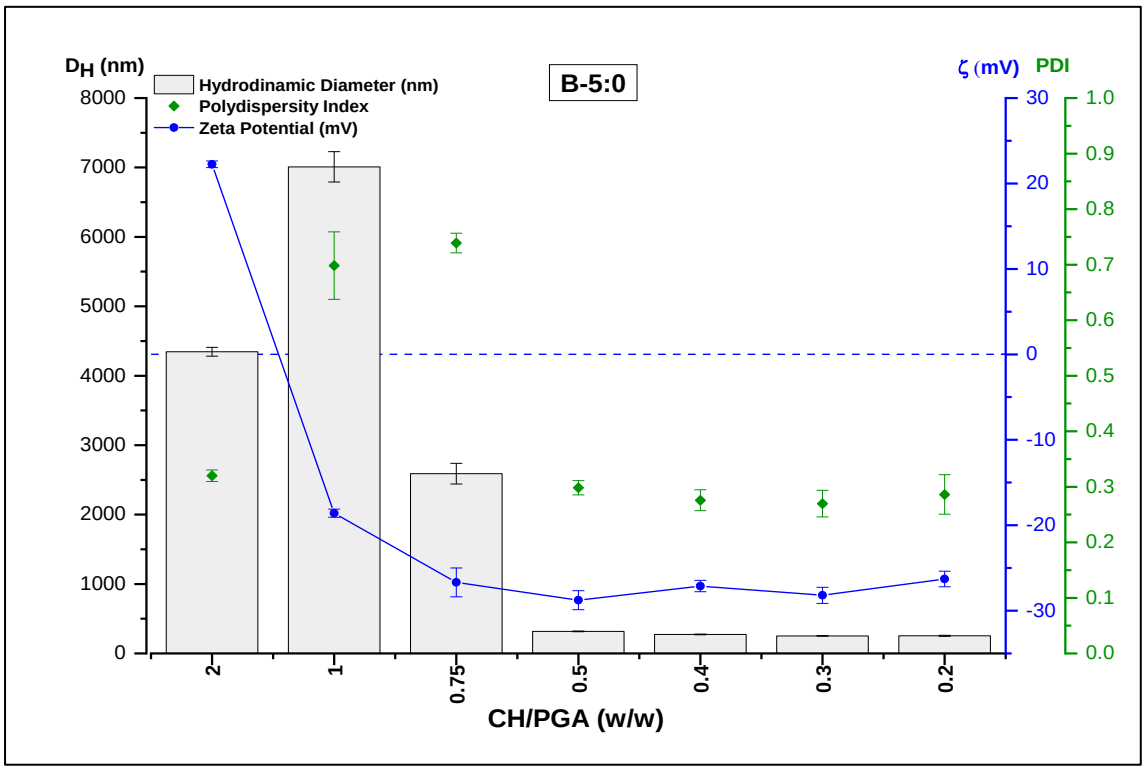

Figure B.16 The D_H (nm) (▭), PDI (●) and ζ potential (mV) (■) of POPC/DOPG-bilosomes (B-5:0) for different CH/PGA (w/w) ratios. The data represent the mean±SD.

List of References

Abbas, H., El-Feky, Y. A., Al-Sawahli, M. M., El-Deeb, N. M., El-Nassan, H. B., & Zewail, M. (2022). Development and optimization of curcumin analog nano-bilosomes using 21.31 full factorial design for anti-tumor profiles improvement in human hepatocellular carcinoma: In-vitro evaluation, in-vivo safety assay. *Drug Delivery*, *29*(1), 714-727.

Abbas, H., Refai, H., El Sayed, N., Rashed, L. A., Mousa, M. R., & Zewail, M. (2021). Superparamagnetic iron oxide loaded chitosan coated bilosomes for magnetic nose to brain targeting of resveratrol. *International journal of pharmaceutics*, *610*, 121244.

Aburahma, M. H. (2016). Bile salts-containing vesicles: promising pharmaceutical carriers for oral delivery of poorly water-soluble drugs and peptide/protein-based therapeutics or vaccines. *Drug Delivery*, *23*(6), 1847-1867. https://doi.org/10.3109/10717544.2014.976892

Ahad, A., Raish, M., Ahmad, A., Al-Jenoobi, F. I., & Al-Mohizea, A. M. (2018). Development and biological evaluation of vesicles containing bile salt of telmisartan for the treatment of diabetic nephropathy. *Artificial Cells Nanomedicine and Biotechnology*, *46*, S532-S539. https://doi.org/10.1080/21691401.2018.1430700

Al-Mahallawi, A. M., Abdelbary, A. A., & Aburahma, M. H. (2015). Investigating the potential of employing bilosomes as a novel vesicular carrier for transdermal delivery of tenoxicam. *Int J Pharm*, *485*(1-2), 329-340. https://doi.org/10.1016/j.ijpharm.2015.03.033

Aluani, D., Tzankova, V., Yordanov, Y., Zhelyazkova, A., Georgieva, E., & Yoncheva, K. J. P. (2016). Quercetin: An overview of biological effects and recent development of drug delivery systems. *63*, 52-60.

Amalraj, A., Pius, A., Gopi, S., & Gopi, S. (2017). Biological activities of curcuminoids, other biomolecules from turmeric and their derivatives - A review. *J Tradit Complement Med*, *7*(2), 205-233. https://doi.org/10.1016/j.jtcme.2016.05.005

Amenitsch, H., Rappolt, M., Teixeira, C. V., Majerowicz, M., & Laggner, P. (2004). In situ sensing of salinity in oriented lipid multilayers by surface X-ray scattering. *Langmuir*, *20*(11), 4621-4628.

Amnuaikit, T., Limsuwan, T., Khongkow, P., & Boonme, P. (2018). Vesicular carriers containing phenylethyl resorcinol for topical delivery system; liposomes, transfersomes and invasomes. *Asian journal of pharmaceutical sciences*, *13*(5), 472-484.

Amri, A., Chaumeil, J., Sfar, S., & Charrueau, C. (2012). Administration of resveratrol: what formulation solutions to bioavailability limitations? *Journal of Controlled Release*, *158*(2), 182-193.

Andishmand, H., Hamishehkar, H., Babazadeh, A., Taghvimi, A., Mohammadifar, M. A., & Tabibiazar, M. (2016). A colon targeted delivery system for resveratrol enriching in pH responsive-model. *Pharmaceutical Sciences*, *23*(1), 42-49.

Antipov, A. A., Sukhorukov, G. B., Leporatti, S., Radtchenko, I. L., Donath, E., & Möhwald, H. (2002). Polyelectrolyte multilayer capsule permeability control. *Colloids and Surfaces A: Physicochemical and Engineering Aspects*, *198*, 535-541.

Ares, A. M., Soto, M. E., Nozal, M. J., Bernal, J. L., Higes, M., & Bernal, J. (2015). Determination of resveratrol and piceid isomers in bee pollen by liquid

chromatography coupled to electrospray ionization-mass spectrometry. *Food Analytical Methods*, *8*(6), 1565-1575.

Ariyarathna, I. R., Karunaratne, D. N. J. F., & Processing, B. (2015). Use of chickpea protein for encapsulation of folate to enhance nutritional potency and stability. *95*, 76-82.

Arora, D., Khurana, B., & Nanda, S. (2020). DoE directed optimization, development and evaluation of resveratrol loaded ultradeformable vesicular cream for topical antioxidant benefits. *Drug Development and Industrial Pharmacy*, *46*(2), 227-235.

Arzani, G., Haeri, A., Daeihamed, M., Bakhtiari-Kaboutaraki, H., & Dadashzadeh, S. (2015). Niosomal carriers enhance oral bioavailability of carvedilol: Effects of bile salt-enriched vesicles and carrier surface charge [Article]. *International Journal of Nanomedicine*, *10*, 4797-4813. https://doi.org/10.2147/IJN.S84703

Assadpour, E., & Jafari, S. M. (2019). An overview of lipid-based nanostructures for encapsulation of food ingredients. *Lipid-based nanostructures for food encapsulation purposes*, 1-34.

Badran, M. (2014). Formulation and in vitro evaluation of flufenamic acid loaded deformable liposomes for improved skin delivery. *Digest Journal of Nanomaterials & Biostructures (DJNB)*, *9*(1).

Balanč, B. D., Ota, A., Djordjević, V. B., Šentjurc, M., Nedović, V. A., Bugarski, B. M., & Ulrih, N. P. (2015). Resveratrol-loaded liposomes: Interaction of resveratrol with phospholipids. *European journal of lipid science and technology*, *117*(10), 1615-1626.

Bandara, S. R., Molley, T. G., Kim, H., Bharath, P. A., Kilian, K. A., & Leal, C. (2020). The structural fate of lipid nanoparticles in the extracellular matrix. *Materials horizons*, *7*(1), 125-134.

Bang, S., Hwang, I., Yu, Y., Kwon, H., Kim, D., & Park, H. (2011). Influence of chitosan coating on the liposomal surface on physicochemical properties and the release profile of nanocarrier systems. *Journal of Microencapsulation*, *28*(7), 595-604.

Barea, M., Jenkins, M., Lee, Y., Johnson, P., & Bridson, R. (2012). Encapsulation of liposomes within pH responsive microspheres for oral colonic drug delivery. *International journal of biomaterials*, *2012*.

Barone, A., Cristiano, M. C., Cilurzo, F., Locatelli, M., Iannotta, D., Di Marzio, L., . . . Paolino, D. (2020). Ammonium glycyrrhizate skin delivery from ultradeformable liposomes: a novel use as an anti-inflammatory agent in topical drug delivery. *Colloids and Surfaces B: Biointerfaces*, *193*, 111152.

Battaglia, G., & Ryan, A. J. (2005). Bilayers and interdigitation in block copolymer vesicles. *Journal of the American Chemical Society*, *127*(24), 8757-8764.

Beaucage, G. (1995). Approximations leading to a unified exponential/power-law approach to small-angle scattering. *Journal of applied crystallography*, *28*(6), 717-728.

Beaucage, G. (1996). Small-angle scattering from polymeric mass fractals of arbitrary mass-fractal dimension. *Journal of applied crystallography*, *29*(2), 134-146.

Beaucage, G. (2012). 2.14—combined small-angle scattering for characterization of hierarchically structured polymer systems over nano-to-micron meter: part II theory. *Polymer science: a comprehensive reference. Elsevier, Amsterdam*, *399*.

Berr, S. (1987). Solvent isotope effects on alkytrimethylammonium bromide micelles as a function of alkyl chain length. *Journal of Physical Chemistry*, *91*(18), 4760-4765.

Berti, D., Caminati, G., & Baglioni, P. (2011). Functional liposomes and supported lipid bilayers: towards the complexity of biological archetypes. *Physical Chemistry Chemical Physics*, *13*(19), 8769-8782.

Bhattacharjee, S. (2016). DLS and zeta potential - What they are and what they are not? *J Control Release*, *235*, 337-351. https://doi.org/10.1016/j.jconrel.2016.06.017

Bonechi, C., Martini, S., Ciani, L., Lamponi, S., Rebmann, H., Rossi, C., & Ristori, S. (2012). Using liposomes as carriers for polyphenolic compounds: the case of trans-resveratrol. *PLoS One*, *7*(8), e41438. https://doi.org/10.1371/journal.pone.0041438

Borel, T., & Sabliov, C. (2014). Nanodelivery of bioactive components for food applications: types of delivery systems, properties, and their effect on ADME profiles and toxicity of nanoparticles. *Annual review of food science and technology*, *5*, 197-213.

Boseila, A. A., Abdel-Reheem, A. Y., & Basalious, E. B. (2019). Design of bile-based vesicles (BBVs) for hepatocytes specific delivery of Daclatasvir: Comparison of ex-vivo transenterocytic transport, in-vitro protein adsorption resistance and HepG2 cellular uptake of charged and β-sitosterol decorated vesicles [Article]. *Plos One*, *14*(7), Article e0219752. https://doi.org/10.1371/journal.pone.0219752

Bouarab, L., Maherani, B., Kheirolomoom, A., Hasan, M., Aliakbarian, B., Linder, M., . . . Biointerfaces, s. B. (2014). Influence of lecithin–lipid composition on physico-chemical properties of nanoliposomes loaded with a hydrophobic molecule. *115*, 197-204.

Brittes, J., Lucio, M., Nunes, C., Lima, J., & Reis, y. (2010). Effects of resveratrol on membrane biophysical properties: relevance for its pharmacological effects. *Chemistry and Physics of Lipids*, *163*(8), 747-754.

Brodkorb, A., Egger, L., Alminger, M., Alvito, P., Assunção, R., Ballance, S., . . . Carrière, F. (2019). INFOGEST static in vitro simulation of gastrointestinal food digestion. *Nature protocols*, *14*(4), 991-1014.

Brooksbank, D. V., Leaver, J., & Horne, D. S. (1993). Adsorption of milk proteins to phosphatidylglycerol and phosphatidylcholine liposomes. *Journal of Colloid and Interface Science*, *161*(1), 38-42.

Brown, V. A., Patel, K. R., Viskaduraki, M., Crowell, J. A., Perloff, M., Booth, T. D., . . . Piccirilli, G. J. C. r. (2010). Repeat dose study of the cancer chemopreventive agent resveratrol in healthy volunteers: safety, pharmacokinetics, and effect on the insulin-like growth factor axis. *70*(22), 9003-9011.

Caddeo, C., Pons, R., Carbone, C., Fernandez-Busquets, X., Cardia, M. C., Maccioni, A. M., . . . Manconi, M. (2017). Physico-chemical characterization of succinyl chitosan-stabilized liposomes for the oral co-delivery of quercetin and resveratrol. *Carbohydr Polym*, *157*, 1853-1861. https://doi.org/10.1016/j.carbpol.2016.11.072

Can, A., Kiraz, A., & Pala, C. U. (2019). In vitro Evaluation of the Antibacterial Potential of Niosome-Encapsulated Olive Leaf Extract. *International Journal of Scientific and Technological Research*, *5*, 1-8.

Can, A., Tyler, A. I., & Mackie, A. R. (2021). Potential use of bile salts in lipid self-assembled systems for the delivery of phytochemicals. *Current Opinion in Colloid & Interface Science*, 101502.

Carbonell-Capella, J. M., Buniowska, M., Barba, F. J., Esteve, M. J., & Frígola, A. (2014). Analytical Methods for Determining Bioavailability and Bioaccessibility of Bioactive Compounds from Fruits and Vegetables: A Review. *Comprehensive Reviews in Food Science and Food Safety*, *13*(2), 155-171. https://doi.org/10.1111/1541-4337.12049

Catalgol, B., Batirel, S., Taga, Y., & Ozer, N. K. (2012). Resveratrol: French paradox revisited. *Frontiers in pharmacology*, *3*, 141.

Chawda, P. J., Shi, J., Xue, S., & Young Quek, S. (2017). Co-encapsulation of bioactives for food applications. *Food Quality and Safety*, *1*(4), 302-309. https://doi.org/10.1093/fqsafe/fyx028

Cheewatanakornkool, K., & Sriamornsak, P. (2015). Pectin-Chitosan Multilayer Coated Microbeads of Diclofenac Sodium Prepared by Layer-by-Layer Technique. *Advanced Materials Research*, *1060*, 45-49.

Chen, B., Wang, X., Lin, D., Xu, D., Li, S., Huang, J., . . . Yao, H. (2019). Proliposomes for oral delivery of total biflavonoids extract from Selaginella doederleinii: formulation development, optimization, and in vitro–in vivo characterization. *International journal of nanomedicine*, *14*, 6691.

Chen, H., Pan, H., Li, P., Wang, H., Wang, X., Pan, W., & Yuan, Y. (2016). The potential use of novel chitosan-coated deformable liposomes in an ocular drug delivery system [Article]. *Colloids and Surfaces B: Biointerfaces*, *143*, 455-462. https://doi.org/10.1016/j.colsurfb.2016.03.061

Chen, L., Zhu, H., & Cui, H. (2017). A study of the Brownian motion of the non-spherical microparticles on fluctuating lattice Boltzmann method. *Microfluidics and Nanofluidics*, *21*, 1-10.

Chen, R., Poger, D., & Mark, A. E. (2011). Effect of high pressure on fully hydrated DPPC and POPC bilayers. *The Journal of Physical Chemistry B*, *115*(5), 1038-1044.

Chen, W.-T., Kuo, Y.-L., Chen, C.-H., Wu, H.-T., Chen, H.-W., & Fang, W.-P. (2022). Improving the stability and bioactivity of curcumin using chitosan-coated liposomes through a combination mode of high-pressure processing. *Lwt*, *168*, 113946.

Chen, X., McClements, D. J., Zhu, Y. Q., Chen, Y., Zou, L. Q., Liu, W., . . . Liu, C. M. (2018). Enhancement of the solubility, stability and bioaccessibility of quercetin using protein-based excipient emulsions. *Food Research International*, *114*, 30-37. https://doi.org/10.1016/j.foodres.2018.07.062

Cheng, C., Wu, Z., McClements, D. J., Zou, L., Peng, S., Zhou, W., & Liu, W. (2019). Improvement on stability, loading capacity and sustained release of rhamnolipids modified curcumin liposomes. *Colloids and Surfaces B: Biointerfaces*, *183*, 110460.

Chimento, A., De Amicis, F., Sirianni, R., Sinicropi, M. S., Puoci, F., Casaburi, I., . . . Pezzi, V. (2019). Progress to improve oral bioavailability and beneficial effects of resveratrol [Review]. *International Journal of Molecular Sciences*, *20*(6), Article 1381. https://doi.org/10.3390/ijms20061381

Chu, B.-S., Gunning, A. P., Rich, G. T., Ridout, M. J., Faulks, R. M., Wickham, M. S., . . . Wilde, P. J. (2010). Adsorption of bile salts and pancreatic colipase and lipase onto digalactosyldiacylglycerol and dipalmitoylphosphatidylcholine monolayers. *Langmuir*, *26*(12), 9782-9793.

Cieślik-Boczula, K., Maniewska, J., Grynkiewicz, G., Szeja, W., Koll, A., & Hendrich, A. B. (2012). Interaction of quercetin, genistein and its derivatives with lipid bilayers–An ATR IR-spectroscopic study. *Vibrational Spectroscopy*, *62*, 64-69.

Colvin, J., & Stapleton, H. (1985). Fractal and spectral dimensions of biopolymer chains: Solvent studies of electron spin relaxation rates in myoglobin azide. *The Journal of chemical physics*, *82*(10), 4699-4706.

Coreta-Gomes, F. M., Martins, P. A., Velazquez-Campoy, A., Vaz, W. L., Geraldes, C. F., & Moreno, M. J. (2015). Interaction of Bile Salts with Model Membranes Mimicking the Gastrointestinal Epithelium: A Study by Isothermal Titration Calorimetry. *Langmuir*, *31*(33), 9097-9104. https://doi.org/10.1021/acs.langmuir.5b01810

Craft, B. D., Kerrihard, A. L., Amarowicz, R., & Pegg, R. B. (2012). Phenol-Based Antioxidants and the In Vitro Methods Used for Their Assessment. *Comprehensive Reviews in Food Science and Food Safety*, *11*(2), 148-173. https://doi.org/10.1111/j.1541-4337.2011.00173.x

Cuomo, F., Cofelice, M., Venditti, F., Ceglie, A., Miguel, M., Lindman, B., & Lopez, F. (2018). In-vitro digestion of curcumin loaded chitosan-coated liposomes. *Colloids Surf B Biointerfaces*, *168*, 29-34. https://doi.org/10.1016/j.colsurfb.2017.11.047

Danaei, M., Dehghankhold, M., Ataei, S., Hasanzadeh Davarani, F., Javanmard, R., Dokhani, A., . . . Mozafari, M. (2018). Impact of particle size and polydispersity index on the clinical applications of lipidic nanocarrier systems. *Pharmaceutics*, *10*(2), 57.

Dash, K. K., Fayaz, U., Dar, A. H., Shams, R., Manzoor, S., Sundarsingh, A., . . . Khan, S. A. (2022). A comprehensive review on heat treatments and related impact on the quality and microbial safety of milk and milk-based products. *Food Chemistry Advances*, 100041.

Davidov-Pardo, G., & McClements, D. J. (2014). Resveratrol encapsulation: Designing delivery systems to overcome solubility, stability and bioavailability issues. *Trends in Food Science & Technology*, *38*(2), 88-103. https://doi.org/10.1016/j.tifs.2014.05.003

de Ghellinck, A., Shen, C., Fragneto, G., & Klösgen, B. (2015). Probing the position of resveratrol in lipid bilayers: A neutron reflectivity study. *Colloids and surfaces B: biointerfaces*, *134*, 65-72.

Delgado, Á. V., González-Caballero, F., Hunter, R., Koopal, L., & Lyklema, J. (2007). Measurement and interpretation of electrokinetic phenomena. *Journal of colloid and interface science*, *309*(2), 194-224.

Delmas, D., Aires, V., Limagne, E., Dutartre, P., Mazue, F., Ghiringhelli, F., & Latruffe, N. (2011). Transport, stability, and biological activity of resveratrol. *Ann N Y Acad Sci*, *1215*, 48-59. https://doi.org/10.1111/j.1749-6632.2010.05871.x

Devi, G. K., Suruthi, P., Veerakumar, R., Vinoth, S., Subbaiya, R., & Chozhavendhan, S. (2019). A review on metallic gold and silver nanoparticles. *Research Journal of Pharmacy and Technology*, *12*(2), 935-943.

Devi, P., Sharma, P., Rathore, C., & Negi, P. (2019). Novel Drug Delivery Systems of Resveratrol to Bioavailability and Therapeutic Effects. In *Resveratrol - Adding Life to Years, Not Adding Years to Life*. https://doi.org/10.5772/intechopen.79739

Dias, D. R., Botrel, D. A., Fernandes, R. V. D. B., & Borges, S. V. (2017). Encapsulation as a tool for bioprocessing of functional foods. *Current Opinion in Food Science*, *13*, 31-37.

Dupont, D., Mandalari, G., Molle, D., Jardin, J., Léonil, J., Faulks, R. M., . . . Mackie, A. R. (2010). Comparative resistance of food proteins to adult and infant in vitro digestion models. *Molecular nutrition & food research*, *54*(6), 767-780.

EC. (2011). *Commission Recommendation of 18 October 2011 on the definition of nanomaterial (2011/696/EU)*. Retrieved 21/07/2023 from https://eur-lex.europa.eu/eli/reco/2011/696/oj

Elnaggar, Y. S. R. (2015). Multifaceted applications of bile salts in pharmacy: an emphasis on nanomedicine. *International Journal of Nanomedicine*, *10*, 3955-3971. https://doi.org/10.2147/ijn.S82558

Elnaggar, Y. S. R., Omran, S., Hazzah, H. A., & Abdallah, O. Y. (2019). Anionic versus cationic bilosomes as oral nanocarriers for enhanced delivery of the hydrophilic drug risedronate [Article]. *International Journal of Pharmaceutics*, *564*, 410-425. https://doi.org/10.1016/j.ijpharm.2019.04.069

Elsayed, M. M., & Cevc, G. (2011). The vesicle-to-micelle transformation of phospholipid–cholate mixed aggregates: a state of the art analysis including membrane curvature effects. *Biochimica et biophysica acta (BBA)-biomembranes*, *1808*(1), 140-153.

Esfanjani, A. F., Assadpour, E., & Jafari, S. M. (2018). Improving the bioavailability of phenolic compounds by loading them within lipid-based nanocarriers. *Trends in Food Science & Technology*, *76*, 56-66.

Espinal-Ruiz, M., Parada-Alfonso, F., Restrepo-Sánchez, L.-P., Narváez-Cuenca, C.-E., & McClements, D. J. (2014). Impact of dietary fibers [methyl cellulose, chitosan, and pectin] on digestion of lipids under simulated gastrointestinal conditions. *Food & function*, *5*(12), 3083-3095.

Faizi, H. A., Frey, S. L., Steinkühler, J., Dimova, R., & Vlahovska, P. M. (2019). Bending rigidity of charged lipid bilayer membranes. *Soft Matter*, *15*(29), 6006-6013.

Fan, Q., Zhang, Y., Hou, X., Li, Z., Zhang, K., Shao, Q., & Feng, N. (2018). Improved oral bioavailability of notoginsenoside R1 with sodium glycocholate-mediated liposomes: preparation by supercritical fluid technology and evaluation in vitro and in vivo. *International Journal of Pharmaceutics*, *552*(1-2), 360-370.

Fang, J.-Y., Hwang, T.-L., Huang, Y.-L., & Fang, C.-L. (2006). Enhancement of the transdermal delivery of catechins by liposomes incorporating anionic surfactants and ethanol. *International Journal of Pharmaceutics*, *310*(1-2), 131-138.

Faridi Esfanjani, A., Assadpour, E., & Jafari, S. M. (2018). Improving the bioavailability of phenolic compounds by loading them within lipid-based nanocarriers. *Trends in Food Science & Technology*, *76*, 56-66. https://doi.org/10.1016/j.tifs.2018.04.002

Fernández-Nieves, A., Fernández-Barbero, A., Vincent, B., & De las Nieves, F. (2003). Osmotic de-swelling of ionic microgel particles. *The Journal of chemical physics*, *119*(19), 10383-10388.

Ferreira, S., & Domingues, F. (2016). The antimicrobial action of resveratrol against Listeria monocytogenes in food-based models and its antibiofilm properties. *J Sci Food Agric*, *96*(13), 4531-4535. https://doi.org/10.1002/jsfa.7669

Foo, K. S., Bavoh, C. B., Lal, B., & Mohd Shariff, A. (2020). Rheology Impact of Various Hydrophilic-Hydrophobic Balance (HLB) Index Non-Ionic Surfactants on Cyclopentane Hydrates. *Molecules*, *25*(16), 3725.

Fornasier, M., Pireddu, R., Del Giudice, A., Sinico, C., Nylander, T., Schillén, K., . . . Murgia, S. (2021). Tuning lipid structure by bile salts: Hexosomes for topical administration of catechin. *Colloids and Surfaces B: Biointerfaces*, *199*, 111564.

Frenzel, M., Krolak, E., Wagner, A., & Steffen-Heins, A. (2015). Physicochemical properties of WPI coated liposomes serving as stable transporters in a real food matrix. *LWT-food science and technology*, *63*(1), 527-534.

Gambini, J., Inglés, M., Olaso, G., Lopez-Grueso, R., Bonet-Costa, V., Gimeno-Mallench, L., . . . longevity, c. (2015). Properties of resveratrol: in vitro and in vivo studies about metabolism, bioavailability, and biological effects in animal models and humans. *2015*.

Garidel, P., Hildebrand, A., Knauf, K., & Blume, A. (2007). Membranolytic activity of bile salts: influence of biological membrane properties and composition. *Molecules*, *12*(10), 2292-2326.

Gass, J., Vora, H., Hofmann, A. F., Gray, G. M., & Khosla, C. (2007). Enhancement of dietary protein digestion by conjugated bile acids. *Gastroenterology*, *133*(1), 16-23.

Gibis, M., Rahn, N., & Weiss, J. (2013). Physical and oxidative stability of uncoated and chitosan-coated liposomes containing grape seed extract. *Pharmaceutics*, *5*(3), 421-433.

Gokce, Y., Cengiz, B., Yildiz, N., Calimli, A., & Aktas, Z. (2014). Ultrasonication of chitosan nanoparticle suspension: Influence on particle size. *Colloids and Surfaces A: Physicochemical and Engineering Aspects*, *462*, 75-81.

Goldberg, D. M., Yan, J., & Soleas, G. J. J. C. b. (2003). Absorption of three wine-related polyphenols in three different matrices by healthy subjects. *36*(1), 79-87.

Goniotaki, M., Hatziantoniou, S., Dimas, K., Wagner, M., & Demetzos, C. (2004). Encapsulation of naturally occurring flavonoids into liposomes: physicochemical properties and biological activity against human cancer cell lines. *Journal of pharmacy and pharmacology*, *56*(10), 1217-1224.

Gradauer, K., Vonach, C., Leitinger, G., Kolb, D., Fröhlich, E., Roblegg, E., . . . Prassl, R. J. I. j. o. n. (2012). Chemical coupling of thiolated chitosan to preformed liposomes improves mucoadhesive properties. *7*, 2523.

Grillo, I. (2008). 13 Small-Angle Neutron Scattering and Applications in Soft Condensed Matter.

Guan, P., Lu, Y., Qi, J., Niu, M., Lian, R., Hu, F., & Wu, W. (2011). Enhanced oral bioavailability of cyclosporine A by liposomes containing a bile salt. *International journal of nanomedicine*, *6*, 965.

Guan, P., Lu, Y., Qi, J., & Wu, W. (2016). Readily restoring freeze-dried probilosomes as potential nanocarriers for enhancing oral delivery of cyclosporine A. *Colloids Surf B Biointerfaces*, *144*, 143-151. https://doi.org/10.1016/j.colsurfb.2016.04.006

Guinier, A., & Fournet, G. (1955). *Small-angle Scattering of X-rays*. John Wiley and Sons, New York.

Guo, L., Peng, Y., Li, Y., Yao, J., Zhang, G., Chen, J., . . . Sui, L. (2015). Cell death pathway induced by resveratrol-bovine serum albumin nanoparticles in a

human ovarian cell line. *Oncol Lett*, *9*(3), 1359-1363. https://doi.org/10.3892/ol.2015.2851

Gómez-Mascaraque, L. G., Sipoli, C. C., de La Torre, L. G., & López-Rubio, A. (2017). Microencapsulation structures based on protein-coated liposomes obtained through electrospraying for the stabilization and improved bioaccessibility of curcumin. *Food Chemistry*, *233*, 343-350.

Hammouda, B. (2010). Analysis of the Beaucage model. *Journal of Applied Crystallography*, *43*(6), 1474-1478.

Hao, F., He, Y., Sun, Y., Zheng, B., Liu, Y., Wang, X., . . . Xie, J. (2016). Improvement of oral availability of ginseng fruit saponins by a proliposome delivery system containing sodium deoxycholate. *Saudi J Biol Sci*, *23*(1), S113-125. https://doi.org/10.1016/j.sjbs.2015.09.024

Hasan, M., Messaoud, G. B., Michaux, F., Tamayol, A., Kahn, C., Belhaj, N., . . . Arab-Tehrany, E. J. R. a. (2016). Chitosan-coated liposomes encapsulating curcumin: Study of lipid–polysaccharide interactions and nanovesicle behavior. *6*(51), 45290-45304.

Hashemzadeh, H., Javadi, H., & Darvishi, M. (2020). Study of Structural stability and formation mechanisms in DSPC and DPSM liposomes: A coarse-grained molecular dynamics simulation. *Scientific reports*, *10*(1), 1-10.

He, H., Lu, Y., Qi, J., Zhu, Q., Chen, Z., & Wu, W. (2019). Adapting liposomes for oral drug delivery. *Acta Pharm Sin B*, *9*(1), 36-48. https://doi.org/10.1016/j.apsb.2018.06.005

He, Q., Zhang, Y., Lu, G., Miller, R., Möhwald, H., & Li, J. (2008). Dynamic adsorption and characterization of phospholipid and mixed phospholipid/protein layers at liquid/liquid interfaces. *Advances in colloid and interface science*, *140*(2), 67-76.

Hejazi, R., & Amiji, M. J. J. o. c. r. (2003). Chitosan-based gastrointestinal delivery systems. *89*(2), 151-165.

Henriksen, I., Smistad, G., & Karlsen, J. (1994). Interactions between liposomes and chitosan. *International journal of pharmaceutics*, *101*(3), 227-236.

Hildebrand, A. B., K.: Neubert, R.: Garidel, P.: Blume, A. (2004). Solubilization of negatively charged DPPC/DPPG liposomes by bile salts. *Journal of Colloid and Interface Science*, *279*(2), 559-571. https://doi.org/10.1016/j.jcis.2004.06.085

Holm, R., Østergaard, J., Schönbeck, C., Jensen, H., Shi, W., Peters, G. H., & Westh, P. (2014). Determination of stability constants of tauro-and glyco-conjugated bile salts with the negatively charged sulfobutylether-β-cyclodextrin: comparison of affinity capillary electrophoresis and isothermal titration calorimetry and thermodynamic analysis of the interaction. *Journal of inclusion phenomena and macrocyclic chemistry*, *78*(1-4), 185-194.

Hosny, K. M., Alharbi, W. S., Almehmady, A. M., Bakhaidar, R. B., Alkhalidi, H. M., Sindi, A. M., . . . Zaki, R. M. (2020). Preparation and optimization of pravastatin-naringenin nanotransfersomes to enhance bioavailability and reduce hepatic side effects. *Journal of Drug Delivery Science and Technology*, *57*, 101746.

Hu, D., Xu, Y., Xie, J., Sun, C., Zheng, X., & Chen, W. (2018). Systematic evaluation of phenolic compounds and protective capacity of a new mulberry cultivar J33 against palmitic acid-induced lipotoxicity using a simulated digestion method. *Food Chemistry*, *258*, 43-50.

Hu, S., Niu, M., Hu, F., Lu, Y., Qi, J., Yin, Z., & Wu, W. (2013). Integrity and stability of oral liposomes containing bile salts studied in simulated and ex vivo gastrointestinal media. *International Journal of Pharmaceutics*, *441*(1-2), 693-700.

Hua, Y., Wei, Z., & Xue, C. (2021). Chitosan and its composites-based delivery systems: advances and applications in food science and nutrition sector. *Critical Reviews in Food Science and Nutrition*, 1-20.

Huang, M., Liang, C., Tan, C., Huang, S., Ying, R., Wang, Y., . . . Zhang, Y. (2019). Liposome co-encapsulation as a strategy for the delivery of curcumin and resveratrol. *Food & function*, *10*(10), 6447-6458.

Huang, X., Dai, Y., Cai, J., Zhong, N., Xiao, H., McClements, D. J., & Hu, K. (2017). Resveratrol encapsulation in core-shell biopolymer nanoparticles: Impact on antioxidant and anticancer activities. *Food Hydrocolloids*, *64*, 157-165. https://doi.org/10.1016/j.foodhyd.2016.10.029

Hui, C., & Huang, H. (2021). A study on chitosan-coated liposomes as a carrier of bovine serum albumin as oral protein drug. *Journal of Dispersion Science and Technology*, *42*(10), 1494-1503.

Hupfeld, S., Moen, H. H., Ausbacher, D., Haas, H., & Brandl, M. (2010). Liposome fractionation and size analysis by asymmetrical flow field-flow fractionation/multi-angle light scattering: influence of ionic strength and osmotic pressure of the carrier liquid. *Chemistry and physics of lipids*, *163*(2), 141-147.

Jackman, J. A., Zhao, Z., Zhdanov, V. P., Frank, C. W., & Cho, N.-J. (2014). Vesicle adhesion and rupture on silicon oxide: Influence of freeze–thaw pretreatment. *Langmuir*, *30*(8), 2152-2160.

Jafari, S. M. (2017). *Nanoencapsulation technologies for the food and nutraceutical industries*. Academic Press.

Jafari, S. M., & McClements, D. J. (2017). Nanotechnology approaches for increasing nutrient bioavailability. *Advances in food and nutrition research*, *81*, 1-30.

Jahan-Mihan, A., Luhovyy, B. L., Khoury, D. E., & Anderson, G. H. (2011). Dietary proteins as determinants of metabolic and physiologic functions of the gastrointestinal tract. *Nutrients*, *3*(5), 574-603.

Jash, A., & Rizvi, S. S. (2022). Heat-stable liposomes from milk fat globule membrane phospholipids for pH-triggered delivery of hydrophilic and lipophilic bioactives. *Innovative Food Science & Emerging Technologies*, *79*, 103030.

Jash, A., Ubeyitogullari, A., & Rizvi, S. S. (2020). Synthesis of multivitamin-loaded heat stable liposomes from milk fat globule membrane phospholipids by using a supercritical-CO 2 based system. *Green Chemistry*, *22*(16), 5345-5356.

Jeon, S., Yoo, C. Y., & Park, S. N. (2015). Improved stability and skin permeability of sodium hyaluronate-chitosan multilayered liposomes by Layer-by-Layer electrostatic deposition for quercetin delivery. *Colloids and surfaces B: biointerfaces*, *129*, 7-14.

Jiang, X., Li, Y., Tang, X., Jiang, J., He, Q., Xiong, Z., & Zheng, H. (2021). Biopolymer-based flocculants: A review of recent technologies. *Environmental Science and Pollution Research*, *28*, 46934-46963.

Jovanović, A. A., Balanč, B. D., Ota, A., Ahlin Grabnar, P., Djordjević, V. B., Šavikin, K. P., . . . Poklar Ulrih, N. (2018). Comparative Effects of Cholesterol and β-Sitosterol on the Liposome Membrane Characteristics. *European Journal of Lipid Science and Technology*, *120*(9). https://doi.org/10.1002/ejlt.201800039

Jubeh, T. T., Barenholz, Y., & Rubinstein, A. (2004). Differential adhesion of normal and inflamed rat colonic mucosa by charged liposomes. *Pharmaceutical research*, *21*, 447-453.

Karim, N., Shishir, M. R. I., & Chen, W. (2020). Surface decoration of neohesperidin-loaded nanoliposome using chitosan and pectin for improving stability and controlled release. *Int J Biol Macromol*, *164*, 2903-2914. https://doi.org/10.1016/j.ijbiomac.2020.08.174

Kasiotis, K. M., Pratsinis, H., Kletsas, D., & Haroutounian, S. A. (2013). Resveratrol and related stilbenes: their anti-aging and anti-angiogenic properties. *Food Chem Toxicol*, *61*, 112-120. https://doi.org/10.1016/j.fct.2013.03.038

Kim, M. S., Yeom, D. W., Kim, S. R., Yoon, H. Y., Kim, C. H., Son, H. Y., . . . Choi, Y. W. (2016). Development of a chitosan based double layer-coated tablet as a platform for colon-specific drug delivery. *Drug Design, Development and Therapy*, 45-57.

King, R., Bomser, J., & Min, D. (2006). Bioactivity of Resveratrol. *Comprehensive Reviews in Food Science and Food Safety*, *5*, 65-70.

Kiselev, M., Janich, M., Hildebrand, A., Strunz, P., Neubert, R., & Lombardo, D. (2013). Structural transition in aqueous lipid/bile salt [DPPC/NaDC] supramolecular aggregates: SANS and DLS study. *Chemical Physics*, *424*, 93-99.

Kokkona, M., Kallinteri, P., Fatouros, D., & Antimisiaris, S. G. J. E. j. o. p. s. (2000). Stability of SUV liposomes in the presence of cholate salts and pancreatic lipases: effect of lipid composition. *9*(3), 245-252.

Kotla, N. G., Chandrasekar, B., Rooney, P., Sivaraman, G., Larrañaga, A., Krishna, K. V., . . . Rochev, Y. (2017). Biomimetic lipid-based nanosystems for enhanced dermal delivery of drugs and bioactive agents. *ACS Biomaterials Science & Engineering*, *3*(7), 1262-1272.

Kotlarchyk, M., & Chen, S. H. (1983). Analysis of small angle neutron scattering spectra from polydisperse interacting colloids. *The Journal of chemical physics*, *79*(5), 2461-2469.

Koukoulitsa, C., Durdagi, S., Siapi, E., Villalonga-Barber, C., Alexi, X., Steele, B. R., . . . Mavromoustakos, T. (2011). Comparison of thermal effects of stilbenoid analogs in lipid bilayers using differential scanning calorimetry and molecular dynamics: correlation of thermal effects and topographical position with antioxidant activity. *European Biophysics Journal*, *40*(7), 865-875.

Kristl, J., Teskač, K., Caddeo, C., Abramović, Z., & Šentjurc, M. (2009). Improvements of cellular stress response on resveratrol in liposomes. *European journal of pharmaceutics and biopharmaceutics*, *73*(2), 253-259.

Krzysko, A. J., Nakouzi, E., Zhang, X., Graham, T. R., Rosso, K. M., Schenter, G. K., . . . Ivory, C. F. (2020). Correlating inter-particle forces and particle shape to shear-induced aggregation/fragmentation and rheology for dilute anisotropic particle suspensions: A complementary study via capillary rheometry and in-situ small and ultra-small angle X-ray scattering. *Journal of Colloid and Interface Science*, *576*, 47-58.

Kubo, Y., Nogita, T., Kimura, I., Chiba, M., & Sakakibara, K. (2016). Interventional evaluation of monoammonium glycyrrhizinate-glycine/DL-methionine combination tablets in mild alopecia areata. *Journal of Clinical & Experimental Dermatology Research*, *7*(1), 322.

Kurien, B. T., Singh, A., Matsumoto, H., Scofield, R. H. J. A., & technologies, d. d. (2007). Improving the solubility and pharmacological efficacy of curcumin by heat treatment. *5*(4), 567-576.

Kučerka, N., Tristram-Nagle, S., & Nagle, J. F. (2006). Structure of fully hydrated fluid phase lipid bilayers with monounsaturated chains. *The Journal of membrane biology*, *208*, 193-202.

Labourdenne, S., Brass, O., Ivanova, M., Cagna, A., & Verger, R. (1997). Effects of colipase and bile salts on the catalytic activity of human pancreatic lipase. A study using the oil drop tensiometer. *Biochemistry*, *36*(12), 3423-3429.

Lancon, A., Delma, D., Osman, H., Thénot, J.-P., Jannin, B., & Latruffe, N. (2004). Human hepatic cell uptake of resveratrol: involvement of both passive diffusion and carrier-mediated process. *Biochemical and biophysical research communications*, *316*(4), 1132-1137.

Langasco, R., Fancello, S., Rassu, G., Cossu, M., Cavalli, R., Galleri, G., . . . Gavini, E. (2019). Increasing protective activity of genistein by loading into transfersomes: A new potential adjuvant in the oxidative stress-related neurodegenerative diseases? *Phytomedicine*, *52*, 23-31.

Laye, C., McClements, D., & Weiss, J. (2008). Formation of biopolymer-coated liposomes by electrostatic deposition of chitosan. *Journal of Food Science*, *73*(5), N7-N15.

Lee, M.-K. (2020). Liposomes for enhanced bioavailability of water-insoluble drugs: In vivo evidence and recent approaches. *Pharmaceutics*, *12*(3), 264.

Li, N. Y. D., Perutková, Š., Iglič, A., & Rappolt, M. (2017). My first electron density map: A beginner's guide to small angle X-ray diffraction. *Elektrotehniski Vestnik*, *84*(3), 69.

Li, Y., Yang, D., Wang, Y., Li, Z., & Zhu, C. (2019). Co-delivery doxorubicin and silybin for anti-hepatoma via enhanced oral hepatic-targeted efficiency. *International journal of nanomedicine*, *14*, 301.

Li, Y. R., Li, S., & Lin, C. C. (2018). Effect of resveratrol and pterostilbene on aging and longevity. *Biofactors*, *44*(1), 69-82. https://doi.org/10.1002/biof.1400

Li, Z., Paulson, A. T., & Gill, T. A. (2015). Encapsulation of bioactive salmon protein hydrolysates with chitosan-coated liposomes. *Journal of Functional Foods*, *19*, 733-743.

Liang, F., & Hua, J. X. (2005). Absorption profiles of sanchinoside R1 and ginsenoside Rg1 in the rat intestine. *European journal of drug metabolism and pharmacokinetics*, *30*(4), 261-268.

Lichtenberg, D., Ahyayauch, H., & Goñi, F. M. (2013). The mechanism of detergent solubilization of lipid bilayers. *Biophysical Journal*, *105*(2), 289-299.

Liu, C., Guo, Y., Cheng, Y., & Qian, H. (2022). Bilosomes: A controlled delivery system for the sustained release of torularhodin during digestion in the small intestine both in vitro and in vivo. *Colloids and Surfaces A: Physicochemical and Engineering Aspects*, *654*, 130055.

Liu, N., & Park, H.-J. J. J. o. m. (2009). Chitosan-coated nanoliposome as vitamin E carrier. *26*(3), 235-242.

Liu, W., Liu, J., Liu, W., Li, T., & Liu, C. (2013). Improved physical and in vitro digestion stability of a polyelectrolyte delivery system based on layer-by-layer self-assembly alginate–chitosan-coated nanoliposomes. *Journal of agricultural and food chemistry*, *61*(17), 4133-4144.

Liu, W., Ye, A., Han, F., & Han, J. (2019). Advances and challenges in liposome digestion: Surface interaction, biological fate, and GIT modeling. *Advances in Colloid and Interface Science*, *263*, 52-67.

Liu, W., Ye, A., Liu, W., Liu, C., Han, J., & Singh, H. (2015). Behaviour of liposomes loaded with bovine serum albumin during in vitro digestion. *Food chemistry*, *175*, 16-24.

Liu, W. L., Liu, W., Ye, A. Q., Peng, S. F., Wei, F. Q., Liu, C. M., & Han, J. Z. (2016). Environmental stress stability of microencapsules based on liposomes decorated with chitosan and sodium alginate. *Food Chemistry*, *196*, 396-404. https://doi.org/10.1016/j.foodchem.2015.09.050

Liu, Y., Liu, D., Zhu, L., Gan, Q., & Le, X. (2015). Temperature-dependent structure stability and in vitro release of chitosan-coated curcumin liposome. *Food Research International*, *74*, 97-105.

Lopes, N. A., Pinilla, C. M. B., & Brandelli, A. (2017). Pectin and polygalacturonic acid-coated liposomes as novel delivery system for nisin: Preparation, characterization and release behavior. *Food hydrocolloids*, *70*, 1-7.

Ma, L., Wang, X., Wu, J., Zhang, D., Zhang, L., Song, X., . . . Wu, S. (2019). Polyethylenimine and sodium cholate-modified ethosomes complex as multidrug carriers for the treatment of melanoma through transdermal delivery. *Nanomedicine*, *14*(18), 2395-2408.

Mackie, A., Gourcy, S., Rigby, N., Moffat, J., Capron, I., & Bajka, B. (2019). The fate of cellulose nanocrystal stabilised emulsions after simulated gastrointestinal digestion and exposure to intestinal mucosa. *Nanoscale*, *11*(6), 2991-2998.

Mackie, A., & Macierzanka, A. (2010). Colloidal aspects of protein digestion. *Current Opinion in Colloid & Interface Science*, *15*(1-2), 102-108.

Mackie, A., Mulet-Cabero, A.-I., & Torcello-Gómez, A. (2020). Simulating human digestion: Developing our knowledge to create healthier and more sustainable foods. *Food & function*, *11*(11), 9397-9431.

Madsen, K. L., & Herlo, R. (2017). Recursive alterations of the relationship between simple membrane geometry and insertion of amphiphilic motifs. *Membranes*, *7*(1), 6.

Mahmood, S., Taher, M., & Mandal, U. K. (2014). Experimental design and optimization of raloxifene hydrochloride loaded nanotransfersomes for transdermal application. *Int J Nanomedicine*, *9*, 4331-4346. https://doi.org/10.2147/ijn.S65408

Manconi, M., Manca, M. L., Valenti, D., Escribano, E., Hillaireau, H., Fadda, A. M., & Fattal, E. (2017). Chitosan and hyaluronan coated liposomes for pulmonary administration of curcumin. *International journal of pharmaceutics*, *525*(1), 203-210.

Manconi, M., Mura, S., Manca, M. L., Fadda, A., Dolz, M., Hernandez, M., . . . Díez-Sales, O. J. I. J. o. P. (2010). Chitosomes as drug delivery systems for C-phycocyanin: Preparation and characterization. *392*(1-2), 92-100.

Marsanasco, M., Calabró, V., Piotrkowski, B., Chiaramoni, N. S., & del V. Alonso, S. (2016). Fortification of chocolate milk with omega-3, omega-6, and vitamins E and C by using liposomes. *European Journal of Lipid Science and Technology*, *118*(9), 1271-1281. https://doi.org/10.1002/ejlt.201400663

Marsanasco, M., Piotrkowski, B., Calabró, V., del Valle Alonso, S., & Chiaramoni, N. S. (2015). Bioactive constituents in liposomes incorporated in orange juice as new functional food: thermal stability, rheological and organoleptic properties. *Journal of food science and technology*, *52*, 7828-7838.

Martínez-Padilla, E., Li, K., Blok Frandsen, H., Skejovic Joehnke, M., Vargas-Bello-Pérez, E., & Lykke Petersen, I. (2020). In vitro protein digestibility and fatty acid profile of commercial plant-based milk alternatives. *Foods*, *9*(12), 1784.

Matloub, A. A., Salama, A. H., Aglan, H. A., AbouSamra, M. M., ElSouda, S. S. M., & Ahmed, H. H. (2018). Exploiting bilosomes for delivering bioactive polysaccharide isolated from Enteromorpha intestinalis for hacking hepatocellular carcinoma. *Drug development and industrial pharmacy*, *44*(4), 523-534.

Matsuura, Y. (1991). Pectic acid degrading enzymes from human feces. *Agricultural and biological chemistry*, *55*(3), 885-886.

Maurer, N., Fenske, D. B., & Cullis, P. R. (2001). Developments in liposomal drug delivery systems. *Expert Opinion on Biological Therapy*, *1*(6), 923-947.

McClements, D. J. (2013). Edible lipid nanoparticles: Digestion, absorption, and potential toxicity. *Progress in lipid research*, *52*(4), 409-423.

McClements, D. J. (2015). Encapsulation, protection, and release of hydrophilic active components: Potential and limitations of colloidal delivery systems. *Advances in colloid and interface science*, *219*, 27-53.

McClements, D. J. (2020). Advances in nanoparticle and microparticle delivery systems for increasing the dispersibility, stability, and bioactivity of phytochemicals. *Biotechnology Advances*, *38*, 107287.

McClements, D. J., Li, F., & Xiao, H. (2015). The nutraceutical bioavailability classification scheme: classifying nutraceuticals according to factors limiting their oral bioavailability. *Annual Review of Food Science and Technology*, *6*, 299-327.

Meng, X., Maliakal, P., Lu, H., Lee, M.-J., Yang, C. S. J. J. o. A., & Chemistry, F. (2004). Urinary and plasma levels of resveratrol and quercetin in humans, mice, and rats after ingestion of pure compounds and grape juice. *52*(4), 935-942.

Minekus, M., Alminger, M., Alvito, P., Ballance, S., Bohn, T., Bourlieu, C., . . . Brodkorb, A. (2014). A standardised static in vitro digestion method suitable for food - an international consensus. *Food Funct*, *5*(6), 1113-1124. https://doi.org/10.1039/c3fo60702j

Mirafzali, Z., Thompson, C. S., & Tallua, K. (2014). Application of liposomes in the food industry. In *Microencapsulation in the Food Industry* (pp. 139-150). Elsevier.

Moghimipour, E., Ameri, A., & Handali, S. (2015). Absorption-enhancing effects of bile salts. *Molecules*, *20*(8), 14451-14473.

Molet-Rodríguez, A., Torcello-Gómez, A., Salvia-Trujillo, L., Martín-Belloso, O., & Mackie, A. R. (2023). In vitro digestibility of O/W emulsions co-ingested with complex meals: Influence of the food matrix. *Food Hydrocolloids*, *135*, 108121.

Morel, J., Andreux, F., Habib, L., & Guckert, A. (1987). Comparison of the adsorption of maize root mucilage and polygalacturonic acid on montmorillonite homoionic to divalent lead and cadmium. *Biology and Fertility of Soils*, *5*, 13-17.

Moreno, F. J., Mackie, A. R., & Mills, E. C. (2005). Phospholipid interactions protect the milk allergen α-lactalbumin from proteolysis during in vitro digestion. *Journal of agricultural and food chemistry*, *53*(25), 9810-9816.

Mouhid, L., Corzo-Martínez, M., Torres, C., Vázquez, L., Reglero, G., Fornari, T., & Ramírez de Molina, A. (2017). Improving in vivo efficacy of bioactive

molecules: An overview of potentially antitumor phytochemicals and currently available lipid-based delivery systems. *Journal of oncology*, *2017*.

Müller, M. J., Stachurski, S., Stoffels, P., Schipper, K., Feldbrügge, M., & Büchs, J. (2018). Online evaluation of the metabolic activity of Ustilago maydis on (poly) galacturonic acid. *Journal of Biological Engineering*, *12*(1), 1-17.

Ng, S. W., Chan, Y., Chellappan, D. K., Madheswaran, T., Zeeshan, F., Chan, Y. L., . . . Wark, P. (2019). Molecular modulators of celastrol as the keystones for its diverse pharmacological activities. *Biomedicine & Pharmacotherapy*, *109*, 1785-1792.

Nguyen, S., Alund, S. J., Hiorth, M., Kjøniksen, A.-L., & Smistad, G. (2011). Studies on pectin coating of liposomes for drug delivery. *Colloids and Surfaces B: Biointerfaces*, *88*(2), 664-673.

Nguyen, T. X., Huang, L., Liu, L., Elamin Abdalla, A. M., Gauthier, M., & Yang, G. (2014). Chitosan-coated nano-liposomes for the oral delivery of berberine hydrochloride [Article]. *Journal of Materials Chemistry B*, *2*(41), 7149-7159. https://doi.org/10.1039/c4tb00876f

Niaz, T., Imran, M., & Mackie, A. (2021). Improving carvacrol bioaccessibility using core-shell carrier-systems under simulated gastrointestinal digestion. *Food Chem*, *353*, 129505. https://doi.org/10.1016/j.foodchem.2021.129505

Nikiforidis, C. V. (2019). Structure and functions of oleosomes (oil bodies). *Advances in colloid and interface science*, *274*, 102039.

Nkanga, C. I., Bapolisi, A. M., Okafor, N. I., & Krause, R. W. M. (2019). General perception of liposomes: formation, manufacturing and applications. *Liposomes-advances and perspectives*.

Pabois, O., Lorenz, C. D., Harvey, R. D., Grillo, I., Grundy, M. M.-L., Wilde, P. J., . . . Dreiss, C. A. (2019). Molecular insights into the behaviour of bile salts at interfaces: a key to their role in lipid digestion. *Journal of colloid and interface science*, *556*, 266-277.

Pan, L., Zhang, S., Gu, K., & Zhang, N. (2018). Preparation of astaxanthin-loaded liposomes: characterization, storage stability and antioxidant activity. *CyTA-Journal of Food*, *16*(1), 607-618.

Panya, A., Laguerre, M., Lecomte, J., Villeneuve, P., Weiss, J., McClements, D. J., & Decker, E. A. (2010). Effects of chitosan and rosmarinate esters on the physical and oxidative stability of liposomes. *Journal of agricultural and food chemistry*, *58*(9), 5679-5684.

Park, S. N., Jo, N. R., & Jeon, S. H. (2014). Chitosan-coated liposomes for enhanced skin permeation of resveratrol. *Journal of industrial and engineering chemistry*, *20*(4), 1481-1485.

Pasarin, D., Ghizdareanu, A.-I., Enascuta, C. E., Matei, C. B., Bilbie, C., Paraschiv-Palada, L., & Veres, P.-A. (2023). Coating Materials to Increase the Stability of Liposomes. *Polymers*, *15*(3), 782.

Pattni, B. S., Chupin, V. V., & Torchilin, V. P. (2015). New developments in liposomal drug delivery. *Chemical Reviews*, *115*(19), 10938-10966.

Pecora, R. (2008). Basic concepts–Scattering and time correlation functions. *Soft Matter Characterization*, 1-40.

Peng, R. M., Lin, G. R., Ting, Y., & Hu, J. Y. (2018). Oral delivery system enhanced the bioavailability of stilbenes: Resveratrol and pterostilbene. *Biofactors*, *44*(1), 5-15. https://doi.org/10.1002/biof.1405

Peng, S., Zou, L., Zhou, W., Liu, W., Liu, C., & McClements, D. J. (2019). Encapsulation of lipophilic polyphenols into nanoliposomes using pH-driven

method: Advantages and disadvantages. *Journal of agricultural and food chemistry*, *67*(26), 7506-7511.

Petruzzi, L., Campaniello, D., Speranza, B., Corbo, M. R., Sinigaglia, M., & Bevilacqua, A. (2017). Thermal treatments for fruit and vegetable juices and beverages: A literature overview. *Comprehensive Reviews in Food Science and Food Safety*, *16*(4), 668-691.

Planas, J. M., Alfaras, I., Colom, H., Juan, M. E. J. A. o. b., & biophysics. (2012). The bioavailability and distribution of trans-resveratrol are constrained by ABC transporters. *527*(2), 67-73.

Polozova, A., Li, X., Shangguan, T., Meers, P., Schuette, D. R., Ando, N., . . . Perkins, W. R. (2005). Formation of homogeneous unilamellar liposomes from an interdigitated matrix. *Biochimica et biophysica acta (BBA)-biomembranes*, *1668*(1), 117-125.

Porrini, M., & Riso, P. (2008). Factors influencing the bioavailability of antioxidants in foods: a critical appraisal. *Nutr Metab Cardiovasc Dis*, *18*(10), 647-650. https://doi.org/10.1016/j.numecd.2008.08.004

Priprem, A., Watanatorn, J., Sutthiparinyanont, S., Phachonpai, W., & Muchimapura, S. (2008). Anxiety and cognitive effects of quercetin liposomes in rats. *Nanomedicine: nanotechnology, biology and medicine*, *4*(1), 70-78.

Pynn, R. (2009). Neutron scattering—a non-destructive microscope for seeing inside matter. *Neutron applications in earth, energy and environmental sciences*, 15-36.

Rai, D., Beaucage, G., Jonah, E., Britton, D., Sukumaran, S., Chopra, S., . . . Härting, M. (2012). Quantitative investigations of aggregate systems. *The Journal of chemical physics*, *137*(4).

Rampino, A., Borgogna, M., Bellich, B., Blasi, P., Virgilio, F., & Cesàro, A. (2016). Chitosan-pectin hybrid nanoparticles prepared by coating and blending techniques. *European Journal of Pharmaceutical Sciences*, *84*, 37-45.

Rappolt, M. (2010). Bilayer thickness estimations with “poor” diffraction data. *Journal of Applied Physics*, *107*(8), 084701.

Refai, H., Hassan, D., & Abdelmonem, R. (2017). Development and characterization of polymer-coated liposomes for vaginal delivery of sildenafil citrate. *Drug Delivery*, *24*(1), 278-288.

Rein, M. J., Renouf, M., Cruz-Hernandez, C., Actis-Goretta, L., Thakkar, S. K., & da Silva Pinto, M. (2013). Bioavailability of bioactive food compounds: a challenging journey to bioefficacy. *Br J Clin Pharmacol*, *75*(3), 588-602. https://doi.org/10.1111/j.1365-2125.2012.04425.x

Reza Mozafari, M., Johnson, C., Hatziantoniou, S., & Demetzos, C. (2008). Nanoliposomes and their applications in food nanotechnology. *Journal of Liposome Research*, *18*(4), 309-327.

Rezaei, A., Fathi, M., & Jafari, S. M. (2019). Nanoencapsulation of hydrophobic and low-soluble food bioactive compounds within different nanocarriers. *Food Hydrocolloids*, *88*, 146-162.

Richards, M. H., & Gardner, C. R. (1978). Effects of bile salts on the structural integrity of liposomes. *Biochimica et Biophysica Acta (BBA)-General Subjects*, *543*(4), 508-522.

Riddick, T. M. (1968). *Control of colloid stability through zeta potential: with a closing chapter on its relationship to cardiovascular disease*.

Rideau, E., Dimova, R., Schwille, P., Wurm, F. R., & Landfester, K. (2018). Liposomes and polymersomes: a comparative review towards cell mimicking. *Chemical society reviews*, *47*(23), 8572-8610.

Ridlon, J. M., Harris, S. C., Bhowmik, S., Kang, D.-J., & Hylemon, P. B. (2016). Consequences of bile salt biotransformations by intestinal bacteria. *Gut microbes*, *7*(1), 22-39.

Roberts, J. J., Power, A., Chapman, J., Chandra, S., & Cozzolino, D. (2018). Vibrational spectroscopy methods for agro-food product analysis. In *Comprehensive Analytical Chemistry* (Vol. 80, pp. 51-68). Elsevier.

Roger, E., Lagarce, F., Garcion, E., & Benoit, J.-P. (2010). Biopharmaceutical parameters to consider in order to alter the fate of nanocarriers after oral delivery. *Nanomedicine*, *5*(2), 287-306.

Rohindra, D. R., Nand, A. V., & Khurma, J. R. (2004). Swelling properties of chitosan hydrogels. *The South Pacific Journal of Natural and Applied Sciences*, *22*(1), 32-35.

Sabın, J., Prieto, G., Ruso, J. M., Hidalgo-Alvarez, R., & Sarmiento, F. (2006). Size and stability of liposomes: a possible role of hydration and osmotic forces. *The European Physical Journal E*, *20*, 401-408.

Sarabandi, K., Rafiee, Z., Khodaei, D., & Jafari, S. M. (2019). Encapsulation of food ingredients by nanoliposomes. In *Lipid-based nanostructures for food encapsulation purposes* (pp. 347-404). Elsevier.

SasView. (2022). *Model Functions for small-angle scattering analysis*. Retrieved 01.01.2022 from https://www.sasview.org/docs/user/qtgui/Perspectives/Fitting/models/index.html

Saura-Calixto, F., Serrano, J., & Goñi, I. (2007). Intake and bioaccessibility of total polyphenols in a whole diet. *Food Chemistry*, *101*(2), 492-501. https://doi.org/10.1016/j.foodchem.2006.02.006

Scarano, A., Chieppa, M., & Santino, A. (2020). Plant polyphenols-biofortified foods as a novel tool for the prevention of human gut diseases. *Antioxidants*, *9*(12), 1225.

Schlich, M., Lai, F., Pireddu, R., Pini, E., Ailuno, G., Fadda, A., . . . Sinico, C. (2020). Resveratrol proniosomes as a convenient nanoingredient for functional food. *Food Chemistry*, *310*, 125950.

Scott, H. L., Skinkle, A., Kelley, E. G., Waxham, M. N., Levental, I., & Heberle, F. A. (2019). On the mechanism of bilayer separation by extrusion, or why your LUVs are not really unilamellar. *Biophysical Journal*, *117*(8), 1381-1386.

Sebaaly, C., Haydar, S., & Greige-Gerges, H. (2022). Eugenol encapsulation into conventional liposomes and chitosan-coated liposomes: A comparative study. *Journal of Drug Delivery Science and Technology*, *67*, 102942.

Sebaaly, C., Trifan, A., Sieniawska, E., & Greige-Gerges, H. (2021). Chitosan-coating effect on the characteristics of liposomes: A focus on bioactive compounds and essential oils: A review. *Processes*, *9*(3), 445.

Sene, C. F., McCann, M. C., Wilson, R. H., & Grinter, R. (1994). Fourier-transform Raman and Fourier-transform infrared spectroscopy (an investigation of five higher plant cell walls and their components). *Plant physiology*, *106*(4), 1623-1631.

Shen, Q., Zheng, W., Han, F., Dai, J., Song, R., Li, J., . . . Chen, Y. (2023). Quantitative analysis and interfacial properties of mixed pea protein isolate-

phospholipid adsorption layer. *International Journal of Biological Macromolecules*, *232*, 123487.

Shishir, M. R. I., Karim, N., Gowd, V., Xie, J., Zheng, X., & Chen, W. (2019). Pectin-chitosan conjugated nanoliposome as a promising delivery system for neohesperidin: Characterization, release behavior, cellular uptake, and antioxidant property. *Food Hydrocolloids*, *95*, 432-444.

Shishir, M. R. I., Karim, N., Xie, J., Rashwan, A. K., & Chen, W. (2020). Colonic delivery of pelargonidin-3-O-glucoside using pectin-chitosan-nanoliposome: Transport mechanism and bioactivity retention. *Int J Biol Macromol*, *159*, 341-355. https://doi.org/10.1016/j.ijbiomac.2020.05.076

Shishir, M. R. I., Xie, L., Sun, C., Zheng, X., & Chen, W. (2018). Advances in micro and nano-encapsulation of bioactive compounds using biopolymer and lipid-based transporters. *Trends in Food Science & Technology*, *78*, 34-60.

Silva, C., Aranda, F. J., Ortiz, A., Martínez, V., Carvajal, M., & Teruel, J. A. (2011). Molecular aspects of the interaction between plants sterols and DPPC bilayers: An experimental and theoretical approach. *Journal of colloid and interface science*, *358*(1), 192-201.

Singh, P. (2017). Small-Angle Scattering Techniques (SAXS/SANS). In *Membrane Characterization* (pp. 95-111). Elsevier.

Singla, A., & Chawla, M. (2001). Chitosan: Some pharmaceutical and biological aspects-an update. *Journal of pharmacy and pharmacology*, *53*(8), 1047-1067.

Song, K.-H., Chung, S.-J., & Shim, C.-K. (2005). Enhanced intestinal absorption of salmon calcitonin (sCT) from proliposomes containing bile salts. *Journal of Controlled Release*, *106*(3), 298-308.

Soo, E., Thakur, S., Qu, Z., Jambhrunkar, S., Parekh, H. S., & Popat, A. (2016). Enhancing delivery and cytotoxicity of resveratrol through a dual nanoencapsulation approach. *Journal of Colloid and Interface Science*, *462*, 368-374.

Souza, G. R., & Miller, J. H. (2011). Elastic light scattering of biopolymer/gold nanoparticles fractal aggregates. In *Reviews in Plasmonics 2010* (pp. 39-68). Springer.

Souza, J. E. D., Casanova, L. M., & Costa, S. S. (2015). Bioavailability of phenolic compounds: a major challenge for drug development?

Springer, M., & Moco, S. J. N. (2019). Resveratrol and Its Human Metabolites—Effects on Metabolic Health and Obesity. *11*(1), 143.

Sriamornsak, P. (2011). Application of pectin in oral drug delivery. *Expert opinion on drug delivery*, *8*(8), 1009-1023.

Svajger, U., & Jeras, M. (2012). Anti-inflammatory effects of resveratrol and its potential use in therapy of immune-mediated diseases. *Int Rev Immunol*, *31*(3), 202-222. https://doi.org/10.3109/08830185.2012.665108

Tahara, K., Nishio, M., & Takeuchi, H. (2018). Evaluation of liposomal behavior in the gastrointestinal tract after oral administration using real-time in vivo imaging. *Drug Development and Industrial Pharmacy*, *44*(4), 608-614.

Tai, K., Rappolt, M., Mao, L., Gao, Y., Li, X., & Yuan, F. (2020). The stabilization and release performances of curcumin-loaded liposomes coated by high and low molecular weight chitosan. *Food Hydrocolloids*, *99*, 105355.

Tan, C., Feng, B., Zhang, X., Xia, W., & Xia, S. (2016). Biopolymer-coated liposomes by electrostatic adsorption of chitosan (chitosomes) as novel delivery systems for carotenoids. *Food Hydrocolloids*, *52*, 774-784.

Tan, C., Wang, J., & Sun, B. (2021). Biopolymer-liposome hybrid systems for controlled delivery of bioactive compounds: Recent advances. *Biotechnol Adv*, *48*, 107727. https://doi.org/10.1016/j.biotechadv.2021.107727

Tang, M., Gui, Z., Liang, X., Yan, C., Li, X., Li, Z., . . . Gui, S. (2021). Pueraria flavones-loaded bile salt liposomes with improved intestinal absorption and oral bioavailability: in vitro and in vivo evaluation. *Pharmaceutical Development and Technology*, *26*(10), 1051-1060.

Thakare, M., Israel, B. e., Garner, S., Ahmed, H., Elder, D., & Capomacchia, A. (2017). Nonionic surfactant structure on the drug release, formulation and physical properties of ethylcellulose microspheres. *Pharmaceutical development and technology*, *22*(3), 418-425.

Thomson, A., Keelan, M., Garg, M., & Clandinin, M. (1989). Intestinal aspects of lipid absorption: in review. *Canadian journal of physiology and pharmacology*, *67*(3), 179-191.

Torchilin, V. P. (2005). Recent advances with liposomes as pharmaceutical carriers. *Nat Rev Drug Discov*, *4*(2), 145-160. https://doi.org/10.1038/nrd1632

Toro-Uribe, S., Ibáñez, E., Decker, E. A., McClements, D. J., Zhang, R., López-Giraldo, L. J., & Herrero, M. (2018). Design, fabrication, characterization, and in vitro digestion of alkaloid-, catechin-, and cocoa extract-loaded liposomes. *Journal of agricultural and food chemistry*, *66*(45), 12051-12065.

Tønnesen, H. H., Másson, M., & Loftsson, T. (2002). Studies of curcumin and curcuminoids. XXVII. Cyclodextrin complexation: solubility, chemical and photochemical stability. *International Journal of Pharmaceutics*, *244*(1-2), 127-135.

Uchegbu, I. F., & Florence, A. T. (1995). Non-ionic surfactant vesicles (niosomes): physical and pharmaceutical chemistry. *Advances in Colloid and Interface Science*, *58*(1), 1-55.

Van Hoogevest, P., & Wendel, A. (2014). The use of natural and synthetic phospholipids as pharmaceutical excipients. *European journal of lipid science and technology*, *116*(9), 1088-1107.

Van Tran, V., Moon, J.-Y., & Lee, Y.-C. (2019). Liposomes for delivery of antioxidants in cosmeceuticals: Challenges and development strategies. *Journal of Controlled Release*, *300*, 114-140.

Vang, O., Ahmad, N., Baile, C. A., Baur, J. A., Brown, K., Csiszar, A., . . . Lin, H.-Y. J. P. o. (2011). What is new for an old molecule? Systematic review and recommendations on the use of resveratrol. *6*(6).

Vaz-da-Silva, M., Loureiro, A., Falcao, A., Nunes, T., Rocha, J., Fernandes-Lopes, C., . . . Soares-da-Silva, P. (2008). Effect of food on the pharmacokinetic profile of trans-resveratrol. *Int J Clin Pharmacol Ther*, *46*(11), 564-570.

Vian, M. A., Tomao, V., Gallet, S., Coulomb, P., & Lacombe, J. (2005). Simple and rapid method for cis-and trans-resveratrol and piceid isomers determination in wine by high-performance liquid chromatography using Chromolith columns. *Journal of chromatography A*, *1085*(2), 224-229.

Waglewska, E., Pucek-Kaczmarek, A., & Bazylińska, U. (2020). Novel surface-modified bilosomes as functional and biocompatible nanocarriers of hybrid compounds. *Nanomaterials*, *10*(12), 2472.

Walle, T. (2011). Bioavailability of resveratrol. *Ann N Y Acad Sci*, *1215*, 9-15. https://doi.org/10.1111/j.1749-6632.2010.05842.x

Walle, T., Hsieh, F., DeLegge, M. H., Oatis, J. E., & Walle, U. K. (2004). High absorption but very low bioavailability of oral resveratrol in humans. *Drug Metabolism and Disposition*, *32*(12), 1377-1382.

Wang, L., Huang, X., Jing, H., Ma, C., & Wang, H. (2021). Bilosomes as effective delivery systems to improve the gastrointestinal stability and bioavailability of epigallocatechin gallate (EGCG). *Food Research International*, *149*, 110631.

Wang, M., Liu, M., Xie, T., Zhang, B. F., & Gao, X. L. (2017). Chitosan-modified cholesterol-free liposomes for improving the oral bioavailability of progesterone. *Colloids Surf B Biointerfaces*, *159*, 580-585. https://doi.org/10.1016/j.colsurfb.2017.08.028

Wang, Q., Wei, Q., Yang, Q., Cao, X., Li, Q., Shi, F., . . . Yu, J. (2018). A novel formulation of [6]-gingerol: Proliposomes with enhanced oral bioavailability and antitumor effect. *International Journal of Pharmaceutics*, *535*(1-2), 308-315.

Wang, T., & Luo, Y. (2019). Biological fate of ingested lipid-based nanoparticles: current understanding and future directions. *Nanoscale*, *11*(23), 11048-11063. https://doi.org/10.1039/c9nr03025e

Wang, W., Cui, C., Wang, Q., Sun, C., Jiang, L., & Hou, J. (2019). Effect of pH on physicochemical properties of oil bodies from different oil crops. *Journal of food science and technology*, *56*, 49-58.

Wang, X., Cheng, F., Wang, X., Feng, T., Xia, S., & Zhang, X. (2021). Chitosan decoration improves the rapid and long-term antibacterial activities of cinnamaldehyde-loaded liposomes. *International Journal of Biological Macromolecules*, *168*, 59-66.

Wang, X., Ye, A., Dave, A., & Singh, H. (2022). Structural changes in oat milk and an oat milk–bovine skim milk blend during dynamic in vitro gastric digestion. *Food Hydrocolloids*, *124*, 107311.

Wang, Y., Zhou, Q., Zheng, J., Xiong, H., Zhao, L., Xu, Y., & Bai, C. (2023). Fabricating pectin and chitosan double layer coated liposomes to improve physicochemical stability of beta-carotene and alter its gastrointestinal fate. *International Journal of Biological Macromolecules*, *247*, 125780.

Wechtersbach, L., Ulrih, N. P., & Cigić, B. (2012). Liposomal stabilization of ascorbic acid in model systems and in food matrices. *LWT-food science and technology*, *45*(1), 43-49.

Wei, Y., Cai, Z., Wu, M., Guo, Y., Tao, R., Li, R., . . . Zhang, H. (2020). Comparative studies on the stabilization of pea protein dispersions by using various polysaccharides. *Food Hydrocolloids*, *98*, 105233.

Weiskirchen, S., & Weiskirchen, R. (2016). Resveratrol: how much wine do you have to drink to stay healthy? *Advances in Nutrition*, *7*(4), 706-718.

Wenzel, E., & Somoza, V. (2005). Metabolism and bioavailability of trans-resveratrol. *Molecular nutrition & food research*, *49*(5), 472-481.

Wilde, P., & Chu, B. (2011). Interfacial & colloidal aspects of lipid digestion. *Advances in colloid and interface science*, *165*(1), 14-22.

Wu, P. S., Li, Y. S., Kuo, Y. C., Tsai, S. J., & Lin, C. C. (2019). Preparation and Evaluation of Novel Transfersomes Combined with the Natural Antioxidant Resveratrol. *Molecules*, *24*(3). https://doi.org/10.3390/molecules24030600

Wu, Z., Yang, C., Chen, L., Ma, L., Wu, X., Dai, X., . . . Shi, X. (2019). A Multiscale Study on the Effect of Sodium Cholate on the Deformation Ability of Elastic Liposomes. *AAPS PharmSciTech*, *20*(8), 1-10.

Wüstner, D., Herrmann, A., & Müller, P. (2000). Head group-independent interaction of phospholipids with bile salts: a fluorescence and EPR study. *Journal of lipid research*, *41*(3), 395-404.

Xu, Z., Seddon, J. M., Beales, P. A., Rappolt, M., & Tyler, A. I. (2021). Breaking isolation to form new networks: PH-triggered changes in connectivity inside lipid nanoparticles. *Journal of the American Chemical Society*, *143*(40), 16556-16565.

Yang, G., Wu, F., Chen, M., Jin, J., Wang, R., & Yuan, Y. (2019). Formulation design, characterization, and in vitro and in vivo evaluation of nanostructured lipid carriers containing a bile salt for oral delivery of gypenosides. *International journal of nanomedicine*, *14*, 2267.

Yang, H., Liu, Z., Song, Y., & Hu, C. (2019). Hyaluronic acid-functionalized bilosomes for targeted delivery of tripterine to inflamed area with enhancive therapy on arthritis. *Drug delivery*, *26*(1), 820-830.

Yang, N.-C., Lee, C.-H., Song, T.-Y. J. B., biotechnology,, & biochemistry. (2010). Evaluation of resveratrol oxidation in vitro and the crucial role of bicarbonate ions. 0911281734-0911281734.

Yoshioka, T., Sternberg, B., & Florence, A. T. (1994). Preparation and properties of vesicles (niosomes) of sorbitan monoesters (Span 20, 40, 60 and 80) and a sorbitan triester (Span 85). *International Journal of Pharmaceutics*, *105*(1), 1-6.

Yu, C.-Y., Yin, B.-C., Zhang, W., Cheng, S.-X., Zhang, X.-Z., & Zhuo, R.-X. (2009). Composite microparticle drug delivery systems based on chitosan, alginate and pectin with improved pH-sensitive drug release property. *Colloids and Surfaces B: Biointerfaces*, *68*(2), 245-249.

Yu, J. Y., Chuesiang, P., Shin, G. H., & Park, H. J. (2021). Post-processing techniques for the improvement of liposome stability. *Pharmaceutics*, *13*(7), 1023.

Zhang, B., Xue, A., Zhang, C., Yu, J., Chen, W., & Sun, D. (2016). Bile salt liposomes for enhanced lymphatic transport and oral bioavailability of paclitaxel [Article]. *Pharmazie*, *71*(6), 320-326. https://doi.org/10.1691/ph.2016.5184

Zhang, S., & Wang, X. (2016). Effect of vesicle-to-micelle transition on the interactions of phospholipid/sodium cholate mixed systems with curcumin in aqueous solution. *The Journal of Physical Chemistry B*, *120*(30), 7392-7400.

Zhang, Y., Li, J., Wang, Z., Xu, M.-Z., Zeng, Z., Huang, J.-p., & Guan, Y.-Q. (2020). Natural plant-derived polygalacturonic acid-oleanolic acid assemblies as oral-delivered nanomedicine for insulin resistance treatment. *Chemical engineering journal*, *390*, 124630.

Zhao, C., Zhou, J., Yan, Y., Yang, L., Xing, G., Li, H., . . . Zheng, H. (2021). Application of coagulation/flocculation in oily wastewater treatment: A review. *Science of The Total Environment*, *765*, 142795.

Zhao, J., & Wu, J. (2006). Preparation and characterization of the fluorescent chitosan nanoparticle probe. *Chinese Journal of Analytical Chemistry*, *34*(11), 1555-1559.

Zheng, B., Zhou, H., & McClements, D. J. (2021). Nutraceutical-fortified plant-based milk analogs: Bioaccessibility of curcumin-loaded almond, cashew, coconut, and oat milks. *LWT*, *147*, 111517.

Zhou, F., Xu, T., Zhao, Y., Song, H., Zhang, L., Wu, X., & Lu, B. (2018). Chitosan-coated liposomes as delivery systems for improving the stability and oral bioavailability of acteoside. *Food Hydrocolloids*, *83*, 17-24.

Zhou, W., Cheng, C., Ma, L., Zou, L., Liu, W., Li, R., . . . Li, J. (2021). The Formation of Chitosan-Coated Rhamnolipid Liposomes Containing Curcumin: Stability and In Vitro Digestion. *Molecules*, *26*(3). https://doi.org/10.3390/molecules26030560

Zidovska, A., Ewert, K. K., Quispe, J., Carragher, B., Potter, C. S., & Safinya, C. R. (2009). The effect of salt and pH on block liposomes studied by cryogenic transmission electron microscopy. *Biochimica et Biophysica Acta (BBA)-Biomembranes*, *1788*(9), 1869-1876.

Zou, L.-q., Liu, W., Liu, W.-l., Liang, R.-h., Li, T., Liu, C.-m., . . . Liu, Z. (2014). Characterization and bioavailability of tea polyphenol nanoliposome prepared by combining an ethanol injection method with dynamic high-pressure microfluidization. *Journal of Agricultural and Food Chemistry*, *62*(4), 934-941.

Zou, L.-q., Peng, S.-f., Liu, W., Gan, L., Liu, W.-l., Liang, R.-h., . . . Liu, Z. (2014). Improved in vitro digestion stability of (−)-epigallocatechin gallate through nanoliposome encapsulation. *Food Research International*, *64*, 492-499.

Çağdaş, M., Sezer, A. D., & Bucak, S. (2014). Liposomes as potential drug carrier systems for drug delivery. *Application of nanotechnology in drug delivery*, *1*, 1-50.

List of Abbreviations

$(NH_4)_2CO_3$	Ammonium carbonate
AAT	Alanine amino transaminase
$AUC_{0-\infty}$	Area under the plasma concentration
b	Constant dependent upon the instrument and settings of optics
Bilosomes	Bile salt-containing liposomes
CA	Cholic acid
$CaCl_2(H_2O)_2$	Calcium chloride dihydrate
CDCA	Chenodeoxycholic acid
CH	Chitosan
Chol	Cholesterol
C_{max}	Maximum plasma concentration
CMC	Critical micelle concentration
c-res	Cis-resveratrol
cryo-TEM	Cryo-transmission electron microscopy
Cu	Copper
D	Translational diffusion coefficient
d	Distance in the real space, lattice spacing, bilayer thickness
D_2O	Heavy water
DAD	Diode array detector
DCA	Deoxycholic acid
DE	Degree of esterification
D_H	Hydrodynamic diameter
DI	Deformability index
DLPC	1,2-dilinoleoyl-sn-glycero-3-phosphocholine
DLS	Dynamic light scattering
DMPC	1,2-dimyristoyl-sn-glycero-3-phosphocholine
DOPC	1,2-dioleoyl-sn-glycero-3-phosphocholine
DOPG	1,2-dioleoyl-sn-glycero-3-phospho-(1'-rac-glycerol) (sodium salt)
DPPC	1,2-Dipalmitoyl-sn-glycero-3-phosphocholine
DPPH	1,1-diphenyl-2-picrylhydrazyl
DR	Drug retention
D_{sd}	Sample-to-detector distance

d-spacing	The thickness of lipid plus water layer
DSPC	1,2-Distearoyl-sn-glycero-3-phosphocholine
E	Magnitude of the electric field strength
EDP	Electron density profile
EDTA	Ethylenediaminetetraacetic acid
EE	Encapsulation efficiency
EGCG	Epigallocatechin gallate
$f(kR_H)$	The Henry's function which refers to the ratio of the particle radius to the Debye length
F(q)	Bessel function
F_h	experimentally derived amplitudes (form factors)
FT-IR	Fourier transform infrared spectroscopy
$G1(\tau)$	Field correlation function
$G2(\tau)$	The intensity autocorrelation function
GIT	Gastrointestinal tract
GRAS	Generally recognized as safe
GUV	Giant unilamellar vesicle
h	Hour
HBL	Hydrophilic-lipophilic balance
HCl	Hydrochloric acid
HM-pectin	High methoxy pectin
HMW	High molecular weight
HPLC	High-performance liquid chromatography
I	Intensity
I.D.	Inner diameter
IC_{50}	Half-maximal inhibitory concentration
Isc	Circuit current
j_1	Spherical Bessel function
k_B	The Boltzmann constant
K_c	Bending rigidity
KCl	Potassium chloride
KH_2PO_4	Potassium dihydrogen orthophosphate
LC	Loading capacity

LCA	Lithocholic acid
LC-MS	Liquid chromatography–mass spectrometry
LM-pectin	Low methoxy pectin
LMW	Low molecular weight
LogP	Partition coefficient
LSAS	Lipid self-assembled systems
LUV	Large unilamellar vesicle
MDA	Malondialdehyde
$MgCl_2(H_2O)_6$	Magnesium chloride
min	Minutes
MLV	Multilamellar vesicle
MRP	Multidrug resistance-associated proteins
$MRT_{0-\infty}$	Mean retention time
MTT	3-(4,5-dimethylthiazol-2-yl)-2,5-diphenyl-2H-tetrazolium bromide
N	Structural level
n	Integer (1, 2, 3..) describing the order of the diffraction peak
NaC	Sodium cholate
NaCl	Sodium chloride
NaDC	Sodium deoxycholate
NaGC	Sodium glycocholate
$NaHCO_3$	Sodium bicarbonate
NaOH	Sodium hydroxide
NaTC	Sodium taurocholate
NaTDC	Sodium taurodeoxycholate
N_s	Shell number
OM	Oat milk
P	Power law
P(q)	Form factor
P.D.	Potential difference
PAM	Poly(acrylamide)
P_{app}	Apparent absorption coefficient
PBS	Phosphate-buffered saline
PC	Phosphatidylcholine

PD	Polydispersity
PDI	Polydispersity index
PE	Phosphatidylethanolamine
PEG	Poly(ethylene glycol)
PEI	Polyethylenimine
PGA	Polygalacturonic acid
pKa	Acid dissociation constant
POPC	1-palmitoyl-2oleoyl-sn-glycero-3-phosphocholine
POPE	1-palmitoyl-2-oleoyl-sn-glycero-3-phosphoethanolamine
PS	Phosphatidylserine
PTFE	Polytetrafluoroethylene
Q	Scattering vector
R_C	Core radius
R_e	Equatorial radius perpendicular to the rotational axis of the ellipsoid
R_{eq}	Equatorial radius of core
R_g	Radius of gyration
R_H	Hydrodynamic radius
RH	Relative humidity
RI	Refractive index
R_N	The outer-most shell radius
R_p	Polar radius along the rotational axis of the ellipsoid
R_s	Radius of sphere
RT	Room temperature
R_{total}	Outer radius of the shell
s	Second
S(q)	Structure factor
SANS	Small-angle neutron scattering
SAXS	Small-angle X-ray scattering
SD	Standard deviation
SEM	Scanning electron microscopy
SGF	Simulated gastric fluid
S_h	the peak positions
SIF	Simulated intestinal fluid

SLD	Scattering length density
SPC	Soybean phosphatidylcholine
SSF	Simulated salivary fluid
SUV	Small unilamellar vesicle
T	Temperature
$T_{1/2}$	Elimination half-time
TEER	Transepithelial electrical resistance
TEM	Transmission electron microscopy
T_m	Transition temperature
T_{max}	Time to peak plasma concentration
TPP	Sodium tripolyphosphate pentabasic
t-res	Trans-resveratrol
T_{shell}	Shell thickness
$T_{solvent}$	Solvent thickness
T_{water}	Water thickness
ULV	Unilamellar vesicle
V	Volume of the particle
V(r)	Volume of a sphere of radius r
v/v	Volume concentration
V_{core}	Volume of the core
V_F	Volume fraction of particles
V_{Fshell}	Volume fraction of shell material
V_{no}	Vesicle no
V_p	Electrophoretic velocity of a particle
V_s	Volume of sphere
V_{shell}	Volume of the shell
V_{total}	Total volume
w/v	Mass concentration
wt	Mass fraction
X^2	Chi-square
X_c	Axial ratio of core
X_{ps}	Ratio of the thickness of shell at the pole to that at the equator
z	Peak-to-peak distance

List of Symbols

$\overrightarrow{k_i}$	Incident wave vector
$\overrightarrow{k_s}$	Scattered wave vector
$\Delta\rho$	Contrast factor
n_o	Refractive index of the solvent
α_h	Phase factors of the given amplitudes F_h
ε_0	Permittivity of vacuum
ε_r	Relative permittivity/dielectric constant
ζ	Zeta
η	Zero-shear viscosity of the medium
θ	Scattering angle
λ	Wavelength
λ_o	Wavelength in vacuum
μ_e	Electrophoretic mobility
ρ	Shape factor
$\rho(z)$	Relative electron density
ρ_{shell}	Scattering length density of shell
$\rho_{solvent}$	Scattering length density of solvent
Φ	Particle number density of scattering particle
α	Angle between the axis of the ellipsoid
τ	Delay time